Loughborough University

COMBINED NUMERICAL AND EXPERIMENTAL INVESTIGATION OF TRANSMISSION IDLE GEAR RATTLE

By

Osman A. M. Tangasawi

BEng (Hons.)

Thesis submitted in partial fulfillment of the requirements for the award of the degree of Doctor of Philosophy

Wolfson School of Mechanical and Manufacturing Engineering
Loughborough University
Leicestershire
LE11 3TU
UK

July 2007

Abstract

Gear rattle is caused by engine torsional vibration (engine order response) imparted to the transmission components, further causing the gears to oscillate within their functional backlashes. These oscillations lead to the repetitive impact of gear teeth, which lead to noisy responses, referred to as gear rattle. The lack of in-depth research into the effect of lubricant on gear rattle has been identified as a deficiency in the previous research in rattle. The aim of the current work is to address this shortcoming.

The thesis outlines a new approach in investigating the problem of idle gear rattle. The approach is based on the assumption that under idling condition the teeth-pair impact loads are sufficiently low and the gear speeds are sufficiently high to permit the formation of a hydrodynamic lubricant film between the mating gear teeth. This film acts as a non-linear spring-damper that couples the driver and the driven gears.

A torsional single-degree of freedom model is used in the development of the theory. The model is then expanded into a seven-degree of freedom torsional model and finally into an 11-degree of freedom model that also includes the lateral vibrations of the supporting shafts. The 11-degree of freedom model is based on a real life transmission that is also used in experimental studies to validate the model.

It is found that lubricant viscosity and bearing clearance (lubricant resistance in squeeze) play important roles in determining the dynamics of the system and its propensity to rattle. At low temperatures, the lateral vibrations of the shafts, carrying the gears interfere with the gear teeth impact action. The severity of rattle is determined by the relationship between the entraining and squeeze film actions of the hydrodynamic film. When the latter dominates, the system can rattle more severely.

The numerical results are found to correlate well with the experimental findings obtained from vehicle tests in a semi-anechoic chamber and also with those from a transmission test rig in the powertrain laboratory.

Key words:

Idle gear rattle, iso-viscous rigid regime of lubrication, squeeze film action, entraining motion.

List of publications from this is thesis appears in appendix A.

To my parents, sisters and brothers.

To the memories of my grandmothers Nafeesah and Zeinab.

Acknowledgement

The author wishes to express his gratitude to Professor Homer Rahnejat and Dr Stephanos Theodossiades for their patience and valuable support during the research period. The author would also like to extend his thanks to Wolfson School of Mechanical and manufacturing Engineering, the Department of Aeronautical and Automotive Engineering, the DTA (EPSRC), and Ford Motor Company, who supported this research.

I would like to thank my family for their patience and encouraging support. And I am grateful for our research group members, the technical staff and the undergraduate students, who have been very supportive.

Contents

List of Figures

List of Tables

Notation

$\mathbf{0}$	Zero matrix.
A	Amplitude (general).
A_n	Amplitude of the n^{th} harmonic term.
AL	Rattle index (chapter 2).
b	Clearance boundary (chapter 2).
b_g	Backlash (chapter 2) [m].
C	Clearance between wheel and shaft [m].
c	Torsional damping coefficient [Nm/radian/s].
C_B	Gear blank factor according to ISO 6336.
C_b	Normal backlash [m].
c_c	Centre distance between gear pair [m].
c_g	Contact damping coefficient [Ns/m].
C_R	Basic rack factor according to ISO 6336.
CR_t	The transverse contact ratio.
d_k	The shaft instantaneous displacement at bearing $k(k = a,b,c,d)$; $d_k = x_{1a}, y_{1a}, x_{1b}, y_{1b}, x_{2c}, y_{2c}, x_{2d}$, or y_{2d} [m].
F_f	The hydrodynamic friction force acting on the tooth in contact taken in the normal plane [N].
F_{fit}	The total transverse hydrodynamic flank friction acting on the i^{th} loose wheel [N].
F_{fj}	The hydrodynamic friction force acting on the j^{th} tooth in contact taken in the normal plane [N].
F_{ft}	The sum of the transverse components of the hydrodynamic flank friction acting on each tooth pair in simultaneous contact [N].
f_m	Gear mesh frequency [Hz].
f_{mi}	Gear mesh frequency of the i^{th} gear pair [Hz].

F_p Petrov's hydrodynamic tractive force [N].

F_{pi} Petrov's hydrodynamic tractive force acting on the i^{th} loose wheel bearing [N].

F_r Here, $r = x_1, y_1, x_2, y_2$, see below.

f_{roll} Rolling frequency [Hz].

F_W Gear face width [m]

F_{x1} The resultant force acting on the 1st shaft in the x-direction due to the radial and transverse components of the hydrodynamic film reaction [N].

F_{x2} The resultant force acting on the 2nd shaft in the x-direction due to the radial and transverse components of the hydrodynamic film reaction [N].

F_{y1} The resultant force acting on the 1st shaft in the y-direction due to the radial and transverse components of the hydrodynamic film reaction [N].

F_{y2} The resultant force acting on the 2nd shaft in the y-direction due to the radial and transverse components of the hydrodynamic film reaction [N].

H Hysteresis [Nm].

h Lubricant film thickness between the gear pair tooth surfaces [m].

h_i Lubricant film thickness between the i^{th} gear pair tooth surfaces [m].

h_0 Lubricant central film thickness [m].

$\mathbf{I}$ The mass matrix.

I Overall rattle index (chapter 2).

I_i Mass moment of inertia of the i^{th} wheel (kg m^2).

I_i Rattle index of the i^{th} wheel (chapter 2).

I_{in} Mass moment of inertia of the input shaft (kg m^2).

i_{time} Time step.

I_w Mass moment of inertia the wheel (kg m^2).

$j_{iteration}$ Iteration step.

$\mathbf{K}$ The stiffness matrix.

K The maximum stiffness of a single tooth pair per 1mm of face-width according to ISO 6336 (chapter 2) [N/μm/mm]

k Coefficient of torsional stiffness (chapter 2) [Nm/radian].

k_g Contact stiffness coefficient (chapter 2) [N/m].

K_{0i} The constant term in the Fourier series representing the time-varying linear contact stiffness associated with the i^{th} gear pair (N/m).

$K_{ci\kappa}$ The κ^{th} Fourier coefficient in the cosine Fourier series terms representing the time-varying linear contact stiffness associated with the i^{th} gear pair (N/m).

K_i Linear stiffness coefficient of the i^{th} gear pair contact [N/m].

K_k Coefficient of (non-linear) stiffness of bearing $k(k = a,b,c,d)$ [N/m$^{1.11}$].

K_{kr} Coefficient of (non-linear) stiffness of bearing $k(k = a,b,c,d)$ in the $r(r = x_1, y_1, x_2, y_2)$ direction [N/m$^{1.11}$].

K_r The linearised stiffness coefficient in the direction of $r(r = x_1, y_1, x_2, y_2)$ as a result of differentiating the bearing restoring forces with respect to their radial deformation (N/m).

K_{ri} The linearised stiffness coefficient in the direction of $r(r = x_1, y_1, x_2, y_2)$ as a result of differentiating the radial component of the hydrodynamic contact force with respect to the i^{th} wheel displacement [N/radian].

K_{rin} The linearised stiffness coefficient in the direction of $r(r = x_1, y_1, x_2, y_2)$ as a result of differentiating the radial component of the hydrodynamic contact forces with respect to the input shaft displacement [N/rad].

$K_{si\kappa}$ The κ^{th} Fourier coefficient in the sine Fourier series terms representing the time-varying linear contact stiffness associated with the i^{th} gear pair (N/m).

k'_{th} The theoretical single tooth stiffness according to ISO 6336 (chapter 2) [N/μm/mm].

K_{total} The total mesh stiffness according to ISO 6336 (chapter 2) [N/μm]

L Length of contact line on the contacting gear tooth surfaces [m]

l_j Distance between any contact point and the contact point on the pitch circle along the contact path of the j^{th} tooth [m]

l_1 Length of contact line in the conformal contact between the wheel and shaft [m].

L_{act} The length of the diagonal line in the contact (action) plane [m].

l_j The distance between the point of contact and pitch point measured along the contact path (transverse plane) of the j^{th} tooth [m].

l_k The roller length of bearing $k(k = a,b,c,d)$, [m].

l_l The diagonal parameter on the contact plane such that $0 \le l_l \le L_{act}$ [m].

L_{pitch} The diagonal pitch on the action plane diagonal line [m].

m_k The number of rollers in bearing $k(k = a,b,c,d)$.

N The total number of loose gears in a gearbox (chapter 2) [-].

N_{beh} The number of teeth behind the one described by the diagonal parameter l_l.

N_{front} The number of teeth in front of the one described by the diagonal parameter l_l.

N_i Tooth number of the i^{th} wheel.

N_{total} The total number of teeth in simultaneous contact.

P The pressure in the hydrodynamic conjunction (Pa).

p_{tb} The transverse base pitch [m].

p_{tbp} The pinion's transverse base pitch [m].

p_{tbw} The wheel's transverse base pitch [m].

Q_{kr} The reduced non-linear coefficient of the inner and outer raceways contact with the roller of bearing $k(k = a,b,c,d)$ associated with the bearing reaction in the $r(r = x_1, y_1, x_2, y_2)$direction.

R Ratio of inertia torque to drag torque (rattle ratio, chapter 2) [-].

r_{bp} Base radius of pinion [m]

r_{bw} Base radius of wheel [m]

r_{cjp} The contact radius of the j^{th} pinion [m].

r_{cjw} The contact radius of the j^{th} wheel [m].

r_{eqj} The reduced (equivalent) radius of curvature of the j^{th} meshing tooth pair in the normal plane [m].

r_i The pitch radius of the i^{th} loose wheel [m].

r_{os} Radius of output shaft [m]

r_{op} Outside radius of the pinion [m]

r_{ow} Outside radius of the wheel [m]

r_p Pitch radius of the pinion [m]

r_{p7} The contact radius of the reverse pinion [m].

r_{pi} The pitch radius of the i^{th} pinion [m].

r_s The internal radius of the i^{th} loose wheel [m].

r_w Pitch radius of the wheel [m]

t Time [s].

T_{eng} The total engine torque [Nm]

$\overline{T}_{eng}$ Constant term of the total engine torque [Nm].

T_{ff} The amplitude of the fluctuating (dynamic) torque component [Nm].

T_G Contact elasticity and damping torque (chapter 2) [Nm].

u_{ent} Lubricant entraining velocity [m/s].

u_j Lubricant entraining velocity associated with the j^{th} tooth pair [m/s].

u_{js} The sliding velocity associated with the j^{th} tooth pair [m/s].

v Lubricant entraining velocity in conformal contact between gear and shaft [m/s].

v_{jp} Rolling velocity of the j^{th} pinion tooth [m/s]

v_{jw} Rolling velocity of the j^{th} wheel tooth [m/s]

v_{ppitch} Pitch velocity of the pinion [m/s].

v_{wpitch} Pitch velocity of the wheel [m/s].

W_{ij} The hydrodynamic reaction force acting on the j^{th} tooth of the i^{th} loose wheel [N].

W_{it} The transverse component of the total hydrodynamic reaction force acting on the i^{th} loose wheel [N].

W_{ix} The radial component of the total hydrodynamic reaction force acting on the i^{th} loose wheel [N].

W_j The hydrodynamic reaction force acting on the j^{th} tooth in contact taken in the

normal plane [N].

W_t Hydrodynamic impact force on the transverse plane [N]

x The dimension along the width of contact in the direction of entraining motion [m].

x_1 The first output shaft rigid body translational displacement in the direction along the gear pair line of centres [m].

$\ddot{x}_1$ The first output shaft rigid body translational acceleration in the direction along the gear pair line of centres [m/s^2].

x_2 The second output shaft rigid body translational in the direction along the gear pair line of centres [m].

$\ddot{x}_2$ The second output shaft rigid body translational acceleration in the direction along the gear pair line of centres [m/s^2].

x_e The hydrodynamic conjunction exit position [m].

x_i The hydrodynamic conjunction inlet position [m].

x_{ik} Displacement of the $i^{th}(i=1,2)$ shaft at bearing $k(k=a,b,c,d)$ along the x-direction [m].

y_1 The first output shaft rigid body translational displacement in the direction normal to the gear pair line of centres [m].

$\ddot{y}_1$ The first output shaft rigid body translational acceleration in the direction normal to the gear pair line of centres [m/s^2].

y_2 The second output shaft rigid body translational displacement in the direction normal the gear pair line of centres [m].

$\ddot{y}_2$ The seond output shaft rigid body translational acceleration in the direction normal to the gear pair line of centres [m/s^2].

y_{ik} Displacement of the $i^{th}(i=1,2)$ shaft at bearing $k(k=a,b,c,d)$ along the y-direction [m].

Z_{act} Length of the line of action [m].

z The normal to the contact surface in the direction of the film thickness [m].

α_n Normal pressure angle [rad].

α_t Transverse pressure angle [rad]

β Pitch helix angle [rad]

β_b Base circle helix angle [rad]

γ Chapter 3: The gradient of the diagonal line in the contact (action) plane relative to the face-width line [rad].

γ_k The contact angle of bearing $k(k = a,b,c,d)$ [rad].

δ The relative displacement between the driver and driven gears (chapter 2) [m].

$\dot{\delta}$ The relative velocity between the driver and driven gears (chapter 2) [m/s].

Δ_k The radial clearance of bearing $k(k = a,b,c,d)$.

δ_{kr} The radial deformation of bearing $k(k = a,b,c,d)$ in the $r(r = x_1, y_1, x_2, y_2)$ direction [m].

δh The relative displacement added to tooth separation within the backlash due to shaft's instantaneous displacement [m].

Δu Sliding velocity [m/s].

ε_i The angular distance between the reverse pair centre-line and the axis $x_i(i = 1,2)$, [rad].

η_0 Dynamic viscosity (Pa s).

θ_n Phase angle associated with the nth engine order.

Λ_{kr} The restoring force of bearing $k(k = a,b,c,d)$ in the $r(r = x_1, y_1, x_2, y_2)$ direction [N].

ξ Convergence criterion [rad]

?| Eigen-vector.

?|$_i$ The eigen-vector representing the i^{th} $(i = 1,2,\cdots,12)$normal mode (section 4.5).

ρ_{jp} The transverse radius of curvature of the j^{th} pinion [m].

ρ_{jw} The transverse radius of curvature of the j^{th} wheel [m].

$\dot{\varphi}$ Angular velocity [rad/s].

φ_c Clutch angular displacement [rad].

$\dot{\varphi}_c$ Clutch angular velocity [rad/s^2].

φ_{fw} Flywheel angular displacement [radian].

$\dot{\varphi}_{fw}$ Flywheel angular velocity [rad/s^2].

$\ddot{\varphi}_{fw,ms}$ Mean square of the flywheel angular acceleration (chapter 2) [rad/s^2].

φ_i Angular displacement of the i^{th} $(i = 1,2\cdots 7)$ loose wheel [rad].

$\ddot{\varphi}_i$ Acceleration of the i^{th} $(i = 1,2\cdots 7)$ loose wheel [rad/s^2].

$\ddot{\varphi}_{i,ms}$ Mean square of the i^{th} $(i = 1,2\cdots 7)$ loose wheel acceleration (chapter 2) [rad/s].

φ_{in} Angular displacement of the input shaft [rad]

$\dot{\varphi}_{in}$ Angular velocity of the input shaft [radians/s].

$\ddot{\varphi}_{in}$ Angular acceleration of the input shaft [rad/s^2]

ϕ_{jp} The angle of contact of j^{th} pinion in simultaneous mesh [rad].

ϕ_{jw} The angle of contact of j^{th} wheel in simultaneous mesh [rad].

ϕ_{mp} Mesh angle of the pinion [rad].

ϕ_{mw} Mesh angle of the wheel [rad].

$\dot{\phi}_{os}$ Angular velocity of the output shaft [rad/s]

φ_p Pinion's angular displacement [rad].

ϕ_p The pinion displacement bounded by the meshing cycle ($0 \le \phi_p \le \phi_{mp}$) [rad].

$\dot{\varphi}_p$ Angular velocity of pinion [rad/s]

$\ddot{\varphi}_p$ Angular acceleration of pinion [rad/s^2]

ϕ_w The wheel displacement bounded by the meshing cycle ($0 \le \phi_w \le \phi_{mw}$) [rad].

$\ddot{\varphi}_w$ Angular acceleration of wheel [rad/s^2]

φ_{w0} Wheel's initial angular displacement [rad].

ω Engine mean rotational velocity [radians/s].

ω_{ff} The engine fundamental firing frequency [radians/s].

ω_n The natural frequency (square root of the eigen-value) [rad/s].

$\omega_n^2\big|_i$ The eigen value of the i^{th} $(i = 1,2,\cdots,12)$ normal mode (section 4.5).

Glossary of Terms

FEM Finite element method.

RMS Root mean square.

Chapter 1: Introduction

1.1 Automotive Noise, Vibration, and Harshness

Noise, Vibration and Harshness (NVH) are related to vehicle quality, reliability and refinement (Hall 2001). They describe the noise level inside or in the vicinity of the vehicle (acoustic vibration), the oscillatory motion felt by the vehicle occupants (mechanical vibration), and the quality of vehicle response to transient excitations (e.g. bump). Environmental concerns and the legislative regulations issued by governments have put considerable pressure on vehicle manufacturers to lower noise emissions; for instance, noise legislations in the EU and the UK cost the industry several millions Euros. Moreover, ride comfort has become the current marketing trend in automotive industry and influences customer perception of quality. Therefore, it affects sales. As a result, the competition between vehicle manufacturers has converged into the field of sound quality as can be seen in various commercials and advertisements (Wang et al, 2001). Hence, manufacturers are researching into refining vehicle acoustic performance (Wang et al, 2001).

Controlling and quantifying noise and vibration in vehicles have proved to be a difficult task for design engineers to accomplish. This is due to the existence of several noise and vibration sources (figure 1.1), notably (Hall, 2001; and Laschet, 1994):

- Engine (combustion fluctuation).
- Drive-train (lash zones).
- Road input (surface undulations).
- Exhaust manifold (high speed exhaust gases).

NVH issues are typically addressed in the final stages of vehicle design due to the following reasons (Shih et al, 2001):

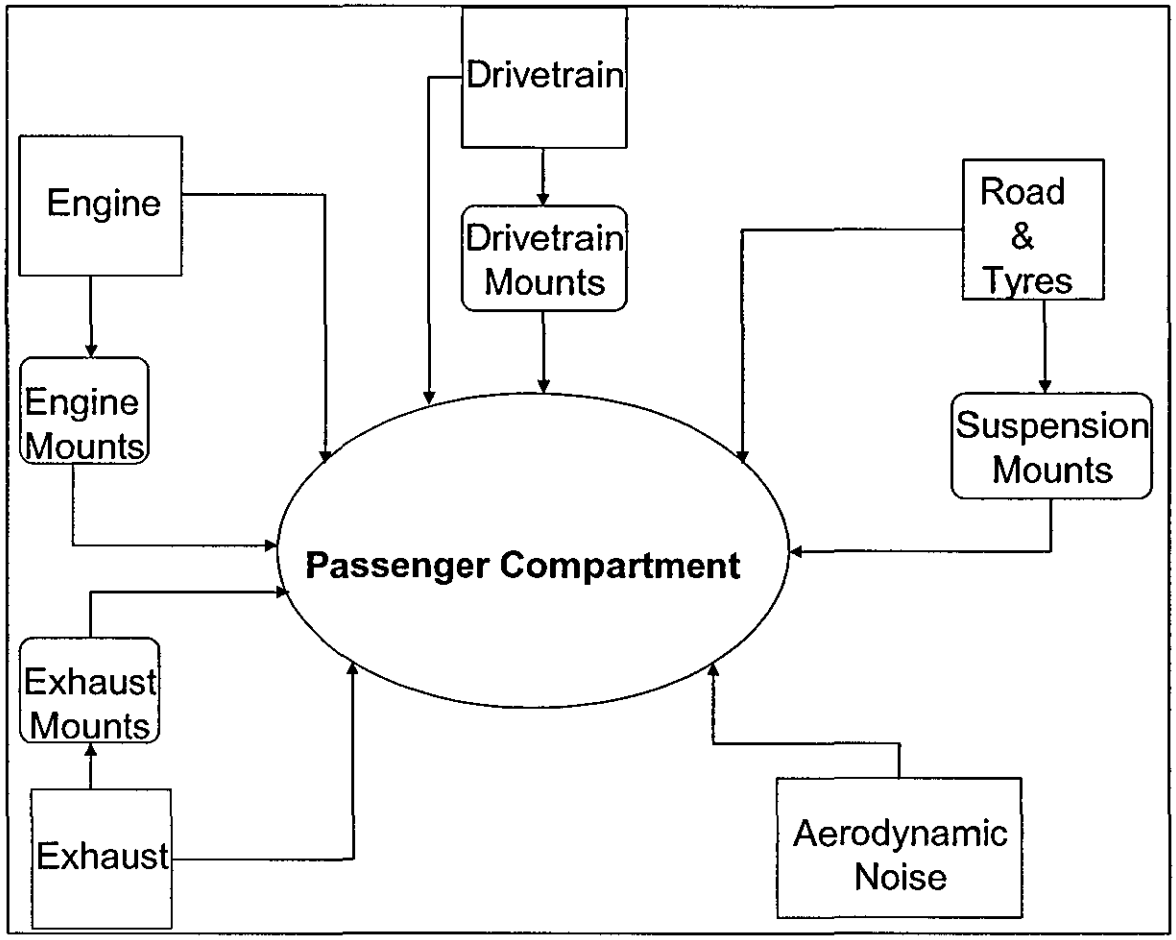

Figure 1. 1: Noise and vibration sources (adapted from Gnanakumarr, 2001)

1. The priority in vehicle design is given for functionality and durability.
2. In the case of heavy and medium duty vehicles, most powertrain components are manufactured by several external suppliers, which make it difficult for an up-front NVH analysis to be carried out.

As a result, NVH issues are generally addressed by adopting palliative measures. Nevertheless, it is necessary to understand the various NVH phenomena and to implement a procedure that considers NVH problems at the design stage, as automotive industry has realised that palliative measures increase costs and often add to vehicle weight, with a direct effect on fuel consumption.

1.2 Rattle

1.2.1 What is rattle?

The internal combustion engine produces a torque that contains alternating components due to combustion irregularities, engine orders (engine speed and its multiples), and inertial effects of the reciprocating motion of the piston assembly (Figure 1.2). When clutch is engaged, the torque fluctuations are transmitted to the gearbox. Inside the transmission, the fixed driving gears (pinions) transfer the fluctuations to the driven unselected gears* (idle gears), which rotate freely on their bearings (Figure 1.3). As a result of the fluctuations, the loose gears oscillate within their backlash (Figure 1.4), leading to collisions (impacts) with the driving gears (Figure 1.5); some of the mechanical energy is lost during these collisions in the form of audible sound energy (rattle). The stars in figure 1.3 indicate the meshing zones susceptible to rattling.

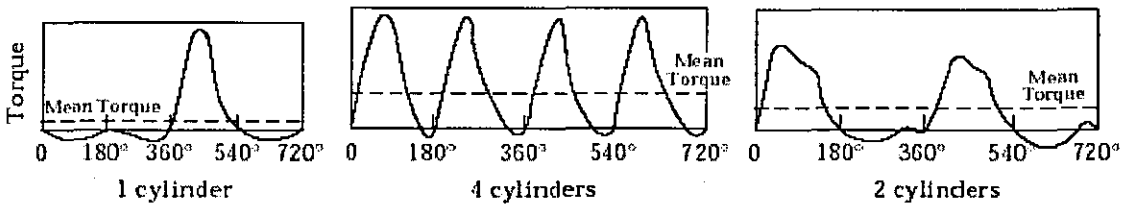

Figure 1. 2: Engine torque fluctuations in single-, dual-, and four-cylinder engines (Couderc et al, 1998)

Gear rattle is usually associated with manual transmissions, which have a dominant share in the European passenger car transmission market (Figure 1.6). On the other hand, rattle is not usually associated with automatic transmissions; this is because the torque converter acts as a viscous damper to mitigate vibro-impact oscillations of gear teeth (Wang et al 2001). According to Bellomo et al (2000), rattle is a "luxury" problem, since it does not affect the functionality of the drive system, and it does not increase with vehicle age.

* The terms "unselected gear", "idle gear", and "loose wheel" are used interchangeably throughout the thesis.

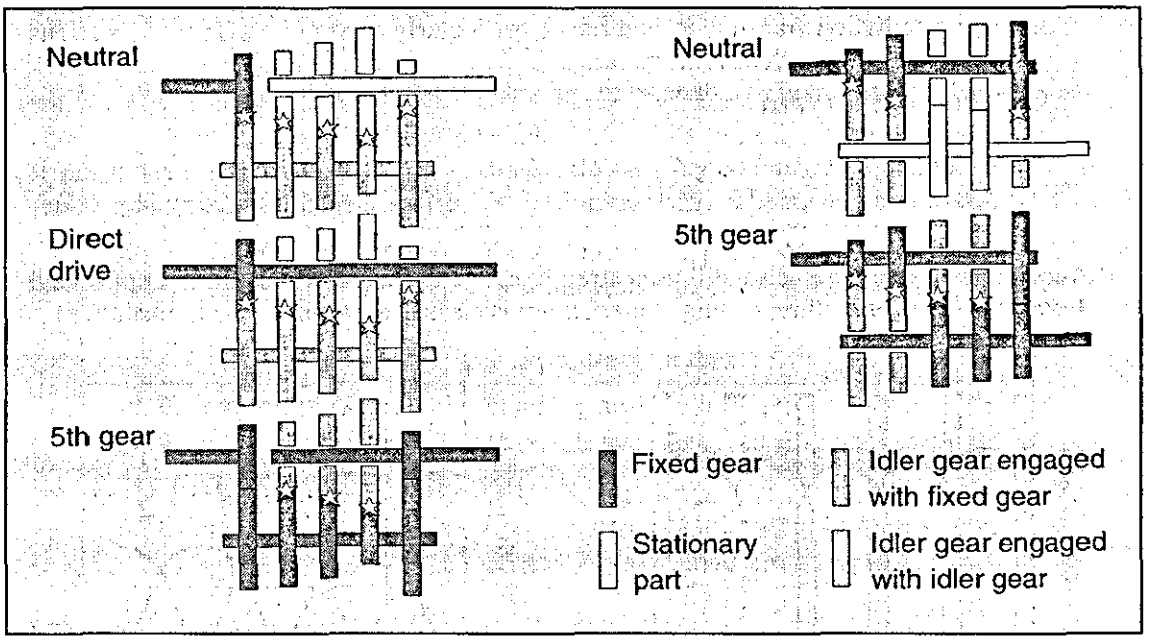

Figure 1. 3: Sources of rattle in RWD and FWD manual transmissions (Lechner and Naunheimer, 1999)

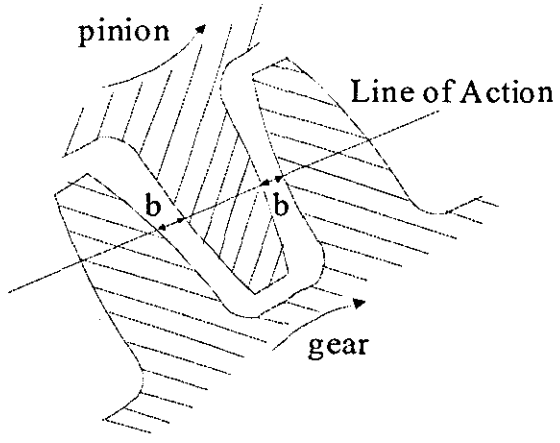

Figure 1. 4: Gear tooth backlash, denoted by b, (Theodossiades, 2000)

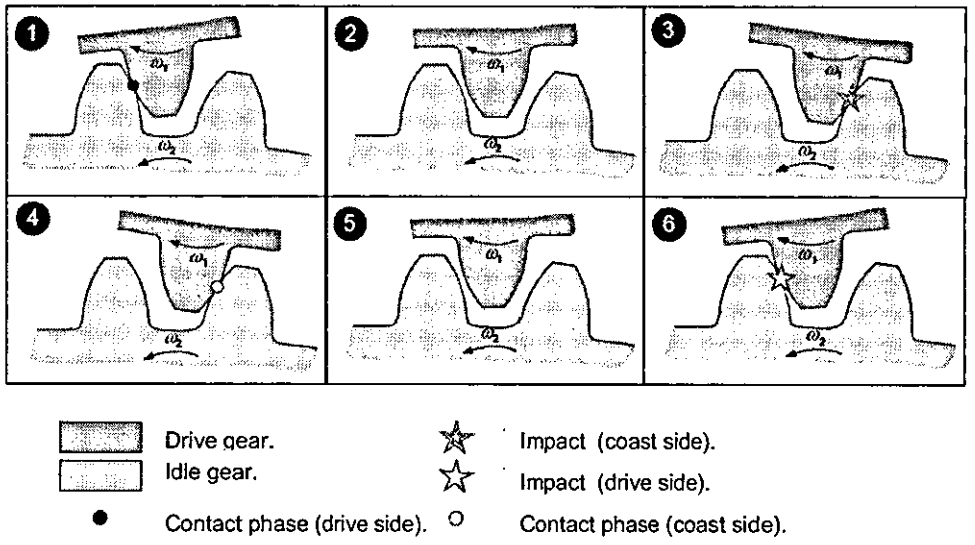

Figure 1. 5: Gear tooth oscillation and impacts within the backlash (Dogan, 2001)

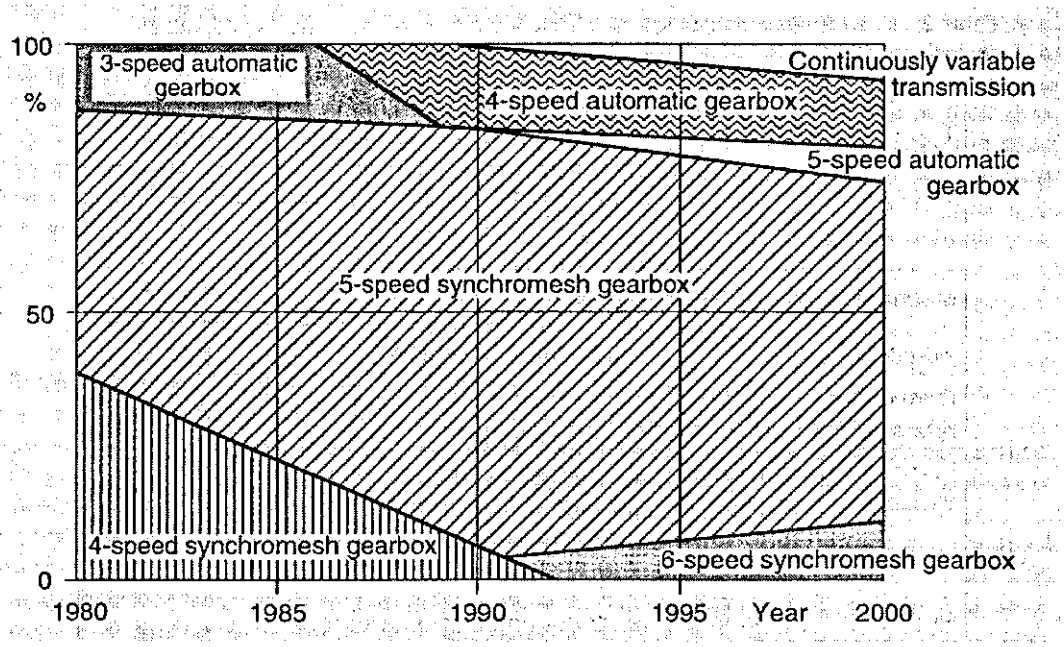

Figure 1. 6: Passenger car transmissions in Europe (Lechner and Naunheimer, 1999)

In the past, petrol engine output torque was lower than that of today's diesel engines, and the problem was not as noticeable in passenger cars. Furthermore, rattle was

buried within the noise of old engines. As modern engines are quieter, drivetrain noise, in general, and rattle, in particular, have become more noticeable.

Rattle noise gives the impression of transmission failure (or impending failure) leading to warranty claims (Wang et al, 2001). Rattle noise can also be mistaken for an engine problem (Bellomo et al 2000), such as tappet bounce.

1.2.2 Types of transmission rattle

The main types of rattle are idle (neutral) rattle, drive (creep) rattle and over-run (coast) rattle. When the engine is idling and the transmission is set to neutral, many unselected gear pairs exist at the same time. Furthermore, other noise sources (e.g. engine and tyres), and aerodynamically induced noises are at a minimum or do not exist (e.g. tyres). Hence, contribution of idle rattle noise is more significant and noticeable. In the past, this has led many researchers to assume that rattle is only an idling issue.

Creeping (drive) rattle occurs when vehicle is in gear and in motion with the engine providing the driving force. On the other hand, over-run (coast) rattle occurs while the vehicle is coasting with the wheels providing the driving load, while the engine acts as a brake. In this thesis, only idle rattle is considered.

1.3 Other types of drivetrain NVH

1.3.1 Clonk

Clonk occurs at high torque and high transient impact at low road speeds. Unlike rattle, it is independent of engine speed. Clonk is described by Gnanakumarr et al (2003) as an elasto-acoustic coupling phenomenon that occurs due to load reversals in the presence of lashes, it is characterised by being of short duration, audible and of high frequency. Clonk occurs during axial shunting or sudden (transient) input action such as clutch actuation or throttle tip-in or tip-out. The

elasto-acoustic coupling usually appears in thin hollow driveshaft tubes; the frequency band of clonk is wide and may overlap with rattle.

1.3.2 Thud

The thud phenomenon is a particular case of clonk. It is a low-energy non-metallic structure-born clonk. Nevertheless, the sound is transmitted directly to the passenger compartment.

1.3.3 Shuffle

Shuffle is a torsional mode characterised by being the lowest in the drivetrain vibration modes. Shuffle is accompanied by a longitudinal motion of the vehicle, referred to as shunt. This motion is in the form of oscillation at frequencies between 2 to 8 Hz (Biermann and Hagerodt, 1999). The cause of shuffle is the torque reversal due to throttle tip-out from drive to coast or throttle tip-in from coast to drive (Gnanakumarr, 2004).

1.3.4 Whine

Gear whine is probably the most well known gear NVH phenomenon. It is caused by gear transmission error and characterised by tonal noise at the meshing frequency or its harmonics. It is also caused by the varying tooth stiffness (with the roll angle) thus resulting in a fluctuating torque and transmission ratio (Naas et al, 2001).

1.4 Problem identification

Gear teeth contact is essentially a lubricated contact, the lubricant between the teeth transmits the load from the driving to the driven gear. The rattle system is non-linear mainly due to the existence of gear backlash, and the existence of the lubricant within the backlash would add to the non-linear behaviour of the rattle system. There is a clear lack of research considering the effects of lubricant oil within the meshing

zone. Therefore, the main problem is to develop a numerical model that includes lubricant reaction and its effect on the unselected gears' response.

1.5 Scope of Current work

1.5.1 Aims

- Better understanding of idle rattle phenomenon.
- Investigating the effects of lubrication on idle rattle.

1.5.2 Objectives

- Development of numerical hydrodynamic models to describe the phenomenon by incorporating tribological effects in the various contact zones.
- Validation of the above approach through experimental means.
- Utilisation of the code in driving design guidelines through parametric studies.

1.5.3 Novelty of current work:

The novelty of the work lies in the development and experimental validation of a numerical model describing the lubricated contact during gear engagement, and considering the entrainment and squeeze actions at the line of contact.

1.6 Thesis Structure

Chapter 1 introduces drivetrain noise, vibration, and harshness (NVH) and a brief definition of automotive gear rattle. Also in this chapter, the scope of the current work is defined.

Chapter 2 is a review of theoretical and experimental work that have been reported on the subject of gear rattle and related subjects in the field of gear technology.

Chapter 3 explains the theoretical background and the method of approach of the current work.

Chapter 4 is an application of the methodology explained in chapter 3 to a complete manual transmission.

Chapter 5 is a description of the experimental procedures used for the purpose of validation of the methodology outlined in chapter 3.

Chapter 6 highlights the results obtained from the transmission models (chapter 4) and experimental work (chapter 5). These are compared and analysed on the basis of the methodology outlined in chapter 3.

Chapter 7 contains a summary and assessment of the current work, the contributions to knowledge, in addition to suggestions for future work on the subject. It represents the link between the current research work and future research in the subject.

The thesis is sealed with a list of references to the cited sources and a further bibliography of the uncited sources.

Chapter 2: Literature Review

2. 1 Introduction

This chapter reviews the work performed thus far on automotive gear rattle and related work. The second section of the chapter explains the mechanism of gear rattle in automotive transmissions, and then reviews its association with lightly loaded gears. The third section focuses on the three common types of automotive transmission gear rattle cited in the literature, it also gives brief descriptions of other types of gear rattle. The fourth section is a review of the methodologies followed by the various researchers in the field to model the transmission components. The fifth section shows the numerical methods adopted to study the vibratory motion of gear pairs. In the sixth section some rattle evaluation indexes are presented. The seventh section is on the experimental methodologies in gear tests. The eighth and ninth sections consider the driveline parameters affecting rattle, and the counter-measures that have been considered to attenuate gear rattle, respectively. The chapter concludes with a summary of the literature review and highlight the deficiencies in the reported rattle research.

2. 2 Gear rattle

2.2.1 The mechanism of rattle

The main cause of automotive gear rattle is the torsional vibration due to the IC engine firing frequency and inertial unbalance (Dogan, 1999, Shih et al, 2001). This initiates cyclic angular accelerations to be transmitted from the engine to the transmission input-shaft, leading to impacts of gear and spline teeth and resulting in radiated noise (Seaman et al, 1984). These impacts occur due to gear teeth oscillating within their backlash limits (Dogan and Lechner, 1998). These impacts could be

single- or double-sided (Padmanabhan et al, 1995a) and are transmitted as vibrations via the shafts' support bearings to the transmission case (Fujimoto and Kizuka, 2001), which vibrates as a membrane, hence, acting as a sound radiator (Sakai et al, 1981, and Davis and Brooks, 2006) to the outside, where the air molecules' vibrations are perceived as audible sound (Wang et al, 2001).

2.2.2 Why idle gears?

Kim and Singh (2001) pointed out that rattle favours loose (idle) gears, because they are lightly loaded. This can be explained in the context that idle gears are not constrained from moving freely when separation occurs. The condition for separation to occur is when the inertia torque of the idle gear is larger than the load (i.e. resisting) torque (Comparin and Singh, 1990). In kinematic terms, the gears separate when the driving gear deceleration is larger than the driven gear deceleration due to drag or load (Johnson and Hirami, 1991) or when the driven gear speed is higher than the driving gear speed (Dogan, 2001). On the other hand, the loaded gear pair (the pair transmitting the load) maintain contact even with the presence of their backlash (Wang et al, 2001).

According to Dogan (1999), vibrations of each idle gear are independent from the vibrations of the other gears. Wang et al (2001) also pointed out that the vibrations of the laden wheels are not significantly affected by the vibrations of the loose wheels. On the other hand, Kim and Singh (2001) have concluded from an experimental and theoretical study of drive rattle that the loose wheels can invoke rattle in the (loaded) wheels transmitting torque. The general trend in the literature links rattle with the loose gear vibrations. The separation of loaded wheels reported by Kim and Singh (2001) may be attributed to other factors that causes it such as shaft deviation errors or pressure angle errors, which have been cited as causes for tooth separation of laden gear pairs by Cai (1995). Smith (1983) also reported that loss of contact could occur in a system with high inertia under high loads if tooth errors are larger than their deflections.

2.3 Types of rattle

2.3.1 Neutral (idle) rattle

Neutral rattle occurs as the engine runs at its idling speed, the transmission is set to neutral (no gear is selected), and the clutch is engaged (Rust et al, 1990). The neutral rattle produces the highest rattle intensity compared to other forms of rattle (Wang et al, 2001). An explanation for this is that while the engine is idling, its noise is level at a minimum. Hence, rattle noise is more audible than when the vehicle is in drive or under coast conditions.

2.3.2 Drive rattle

Seaman et al (1984) suggested that drive rattle occurs in any gear and under variety of throttle conditions. Rust et al (1990) reported that drive rattle occurs at higher loads and lower speeds. Kamo et al (1996) described the conditions of drive rattle to be while vehicle is accelerating. Kim and Singh (2001) specified the conditions to be during light acceleration. Drive rattle increases at high torque demands or direct drive, but at engine speeds higher than 2000 rpm, drive rattle diminishes, (Seaman et al, 1984; and Shaver, 1997). Drive rattle at lightly loaded contacts is also influenced by frictional losses and tyre contact patch conditions (Gnanakumarr et al, 2002).

The definition of drive rattle conditions given by Seaman et al (1984) is the most general, while the other descriptions could be related to particular driving conditions, e.g. Kim and Singh (2001) may be considering creeping conditions like those observed during traffic jams. In such situation drive rattle could be observed even when the gas pedal is not applied and acceleration/deceleration is controlled by clutch actuation (Heinrichs and Bodden, 1999). Based on the various definitions above, drive rattle could be divided into two modes: creeping such as when controlling acceleration by the clutch, and in-gear such as at wide open throttle or partial load.

2.3.3 Coast (overrun) rattle

While coasting (wheel speed is faster than engine speed), the power flow is from the driving wheels to the engine, which provides the braking resistance (Lechner and Naunheimer, 1999), figure 2.1. Under coast rattle the compression pulses from the engine are the exciting force (Fudala et al, 1987). Shih et al (2001) added that coast rattle is also caused by joints and driveline excitations, gear tooth errors and backlash. According to Fudala et al (1987) coast rattle occurs at higher frequencies than drive rattle (>100Hz), especially in low gears (Fudala et al, 1987).

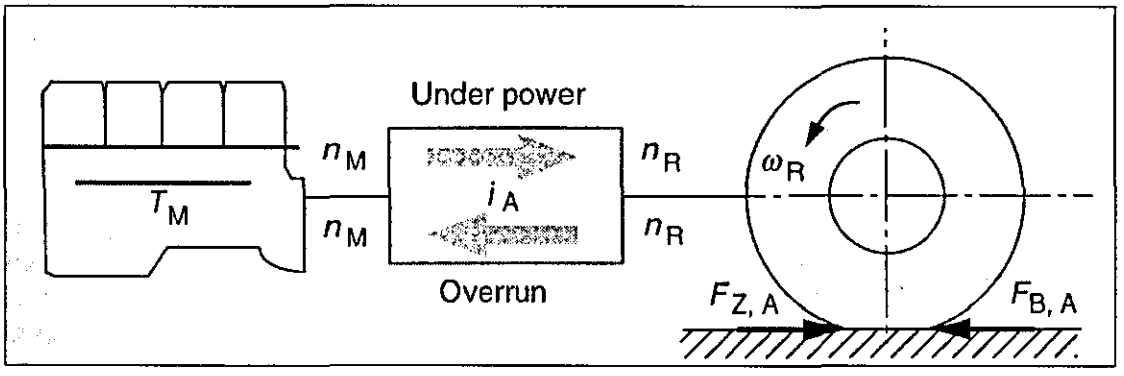

Figure 2.1: Power flow in drive and coast conditions (Lechner and Naunheimer, 1999)

2.3.4 Other types of rattle

Other than manual transmission, gear rattle is also found in engine timing gears (see Wilhelm et al, 1990; Miura and Nakamura, 1998; and Miura and Kojima, 2003). Rattle is also investigated in root blower vacuum pumps, where the main excitation is evoked by eccentricities in gear mounting (see Mason et al, 2006; and Halse et al, 2006).

2.4 Mathematical Modelling

Mathematical modelling, here, refers to modelling of the main interactions across the powertrain, in order to realistically represent the phenomena of interest (in this case gear rattle).

2.4.1 Engine excitations:

The engine excitations to the transmission system have been mainly modelled as velocity or torque fluctuations. Velocity fluctuations were used by Sakai et al (1981) and Kamo et al (1996) in a simple form containing only the fundamental firing frequency ω_{ff} as follows:

$\dot{\varphi} = A\sin\omega_{ff}t$.

Seaman et al (1984) added the mean rotational velocity of the engine, ω:

$\dot{\varphi} = \omega + A\sin\omega_{ff}t$.

Bellomo et al (2000) considered the effects of the higher harmonics of the engine firing frequency:

$\dot{\varphi} = \omega + \sum_n A_n \cos(n\omega_{ff}t)$.

In a similar fashion, the torque excitations have been modelled as follows:
Wang et al (2001) and Gnanakumarr et al (2002) adopted the form:

$T_{eng} = \overline{T}_{eng} + T_{ff}\sin\omega_{ff}t$.

In their cases ω_{ff} is the dominant engine order (e.g. the second order for a 4-cylinder engine); $\overline{T}_{eng}$ is the mean engine torque, and T_{ff} is the amplitude of the fluctuating component.

On the other hand, Singh et al (1989) and Kim and Singh (2001) included multiple harmonic excitations:

$T_{eng} = \overline{T}_{eng} + \sum_n T_{ffn}\sin(n\omega_{ff}t + \theta_n)$. Where, the angle θ_n is the phase angle corresponding to the n^{th} harmonic.

However, Singh et al (1989) utilised only the first two harmonics in their clutch design study. According to Wang (1998) and Wang et al (2001), the dominant engine order is the firing frequency; Gnanakumarr et al (2002) concluded that the impact response in a lubricated conjunction is not due to the forcing frequency, but rather to the contact stiffness non-linearity. Thus, it may be sufficient to model only the firing frequency.

2.4.2 Clutch:

Clutches have been modelled according to their structure: single-stage clutches (Sakai et al, 1981; Meisner and Campbell, 1995; and Bellomo et al, 2000), or multi-stage clutches (Ohnuma et al, 1985; Singh et al, 1989; Couderc et al, 1998; and Kim and Singh, 2001) with constant stiffness and hysteresis coefficients. Sakai et al (1981) and Bellomo et al (2000) added constant damping coefficients; Couderc et al (1998) added a preload. Examples for such stiffness, hysteresis, and damping coefficients are:

$$\text{Stiffness} = k(\varphi_c - \varphi_{fw}).$$

$$\text{Hysteresis} = \begin{cases} +H & if\ \varphi_c - \varphi_{fw} \geq 0 \\ -H & if\ \varphi_c - \varphi_{fw} < 0 \end{cases}.$$

$$\text{Damping} = c(\dot{\varphi}_c - \dot{\varphi}_{fw}).$$

The coefficients k, H and c are for stiffness, hysteresis, and damping respectively; the subscripts c and fw refer to clutch and flywheel respectively. Figure 2.2 illustrates an example of a multi stage clutch model. The figure depicts the non-linearity of the clutch behaviour: piecewise linear stiffness, Coulomb friction (hysteresis), and preload. The piecewise linear stiffness (multiple-stage) is to maintain progressive stiffness that isolate the engine vibrations from being transferred to the transmission. For instance, by having low stiffness in the low-torque first stage, the vibrations during idling are absorbed by the spring and hysteretic damping while the natural frequency of the stage is kept below the operation range (due to low stiffness). As the input torque increases, the progressive stiffness accommodates the high torque vibrations with minimum deflections.

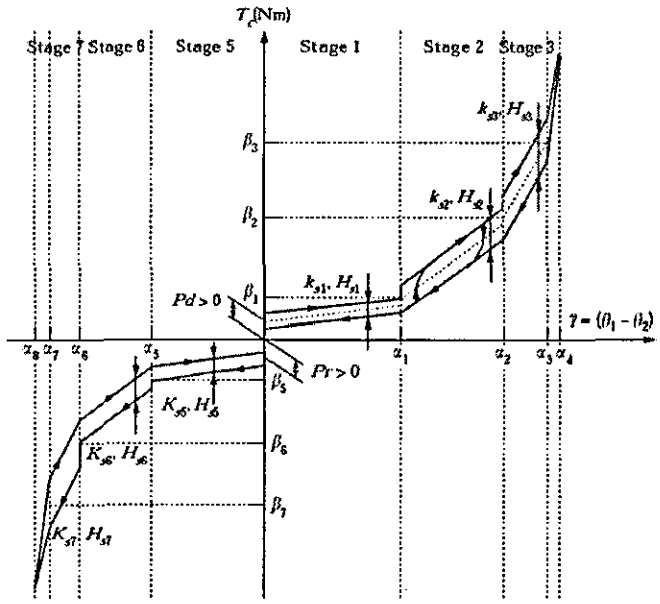

Figure 2.2: Multi-stage clutch model with preload and constant stiffness and hysteresis coefficients (Couderc et al, 1998)

2.4.3 Gear tooth contact:

Sakai et al (1981) modelled the contact through backlash by the dead space function and assuming constant contact stiffness coefficient:

$$y(\delta, b_g) = \begin{cases} \delta - b_g/2, & \delta \geq b_g/2 \\ 0, & -b_g/2 < \delta < b_g/2 \\ \delta + b_g/2, & \delta \leq -b_g/2 \end{cases} .$$

Where, δ is the relative displacement between the driver and driven gears as shown in Figure 2.3. The contact force is:

Contact force $= k_g \times y(\delta, b_g)$.

Where, k_g is the contact stiffness coefficient as shown in figure 2.3.

Similar action has been taken by Singh et al (1989), Comparin and Singh (1990), Couderc et al (1998), and Kim and Singh (2001).

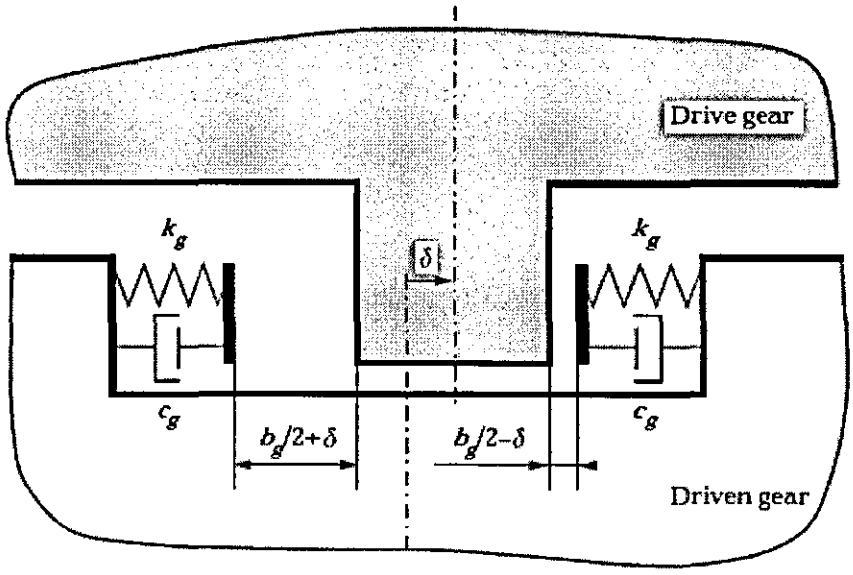

Figure 2.3: Gear backlash model (Couderc et al, 1998)

The stiffness coefficient that has been proposed by Wang et al (2001) is time-dependent and with the presence of backlash, the system becomes a time-varying piece-wise linear system as shown in figure 2.4.

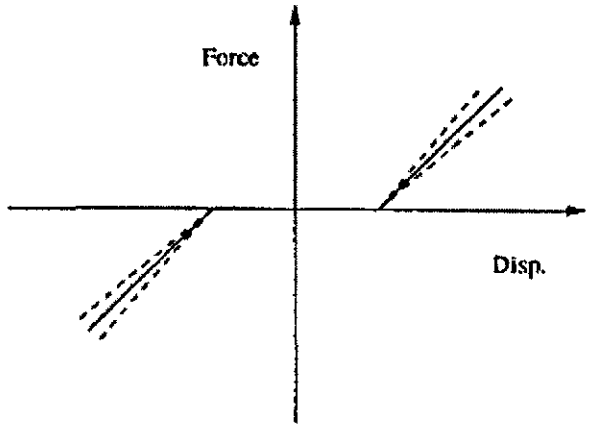

Figure 2.4: Time-varying contact force (Wang et al, 2001)

Bellomo et al (2000) have represented the contact force with Hertzian contact and included a coefficient of restitution. Yakoub et al (2004) and Brancati et al (2005) modelled the stiffness based on previous works by Umezawa et al (1986) and Cai (1995). Umezawa et al (1986) provided an approximate stiffness equation, in which the stiffness depends on the position of the pinion in the contact zone, tooth width,

tooth depth, and helix angle. Cai (1995) modified this approximate equation by incorporating the effects of tooth numbers and addendum modifications. Gnanakumarr et al (2003) calculated tooth stiffness using the ISO 6336, in which the total mesh stiffness K_{total} is calculated as follows:

$K_{total} = K \times$ total length of contact lines.

Where, K is the maximum stiffness of a single tooth pair per 1mm of face-width, producing deformation of 1μm ; the calculations involve the use of K being in the plane normal to the helix of the tooth pair and along the line of action. The value of K is calculated as follows (Gnanakumarr et al, 2003):

$K = 0.8 k'_{th} C_R C_B \cos\beta$.

Where, β is the helix angle at the pitch cylinder; k'_{th}, C_R, and C_B are the theoretical single stiffness, gear blank factor, and basic rack factor, respectively, which can be determined from the ISO 6336 (Gnanakumarr et al, 2003).

Damping has been modelled to be only consisting of bearing drag torque by various researchers, e.g. Sakai et al (1981), Seaman et al (1984), Ohnuma et al (1984), and Kim and Singh (2001). Contact damping was considered insignificant by Ohnuma et al (1985). Cai (1995) suggested a constant contact damping ratio for gear vibrations in general. Couderc et al (1998) also considered impact damping in backlash environment and represented its dead space function in a similar fashion to contact stiffness:

$$\dot{y}(\delta, b_g) = \begin{cases} \dot{\delta}, & \delta \geq b_g/2 \\ 0, & -b_g/2 < \delta < b_g/2 \\ \dot{\delta}, & \delta \leq -b_g/2 \end{cases} .$$

And the damping force is:

Damping force $= c_g \times \dot{y}(\delta, b_g)$.

The coefficient c_g is the contact damping coefficient as shown in figure 2.3. Bellomo et al (2000) utilised a contact damping coefficient that depends on the impact velocity, relative stiffness of contacting teeth, and a coefficient of restitution. Yakoub et al (2004) considered a linear contact damping, where the damping force is proportional to the pseudo-penetration velocity, which is similar to Couderc et al (1998). Kim et al (2005b) modelled the (torque) effect of contact elasticity and damping, T_G, in the

form $T_G = Kf(\delta,\dot{\delta})$, where K is the contact stiffness and the function $f(\delta,\dot{\delta})$ is defined as follows:

$$f(\delta,\dot{\delta}) = \begin{cases} (\delta-(1-\alpha)b)(1+\beta\dot{\delta}), & \delta > b \\ \alpha\delta(1+\beta\dot{\delta}), & -b \le \delta \le b \\ (\delta+(1-\alpha)b)(1+\beta\dot{\delta}), & \delta < -b \end{cases} .$$

Where, δ and $\dot{\delta}$ are the relative displacement and velocity, respectively; α is the first stage stiffness as shown in figure 2.5; β is the damping coefficient; and $\pm b$ define the clearance boundaries.

Kim et al (2005b) emphasised the importance of the inclusion of impact damping; according to them, when impact damping is included, the amplitudes at resonance, the chaotic and quasi-periodic regimes are reduced, and the dynamic stability of the system is improved. Furthermore, a frequency shift is observed by Kim et al (2005b). Damping is also believed to reduce the noise radiation due to ensuing impacts (Chow and Pinnington, 1989).

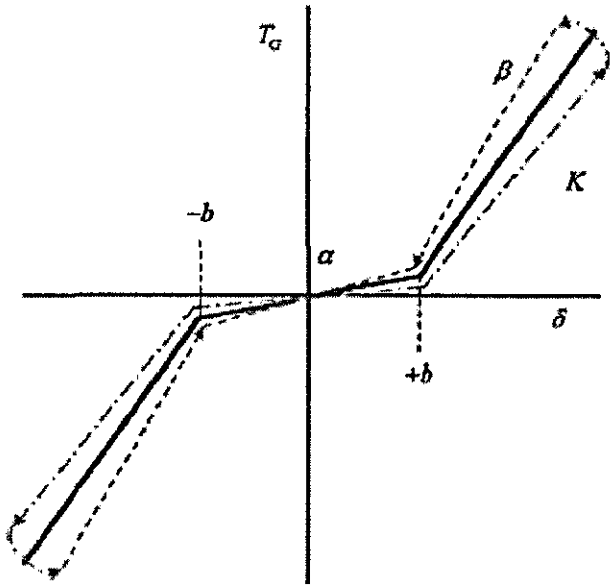

Figure 2.5: Impact stiffness and damping non-linearities (Kim et al, 2005b)

Brancati et al (2005) assumed a non-linear damping due to the squeeze action at the adsorbent oil film while the teeth are not in contact. A similar approach was assumed by Gnanakumarr et al (2002), but in their case metal to metal contact does not take place at all, it is rather the lubricant reaction which transmits the contact force between the teeth at all times. This is because Gnanakumarr et al (2002) have assumed fully flooded conditions and low contact loads such that the pressure in the contact area is too low to affect the viscosity of the lubricant or cause an elastic deformation on the tooth surfaces. Thus, in the work of Gnanakumarr et al (2002), the oil film functions as a non-linear damper-spring element. It should be noted that under loaded conditions, where high pressures are generated in the contact area, elastic deformation of gear teeth becomes also important. Asperity contact (the contact region is partially lubricated) could occur under high pressure and low speed conditions. Detailed description of lubrication types and regimes can be found in Hamrock et al (2004).

2.4.4 Shafts:

Shafts were modelled as constant stiffness elements by Singh et al (1989), Couderc et al (1998), and Kim and Singh (2001). Ohnuma et al (1985), and Wang et al (2001 and 2002) added damping elements to the constant stiffness. Sakai et al (1981) proposed piece-wise linear stiffness such that the effects of splines are accommodated.

2.4.5 Bearings:

Bearings were approximated as journal oil bearings by Kim and Singh (2001), Theodossiades and Natsiavas (2001a), and Gnanakumarr et al (2002). An equivalent linear bearing and shaft stiffness was considered by Özgüven (1991); a piece-wise linear bearing is proposed by Kahraman and Singh (1991); while Theodossiades and Natsiavas (2001b) considered the non-linear Hertzian expression for roller bearing reactions. Mayeux et al (2002) calculated the bearing stiffness using the finite element method (FEM).

The literature has shown a wide range of methodologies for modelling the drivetrain components. The choice of modelling methodology for components affects the

results of the model, yet it may be necessary to concentrate on specific components while making simplifying assumptions for the remaining components. For instance, Gnanakumarr et al (2002) approximated the needle bearings commonly used in manual transmissions by journal bearings and concentrated on the issue of having a lubricated contact, while Dogan (2001) used an approximated formula based on empirical observations, which consider the type and size of the bearing; the work of Dogan (2001) was mainly experimental.

2.5 Solution Methodology

The non-linearity of rattle problem presents difficulties for numerical modelling such as ill-conditioning and numerical stiffness (Wang et al, 2002). Numerical stiffness is defined as being the ratio of the highest eigen-value of the Jacobian to its lowest non-zero eigen-value (Padmanabhan et al, 1995b). Approximate analytical solutions have been considered in literature. For instance, Kahraman and Singh (1991) reduced a non-linear time-varying system into a linear time-varying system by neglecting the backlash. They used the method of multiple scales under further simplifying assumptions: neglecting the input torque fluctuations, and assuming that the mesh stiffness and static transmission error excitations vary in a sinusoidal manner. Whiston (1979) assumed light damping in a one-dimensional oscillator, impacting on a rigid obstruction, while subjected to harmonic excitation using impact dynamics.

Comparin and Singh (1990) sought a simplified analytical solution for the neutral rattle case using the harmonic balance method and assuming a single frequency excitation. They assumed a response without sub- and super-harmonics of the excitation. Karagiannis and Pfeiffer (1991) used the generalised impact theory, neglecting the engine higher harmonics and assumed lubricant damping to be linear. Rook and Singh (1995) used the Galerkin method as being suitable for multiple clearance problems; nevertheless it did not agree with the numerical findings at low excitation frequencies. Kim and Singh (2002), Kim et al (2005a) presented a solution methodology based on the multi-term harmonic balance method, which was capable

of tracking stable and unstable solutions. Further semi-analytical methods were utilised by Kim et al (2005b): the describing function method, and the stochastic linearization method. The main features of the describing function method are (see Kim et al, 2005b):

- A periodic steady state solution is assumed.
- The solution is expanded in terms of Fourier series using only the constant term and the sine and cosine terms of the fundamental frequency.
- The coefficients of these terms are proportional to (describing) functions that mainly depend on the relative displacement.
- The solution is substituted into the equation of motion and the coefficients of like harmonics are equated.
- A set of non-linear algebraic equations in terms of amplitudes and phases is formed and solved using Newton-Raphson method.

The main features of the stochastic linearization method are (see Kim et al, 2005b):

- A combined function of stiffness and damping is linearly estimated, with the linear coefficients being effective stiffness and damping coefficients.
- The effective stiffness and damping coefficients are calculated based on the time domain averages (expectations) of the displacement, velocity, and the non-linear combined function.
- The error due to the difference between the non-linear combined function and the estimated one is minimised using the least square method.

The Runge-Kutta methods were employed by Ohnuma et al (1985), Singh et al (1989), Kamo et al (1996), and Kim and Singh (2001); the latter used a variable time step. Couderc et al (1998), Parker et al (2000), and Gnanakumarr et al (2002) used Newmark integration methods. The natural frequencies were obtained by solving the eigen-value problem (Singh et al, 1989; and Couderc et al, 1998). Kim and Singh (2001) considered non-dimensionalisation, in order to reduce numerical stiffness. The limitations of numerical simulations are that they are not capable of tracking unstable results and that they cannot provide multi-valued solutions (Kim and Singh, 2002).

Statistical methods (Taguchi's and Monte-Carlo methods) were utilised by Driot et al (2000, 2001) to study the effect of tolerance-related geometrical variations on the variability of gear noise and vibrations. These investigations were not related directly to gear rattle, but there could be possible future applications on rattle problems.

2.6 Objective evaluation of rattle:

Sakai et al (1981) found experimentally that rattle occurs when the inertia torque of the loose gear exceeds the drag torque acting on that gear figure 2.6:

$$R = \frac{I_w \ddot{\varphi}_w}{\text{drag torque}}$$

Where: I_w is the inertia of the loose gear; and $\ddot{\varphi}_w$ is its acceleration.

$R < 1.0$ no rattle.
$R \geq 1.0$ rattle.

Seaman et al (1984) theoretically explained the Sakai et al (1981) finding and defined the threshold of rattle as the angular acceleration at which the inertia torque at the unloaded teeth/spline mesh exceeds the drag torque at the same unloaded teeth/spline mesh. A similar argument can be found in (Smith,1999).

Kamo et al (1996) proposed an index for objective evaluation of rattle as follows: $AL = 20\log\sqrt{\text{mean}\left(\left(\ddot{\varphi}_p - \ddot{\varphi}_w\right)^2\right)}$, where, the mean is taken within a specified time and $\ddot{\varphi}_p$ is the acceleration of the pinion. The AL index is a measure of the RMS relative acceleration amplitude of the contacting gear pair. Ideally, it should be $-\infty$ for non-rattling gears. Nonetheless, such an index, when used with pseudo-penetration models, such as the one utilised by Kamo et al (1996), does not determine whether or when the teeth have actually lost contact, and it does not give the whole picture in terms of which parameters are responsible for increasing/decreasing rattle.

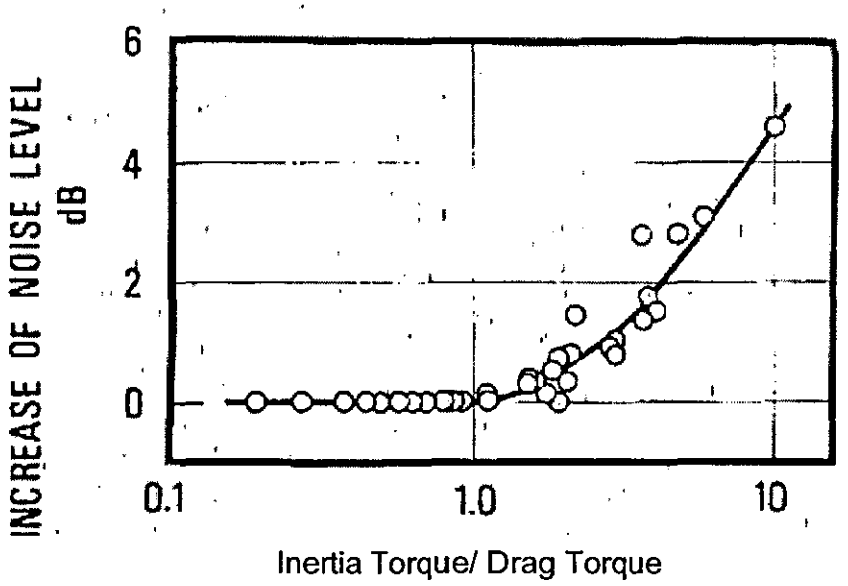

Figure 2.6: Effects of inertia and drag torques on rattle noise (Sakai et al 1981)

Padmanabhan et al (1995a) suggested the use of the ratio of the mean square of the loose gear acceleration to that of the flywheel acceleration as an index. Wang et al (2001) adopted Padmanabhan et al (1995a) index and formed an overall index that encompasses all the loose gears; this index is the square root of the sum of squared indices of the loose gears:

$$I = \left[\sum_{i=1}^{N} I_i^2\right]^{1/2}; I_i = \frac{\ddot{\varphi}_{i,ms}}{\ddot{\varphi}_{fw,ms}}.$$

Where, $\ddot{\varphi}_{i,ms}$ is the mean square of the acceleration of the i^{th} loose gear; $\ddot{\varphi}_{fw,ms}$ is the mean square of the acceleration of the flywheel; and N is the total number of loose gears.

Sakai et al (1981) had proposed a similar index to Padmanabhan et al (1995a) index, but used a decibel scale.

2.7 Experimental Methods:

2.7.1 Excitations:

In order to simulate engine excitation experimentally, Sakai et al (1981) and Forcelli et al (2004) used hydraulic actuators. Croker et al (1990) used a variable speed DC motor coupled to a Hooke joint, about which the test transmission could be pivoted in order to create rotational fluctuations. Dogan (1999, 2001) used an AC synchronous motor and the fluctuations were generated by a computer. Johnson and Hirami (1991), Kamo et al (1996), Heinrichs and Bodden (1999), and Fujimoto and Kizuka, (2003a) experimented with actual vehicles, where excitations were provided using the engine. Rivin (2000), on the other hand, developed a rattle test rig, which consisted of a gear pair and a flywheel/brake; the drive was provided by a hand-operated crank, while the excitations (rectangular load pulses) were delivered through periodic applications of the brake.

2.7.2 Vibration and noise measurements:

Accelerometers were used to measure transmission housing vibrations (Sakai et al, 1981; Johnson and Hirami, 1991; and Forcelli et al, 2004). They can also be mounted on other housings in the drive train, such as the front axle carrier (Shih et al, 2001), or the transfer case (Kamo et al, 1996). Housing vibrations can be measured using a PiezoVelocity Transducer (PVT) or electrodynamic pick-ups. The piezoelectric accelerometer is generally the best choice for transmission gear rattle. According to Wilcoxon Research (undated) the main weakness of electrodynamic pickup is that it has a limited response band (10 Hz– 1 kHz). The PVT tends to have an increasing output voltage with frequency, and this output is only higher than the accelerometer output below 61.4 Hz (Wilcoxon Research, undated).

Rotational fluctuations have been measured by various methods: pulse pick-ups (Sakai et al, 1981), encoders (Johnson and Hirami, 1991, Fujimoto and Kizuka, 2001, and Dogan, 2001), electromagnetic pick-up (Miura and Nakamura, 1998, and Miura and Kojima, 2003), magnetic sensors (Dogan, 2001, and Forcelli et al, 2004), inductive pulse sensors (Steinel, 2000), and Laser Doppler Interferometer (Ryborz,

2003). Axial motion was measured using inductive displacement transducer (Croker et al, 1990, Johnson and Hirami, 1991, and Dogan, 2001). Johnson and Hirami (1991) also used inductive probes to measure the velocities and angular positions of all the gears in their test transmission. The advantages of the inductive proximity transducers are (Eren, 1999):

- Robust.
- Compact.
- Less affected by environmental factors (when compared to capacitive transducers).
- Can be self generating or passive (require power source).

According to Lin (1997) errors can be introduced to eddy current (inductive) proximity transducers by shaft surface roughness, magnetic fields, geometrical inconsistencies, and metallurgical irregularities. According to Lin (1997) capacitive type proximity transducers can be considered as an alternative, since they are not affected by magnetic fields, and surface and metallurgical irregularities. Other advantages of the capacitive type are reported by Chu et al (1995):

- Simple to install.
- Adds no mass or restraints to the measured system.
- Low background noise.
- Wide frequency range.
- With proper insulation could work up to 1093°C.

On the other hand, Wilson (1999) pointed out that both inductive and capacitive proximity transducers work only with electrically conductive targets. According to Wilson (1999) they are sensitive to the gap size, and usually they must be recalibrated when either the target or the material filling the gap changes (e.g. changing of the lubricant or lubricant contamination).

Laser Rotational Vibrometers (LRV) have the following advantages:

- Non contact transducer; thus no mass loading to the measured object (Chu et al, 1995).
- Remote measurement capability (Chu et al, 1995).
- High sensitivity and accuracy (Wilson, 1999).

- Not sensitive to target shape and translational motion (Martin and Rothberg, 2006; and Halkon and Rothberg, 2006).

The limitations of the LRV are:

- The speckle effect, which is a pattern of random constructive and destructive interferences caused by the de-phased wavelets scattered from an optically rough surface, appears as a noise in the signal output (Chu et al, 1995; and Martin and Rothberg, 2006).
- Due to geometrical constraints (location, alignment, and distance), the laser vibrometer is limited to laboratory use (Wilson, 1999).

Sound pressure measurements were carried out using microphones, in the near field (Dogan, 1999, 2001; Fujimoto and Kizuka, 2000; Forcelli et al, 2004), or with an artificial head placed inside the vehicle (Heinrichs and Bodden, 1999, and Steinel, 2000).

Transmission oil temperature control was reported by Croker et al (1990) and Dogan (1999, 2001). Ryborz (2003) used a PT-100 Platinum film probe to measure oil and transmission housing temperatures.

Other measurements include, input torque measurement, using a torque meter (Croker et al, 1990) and torque shaft (Dogan, 2001). Johnson and Hirami (1991) utilised special purpose spark plugs to measure combustion pressure. Heinrichs and Bodden (1999) carried out psycho-acoustic tests by replaying rattle sound to subjects via head phones. Fujimoto and Kizuka (2003b) conducted experiments to produce audible sound from a mathematical model.

2.7.3 Data Analysis:

The impulses due to gear tooth impacts excite the resonances in its transmission path, causing oscillations at broad frequency bands (McFadden, 1985). According to Smith (1983, 1999), cyclic torque variations produce amplitude modulation in the signal; also the speed fluctuation produces frequency modulation to appear in the signal. Furthermore, loss of contact can produce sub-harmonics at the

excitation frequency if the tooth contact is re-established after more than one cycle of excitation (Smith, 1999; and Johnson, 1958).

2.8 Driveline parameters affecting rattle

2.8.1 Engine parameters:

Engine rotational fluctuations:

The gear vibration levels increase with an increase in the fluctuation of engine velocity and acceleration (Sakai et al, 1981). According to Shaver (1997), the crankshaft acceleration amplitude depends only on the throttle opening and is independent of engine speed (Figure 2.7). Furthermore, Shaver (1997) reported that the amplitude of the speed fluctuation, however, is inversely proportional to the engine speed; the amplitude of the instantaneous displacement is inversely proportional to the square of engine speed (Figure 2.7). Lutz (1988) also reported that for a 6-cylinder engine, the engine rotational speed fluctuations decrease as the engine rotational speed increases. In coast (overrun) conditions, however, the acceleration amplitude increases with crankshaft speed (Figure 2.8) and as a result of this, coast rattle occurs at speed higher than 2000 rpm, (Shaver, 1997). The above suggests that at lower excitation frequencies, stronger amplitudes are observed.

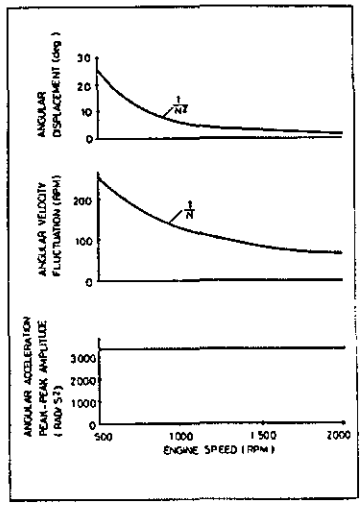

Figure 2.7: Angular fluctuation vs. engine speed (Shaver, 1997)

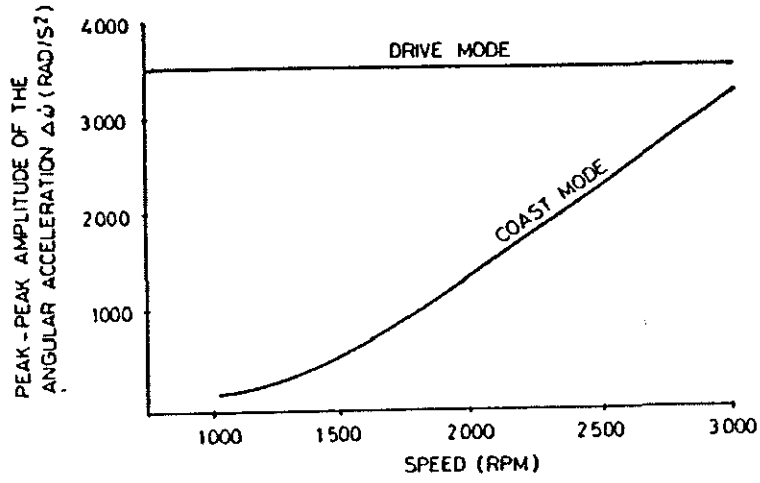

Figure 2.8: Angular acceleration fluctuation vs. engine speed in drive and coast modes (Shaver, 1997)

2.8.2 Shafts and gears parameters:

Backlash:

Decreasing the backlash of either the input shaft splines or gear teeth backlash reduces the vibration levels, figure 2.9, (Sakai et al 1981). Nevertheless, in practice, it is difficult to obtain a reduction in backlash that significantly reduces rattle noise (Sakai et al, 1981; and Seaman et al, 1984). Dogan (2001) have proved experimentally that noise level increases and decreases if the backlash is increased and decreased, respectively. Nevertheless, according to Dogan (2001), it is not feasible to reduce the backlash below 60μm; this is because an allowance for thermal expansion is necessary.

Pitch diameter eccentricities and tooth spacing errors (Seaman et al, 1984):

Pitch diameter eccentricities and tooth spacing errors cause angular accelerations of the gear train, figure 2.10. However, these angular accelerations are much lower than the angular acceleration of the engine itself.

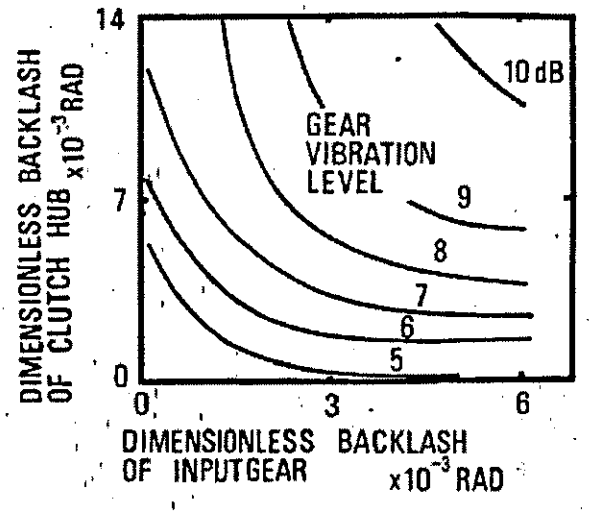

Figure 2. 9: Effect of backlash on gear rattle (Sakai et al 1981)

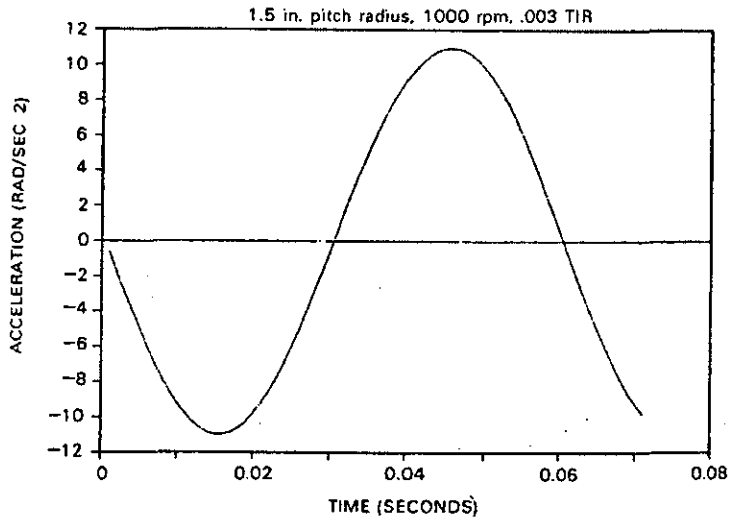

Figure 2. 10: Acceleration fluctuation due to gear eccentricity (Seaman et al, 1984)

Centre distance (Dogan, 2001):

When the centre distance is decreased, the noise level is decreased. Nevertheless, the base line noise level (noise before commencement of rattle) increases as the centre distance decreases.

Effects of oil temperature:

Drag torque is higher at lower temperatures, figure 2.11, (Sakai et al, 1981; Seaman et al, 1984; and Fujimoto et al 1987); rattle noise is lower at lower temperatures (Sakai et al, 1981) and (Seaman et al, 1984). As the oil viscosity decreases with an increase in temperature, the damping at tooth contacts decreases (Seaman et al, 1984). Hence, it can be understood that the oil viscosity plays a dual role: it introduces a drag torque between the gear and the shaft and dampens the impacts between gear pair teeth during meshing, thus attenuating the noise produced. Figure 2.11 shows that at the same sump temperature, drag torque is higher at higher rotational speeds; but as temperature increases, the variation between different values of drag torque at different rotational speeds decreases in magnitude. Therefore, theoretically, there could be a temperature, at which drag torque is the same for all rotational speeds.

However, Fujimoto and Kizuka (2001) reported that there is an optimum temperature range, at which rattle is minimum, Figure 2.12; here, the neutral rattle noise is a result of the easier motion of gears in the high temperature zone above the optimum temperature (Fujimoto and Kizuka, 2001). Comparing this with the previous paragraph, it can be concluded that rattle level does not depend exclusively on oil temperature; other factors such as the rotational speed can also affect the drag torque values.

Other lubricant effects:

In most literature, lubricant effects were regarded only as resistive action. Rust et al (1990) proposed that lubricant viscosity and oil depth are major components contributing to drag torque. Dogan (2001) considered the oil squeeze action between the meshing teeth and gear churning action in the oil sump as resistive torques. Taking the oil effect further, Gnanakumarr et al (2002) assumed line contacts in lightly loaded counterformal lubricated contacts, and the contact force as a hydrodynamic impact force. In the same work, a formula proposed by Rahnejat (1984) was used, which takes both forcing (due to lubricant entraining motion) and damping effects into consideration.

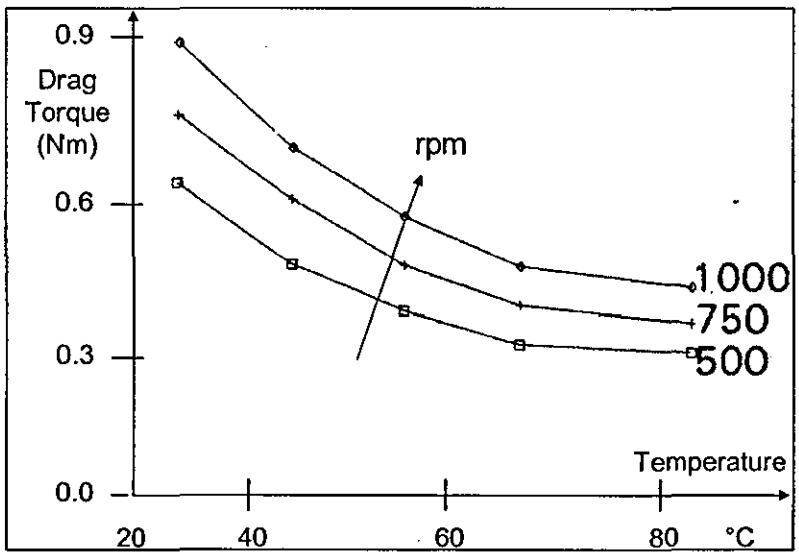

Figure 2. 11: Effect of temperature on drag torque (see Seaman et al 1984)

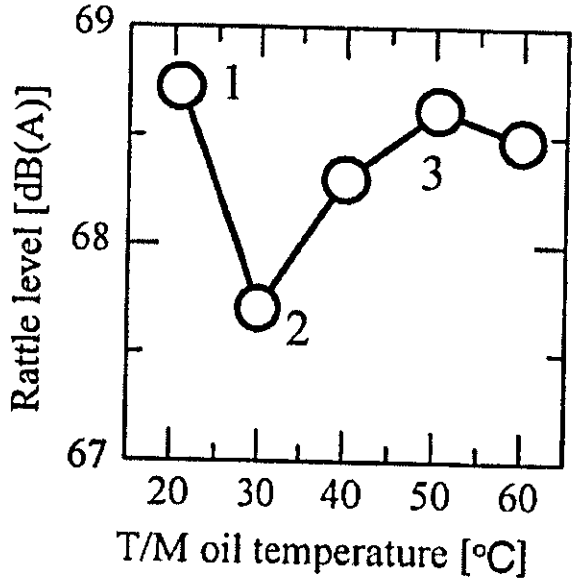

Figure 2. 12: Transmission oil temperature vs. rattle noise (Fujimoto and Kizuka, 2001)

Brancati et al (2005) considered the damping effects of oil only. They assumed an elastic force when the teeth are in contact and non-linear damping force during separation. Unlike Gnanakumarr et al (2002), who assumed the drag (caused by the bearings) in idler gears to behave according to the (linear) Petrov's formula (see Hamrock et al, 2004), Brancati et al (2005) assumed a constant drag torque.

The contact damping force introduced by Brancati et al (2005) is based on various assumptions: constant radii of curvature (taken at the pitch points), constant viscosity, and ignoring sliding velocity. Similar assumptions were used by Gnanakumarr et al (2002). Brancati et al (2005) concluded that the presence of oil in the contact zone, as well as an increase in oil viscosity, lead to a reduction in rattle.

Tooth surface finish:

Dogan (2001) experimented with a gear coated such that its tooth surface would be hemispherically undulated and found that gears with such topography produce lower rattle noise level than when polished. Dogan (2001) explained this by concluding that the undulated topography is rich with oil deposited in its troughs thus damping the impacts.

2.9 Rattle counter measures/control

2.9.1 Increasing engine idle speed:

When engine idle speed increases, the piston pressure torque pulses occur more frequently, causing a more uniform rotation of crankshaft and flywheel, therefore angular accelerations at the flywheel are reduced (Seaman et al, 1984). However, according to Shaver (1997) the acceleration amplitude is independent of engine speed. A suitable interpretation could be that by sufficiently increasing the engine speed, the firing frequency increases such that there is not enough time for large tooth separations to form, thus, reducing the tooth impact intensities and consequently rattle.

The disadvantages of increasing idle speed, however, are (Seaman et al, 1984):

-Increase in fuel consumption.

-Transmission drag increases with increasing engine speed.

2.9.2 Flywheel measures:

Increasing flywheel inertia would decrease angular acceleration, thus, reduces both drive and neutral rattle (Seaman et al, 1984). The disadvantages of increasing flywheel inertia are (Seaman et al, 1984):

-Engine response decreases.

-Fuel consumption increases.

-Crankshaft stresses increase.

-Vehicle weight increases.

Another countermeasure is the use of dual mass flywheels (DMF), Figure 2.13. The DMF consists of a primary and a secondary mass connected via a spring or damper (Shaver, 1997), which is simply a distribution of the inertia of the single flywheel system so as to lower the resonant frequencies (Sebulke, 1987). It decreases both the torsional vibrations in the drive train (Dogan and Lechner, 1998) and the natural frequencies of the transmission rotating components (Yamamoto et al, 1991; Shaver, 1997) such that the resonance peaks lie below the operation range and the transmissibility is low within the operation range (Yamamoto et al, 1991). In other words, the DMF acts as a mechanical low-pass filter, which transmits vibrations at low rotational speeds only (Sebulke, 1987). Laschet (1994) also reported that the DMF separates the engine excitations from the transmission, leading to less number of impacts between gear teeth. Nevertheless, some drawbacks were reported by Fudala et al (1987), which include cost, engine torsional vibration increases due to the primary mass being lower, and DMF spring damper reliability problems. Wang et al (2001) concluded that the DMF is more effective at lower speeds, while the standard clutch-flywheel (single flywheel) is more effective at higher speeds.

In order to optimise the DMF, (Yamamoto et al, 1991) proposed a DMF that has large friction at speeds below the operation range to decrease the resonance peaks, while it has low friction at operational speeds allowing minimum transmissibility. Bertin et al (1995) presented a DMF design in which the springs were arranged radially allowing for more torque to be transmitted at higher speeds due to the centrifugal force

hardening the spring. They also utilised friction hysteresis to absorb energy at speeds below the operation range.

1 Dual Mass Flywheel;
2 Flexible Element;
3 Pressure Plate;
4 Diaphragm Spring;
5 Driven Plate;
6 Release Bearing.

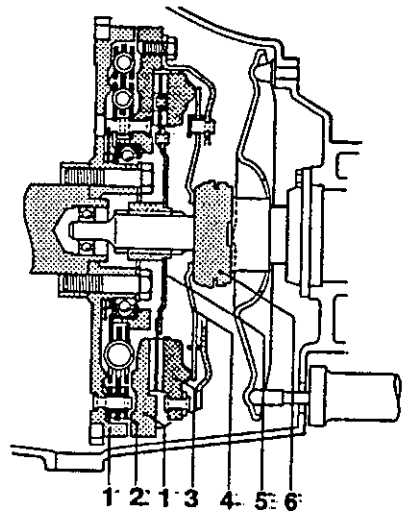

Figure 2.13: Clutch with dual mass flywheel (Shaver 1997)

It is clear that the costs of designing and manufacturing the DMF are higher than the costs of manufacturing the conventional single-mass flywheel. In addition to that, Cavina and Serra (2004) reported two issues pertaining to the DMF, the first occurs in poor starting condition, resulting in crankshaft resonance (and apparently engine stall), which necessitates restarting the engine. The second problem occurs below the idle speed, while braking, keeping the vehicle in gear, and sudden slip of the clutch leading to oscillations in the crankshaft that are transmitted to the vehicle interior (Cavina and Serra, 2004).

2.9.3 Acoustic isolation:

This could be accomplished by isolating the clutch, transmission and the gear-stick from the passenger compartment (Seaman et al, 1984); or bodywork insulation (Ryborz, 2003). A disadvantage of this solution is that noise may be reflected from nearby bodies e.g. walls. Dogan and Lechner (1998) also agree that encapsulation of transmission housing would decrease sound transmission and radiation, but they pointed out that this measure is not economical.

2.9.4 Clutch measures:

According to Seaman et al (1984), using a long travel damper (low spring rate), figure 2.14, reduces angular acceleration at transmission input shaft and eliminates neutral rattle, but not drive rattle. Another disadvantage of a long travel damper is that it promotes drive line clonk (Seaman et al, 1984; Fudala et al, 1987). Fujimoto et al (1987) reported that when the engine is idling (Ne = Neo), there was an optimum value of first stage spring constant (K1 normalised to a reference K1o), at which the A-weighted idle rattle noise level (L) is minimum, figure 2.15 (a). Their findings agree with Seaman et al (1984), but they did not mention clonk, they rather explained that idle rattle will increase if the first stage spring constant is low enough to be bypassed to the second stage spring. A similar behaviour was reported by Fujimoto et al (1987) regarding first stage hysteresis (H1 normalised to a reference H1o), figure 2.15 (b), where the A-weighted idle rattle noise level decreases with increasing hysteresis up to a minimum, before it starts to increase again.

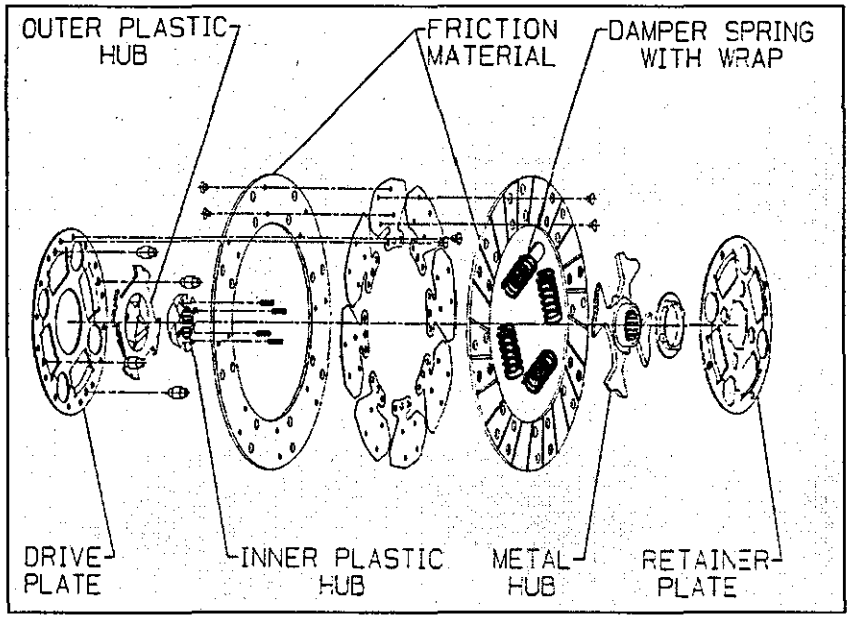

Figure 2.14: Clutch with a long travel damper (Seaman et al 1984)

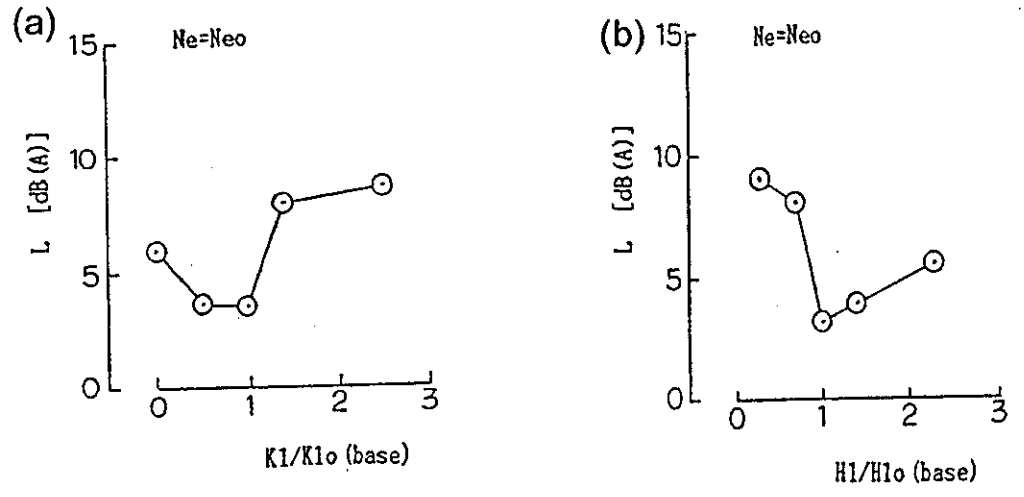

Figure 2.15: Influence of 1st stage (a) spring const. (rate) and (b) hysteresis (Fujimoto et al, 1987)

Regarding the second stage damper, figure 2.16 (a), Fujimoto et al (1987) found that there was a value of spring constant (K2 normalised to a reference K2o), at which idle rattle drops and remains unchanged for lower spring constants. The second stage hysteresis (H2 normalised to a reference H2o), as reported by Fujimoto et al (1987), behaves in a similar way as the first stage hysteresis, figure 2.16(b). The results obtained by Fujimoto et al (1987) agree well with earlier results obtained by Sakai et al (1981).

Fudala et al (1987) found experimentally that damping in clutch changes with rotational speed; increasing with speed in drive condition, while decreasing in coast condition.

For drive condition, the clutch damper and hysteresis should be tuned such that the rattle noise would be less audible (Shaver, 1997). Shaver (1997) also quoted a high value of damper rates (+10 Nm/degree) to eliminate coast rattle. According to Steinel (2000), tuning clutch dampers may produce conflicting results regarding different drivetrain vibration phenomena, in this case using dual-mass flywheel is the optimum remedy.

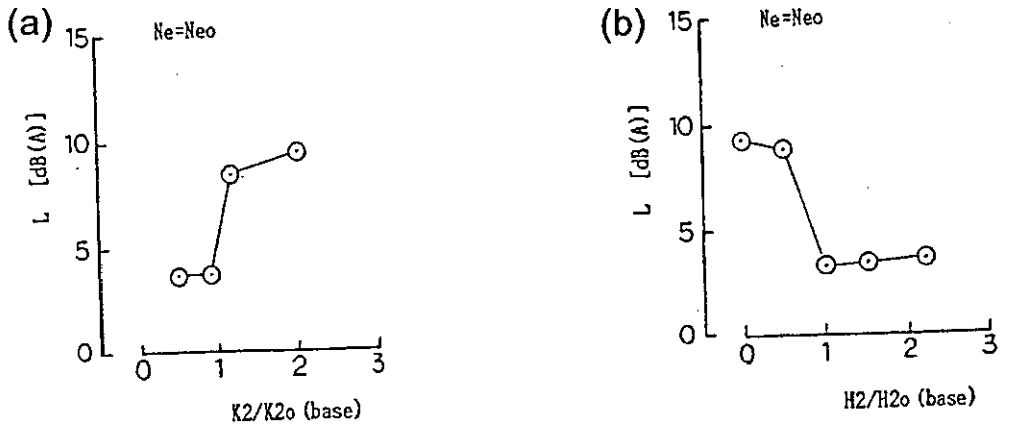

Figure 2.16: Influence of 2nd stage (a) spring const. (rate) and (b) hysteresis (Fujimoto et al, 1987)

2.9.5 Torsional damping:

Torsional dampers lower the resonance peaks of the drive system (Dogan and Lechner, 1998). By placing a rubber torsional damper in the head set (drop) gear, the angular accelerations are reduced at gear meshes (Seaman et al, 1984), figure 2.17. The disadvantages of such torsional dampers, as reported by Seaman et al (1984) are:

-Clonk is promoted.

-Could be expensive.

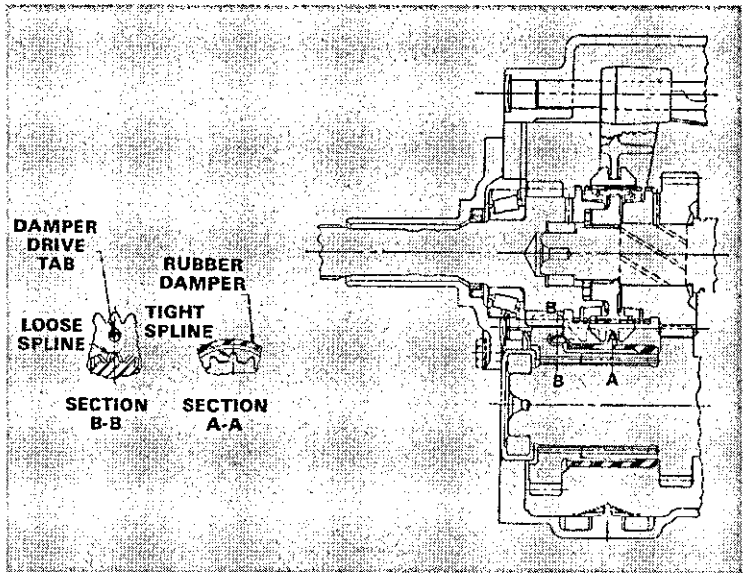

Figure 2.17: headset torsional damper (Seaman et al 1984)

2.9.6 Using zero backlash:

Using zero backlash for gears and splines - by implementing tighter tolerances, eliminates gear rattle (Seaman et al 1984). Biermann and Hagerodt (1999) also concluded that zero backlash eliminates gear contact changes (which causes rattle). The disadvantages are:

-Manufacturing gears with zero backlash is difficult (Seaman et al, 1984; Biermann and Hagerodt, 1999). According to Dogan (2001), the feasible minimum backlash size is 60μm.

-Zero backlash causes gear growl (or howl) – a low guttural sound, like an angry dog (Seaman et al, 1984).

Haberhauer and Bodenstein (2003) have pointed out that the existence of backlash is necessary to allow for manufacturing tolerances, thermal expansion as well as for the build-up of lubricant film.

2.9.7 Decreasing inertia torque:

Seaman et al (1984) concluded the following:

> By reducing the reflected inertia at gear/spline mesh point, improvement in gear rattle and shiftability can be achieved. Rattle occurs at higher gear accelerations when the effective inertia is lowered. Nevertheless, reducing components' inertia is limited by material strength and costs. The inertia can be minimised by rearranging transmission components. When component inertia is sufficiently reduced, the inertia torque is decreased, thus increasing the ratio of drag torque to inertia torque above the rattle threshold.

Rust et al (1990) experimented with loose gear inertia and observed that when reducing the inertia, the rattle threshold is increased, the resonance speed is raised, the number of tooth impacts is increased, and the noise level is reduced. Dogan (2001) explained the effect from the impact point of view; by reducing the inertia of the loose gear, the intensity of impacts and subsequently the radiated noise levels are reduced.

2.9.8 Increasing drag torque:

By sufficiently increasing the drag torque, the ratio of drag torque to inertia torque can be kept above 1.0 (the rattle threshold); thus eliminating rattle (Seaman et al, 1984). Bellomo et al (2000) also concluded that increasing the drag torque decreases rattle noise. However, increasing drag torque yields the following negative results (Seaman et al,1984):

1- Increase in shift effort.

2- Friction heat is created, thus increasing transmission operating temperature.

3- Increase in frictional losses (decreasing mechanical efficiency).

Kim and Singh (2001) also concluded that while controlling the drag torque is a cheap solution to gear rattle, the issue of operating temperature remains a limitation to this countermeasure. Other ways to increase drag torque in the transmission are by pre-loading the transmission bearings or using anti-rattle plate at the gear headset (drop gear) (Seaman et al, 1984). The downside of using anti-rattle plates is the expense, as well as creating other gear noise (Seaman et al, 1984).

The relation between the inertia torque and drag torque at rattle and non-rattle conditions is shown in figures 2.18, and 2.19. When the drag torque is higher than the inertia torque, the loose gear cannot detach itself into a free flight, and as a result the impacts that occur after the gear loses its free flight energy are prevented (Figure 2.18). On the other hand, when the drag torque is less than the inertia torque, the loose gear releases itself from contact once the driving gear starts to slow down (Figure 2.19) leading to free flight followed by an impact.

2.9.9 Anti-backlash measures:

Rivin (2000) proposed modified gears that have shims added to their idle (coast) sides (Figure 2.20) in order to elongate the duration of teeth impacts. These modified gears, according to Rivin (2000), have reduced rattle noise (in the order of 10 dB).

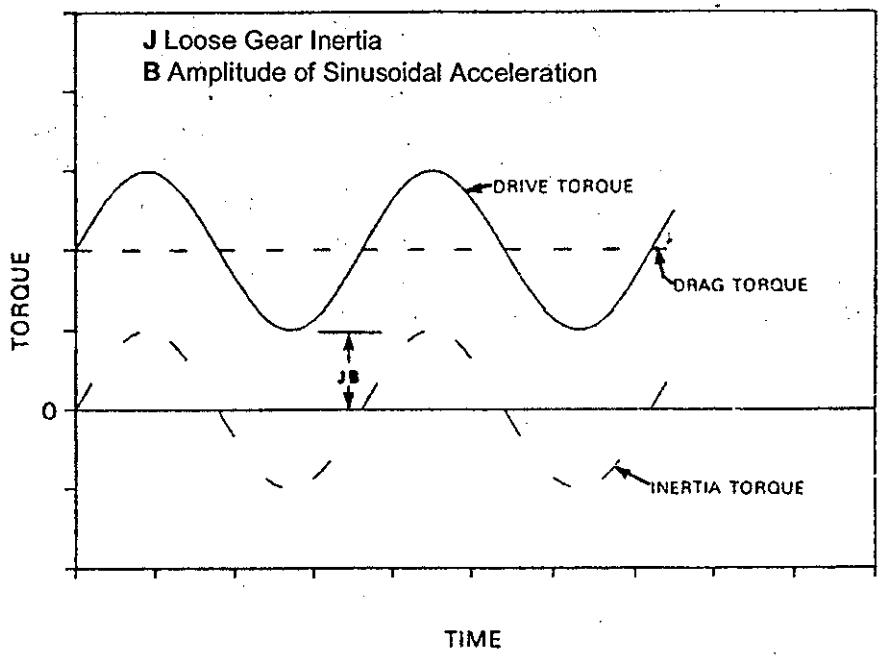

Figure 2.18: Drive torque at non-rattle condition (Seaman et al 1984)

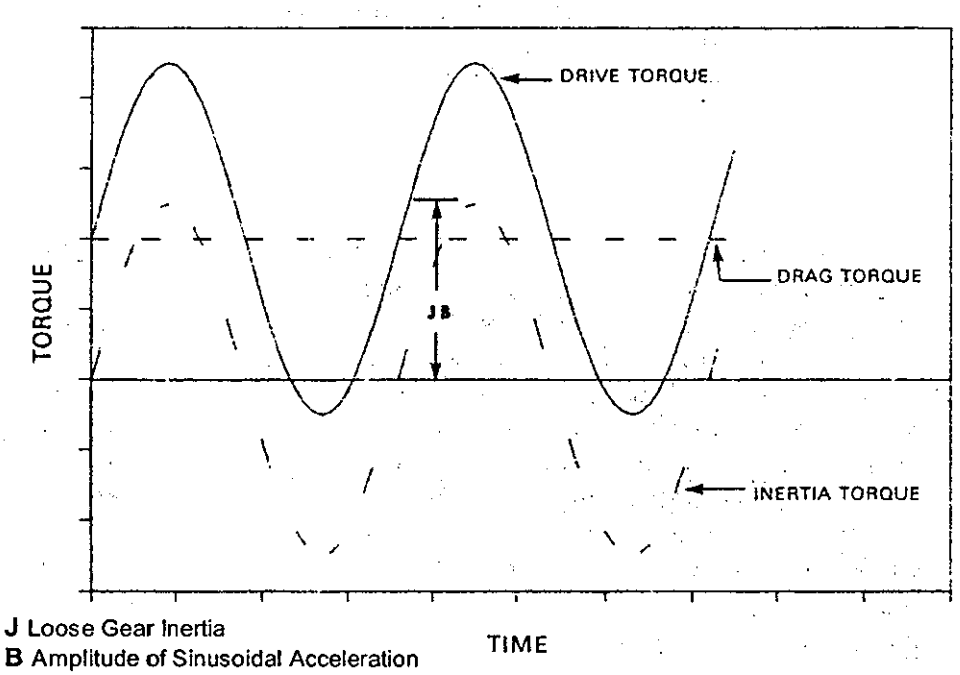

Figure 2.19: Drive torque at rattle condition (Seaman et al 1984)

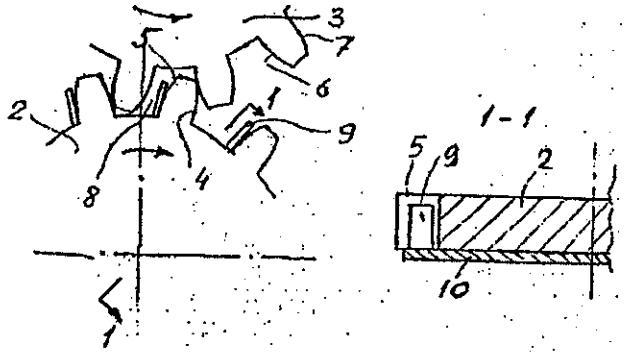

1-1 Sectional View
2 Driving Gear;
3 Driven Gear;
4 Drive Side of Driving Gear;
5 Idle Side of Driving Gear;
6 Drive Side of Driven Gear;
7 Idle Side of Driven Gear;
8 Backlash;
9 Shim;
10 Shim Holding-Disc

Figure 2.20: Rivin's modified gear (Rivin, 2000)

Anti-backlash gears, figures 2.21, 2.22 and 2.23, also decrease rattle noise, but the spring loaded contact produces friction losses and heat, Rivin (2000).

Fujimoto and Kizuka (2003a) reported that the vibrations between the input-shaft and countershaft were found to be suppressed when a backlash eliminator is added, figure 2.23. By preloading the backlash eliminator and increasing the first stage constant of the clutch disk, noise levels can be reduced (Fujimoto and Kizuka, 2003a). Nevertheless, Fujimoto and Kizuka (2003a) found that in practice, increasing the initial force (preloading) in the backlash eliminator could produce a whistling noise.

Magnetic attraction between the contacting gears was utilised to raise the rattle threshold and attenuate gear noise above the rattle threshold (Dogan and Lechner, 1998), figure 2.24.

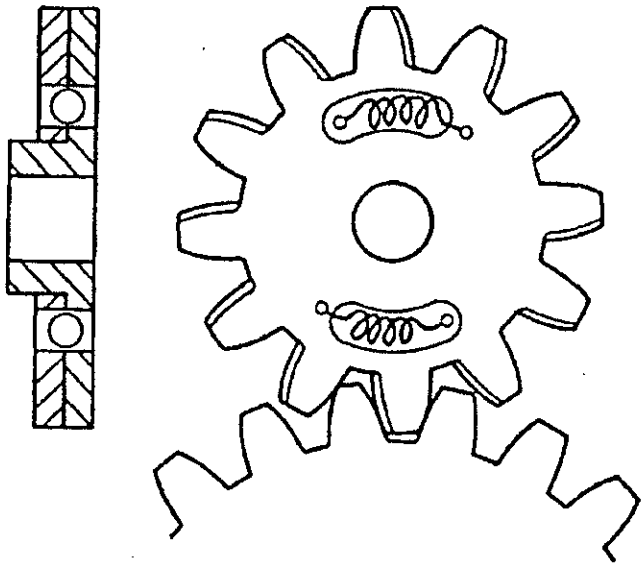

Figure 2.21: Concept of anti-backlash gear (Rivin, 2000)

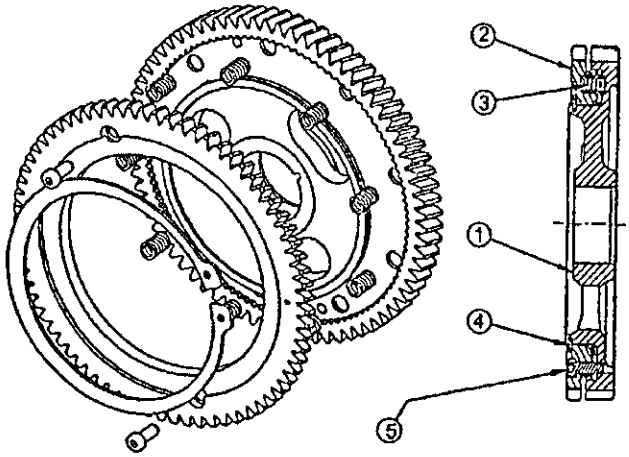

1 Main Gear;
2 Backlash Control Gear;
3 Springs;
4 Retaining Ring;
5 Screws

Figure 2.22: Cummings 4B anti-backlash gear (Rivin, 2000)

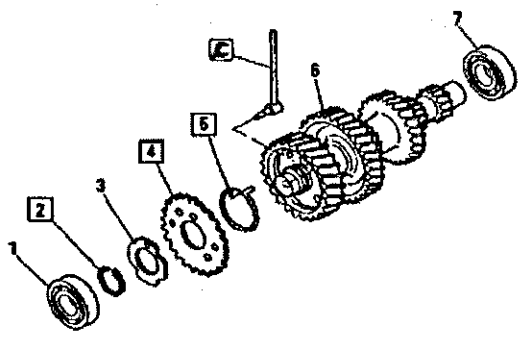

1. c/s front bearing
2. snap ring
3. sub gear plate
4. sub gear
5. sub gear spring
6. c/s
7. bearing in c/s

Figure 2. 23: Countershaft with backlash-eliminator (Fujimoto and Kizuka, 2003a)

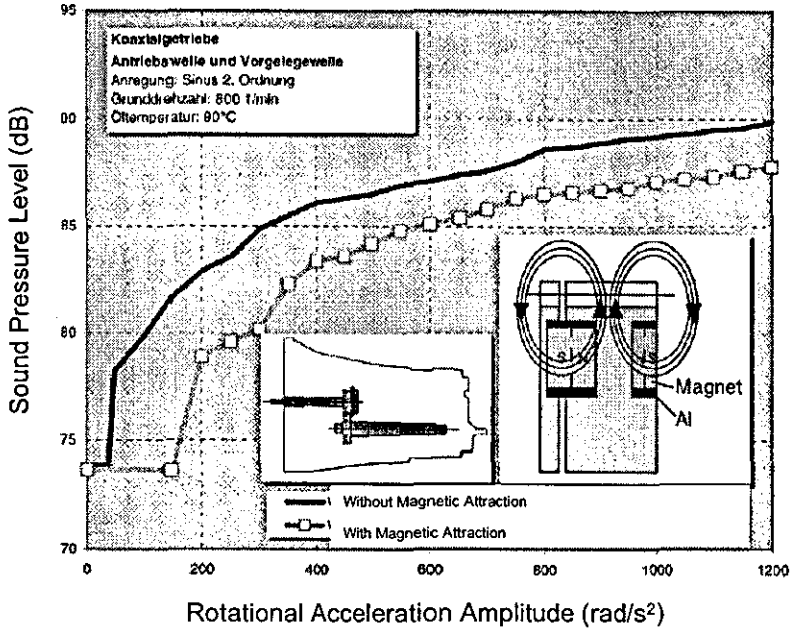

Figure 2.24: Magnetic attraction as anti-rattle measure (Dogan and Lechner 1998)

Dogan (2001) tested other measures to limit the motion of loose gears and reduce the intensity of tooth impacts:

- O-ring at gear hub to provide friction damping, figure 2.25: it doubled the rattle threshold on the tested transmission (at reverse) and reduced the sound pressure level by 2 dB(A). Nevertheless, at acceleration amplitudes from 600 rad/s^2, wear problems decrease the efficiency of the O-ring leading to the sound pressure level to increase.
- Elastomer inset at pinion bottom land (Figure 2.26): the Elastomer prevents tooth separation when it comes into contact with the loose wheel as shown in figure 2.26 (point 2). The gear pair tested with elastomer inset were up to 3.5 dB (A) noisier at low acceleration amplitudes, but more quiet at higher amplitudes (4 dB (A) lower).
- Eddy current brake (Figure 2.27): an eddy current brake functions as a damping element to raise the rattle threshold. The gear pair tested with eddy current brakes has a four-time higher rattle threshold. Nevertheless, they produce higher noise levels below the rattle threshold.

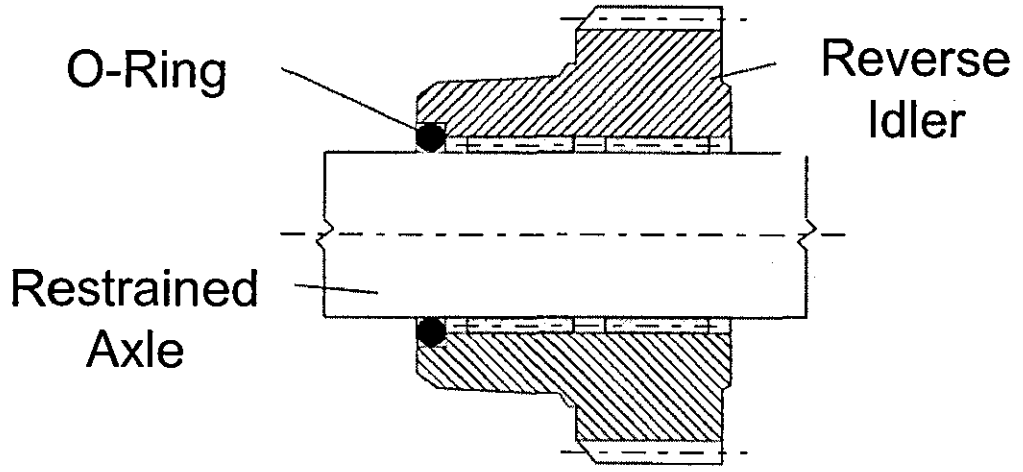

Figure 2.25: O-ring as friction damper (Dogan, 2001)

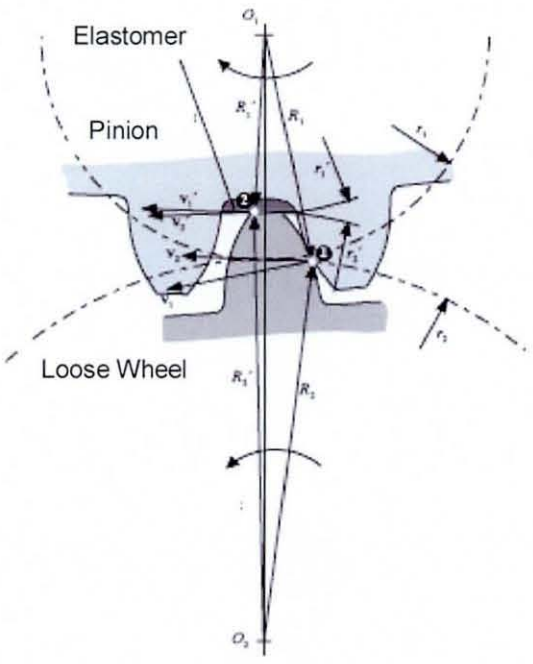

Figure 2.26: Pinion elastomer insert (Doğan, 2001)

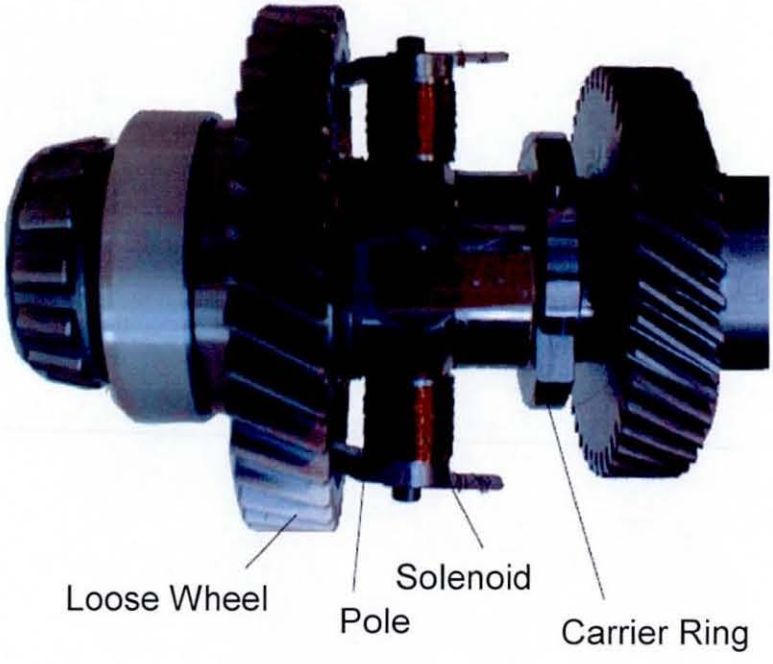

Figure 2. 27: Eddy current brake (Doğan, 2001)

2.10 Conclusions

It is clear that a considerable amount of work has been undertaken over the last 25 years on the issue of gear rattle. The main features of those works are summarised below:

- Most literature concentrated on idle rattle with minimum attention to coast rattle.
- The powertrain components have been modelled with various levels of complexity and both analytical and numerical solutions have been sought.
- Nevertheless, due to the high non-linearity of the problem, numerical solutions are more accurate (because of less simplifying assumptions) and more efficient, especially from the repeatability and parametric studies point of view.
- Basic, complete transmission and whole vehicle experiments have been conducted.
- While basic experiments help in building the core science and design guidelines of gear rattle, complete transmission and whole vehicle experiments help understanding gear rattle as a system problem.
- Most of gear rattle counter-measures tend to be internal and structural measures.
- Tribological measures are the new direction in gear rattle research.
- Most of the literature treats the lubricant as a damping factor rather than a forcing medium; the aim of the current work is to address this deficiency in the research effort.

Chapter 3 Method of Approach

3.1 Introduction

This chapter introduces the physics of the problem, as well as the analysis methods employed. Through a single degree-of-freedom model, an explanation of the meshing process and the kinematics of the contact are provided. The kinetics of gear impacts problem under lightly loaded hydrodynamic conditions is explained, together with drag and friction forces under the same conditions. The effects of various parameters are analysed. The physical concepts introduced in this chapter are later applied to a full transmission system (a multiple-degree-of-freedom gear cluster model) in chapter 4.

3.2 The Single Degree of Freedom Model

The single degree of freedom model comprises a driving gear (pinion) and a driven gear (wheel), which is idling (i.e. not loaded) (see figure 3.1). The angular displacement $\varphi_p(t)$, velocity $\dot{\varphi}_p(t)$ and acceleration $\ddot{\varphi}_p(t)$ time histories of the pinion are known from given engine running conditions.

The wheel is driven by a repetitive impacting hydrodynamic (contact) force, W_t, applied by the teeth of its pinion. The motion is resisted by the hydrodynamic friction force, F_{fl}, acting on the teeth flanks, and the Petrov tractive force, F_p, due to the action of the lubricant between the wheel and its supporting shaft (see figures 3.1 and 3.2). The equation of motion is obtained as follows:

$$I_w\ddot{\varphi}_w = W_t r_w - F_{fl} r_w - F_p r_{os} \qquad (3.1)$$

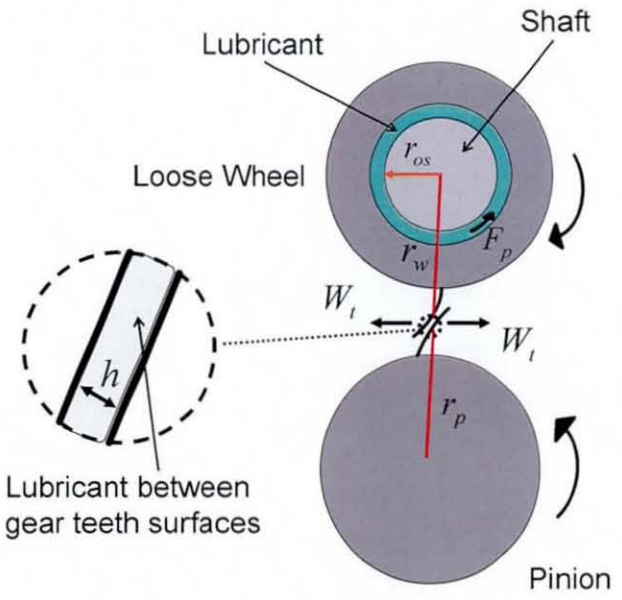

Figure 3.1: Gear Pair

The radius r_w is the pitch radius of the loose wheel, while the radius r_{os} is its inside radius at the interface with its supporting shaft. The hydrodynamic reaction force W_t and the hydrodynamic friction force F_{ft} are, respectively, the sum of the hydrodynamic and friction forces acting on each pair of the teeth in simultaneous contact. These forces are taken in the transverse plane (see figure 3.2), thus:

$$W_t = \sum_{j=1}^{N_{total}} W_j \cos\alpha_n \cos\beta . \qquad (3.2)$$

$$F_{ft} = \sum_{j=1}^{N_{total}} F_{fj} \sin\alpha_t . \qquad (3.3)$$

Here, W_j and F_{fj} are the hydrodynamic reaction and friction forces acting on the j^{th} tooth in contact taken in the normal plane, and N_{total} is the number of teeth in simultaneous contact. The details of hydrodynamic reaction and friction forces W_j, F_{fj} and the Petrov force F_p are given later in this chapter.

In order to determine the hydrodynamic force and friction (W_j and F_j), the geometric and kinematic characteristics of the contact between each idle gear and its pinion must be established.

3.3 Simulation of the Meshing Sequence of Conventional Helical Gear Pairs

A procedure is developed to determine the radii of contact and radii of curvature for the teeth in simultaneous contact for a pair of gear teeth. The procedure is then used to determine the simultaneous hydrodynamic reaction and friction, which depend on the geometry of the mating surfaces. In order to simplify the computational effort, the teeth are assumed to be perfectly helical and involute.

Length of the line of action (Chao, 1991) in the meshing plane is given by (see figure 3.3):

$$Z_{act} = \sqrt{r_{op}^2 - r_{bp}^2} + \sqrt{r_{ow}^2 - r_{bw}^2} - c_c \sin\alpha_t . \qquad (3.4)$$

Hence, the angles of inclination for the line of action that describes a complete meshing cycle for the pinion and wheel respectively (see figure 3.4) are given by (Drago, 1988):

$$\left.\begin{aligned} \phi_{mp} &= \frac{Z_{act}}{r_{bp}} \\ \phi_{mw} &= \frac{Z_{act}}{r_{bw}} \end{aligned}\right\} \qquad (3.5)$$

Since the meshing action is cyclic, it is sufficient to describe the angular displacement relative to the meshing cycle of the pinion and wheel by normalising the global displacements φ_p and φ_w respectively, as follows:

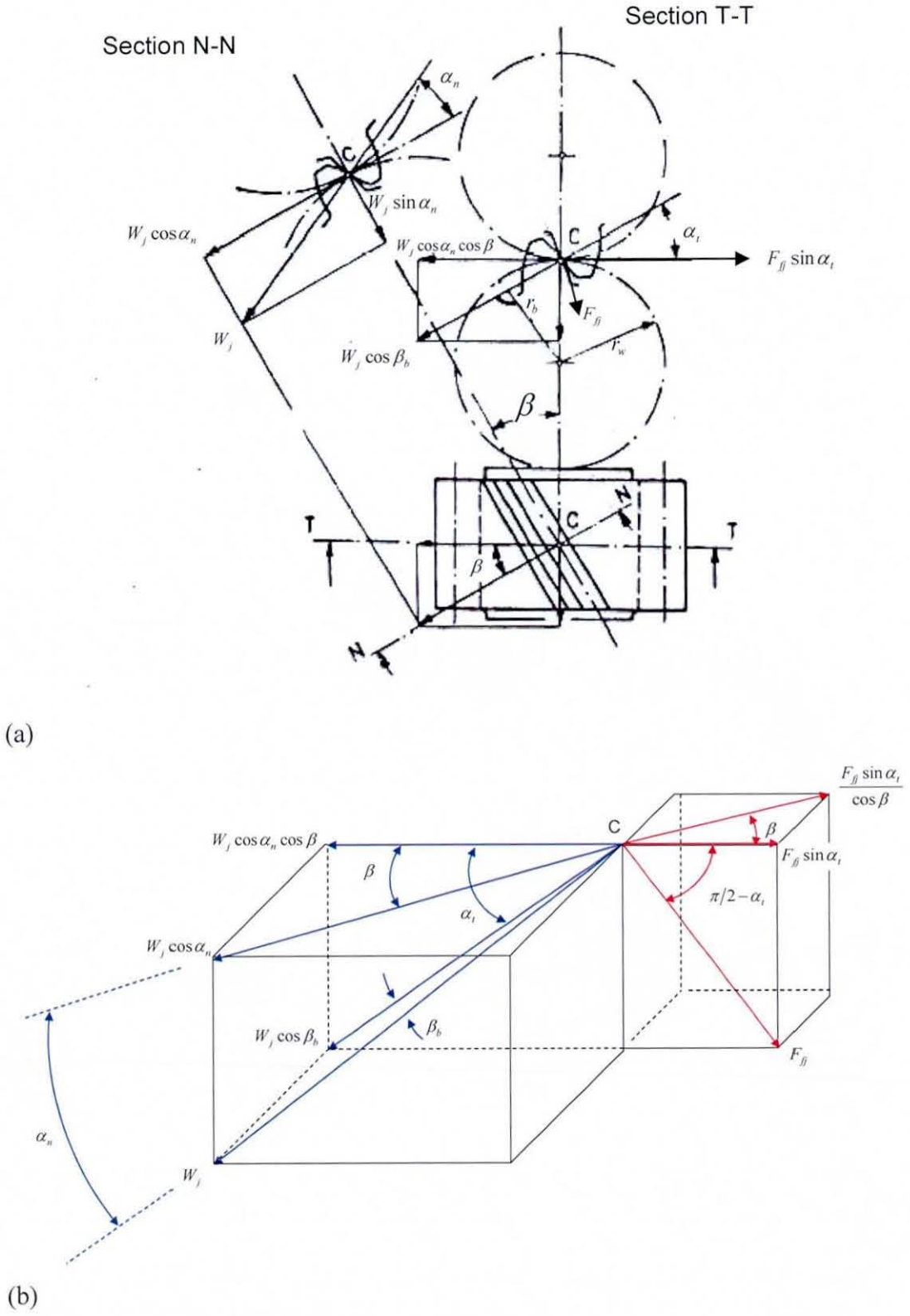

Figure 3.2: The contact and friction forces (Graikousis, 1985)

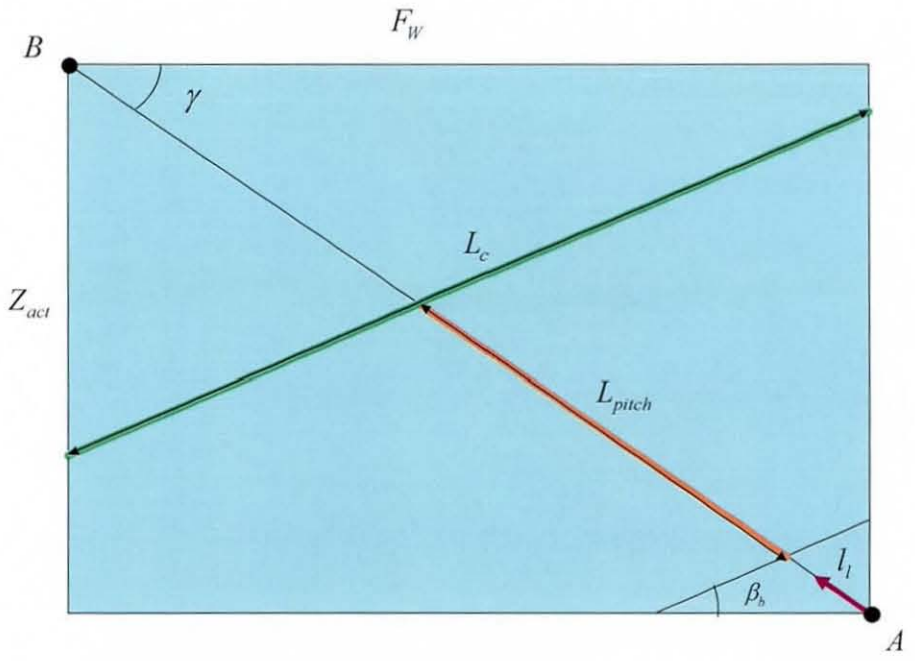

Figure 3.3: Contact Plane

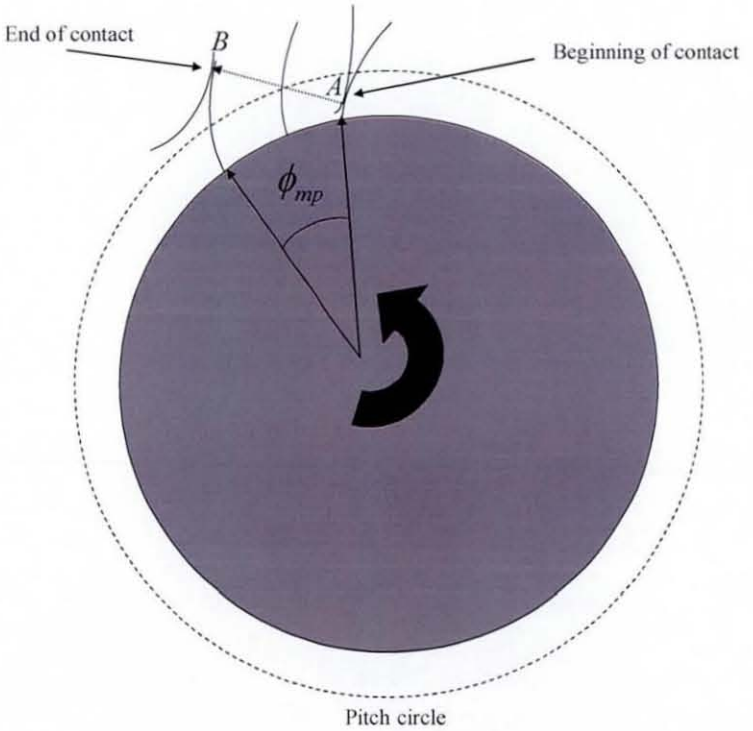

Figure 3.4: Mesh cycle of pinion tooth

$$\left.\begin{aligned}\phi_p &= \phi_{mp}\left(\frac{\varphi_p}{\phi_{mp}} - Integer\left(\frac{\varphi_p}{\phi_{mp}}\right)\right)\\ \phi_w &= \phi_{mw}\left(\frac{\varphi_w}{\phi_{mw}} - Integer\left(\frac{\varphi_w}{\phi_{mw}}\right)\right)\end{aligned}\right\}, \tag{3. 6}$$

Here ϕ_p and ϕ_w are bounded by the meshing cycle, such that $0 \le \phi_p \le \phi_{mp}$ and $0 \le \phi_w \le \phi_{mw}$, while the global displacements φ_p and φ_w are only bounded by their initial conditions, thus: $\varphi_{p0} < \varphi_p < +\infty$ and $\varphi_{w0} < \varphi_w < +\infty$. The function *Integer* returns the integer portion of the real argument.

From the contact plane diagram in figure 3.3, it follows that:

a- The length of the diagonal line in the contact (action) plane:

$$L_{act} = \sqrt{Z_{act}^2 + F_W{}^2}\,. \tag{3. 7}$$

b- The gradient of the diagonal line in the contact (action) plane relative to the face-width line:

$$\gamma = \tan^{-1}\left(\frac{Z_{act}}{F_W}\right). \tag{3. 8}$$

c- The diagonal pitch on the action plane diagonal line:

$$L_{pitch} = \frac{p_{tb}\cos\beta_b}{\sin(\gamma + \beta_b)}, \quad \left(where,\ p_{tb} = p_{tbp} = p_{tbw}\right). \tag{3. 9}$$

A diagonal parameter, l_l, on the contact plane needs to be defined in order to describe the position of each tooth during the meshing cycle along the diagonal line of the contact plane. This parameter depends on the angular displacements of the pinion and the wheel, and starts with a value of zero at the beginning of the tooth contact (point A in figure 3.3), at the end of the contact (point B in figure 3.3) the parameter takes the value L_{act} such that $0 \le l_l \le L_{act}$. Since the amount of backlash is negligible when compared to the length of the line of action, the contact plane is common for both the

pinion and the wheel. Hence, (from figure 3.3) the length of the diagonal parameter is:

$$l_l = \frac{\phi_p r_{bp}}{\sin\gamma} = \frac{\phi_w r_{bw}}{\sin\gamma} \tag{3. 10}$$

The diagonal parameter l_l follows the motion of one tooth only across the contact plane. However, since more than one pair of teeth remain in simultaneous contact; their total number must be determined.

The number of teeth following any given tooth considered in contact (the one described by the diagonal parameter l_l) equals the integer portion of the ratio of the diagonal parameter to the pitch diameter of the action plane, thus:

$$N_{beh} = Integer\left(\frac{l_l}{L_{pitch}}\right). \tag{3. 11}$$

The number of teeth preceding the considered tooth is then calculated as follows:

$$N_{front} = Integer\left(\frac{L_{act} - l_l}{L_{pitch}}\right). \tag{3. 12}$$

The total number of teeth in simultaneous contact at each instant of time (also adding the considered tooth) is given by:

$$N_{total} = N_{beh} + N_{front} + 1. \tag{3. 13}$$

The respective angles of contact of j^{th} teeth pair in simultaneous mesh for the pinion and the wheel, respectively, are:

$$\left.\begin{aligned} \phi_{jp} &= \phi_p \frac{\left[l_l + (n - N_{beh})L_{pitch}\right]}{l_l} \\ \phi_{jw} &= \phi_w \frac{\left[l_l + (n - N_{beh})L_{pitch}\right]}{l_l} \end{aligned}\right\} \; n = 0,1,...(N_{beh} + N_{front}). \tag{3. 14}$$

When $n = N_{beh}$, $\phi_{jp} = \phi_p$, which is the angular displacement of the considered main tooth relative to the mesh angle, and $j = n+1$.

The transverse radii of curvature of the j^{th} meshing teeth pair wheel and pinion, respectively are:

$$\left.\begin{aligned} \rho_{jw} &= \frac{\sqrt{r_{ow}^2 - r_{bw}^2} - \phi_{jp} r_{bp}}{\cos\beta} \\ \rho_{jp} &= \frac{c_c \sin\alpha_t}{\cos\beta} - \rho_{jw} \end{aligned}\right\} \qquad (3.15)$$

The contact radii of the j^{th} meshing pair of teeth (wheel and pinion, respectively) are:

$$\left.\begin{aligned} r_{cjp} &= \sqrt{\left(r_{bp}^2 + \rho_{jp}^2\right)} \\ r_{cjw} &= \sqrt{\left(r_{bw}^2 + \rho_{jw}^2\right)} \end{aligned}\right\}. \qquad (3.16)$$

The reduced (equivalent) radius of curvature of the j^{th} meshing tooth pair in the normal plane is given by:

$$r_{eqj} = \frac{\rho_{jp}\rho_{jw}}{\left(\rho_{jp} + \rho_{jw}\right)\cos\beta_b}. \qquad (3.17)$$

The equivalent radius represents the radius of a cylinder in contact with a semi-infinite elastic half-space; this cylinder has a curvature that is equal to the sum of curvatures of the teeth in contact (the curvature of a curve is the inverse of its radius of curvature). Figure 3.5 illustrates the principle behind the equivalent radius of curvature (taken on the transverse plane). In equation (3.17), the division by $\cos\beta_b$ is made in order to transform the equivalent curvature from the transverse plane to the plane orthogonal to the contact.

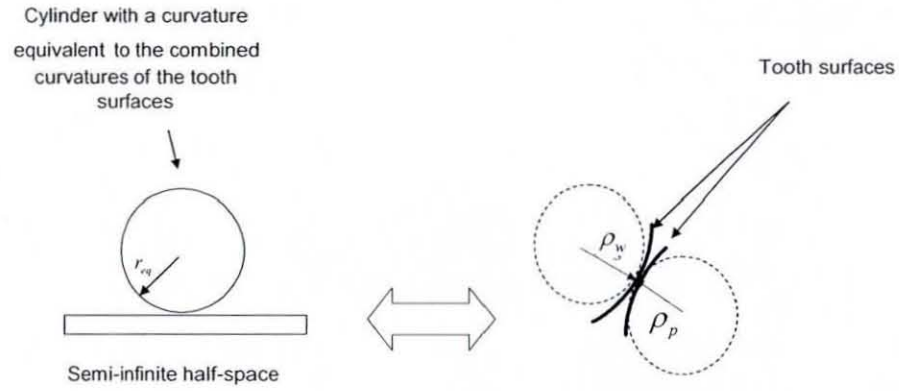

$$r_{eq} = \frac{\rho_p \rho_w}{\rho_p + \rho_w}$$

Figure 3.5: Principle of the equivalent radius of curvature

3.4 Kinematics of contact

The entraining velocity of lubricant between gear flanks can be obtained by considering the kinematics of the contact at any instant of time for any pair of meshing teeth. The entraining motion of the lubricant is as the result of relative motion of contacting surfaces through a converging wedge shape. This action instantaneously takes place orthogonal to the line of contact. Note that the contact in reality is a very long ellipse, where lubricant entrainment occurs along its semi-minor half-width. Therefore, the velocity of rolling of the mating pairs should be determined as a function of the pitch velocity of each of the meshing gear pair. The pitch velocities are given as:

$$\left.\begin{aligned} v_{ppitch} &= r_p \dot{\varphi}_p \\ v_{wpitch} &= r_w \dot{\varphi}_w \end{aligned}\right\} \qquad (3.18)$$

It should be noted that v_{ppitch} and v_{wpitch} are not necessarily equal; this is because separation is a result of the two meshing gears having different tangential velocities.

The transmission gear pairs are helical. Therefore, it is necessary to transform the pitch velocity into the direction of the helix and then obtain the components of surface velocity for each tooth normal to the line of contact (in the direction of relative surface motion). The methodology for this was developed by (Merritt, 1971). Thus, for the pinion and wheel respectively, the rolling velocities are (see Merritt, 1971):

$$\left.\begin{aligned} v_{jp} &= v_{ppitch}\left(\sin\alpha_t + \frac{l_j}{r_p}\right)\cos\beta_b \\ v_{jw} &= v_{wpitch}\left(\sin\alpha_t - \frac{l_j}{r_w}\right)\cos\beta_b \end{aligned}\right\} \qquad (3.19)$$

Where, the length l_j lies on the contact path (transverse plane) of the j^{th} meshing pair of teeth (see figure 3.6) and it can be calculated as follows:

$$l_j = r_w \sin\alpha_t - \rho_{jw} \qquad (3.20)$$

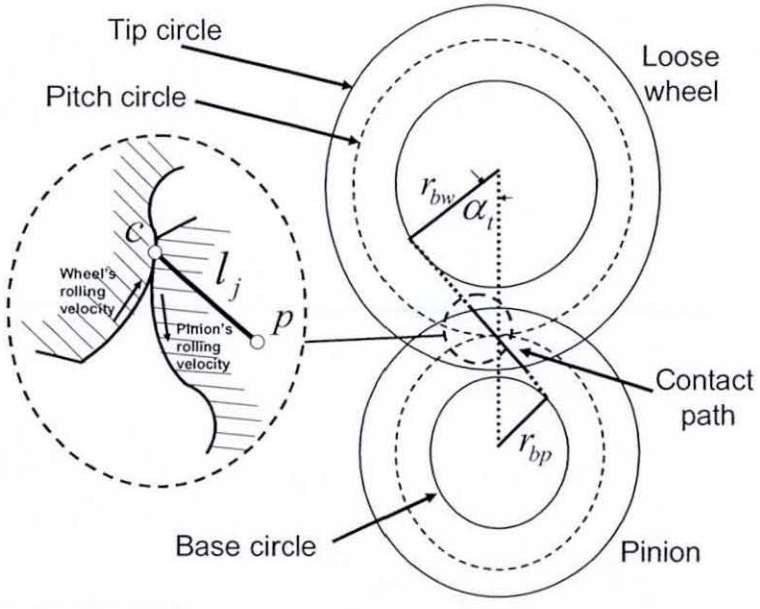

Figure 3. 6: Geometry of impacting pairs

The speed of entraining motion, figure 3.7, is the average of these rolling velocities (see Wedeven, 1975), thus:

$$u_j = \frac{v_{jp} + v_{jw}}{2} \tag{3. 21}$$

And the sliding velocity is the difference between the rolling velocities (Merritt, 1971):

$$u_{js} = v_{jp} - v_{jw} \tag{3. 22}$$

Lubricant film thickness (in the normal plane, see figure 3.1), is given by:

$$h = C_b - \frac{\left|\left(r_w\varphi_w - r_p\varphi_p\right)\right|}{\cos\alpha_n \cos\beta} \tag{3. 23}$$

The squeeze velocity in the normal plane can be obtained by direct differentiation (Rahnejat, 1984) as:

$$\frac{\partial h}{\partial t} = -\frac{\left|\left(r_w\dot{\varphi}_w - r_p\dot{\varphi}_p\right)\right|}{\cos\alpha_n \cos\beta} \tag{3. 24}$$

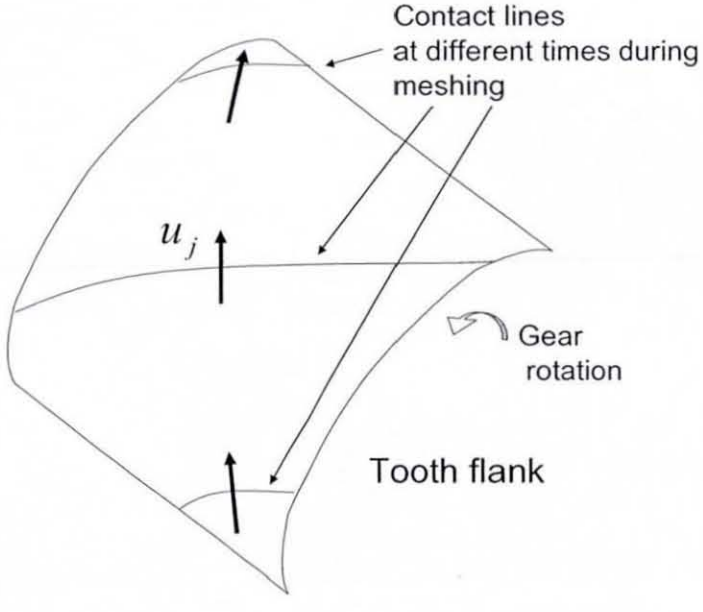

Figure 3.7: Entraining velocity relative to tooth flank

3.5 Hydrodynamic impact condition

Although gear rattle problem has been treated by a number of recent investigations, most models disregard the action of the intervening lubricant in the meshing (contact/impact) zone. This may be assumed as a reasonable assumption for high impact loads as the stiffness of the lubricant film, in parallel to those of the impacting solids, is large compared with them and its effect may be ignored under certain conditions, such as under elastohydrodynamic regime of lubrication. However, under even such conditions the local deformation of the contiguous solids has been shown to be larger than that of a dry impact due to high generated lubricant pressures (Al-Samieh and Rahnejat, 2002).

Under lightly loaded impacts of the order of a few Newtons at most, such as under idle rattle condition, the assumption described above is not permissible as the effective stiffness of the hydrodynamic film plays the key role. This has been shown to some extent by (Gnankumarr et al., 2002), who used an expression for lubricant reaction in terms of oil film thickness and its rate of change, referred to as squeeze film velocity. This expression is for an infinite line contact assumption for an iso-viscous lubricant behaviour. Both these assumptions are justified, as idle rattle is due to low load, precluding any significant viscous action of the lubricant. Furthermore, the average contact width is far less than the length of contact line on the tooth flank in the case of spur gears or involute pairs of low contact conformity. The expression used by (Gnanakumarr et al., 2002) was derived by (Rahnejat 1984), which is also similar to that arrived at independently by (Sasaki et al., 1962). Therefore, hydrodynamic reaction force normal to the surfaces of the j^{th} pair of meshing teeth is given as:

$$\left.\begin{aligned} W_j &= \frac{L\eta_0 r_{eqj}}{h}\left(2u_j - \frac{3\pi}{\sqrt{\frac{2h}{r_{eqj}}}}\frac{\partial h}{\partial t}\right), \quad if \quad \frac{\partial h}{\partial t} < 0 \\ W_j &= \frac{L\eta_0 r_{ejq}}{h}\left(2u_j\right), \qquad\qquad if \quad \frac{\partial h}{\partial t} \geq 0 \end{aligned}\right\} \tag{3.25}$$

Where, r_{eqj} is the instantaneous equivalent radius of curvature taken at the mid-position along the line of contact of the j^{th} pair of meshing teeth, whose radii of contact orthogonal to the line of contact, being the equivalent radius of curvature of a cylinder of radius r_{eqj} in contact with a semi-infinite elastic half-space. The other principal radii of contact describing the profile of the teeth flanks are considered as infinite, rendering them as flat surfaces. This combination leads to contact footprints, which are slanted lines at any instant of time as shown in figure 3.7. In reality the length of the contact line is finite and clearly alters as the time progresses as demonstrated in figure 3.7. This means that equation (3.25), based on an infinite line contact is regarded as an approximation. However, this is quite reasonable under lightly loaded hydrodynamic conditions, since with no deformation of the impacting solids the width of contact is almost negligible.

The transverse component of the hydrodynamic load on each tooth flank is then given as:

$$W_{jt} = W_j \cos\alpha_n \cos\beta . \qquad (3.26)$$

3.6 Resistive forces

3.6.1 Hydrodynamic tractive force:

Resistance to the motion of the loose wheels is provided by hydrodynamic traction induced by a film of lubricant formed between the supporting output shaft convex curvature and the inside concave surface of the mounted gears. This is shown in figure 3.1. This force is known as the Petrov viscous friction, which for a concentric arrangement with zero eccentricity ratio yields (Gnanakumarr et al., 2002):

$$F_p = \frac{\pi \eta_0 v \, l_1 r_{os}}{C} \qquad (3.27)$$

Where, the entraining velocity of the lubricant is given as (Gnanakumarr et al., 2002):

$$v = \frac{1}{2}\left[\left(r_{os} + C\right)\dot{\varphi}_w + \frac{1}{2\pi} r_{os}\dot{\varphi}_{os}\right] \qquad (3.28)$$

In case of the neutral (i.e. idle) condition, the output shaft does not rotate; hence, $\dot{\varphi}_{os} = 0$.

In reality this form of Petrov's equation is meant to be used with journal running concentrically with its bearing (Hamrock et al, 2004). Nevertheless, the loose wheels are mounted on needle roller bearings with many rollers (such that their combined inner surface can be considered as almost a bushing with a wavy surface, waviness of which can be ignored by assuming that the bearing is fully flooded such that there is enough amount of oil to separate the rollers from the inside concave surface of the mounted gear). Therefore, the use of Petrov's equation as an approximation is justified by the fact that under idle conditions radial loads are low, and the idling speed (800 rpm) is high enough to assume concentric running of the loose gears on their bearings.

3.6.2 Hydrodynamic flank friction

The hydrodynamic flank friction F_{fj} acts parallel to the flank end faces (see figure 3.2) and is derived generically by Gohar (2001), using the half-Sommerfeld boundary conditions as follows (see figure 3.8):

$$F_f = L\int_{x_i}^{x_e}\left[\pm\frac{z\,\partial P}{2\,\partial x} + \frac{\eta_0 \Delta u}{z}\right]dx \qquad (3.29)$$

Where, x denotes the dimension along the width of contact (being the direction of entraining motion, figure 3.8), P is the pressure in the conjunction, x_i is the inlet position (where as $x_i \to -\infty$, $P \to 0$), and x_e is the exit position (where at $x_e = 0$, $P = 0$), and z is normal to the contact surface (in the direction of the film thickness) as shown in figure 3.9, L is the length of contact, Δu is the relative sliding velocity between the upper and lower bodies in figure 3.9. It should be mentioned that half-

Sommerfeld condition ignores the effect of suction, film rapture at the exit and also cavitation (see Rahnejat, 1984).

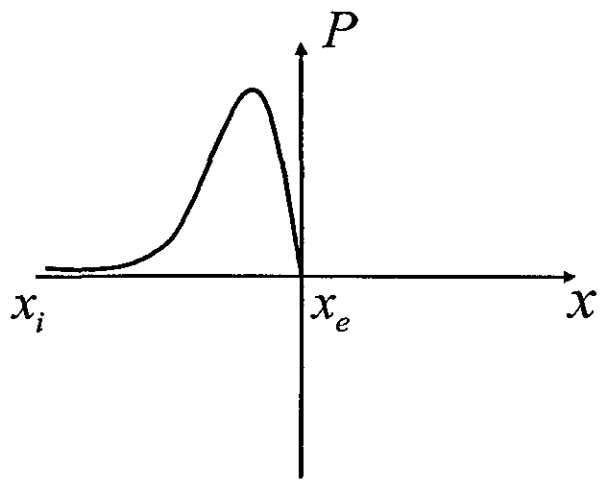

Figure 3.8: Half-Sommerfeld conditions

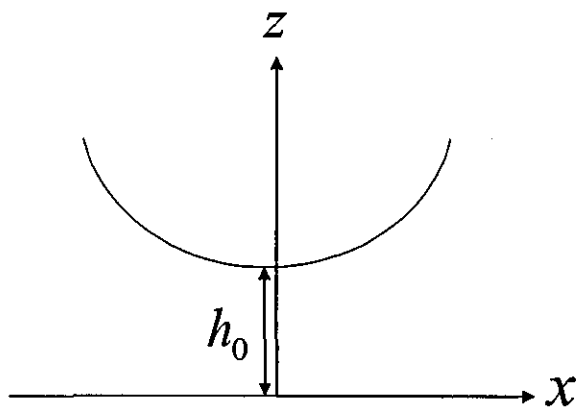

Figure 3.9: Film Shape in Hydrodynamic Infinite Line Contact

For low hydrodynamic pressures, the first term in equation (3.29) can be neglected due to

$$\frac{z\,\partial P}{2\,\partial x} << \frac{\eta_0 \Delta u}{z}$$

Therefore, equation (3.29) becomes:

$$F_f = L\int_{x_i}^{0}\left[\frac{\eta_0 \Delta u}{z}\right]dx = L\eta_0 \Delta u\int_{x_i}^{0}\left[\frac{1}{z}\right]dx \tag{3.30}$$

Assuming an infinite hydrodynamic line contact (figure 3.9), the film thickness variation across the width of contact is given by:

$$z = h_0\left(1+\frac{x^2}{2r_{eq}h_0}\right) \tag{3.31}$$

Then substituting (3.31) back into (3.30):

$$F_f = L\eta_0 \Delta u\int_{x_i}^{0}\left[\frac{1}{h\left(1+\frac{x^2}{2r_{eq}h}\right)}\right]dx \tag{3.32}$$

The following substitution is introduced to simplify the integration in (3.32):

$$\tan\bar{x} = \frac{x}{\sqrt{2r_{eq}h}} \tag{3.33}$$

By implicit differentiation:

$$\sec^2\bar{x}d\bar{x} = \frac{dx}{\sqrt{2r_{eq}h}} \tag{3.34}$$

The integration of (3.32) is subsequently simplified and solved below:

$$F_f = \frac{L\eta_0 \Delta u}{h}\sqrt{2r_{eq}h}\int_{x_i}^{0}d\bar{x} = -\frac{\eta_0 \Delta u}{\sqrt{h}}\sqrt{2r_{eq}}\bar{x}_i \tag{3.35}$$

Rewriting (3.35) in terms of x yields the following analytical expression for hydrodynamic friction:

$$F_f = -\frac{L\eta_0 \Delta u}{\sqrt{h}}\sqrt{2r_{eq}}\tan^{-1}\left(\frac{x_i}{\sqrt{2r_{eq}h}}\right) \tag{3.36}$$

Assuming fully flooded conditions (the oil film thickness at the inlet is equal to the equivalent radius of curvature, thus the contact region is assumed to be fully immersed in oil), the inlet could be assumed to lie at an infinite distance from the exit:

$$x_i \to -\infty \tag{3.37}$$

$$\tan^{-1}(-\infty) \to \frac{-\pi}{2} \tag{3.38}$$

And the hydrodynamic friction reduces to:

$$F_f = \frac{L\pi\eta_0\Delta u}{\sqrt{2h}}\sqrt{r_{eq}} \tag{3.39}$$

Applying the above to gearing action, Δu is the sliding velocity, u_{js}, of the meshing teeth surfaces already defined in equation (3.22), which changes direction as the contact crosses the pitch point. This leads to a negative value for friction, which when substituted into the equations of motion yields forcing terms rather than dissipative terms, contravening the concept of friction. To correct this malfunction of (3.39) and achieving a dissipative hydrodynamic friction force, the sliding velocity u_{js} has been replaced by its absolute value; hence, for the j^{th} gear pair, the hydrodynamic flank friction is obtained as:

$$F_{fj} = \frac{\pi\eta_0 L|u_{js}|\sqrt{r_{eqj}}}{\sqrt{2h}}. \tag{3.40}$$

The sum of torques on all flanks in simultaneous contact is then taken and inserted into the equations of motion as shown in section 3.2.

3.7 Numerical procedure: linear acceleration method

The problem is solved in a series of suitably small time steps, using the Newmark's linear acceleration method, in the same manner described by (Timoshenko et al, 1974; and Rahnejat, 1985). This method assumes that the

acceleration varies in a linear manner within the time step. The following procedure is employed:

1. Using the inertial dynamics (the equations of motion), the angular acceleration, $\ddot{\varphi}_w$ of each component of the system is calculated.
2. The angular velocities and displacements, $\dot{\varphi}_w, \varphi_w$, are calculated in step-by-step integration, using the linear acceleration method.
3. The lubricant entraining speeds and gear meshing characteristics at each contact are determined as described above.
4. Lubricant film thickness is evaluated, using equation (3.23).
5. The squeeze film speed $\frac{\partial h}{\partial t}$ is determined as described above.
6. The hydrodynamic impact force W_j is calculated, using equation (3.25).
7. The hydrodynamic resistive forces are obtained using equations (3.27) and (3.40).
8. The displacements between successive iterations are judged against the following convergence criterion:

$$\left|\varphi(i_{time}, j_{iteration}) - \varphi(i_{time}, j_{iteration} - 1)\right| \leq \xi . \qquad (3.41)$$

   The criterion ξ is selected such that the number of significant figure determines the accuracy of the convergence (Timoshenko et al, 1974; and Rahnejat, 1985).
9. If the convergence criterion is upheld, the time step is advanced: $i_{time} = i_{time} + 1$. Otherwise, the procedure is repeated by advancing the iteration step: $j_{iteration} = j_{iteration} + 1$.

The Newmark integration scheme was used with $\gamma = \frac{1}{2}$ to minimise numerical damping (Reese, 2003), and $\beta = \frac{1}{6}$ to improve its accuracy albeit making it conditionally stable (Timoshenko et al, 1974). To cater for the conditional stability, care had to be taken when selecting the time step size and the initial conditions. The time step used was $1\,\mu s$, the initial displacement $\varphi_{w0} = 10^{-12}$ radians (this is because when using $\varphi_{w0} = 0$, the system was found to be unstable), and the simulation was run

for sufficient real time in order to overcome the initial transience. The initial pinion velocity is taken as the engine idling speed.

3.8 Analysis of the Single Degree-of-Freedom Model:

The examples used here are based on the geometry and properties of the 5th gear in the transaxle transmission (see chapter 4). Under engine idling condition, loose wheels that are not coupled together can be modelled separately as single degree of freedom systems, if the time history of the driving pinion (here the input shaft) is known, and if the contact forces (here the hydrodynamic reaction) depend on the kinematics of the meshing gears.

The frequency spectrum of the pinion motion is shown in figure 3.10; it describes the dominant excitation frequencies of a 4-cylinder Diesel engine, which are the second (approx. 26 Hz), the fourth (approx. 53 Hz), and the sixth (approx. 80 Hz) engine orders. The most influential is clearly the second engine order.

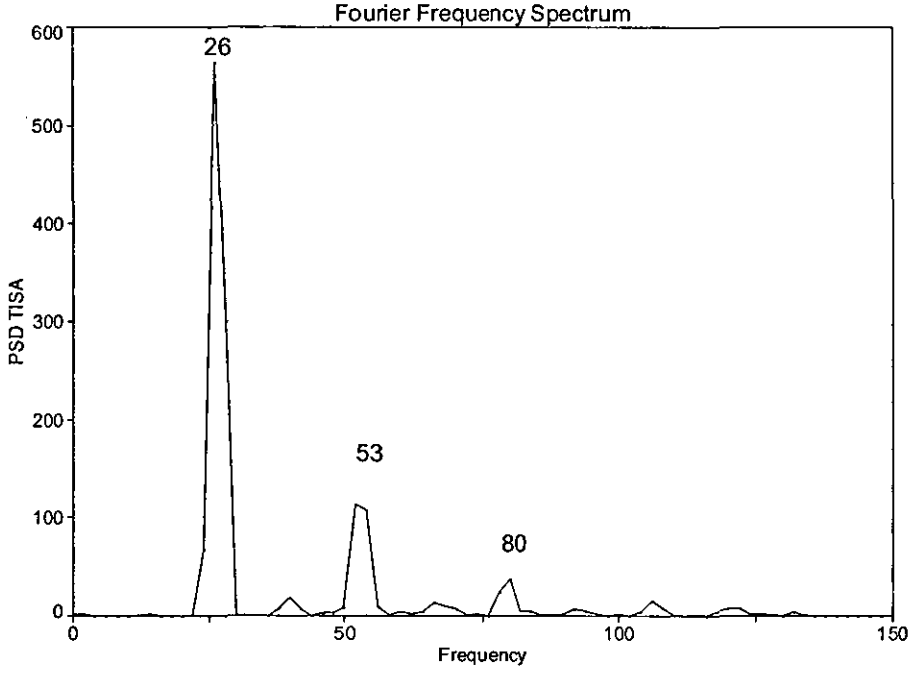

Figure 3.10: Spectrum of the pinion acceleration

3.8.1 The effect of hydrodynamic flank friction torque:

Under fully flooded contact conditions, Table 3.1 shows that the ratio of the hydrodynamic reaction torque to the flank hydrodynamic friction torque is very high, which indicates the insignificance of the flank friction within the tested temperature range 20 – 80 ^{0}C, thus its effect can be ignored; this is inline with Smith (1999), according to whom friction reversal effects may be ignored for helical gears.

Bearing clearance 35 (μm)

RMS of hydrodynamic torque to friction torque	Viscosity (Pa. s.)	Temperature (^{0}C)
303.38	0.11540	20.0
303.66	0.05122	39.4
311.01	0.0152	80.0

Table 3.1: RMS of the ratio of hydrodynamic torque to flank friction torque

3.8.2 The effect of viscosity on the rattle threshold crossing:

At the constant bearing clearance of 35 μm, figures 3.11 to 3.13 show that as the viscosity drops due to a temperature rise, the rattle ratio $(RR = Inertia\ Torque/Drag\ Torque)$increases and crosses the threshold, $RR = 1$, at 80.00^0 C (see figure 3.13), where the separation between the meshing teeth increases considerably as shown by the film thickness variation (see figures 3.11 to 3.13). The initial high values shown in the graphs are transient due to the initial conditions, which smoothen as the system reaches the steady state condition. Figure 3.14 shows that the threshold is mainly crossed, where the pinion velocity and acceleration are rising; this is in agreement with earlier findings by Sakai et al (1984), where rattling noise level is high in the ascending stage of the engine (input) velocity fluctuation. Furthermore, the pinion acceleration (figure 3.14) shows that peaks tend to be stronger at a spacing of 13 Hz (engine rotational frequency) than at the second engine order.

By looking at figures 3.11 to 3.13, the amplitude of the film thickness increases with temperature rise indicating tooth separation (from approx. 3μm p-p at 20°C to more than 10μm p-p at 80°C).

3.8.3 Effect of backlash:

The effect of backlash in fully flooded conditions and constant bearing clearance of $35\,\mu m$ at 20^0 C (as shown in figures 3.15 and 3.16), at 39.40^0 C (see figures 3.17 and 3.18), and at 80^0 C (see figures 3.19 and 3.20) has negligible influence on frequencies and on amplitudes of the response. This is in line with the findings of Sakai et al (1981), Seaman et al (1984), Rust et al (1990) and Dogan (2001).

The dominant effect comes from the change of viscosity; as it decreases with temperature rise, it shifts the active frequencies in acceleration response to the lower frequencies range, and lowers the higher components' amplitudes. This is because the film reaction is directly proportional to the viscosity (equation 3.25). This in turn indicates that as the viscosity decreases, the film stiffness decreases thus lowering the corresponding frequencies. The acceleration response reflects the engine excitations (approx. 26, 52, 78 and 106 Hz) and the squeeze response at 255Hz (fundamental), 510Hz (second harmonic), and 766Hz (third harmonic) in addition to a band of frequencies, which shifts towards the lower spectral components as the temperature increases. Modulation is observed in the spectra at the pinion rotational frequency of 13 Hz.

The fundamental meshing frequency $f_m = 464\,\text{Hz}$ is weak and is buried within the modulation caused by the pinion rotational frequency (13 Hz). The weakness of the meshing frequency indicates significant tooth separation to the extent that any variations due to tooth geometry are not effective (it should be noted that actual metal to metal contact does not take place in the hydrodynamic regime). Furthermore, it is assumed that there are no tooth irregularities and excitation at tooth meshing frequency is not existent.

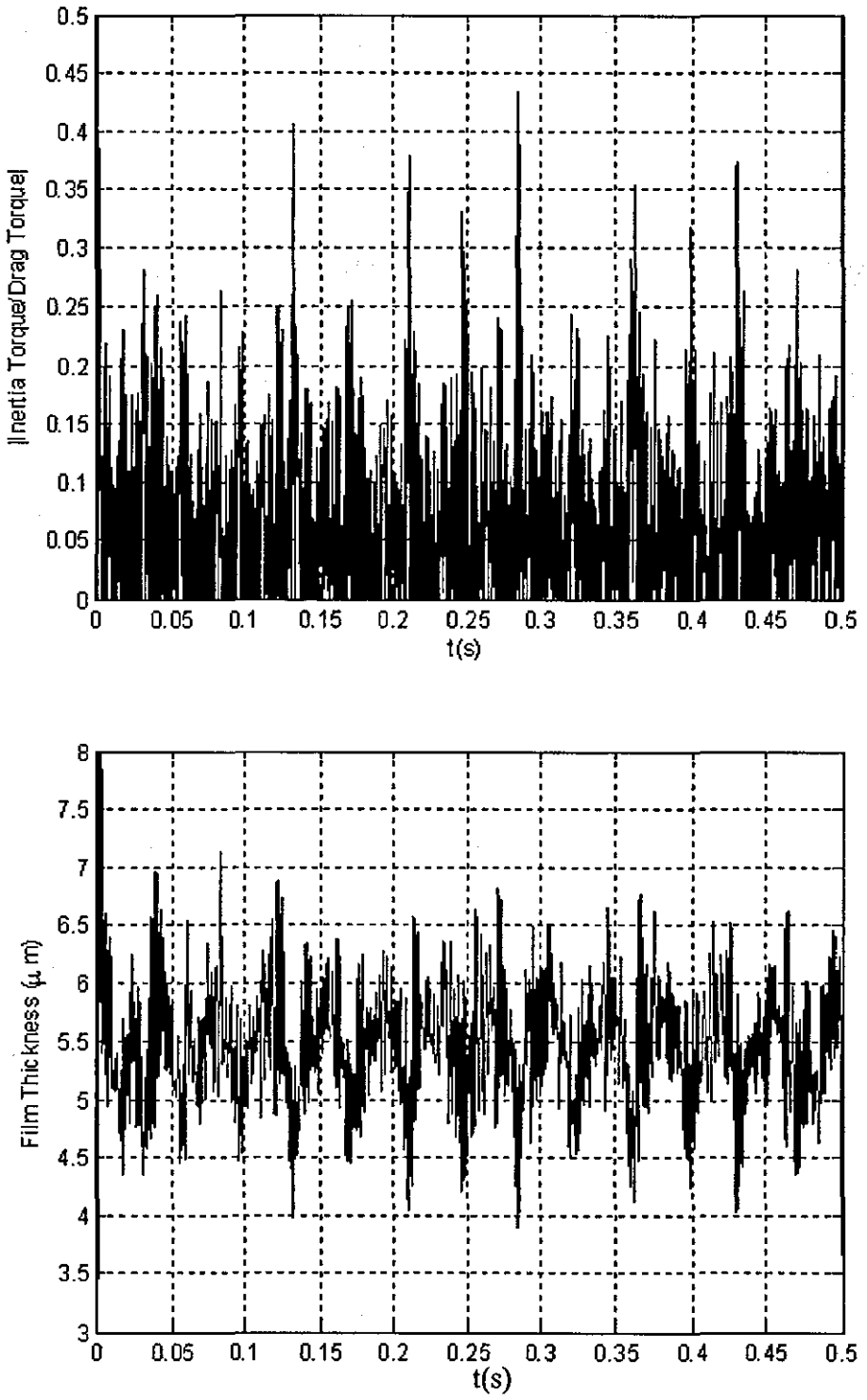

Figure 3.11: The rattle ratio and film thickness ($\eta_0 = 0.1154$ Pa.s. at 20.0^0 C)

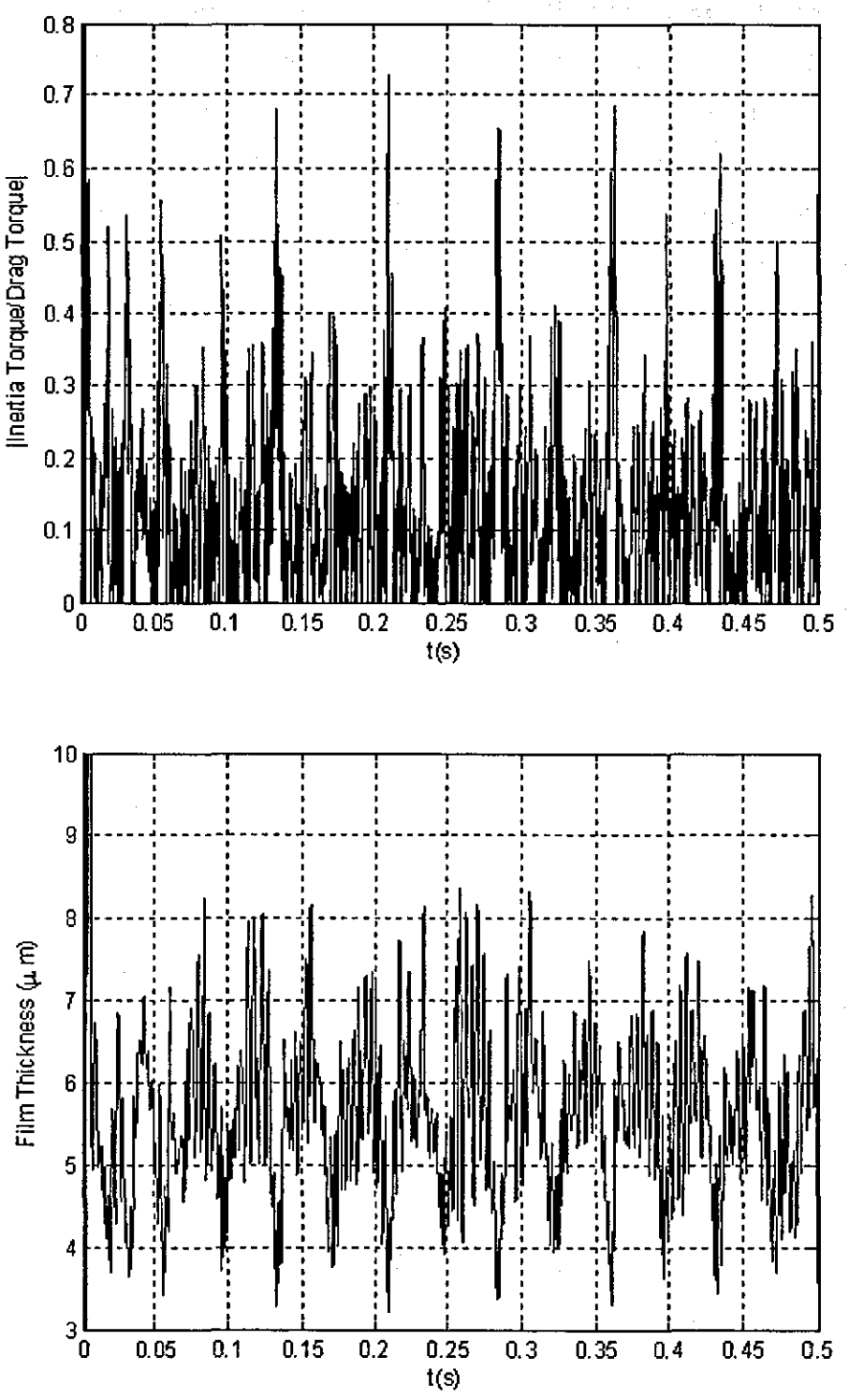

Figure 3.12: The rattle ratio and film thickness ($\eta_0 = 0.05122$ Pa.s. at 39.40^0 C)

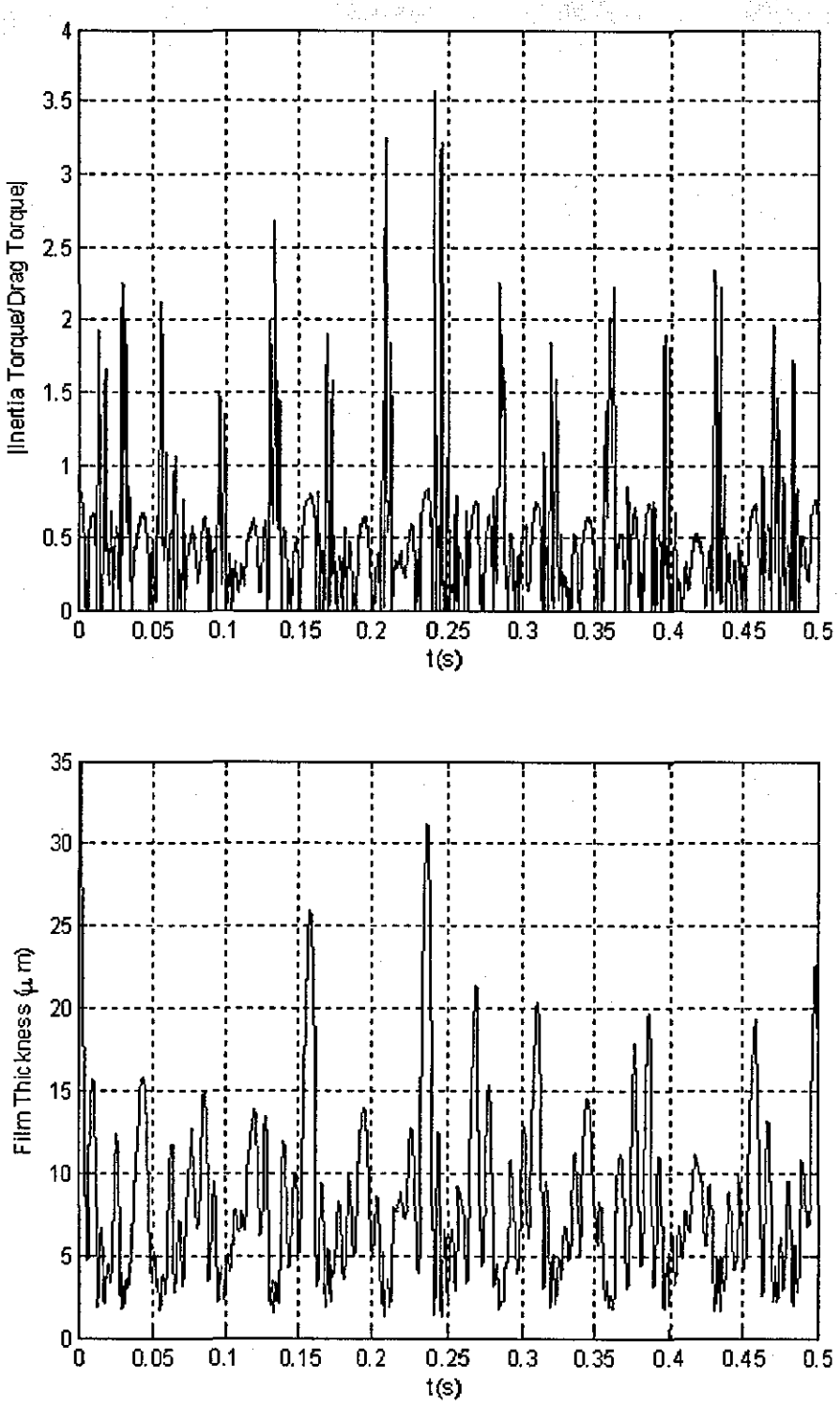

Figure 3.13: The rattle ratio and film thickness ($\eta_0 = 0.01520$ Pa.s. at 80.00^0 C)

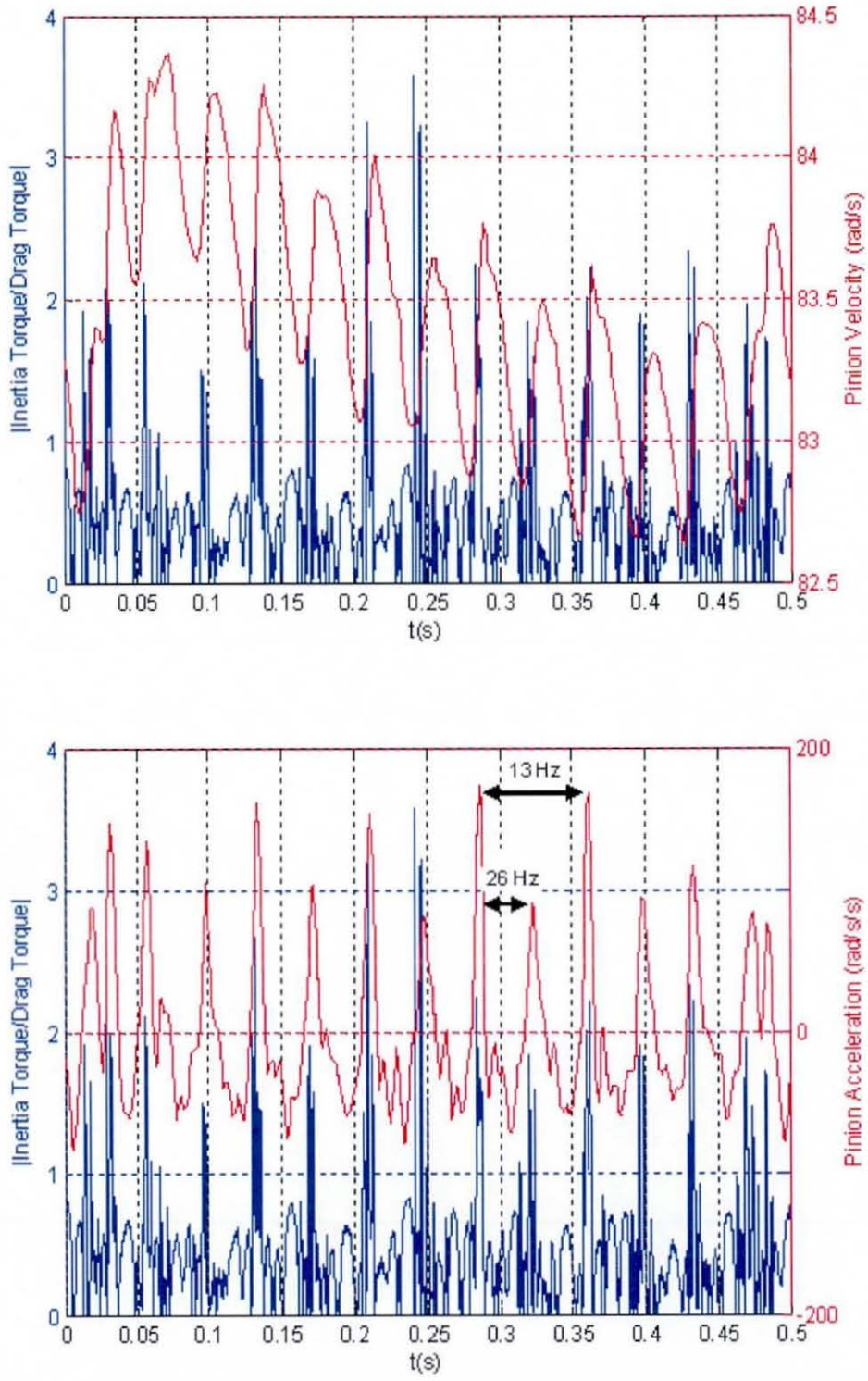

Figure 3.14: The rattle ratio, the pinion velocity and acceleration ($\eta_0 = 0.01520$ Pa.s. at 80.00^0 C)

At 20^0 C (figures 3.15 and 3.16), the second and third harmonics of the 255Hz component (511 and 766 Hz) are dominant and the band is centred on approximately 451Hz. As the temperature rises to 39.40^0 C (figure 3.17 and 3.18), the 255Hz component becomes stronger than its harmonics, this is could be due to the frequency band (with heavy modulation at 13 Hz) having approached it; the stronger frequency in the band is 309Hz.

Figures 3.19 and 3.20 show the wheel response at 80^0 C, and also show that the rattle ratio is well above one. The active frequencies are below the 255Hz and its harmonics and a band of multiples of the pinion rotational frequency (such as 92, 164, 206, 232Hz) dominating (in addition to the excitation frequencies).

It is evident that the change of temperature only affects the amplitudes of the 255Hz and its harmonics. On the other hand, the change of temperature causes a band of frequencies to move towards the lower spectral components. This band can be associated with gear rattle; this is because the band frequency shift can be related to the change in temperature (viscosity) as discussed above. Further more, the frequency 255Hz and its harmonics are attenuated when the system crosses the rattle threshold.

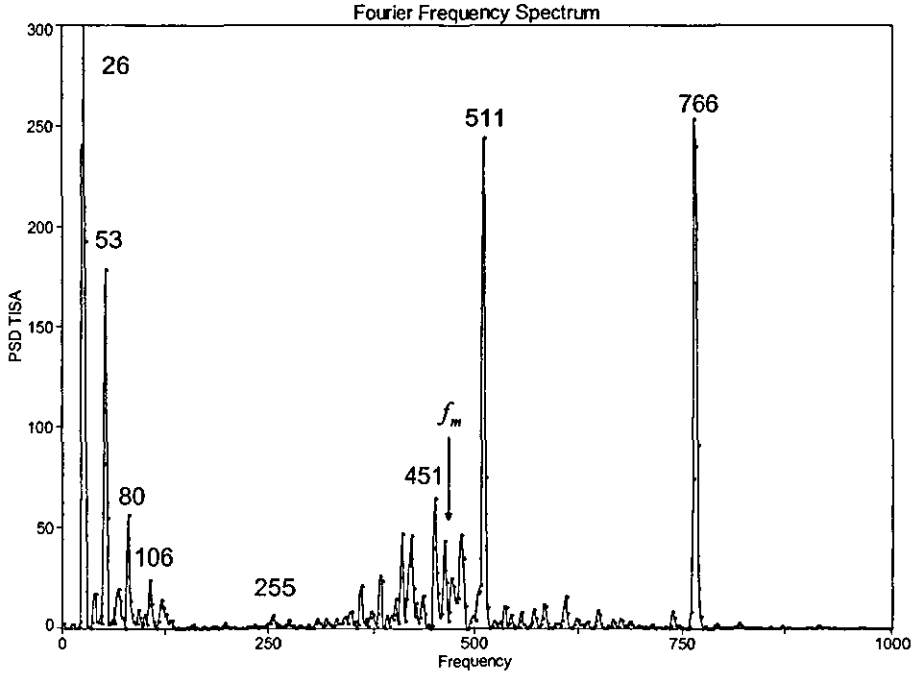

Figure 3. 15 (continued)

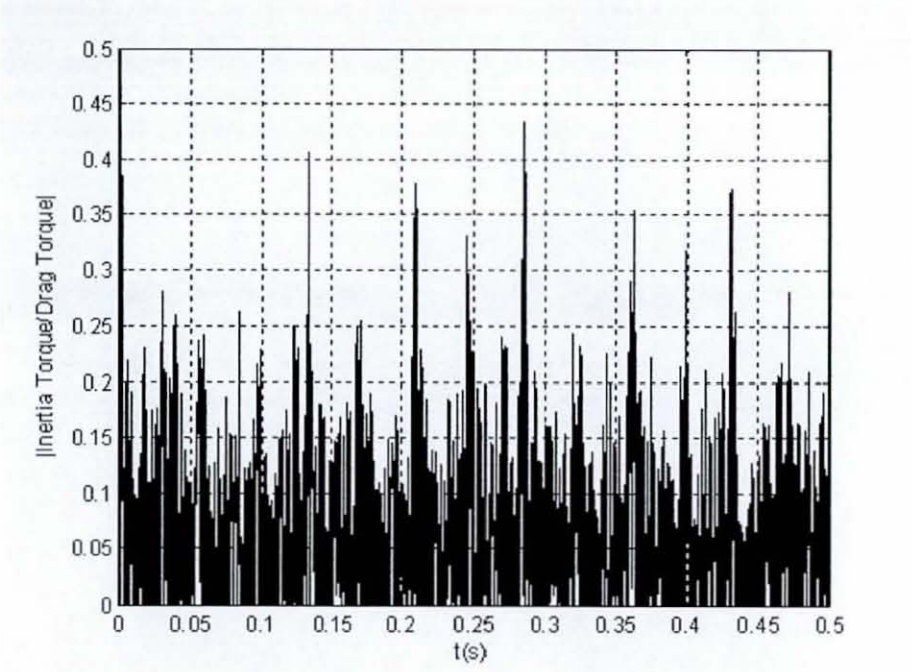

Figure 3. 15: Acceleration response and rattle ratio at 20°C and backlash 79μm

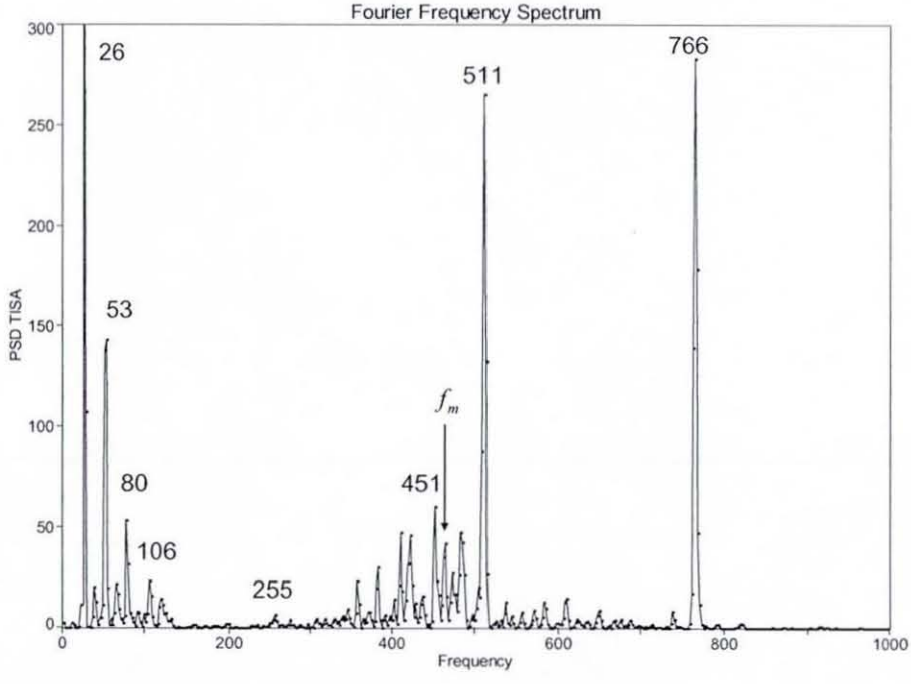

Figure 3.16 (continued)

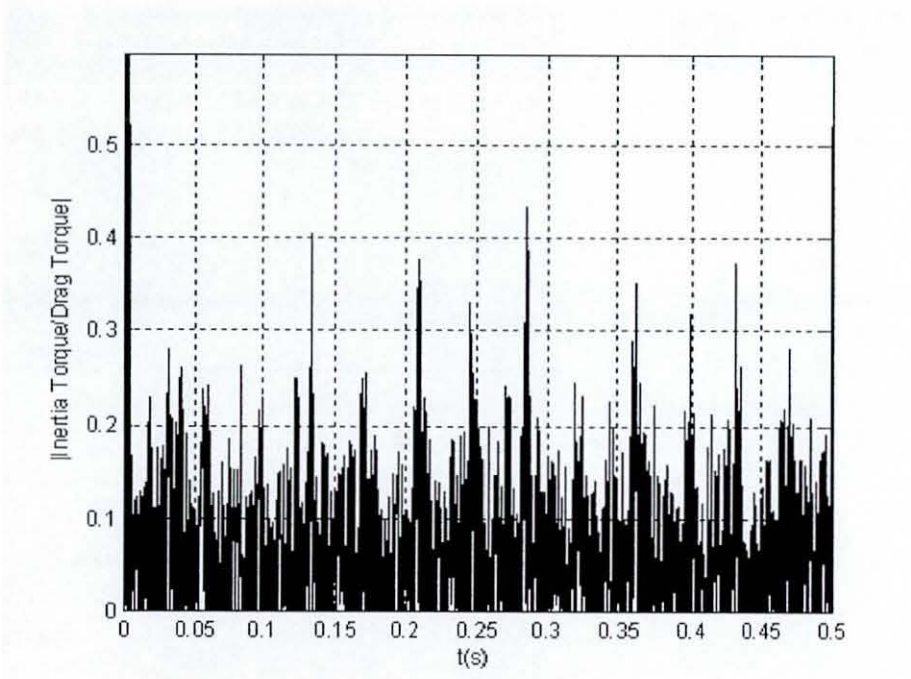

Figure 3. 16: Acceleration response and rattle ratio at 20°C and backlash 158μm

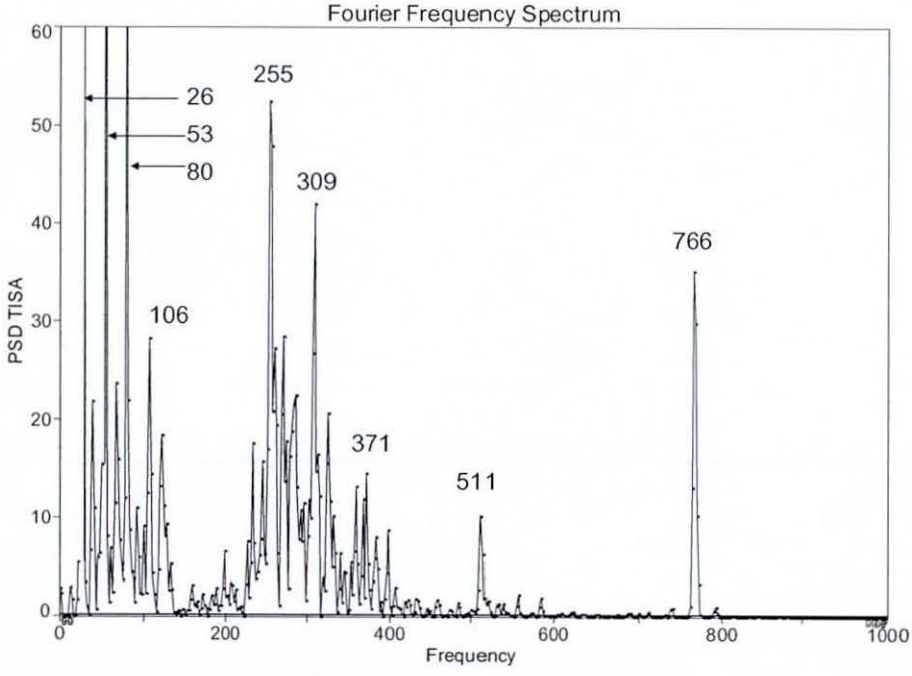

Figure 3.17 (continued)

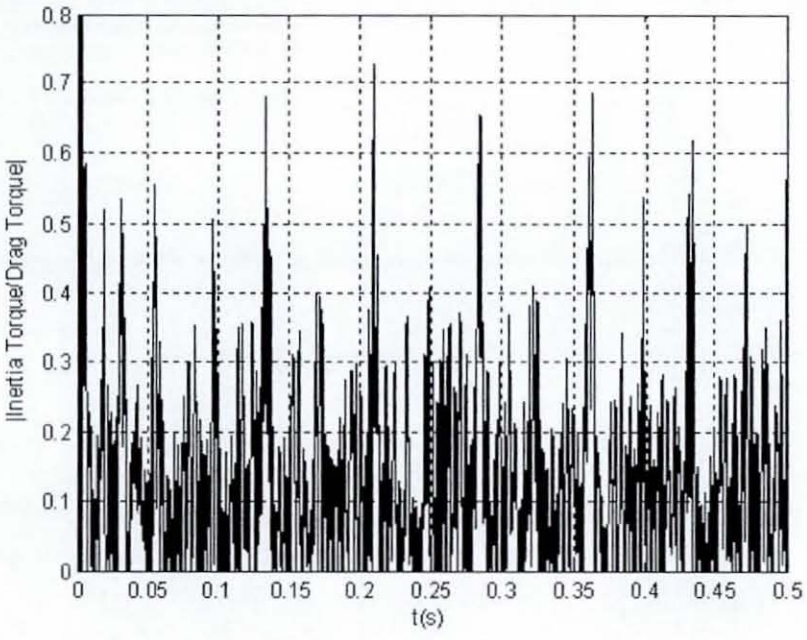

Figure 3. 17: Acceleration response and rattle ratio at 39.4°C and backlash 79μm

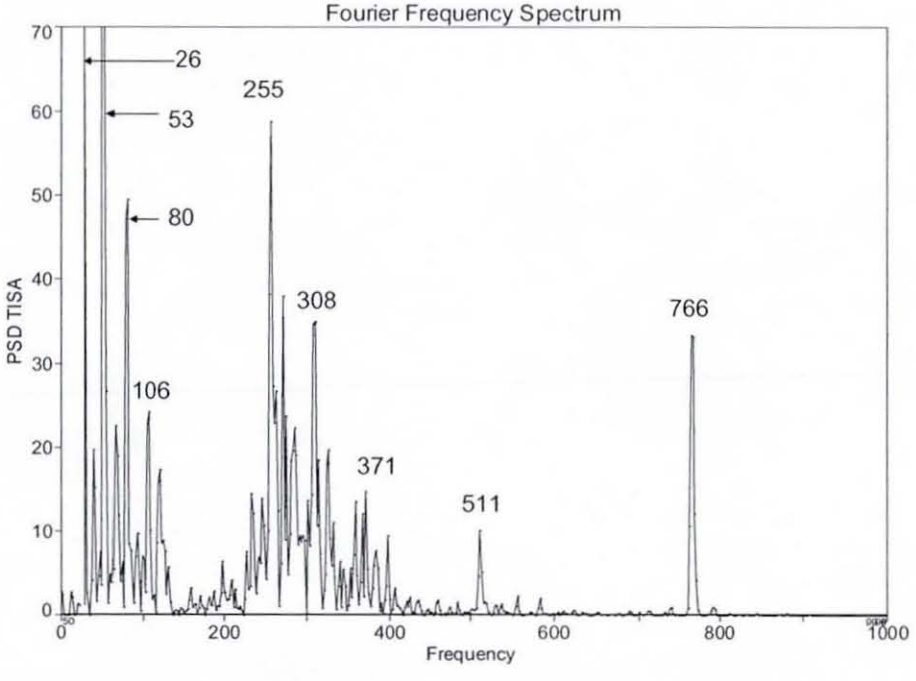

Figure 3.18 (continued)

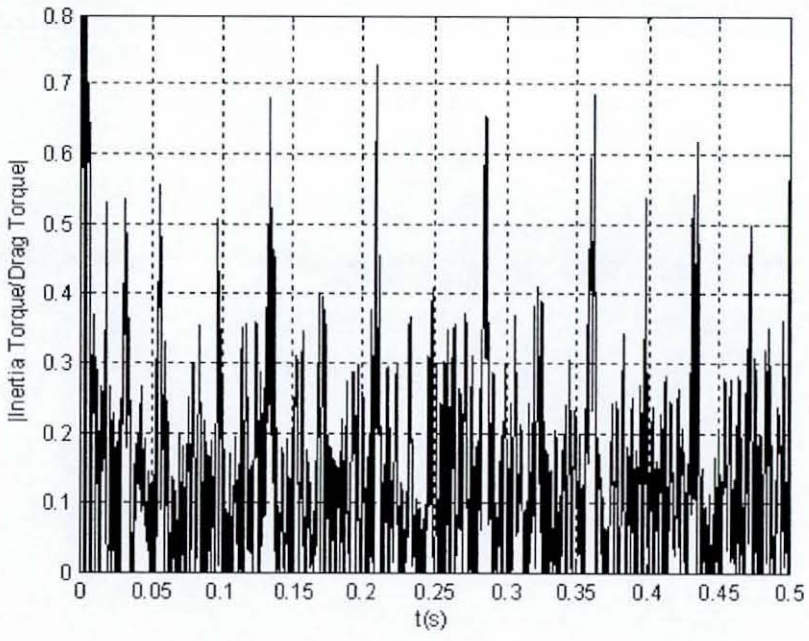

Figure 3. 18: Acceleration response and rattle ratio at 39.4°C and backlash 158μm

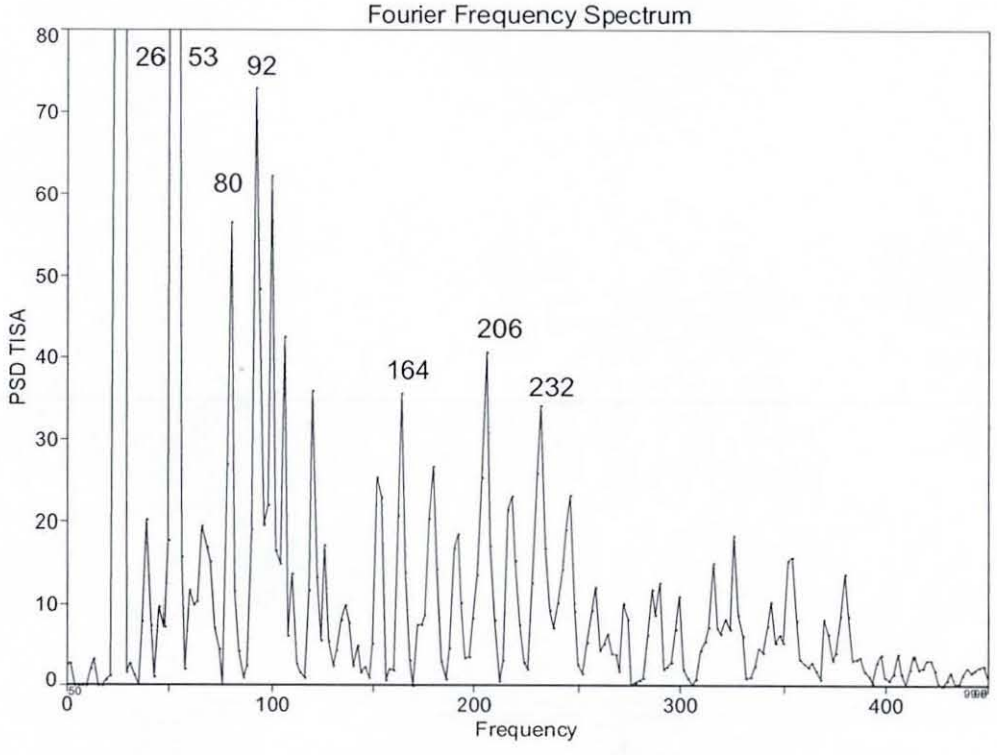

Figure 3.19 (continued)

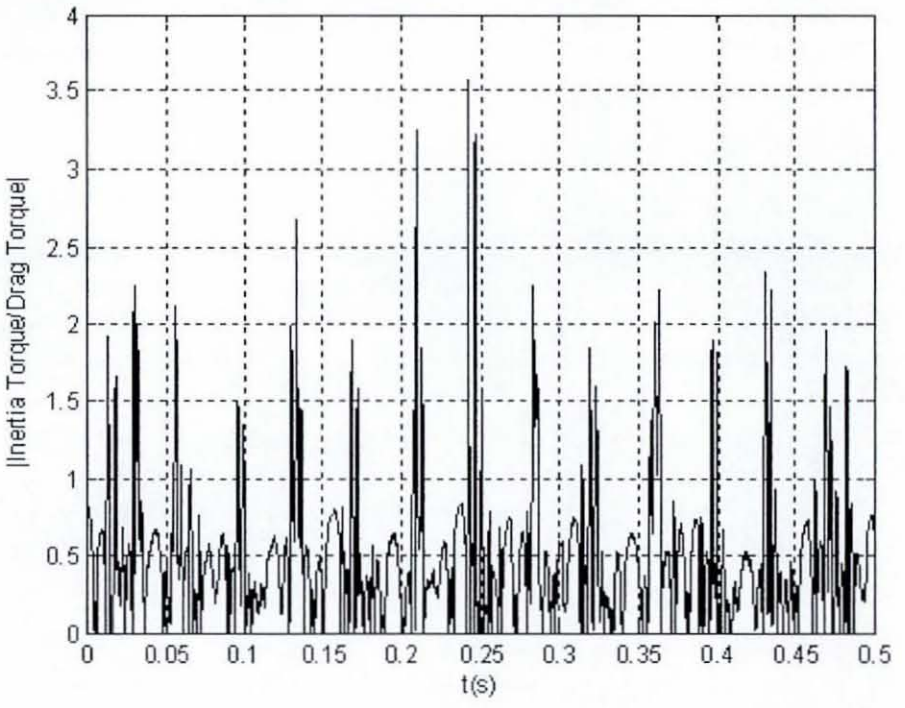

Figure 3. 19: Acceleration response and rattle ratio at 80°C and backlash 79µm

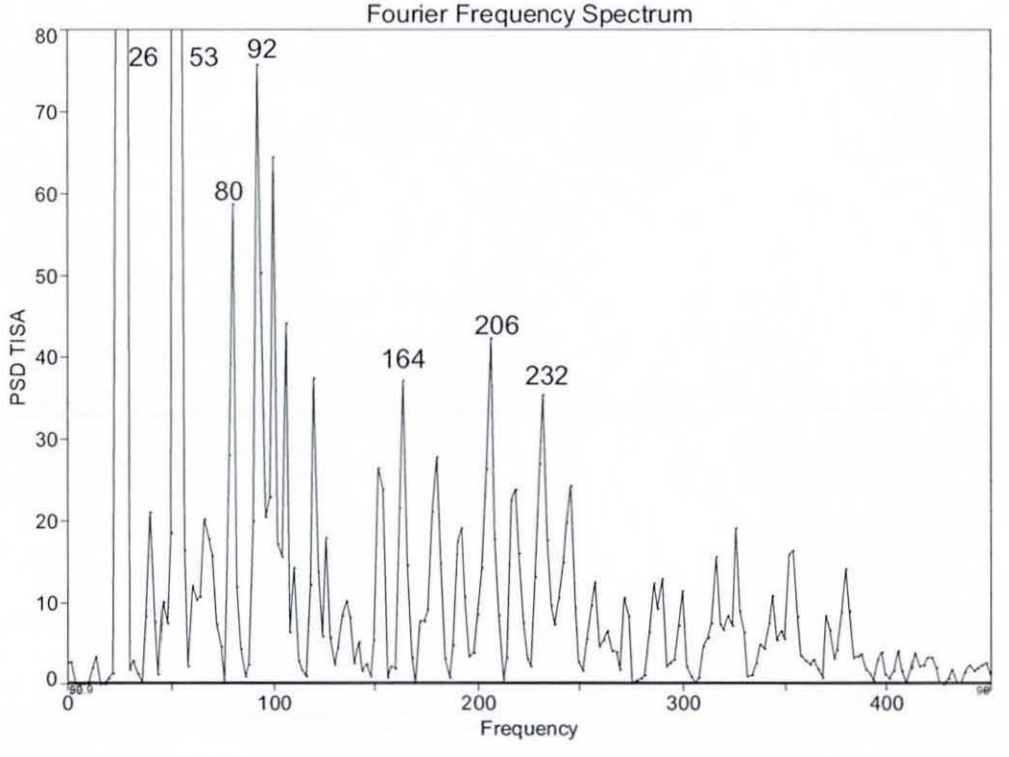

Figure 3.20 (continued)

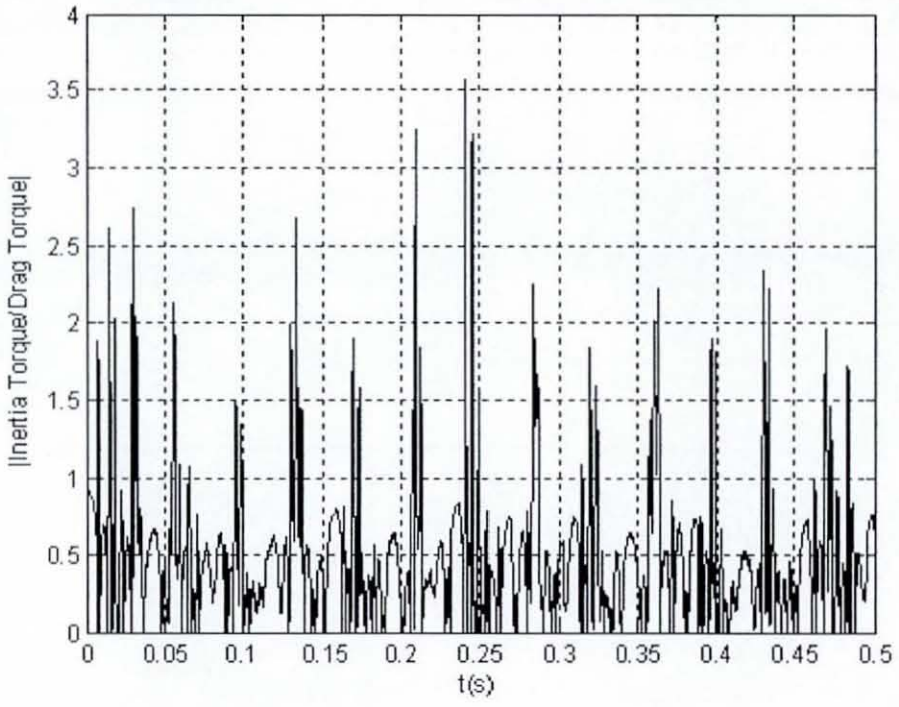

Figure 3. 20: Acceleration response and rattle ratio at 80° C and backlash 158μm

3.8.4 Effect of Bearing Clearance:

With a constant backlash ($79\,\mu m$) and at 20^0 C the frequency response shifts to lower spectral contributions as the bearing clearance increases (figures 3.15, 3.17, 3.19, and figures 3.21 to 3.26). Similar to the findings in section 3.8.3, the responses in the figures show that the frequency 255Hz and its harmonics are affected by the change of bearing clearance only in terms of their amplitude. The response in general is super-harmonics of the pinion rotational frequency (13 Hz).

A band of frequencies initially centred on 1604 Hz when the bearing clearance is 10μm (figure 3.21) moves to 451Hz (figure 3.15) and then to 248Hz (figure 3.22) as the bearing clearance is increased to 35 and 60 μm, respectively; this is similar to what is mentioned in section 3.8.3 regarding the effect of temperature. This band is the response of the wheel due to the squeeze action modulated by the pinion rotational frequency. The size of the band depends on the frequency deviation during modulation: the higher the deviation, the broader the band (see Connor, 1982). The

squeeze action is being sped up and slowed down regularly by the pinion rotational velocity, hence the modulation. The amount, by which the squeeze being sped and slowed, represents the frequency deviation.

A similar effect is seen at 39.40^0 C, but the amplitude remains higher when the clearance is 10 μm (see figures 3.23, 3.17, and 3.24). At bearing clearance of 10 μm (figure 3.23) the band is centred on 1007Hz, then it shifts to 309 Hz when the clearance is 35 μm (figure 3.17), and when the clearance is 60 μm (figure 3.24), the band is centred on 120Hz.

At 80^0 C the dominant frequencies are lower with reduced amplitudes, and the rattle ratio reaches its highest value (see figures 3.25, 3.19. and 3.26). At bearing clearance of 10 μm (figure 3.25) a band of frequencies (478-683Hz) approximately centred on 577Hz is observed, then as the bearing clearance is increased to35 μm (figure 3.19), the band shifts to 206Hz, before it reaches 178 and 184Hz when the bearing clearance is 60 μm (figure 3.26). The system crosses the rattle threshold earlier (compared to the lower temperatures discussed above) at bearing clearance of 35 μm (figure 3.19Figure 3. 19). Figure 3.25 shows that the bearing clearance is still effective (in constraining the system from crossing the rattle threshold) even when the temperature is high (80^0 C).

It is evident from the figures that rattling occurs as a band of low frequencies that shift towards the lower spectral contributions as the drag resisting the wheel motion decreases. This is because the frequency shift can be related to the change in bearing clearance as discussed above. Further more, the frequency 255Hz and its harmonics are attenuated when the system crosses the rattle threshold.

3.9 Conclusions

- Under fully flooded conditions, the hydrodynamic flank friction can be ignored at least within the modelled temperature range 20 – 80 ^{0}C.

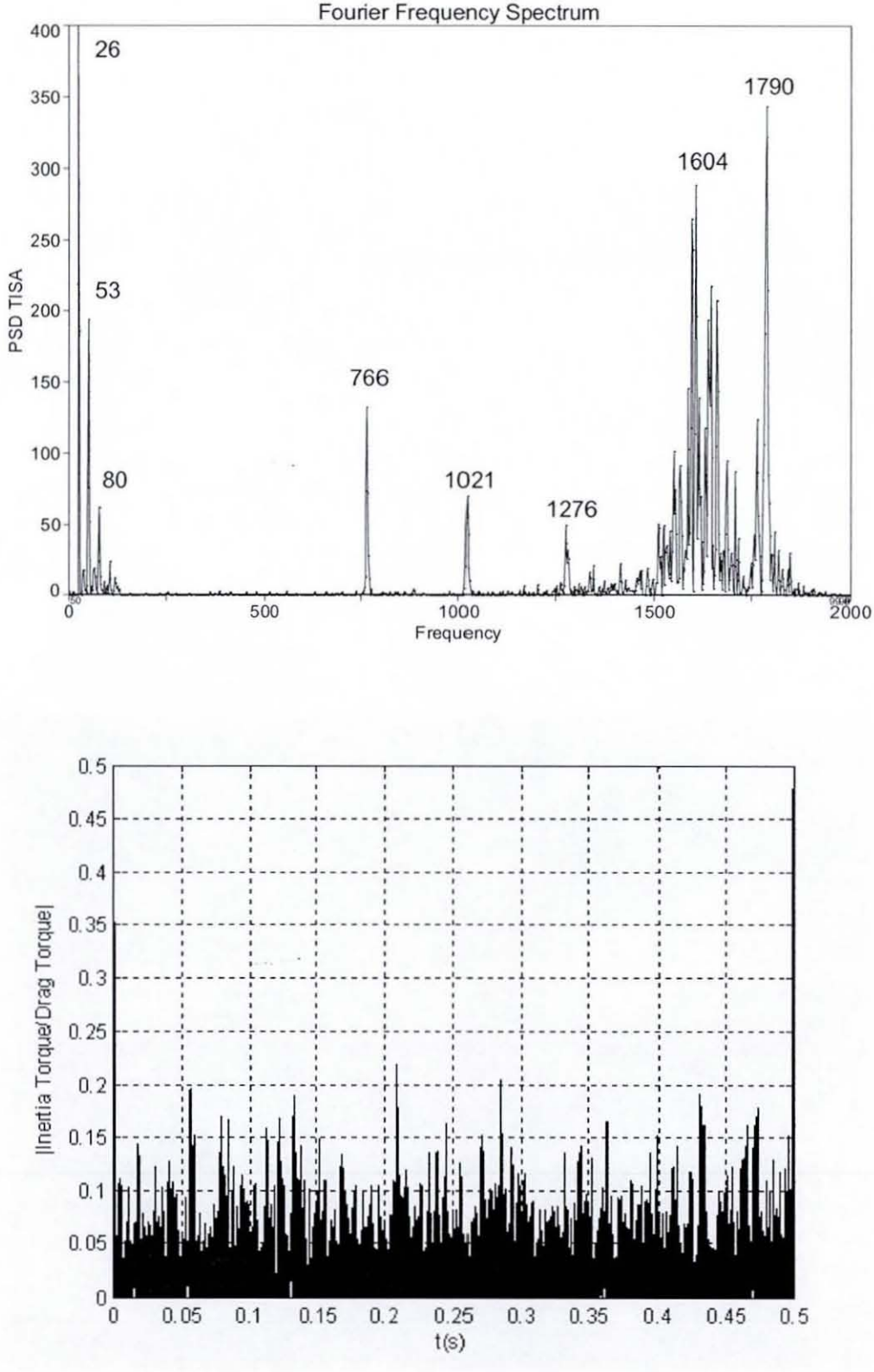

Figure 3. 21: Effect of change in bearing clearance (20 °C and 10μm)

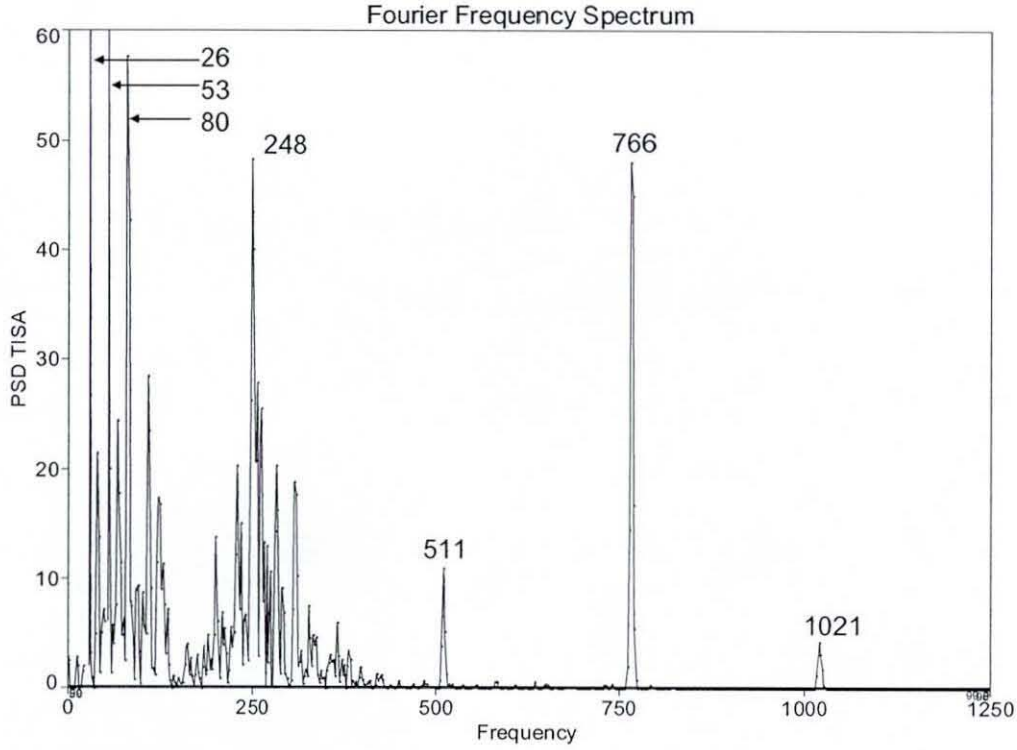

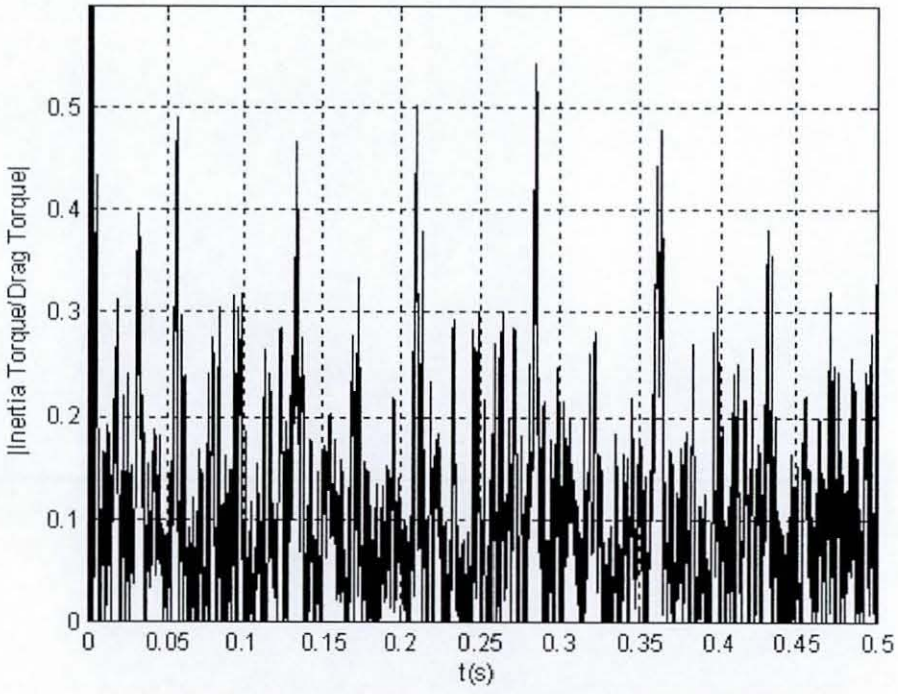

Figure 3. 22: Effect of change in bearing clearance (20 ° C degrees and 60μm)

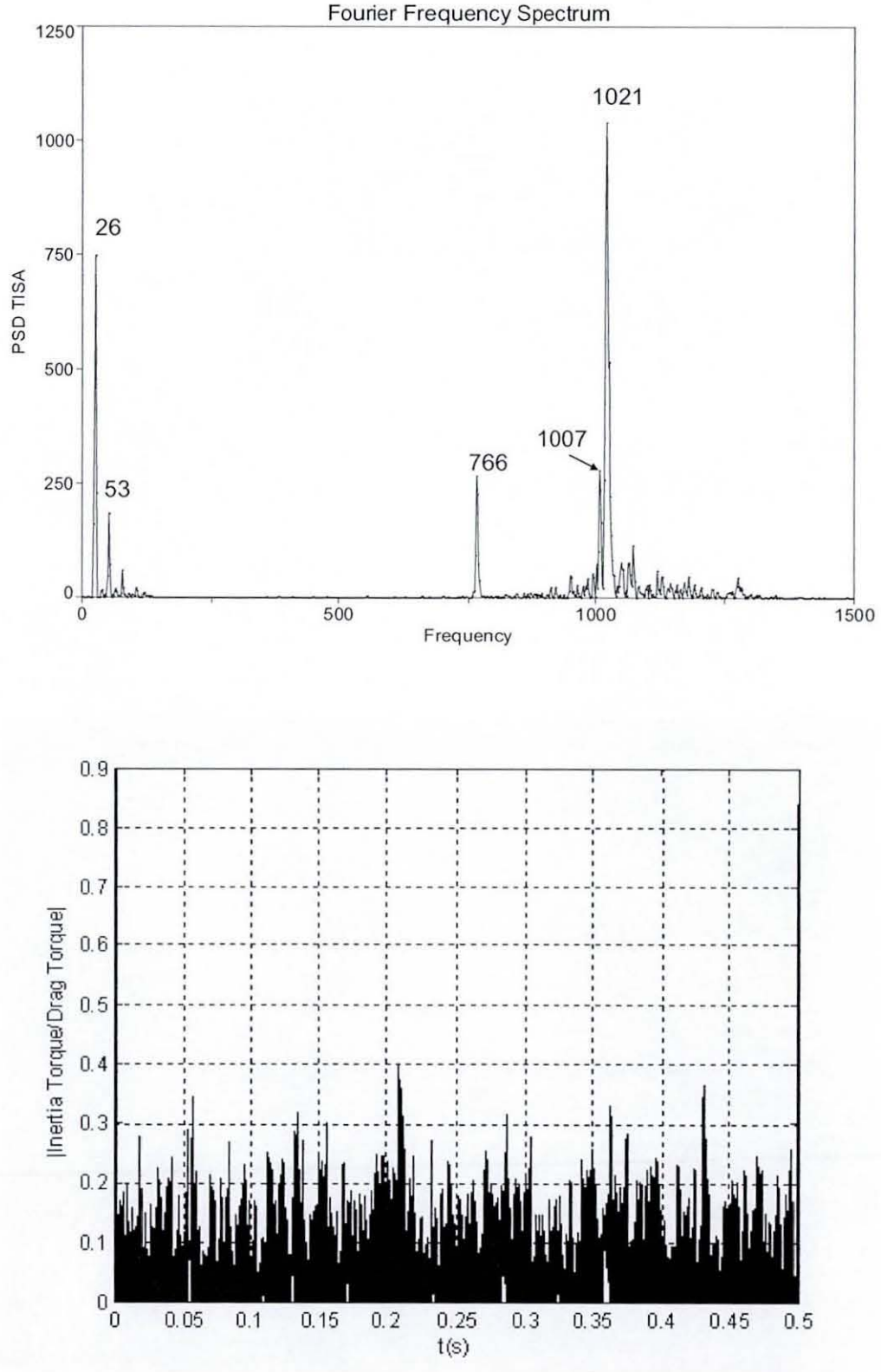

Figure 3. 23: Effect of change in bearing clearance (39.4 ° C and 10μm)

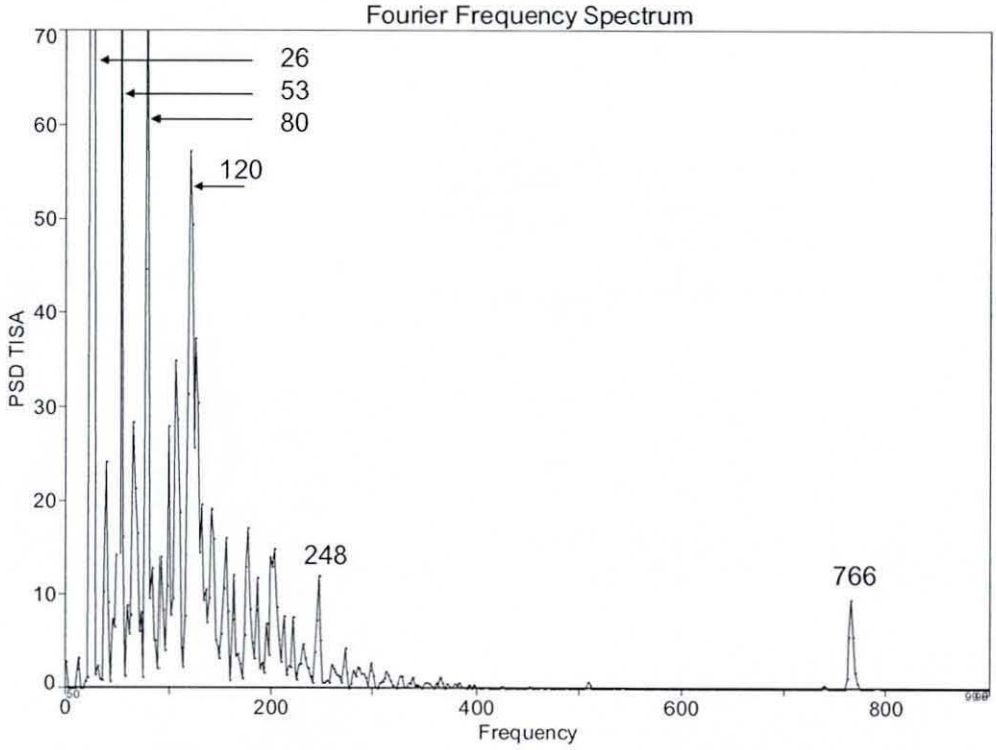

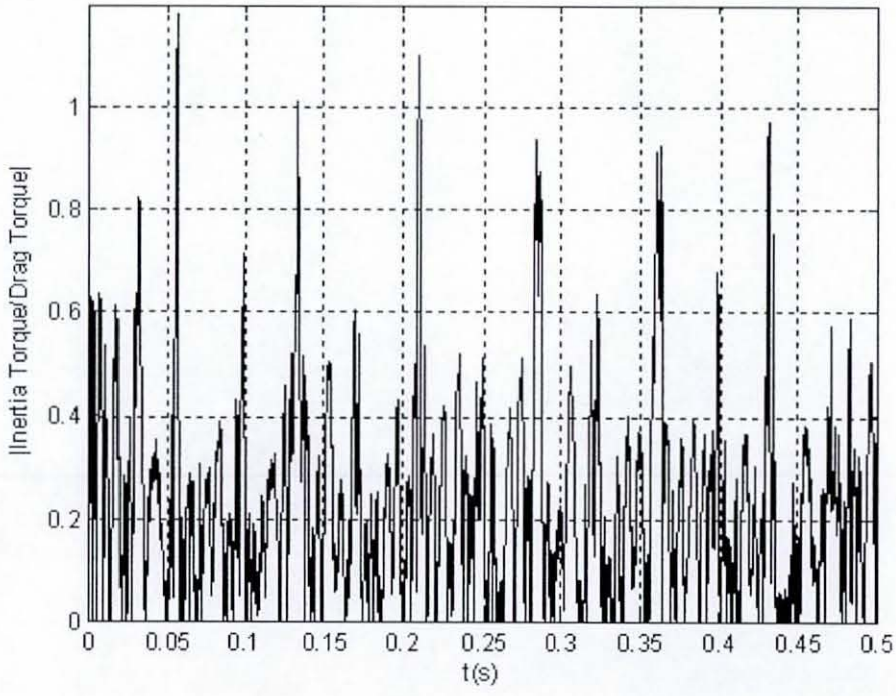

Figure 3. 24: Effect of change in bearing clearance (39.4 °C and 60μm)

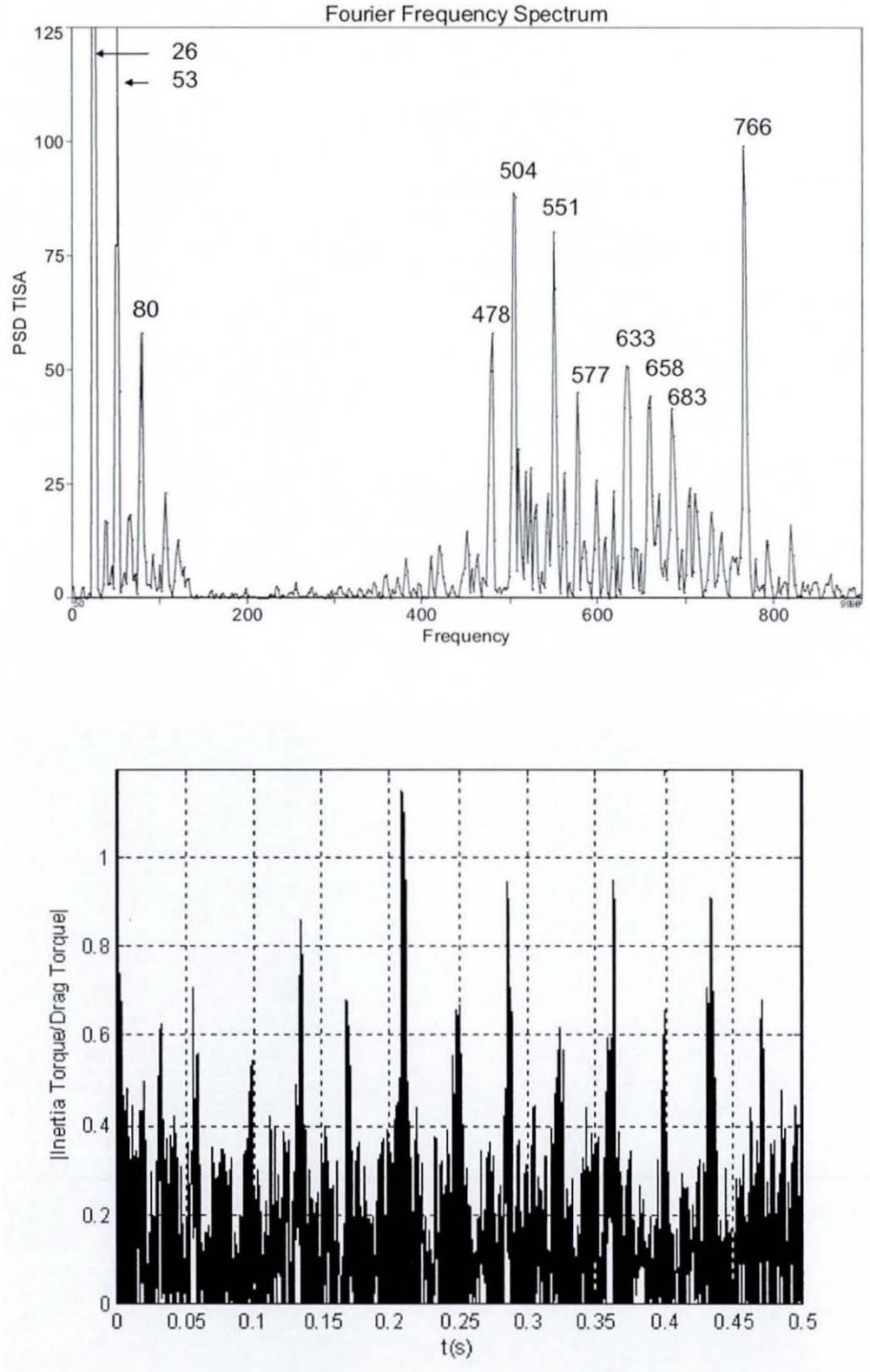

Figure 3. 25: Effect of change in bearing clearance (80 °C and 10μm)

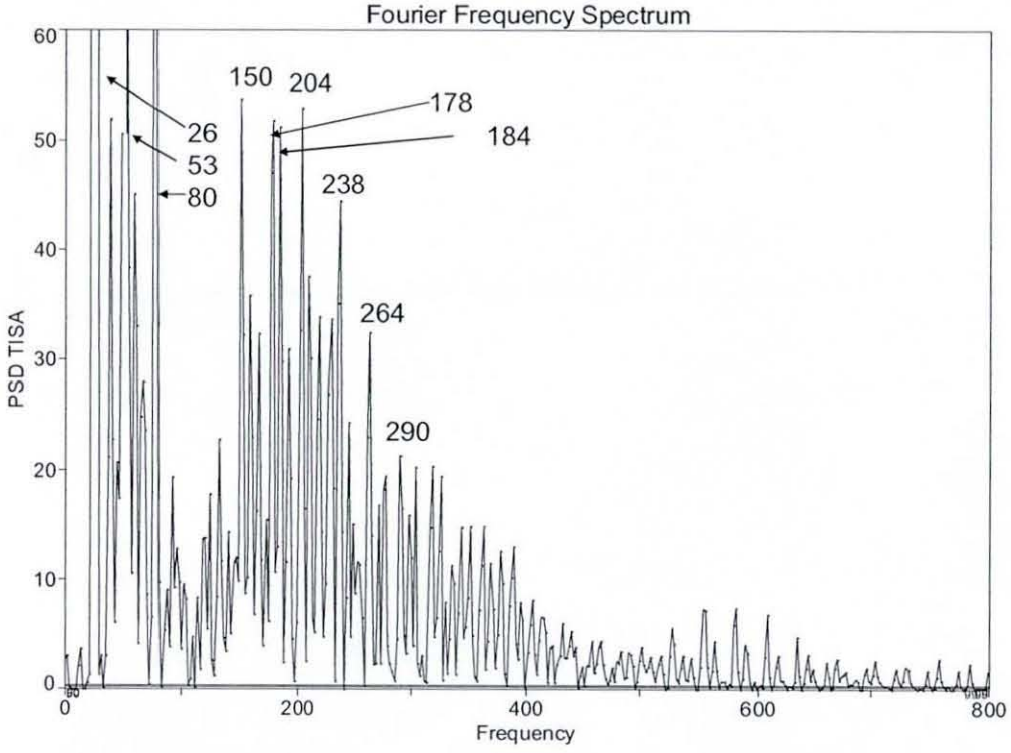

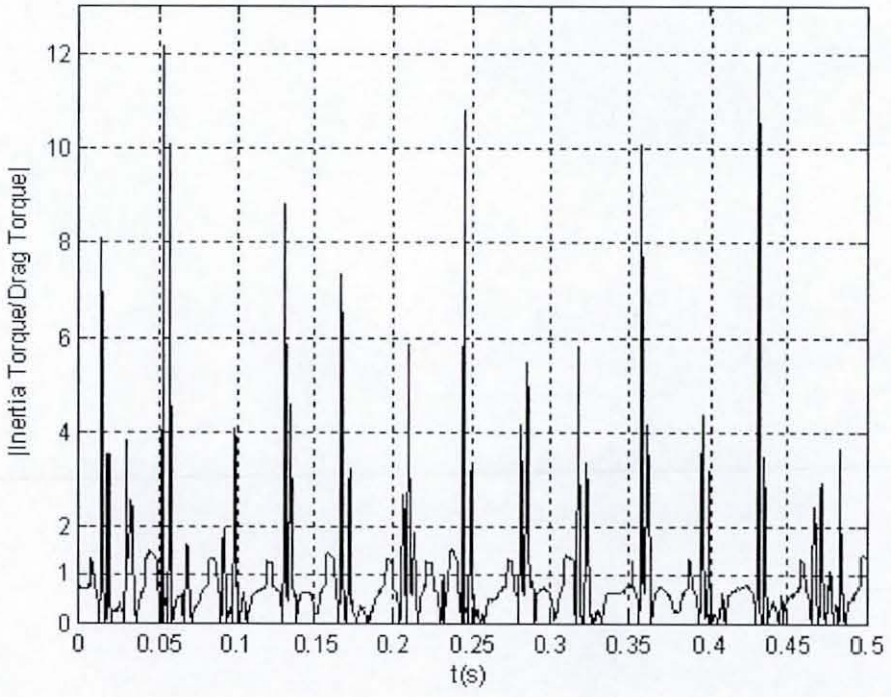

Figure 3. 26: Effect of change in bearing clearance (80 °C and 60μm)

- Assuming hydrodynamic conditions, the rattle ratio $RR = \frac{Inertia\ Torque}{Drag\ Torque}$ increases as temperature rises.

- Under fully flooded conditions, the effect of viscosity is more significant than the amount of backlash. This is because the motion of the tooth within the backlash is governed by the lubricant reaction force.

- The bearing clearance has a strong effect on the system response. The bearing clearance (being in the denominator of Petrov's formula) has a significant contribution to the drag torque, which, together with the inertia torque, determines the threshold at which rattle commences.
- The oil viscosity and bearing clearance play important roles in determining the frequency response of the system, the rattle ratio, and, thus the propensity of the system to rattle.
- A band of frequencies was identified as the possible rattle frequency band as its position in the loose wheel acceleration spectrum is directly affected by the change in either the oil viscosity or the bearing clearance.
- The size of the band is small suggesting long impact time; furthermore, the band tends to be lower in amplitude when compared to the main excitation frequencies (26, 53, and 80 Hz) suggesting effective impact damping particularly at low frequencies. Nevertheless at higher frequencies (figure 3.21 and 3.23), the band shows stronger spectral contribution.

Chapter 4: Transmission Models

4.1 Introduction

In this chapter, the single degree of freedom model concept is extended to a full automotive front wheel drive (FWD) transaxle transmission. Two non-linear models have been developed for this purpose; the first is a seven-degree of freedom torsional model, aiming to depict the rotational vibrations of the idle gears only. The second model is an 11-degree of freedom model, which also takes into account the lateral and transverse motions of the output shafts carrying the idle gears. Finally, a 12-degree of freedom linearised model is developed for the purpose of extracting the natural frequencies of the contact and the corresponding mode shapes.

4.2 The Torsional Model

The layout of the front wheel drive transaxle gearbox is shown in figure 4.1. It comprises an input shaft, which receives the engine torque and two output shafts transmitting torque to the front wheels via the differential unit. When either of the two output shafts is engaged to one of its gears via a synchroniser, the other output shaft rotates on its bearings due to the constant mesh with the differential ring gear. Since all gears on the output shafts are not engaged when the transmission is set to neutral, the two shafts do not transmit torque and they do not rotate. All driving gears (pinions) lie on the input shaft except the reverse pinion, which lies on the first output shaft as shown in figure 4.1. The first wheel and reverse pinion are manufactured as one unit; hence, their rotational speeds are identical.

The angular displacement $\varphi_{in}(t)$, velocity $\dot{\varphi}_{in}(t)$ and acceleration $\ddot{\varphi}_{in}(t)$ time histories of the input shaft are known (using real data from experimental measurements in vehicle). Therefore, the motion of the system is adequately described by the following

set of generalized coordinates $(\varphi_1 \quad \varphi_2 \quad \varphi_3 \quad \varphi_4 \quad \varphi_5 \quad \varphi_6 \quad \varphi_7)^T$, where φ_1 corresponds to the idle gear of the 1st speed and the pinion of the reverse, and $\varphi_{i(i=2...7)}$ corresponds to the idle gears of the 2nd to reverse.

Each idle gear $i(i=1...7)$ is driven by transitive hydrodynamic force, W_{it}, from its pinion and is resisted by the transitive component of the hydrodynamic friction force, F_{fit}, acting on the tooth flanks, and Petrov tractive force, F_{pi}, due to the action of the lubricant between the idle gear and its shaft. The motion of the first idle gear, however, is also resisted by the transverse component of the reaction force due to the contact between the reverse pinion and its idle gear, W_{7t}. The equations of motion describing the system are as follows:

1st speed idle gear:

$$I_1\ddot{\varphi}_1 = W_{1t}r_1 - W_{7t}r_{p7} - F_{f1t}r_1 - F_{p1}r_{s1} \tag{4.1}$$

The rest of the loose wheels $(i=2,\ldots,7)$ are represented by the following equation:

$$I_i\ddot{\varphi}_i = W_{it}r_i - F_{fit}r_5 - F_{pi}r_{si} \tag{4.2}$$

The radii $r_{i=1...7}$ are the pitch radii of the idle gears; and r_{p7} is the pitch radius of the reverse pinion, while $r_{si=1...7}$ are the internal radii of the idle gears, which represent the outside radii of the assumed journal bearings. The hydrodynamic reaction force W_{it} and the hydrodynamic friction force F_{fit} $(i=1,2,\ldots,7)$ are, respectively, the sum of the hydrodynamic and friction forces acting on each tooth in simultaneous contact as described in chapter 3.

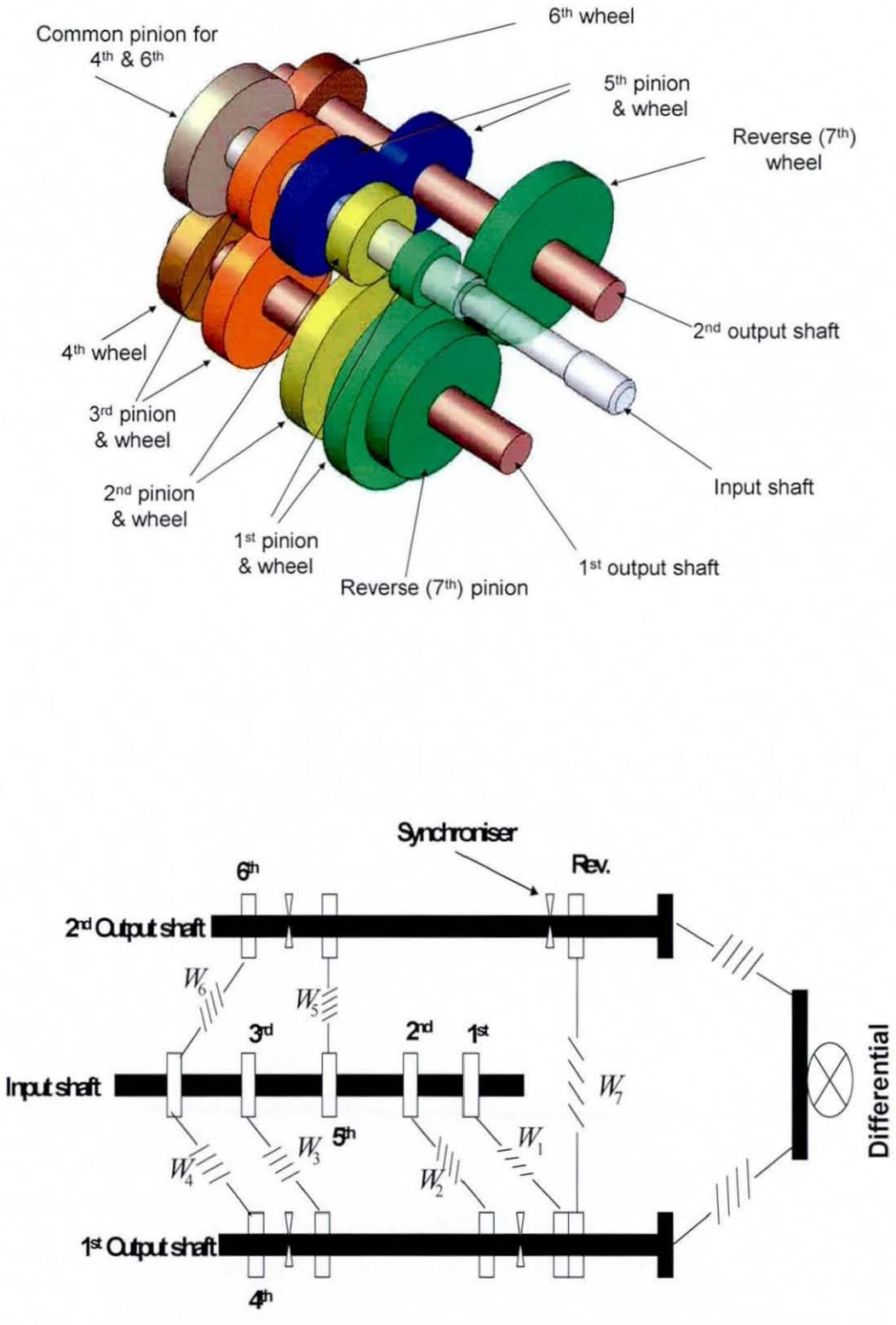

Figure 4.1: FWD Transaxle 3D diagram and schematic

4.3 11-Degree of Freedom Transmission Model:

In section 4.2, a seven-degree of freedom torsional system is presented. This section expands on the torsional model by adding four translational degrees of freedom, describing the lateral and transverse motions of the two output shafts (at their corresponding centres of mass). Therefore, the motion of the expanded system is described by the following set of 11 generalized coordinates $(\varphi_1, \varphi_2, \ldots, \varphi_7, x_1, y_1, x_2, y_2)^T$. The coordinate systems describing the shafts and their bearings are shown in figures 4.2 to 4.5. Figure 4.2 is a front view of the transmission showing the location of the shafts' coordinate systems with respect to the engaged teeth position at the pitch point. The axes x_1 and x_2 lie along the gearing centre lines of the first and second output shafts, respectively. It should be noted that the origins of these coordinate systems lie at the centre of mass of each shaft. It also shows the relative angular locations of the output shafts and the input shaft with respect to their gearing centre-lines. The directions of the film reaction components (in the transverse and radial directions) with respect to those coordinate systems are shown in figure 4.3 for all gear pairs, except for the reverse, which straddles the two output shafts as shown in figure 4.1. Hence, the directions of its film reaction components are as shown in figure 4.4. Figure 4.5 depicts the bearings effect on the system as non-linear springs acting through the centre of masses, thus, assuming that the tapered roller bearings on the shaft are maintained in a preloaded condition and quasi-static shaft/housing temperature, a valid assumption given the low transmission loads and slow temperature rise during idling, only the shafts movement in the transverse planes is considered neglecting the motion in the axial and rotational (rocking) directions.

The additional set of equations of motion (added to the aforementioned torsional equations (4.1) and (4.2) is:

1st shaft (figure 4.5 views A and C) in the x_1 and y_1 directions, respectively:

$$M_1 \ddot{x}_1 = F_{x1} - \Lambda_{ax} - \Lambda_{bx} \qquad (4.3)$$

$$M_1\ddot{y}_1 = F_{y1} - \Lambda_{ay} - \Lambda_{by} \qquad (4.4)$$

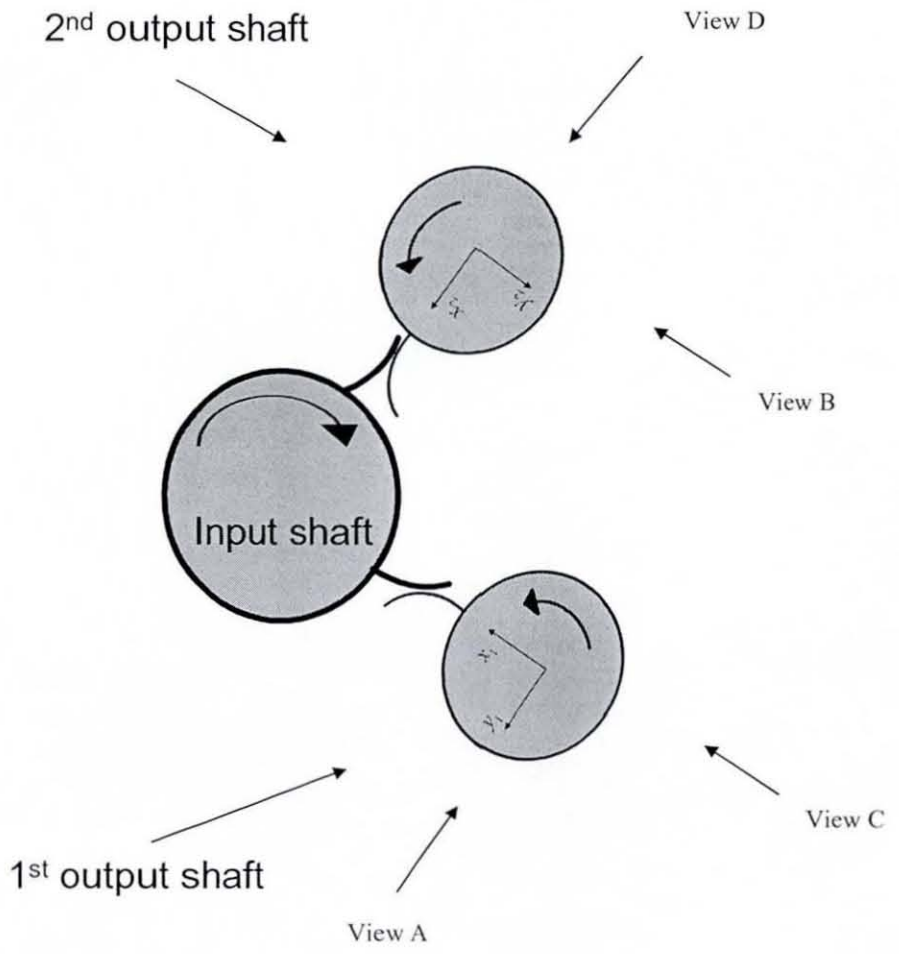

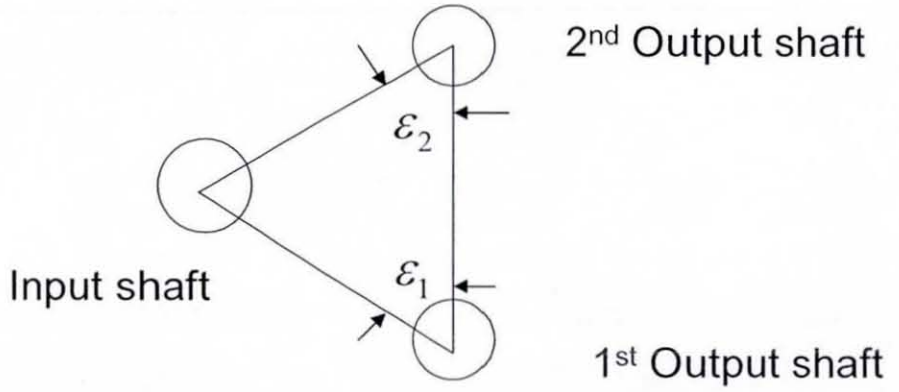

Figure 4.2: Output shafts co-ordinate system relative to tooth contacts

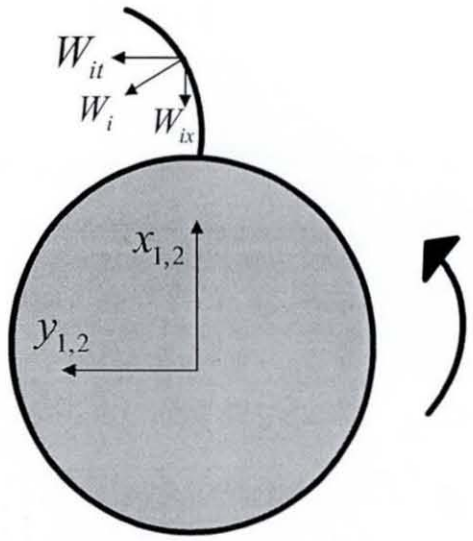

Figure 4.3: Forces acting on idle gears (except reverse) on 1st and 2nd output shafts

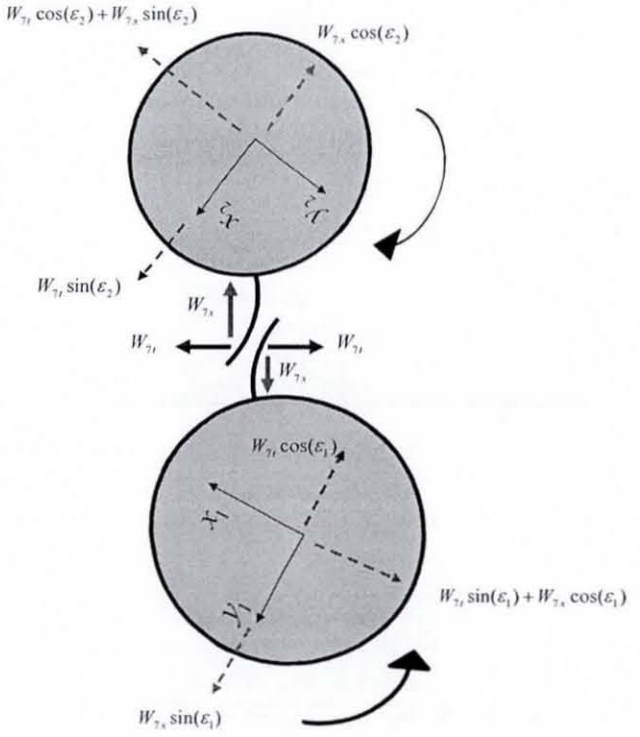

Figure 4.4: Forces acting on the reverse gear pair

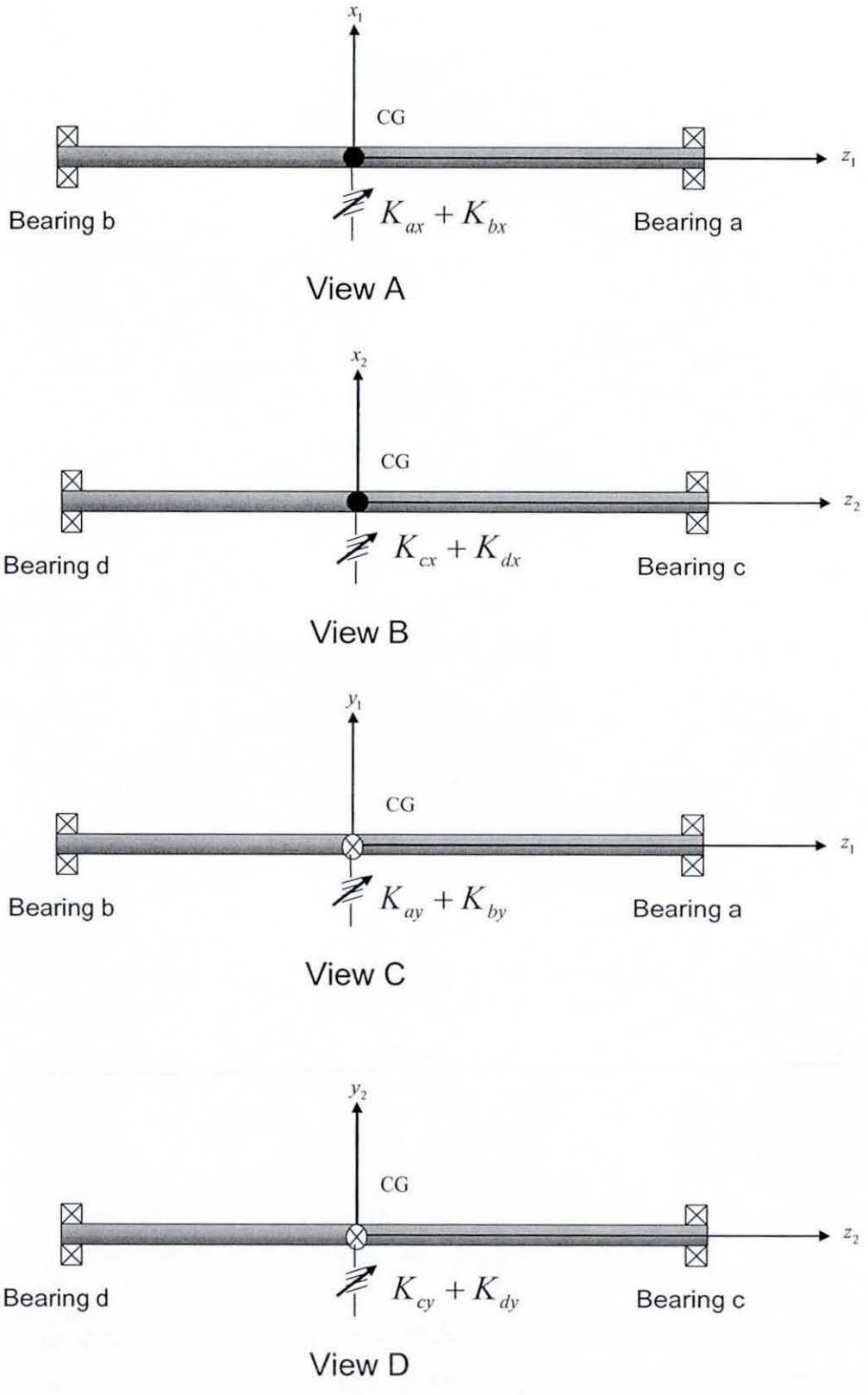

Figure 4.5: Shafts and bearings coordinate systems and bearing stiffness

2^{nd} shaft (figure 4.5 views B and D) in the x_2 and y_2 directions, respectively

$$M_2\ddot{x}_2 = F_{x2} - \Lambda_{cx} - \Lambda_{dx} \tag{4. 5}$$

$$M_2\ddot{y}_2 = F_{y2} - \Lambda_{cy} - \Lambda_{dy} \tag{4. 6}$$

The forces denoted by $\Lambda_{ax}, \Lambda_{ay}, \Lambda_{bx}, \Lambda_{by}, \Lambda_{cx}, \Lambda_{cy}, \Lambda_{dx}, and\ \Lambda_{dy}$ are the bearing reactions. They depend on the stiffness coefficients $K_{ax}, K_{ay}, K_{bx}, K_{by}, K_{cx}, K_{cy}$, K_{dx}, and K_{dy} shown in figure 4.5. The bearing reaction forces are treated in section 4.4.

The rectilinear forces $F_{x1}, F_{y1}, F_{x2}, and\ F_{y2}$ are the resultant forces acting on the shafts due to the radial and transverse components of the hydrodynamic film reaction and are determined as follows:

a- The first output shaft, which contains the 1^{st} to the 4^{th} idle gears and reverse pinion:

The sum of all force components acting along the axis x_1, which includes 1^{st} to 4^{th} gear radial forces (figure 4.3) in addition to the components of the reverse pair radial and transverse forces as a result of their positions in the system (figures 4.2 and 4.4), is given by:

$$F_{x1} = \sum_{i=1}^{4} W_{ix} - W_{7t}\sin(\varepsilon_1) + W_{7x}\cos(\varepsilon_1) \tag{4. 7}$$

The angle ε_1 is the angular distance between the reverse pair centre-line and the axis x_1 (figure 4.2).

The radial component of the hydrodynamic mesh force of the i^{th} gear pair is given by:

$$W_{ix} = -\sum_{j=1}^{N_{total}} W_{ij}\sin\alpha_n\,. \tag{4. 8}$$

Likewise, the sum of all force components acting along the axis y_1, which includes 1st to 4th gear transverse forces (figure 4.3), in addition to the components of the reverse pair radial and transverse forces (figures 4.2 and 4.4), is given by:

$$F_{y1} = \sum_{i=1}^{4} W_{it} - W_{7t}\cos(\varepsilon_1) - W_{7x}\sin(\varepsilon_1) \qquad (4.9)$$

b- The second output shaft, which contains the 5th, 6th, and 7th (idle reverse gear) gears:

As in the case of first output shaft, the sum of all force components acting along the axis x_2, which includes the 5th and 6th gear radial forces (figure 4.3) in addition to the components of the reverse pair radial and transverse forces as a result of their relative positions in the system (figure 4. 2 and 4.4) is given by:

$$F_{x2} = \sum_{i=5}^{6} W_{ix} + W_{7t}\sin(\varepsilon_2) + W_{7x}\cos(\varepsilon_2) \qquad (4.10)$$

The angle ε_2 is the angular distance between the reverse pair centre line and the axis x_2 (figure 4.2).

In a similar fashion, the sum of all force components acting along the axis y_2, which includes the 5th and 6th gear transverse forces (figure 4.3) in addition to the components of the reverse pair radial and transverse forces (figures 4.2 and 4.4) is given by:

$$F_{y2} = \sum_{i=5}^{6} W_{it} - W_{7t}\cos(\varepsilon_2) + W_{7x}\sin(\varepsilon_2) \qquad (4.11)$$

The rectilinear forces $F_{x1}, F_{y1}, F_{x2}, and\ F_{y2}$ represent the coupling terms between the torsional and translational equations of motions. The hydrodynamic reaction depends on the normal film thickness as described by equation (3.25). Hence, when the translational motion of the output shafts are considered, their instantaneous displacement and velocities change the size of the normal film thickness and squeeze

velocity, respectively. When this change is considered, equation (3.23) changes as follows:

$$h = C_b - \frac{\left|\left(r_w\varphi_w + \delta h - r_p\varphi_p\right)\right|}{\cos\alpha_n \cos\beta} \qquad (4.12)$$

Where, δh is the added displacement due to shaft's instantaneous displacement (assuming that the input shaft is rigidly fixed) and is expressed as follows:

For the 1st, 2nd, 3rd, and 4th gear pairs, the value of δh depends on the displacement of the first output shaft in the y_1 direction (figure 4.3):

$$\delta h = y_1 . \qquad (4.13)$$

For the 5th and 6th gear pairs, the value of δh depends on the displacement of the second output shaft in the y_2 direction (figure 4.3):

$$\delta h = y_2 . \qquad (4.14)$$

Since the reverse gear pair straddles the two output shafts, then the corresponding value of δh depends on the relative displacement of both output shafts in the x_1, x_2, y_1, and y_2 directions (figure 4.4):

$$\delta h = \underbrace{\left(x_2 \sin\varepsilon_2 - y_2 \cos\varepsilon_2\right)}_{1} - \underbrace{\left(x_1 \sin\varepsilon_1 + y_1 \cos\varepsilon_1\right)}_{2} . \qquad (4.15)$$

Where, the first term is the amount of change caused by the displacement of the second output shaft and the second term is the amount of change caused by the displacement of the first output shaft.

4.4 Bearing restoring forces:

The transmission under investigation is equipped with tapered roller bearings at the end of the output shafts. As stated above, the 11-degree of freedom model does not consider the motion of the output shafts in the axial direction. Therefore, only the radial components of the bearing restoring forces are considered in the model. It should also be noted that the input shaft is assumed to undergo rotational motion only.

While the vehicle is idling, the output shafts do not rotate. Hence, there are no centrifugal forces or gyroscopic moments affecting the load distribution among the supporting bearing elements. Furthermore, the frictional forces and moments are negligible (see Harris, 2001). The bearing system is assumed to behave as a system of nonlinear springs acting in the x_1, x_2, y_1, and y_2 directions, neglecting each shaft's rocking motion about its centre of mass. Assuming no radial clearance, the total restoring force of the k^{th} bearing acting in the x-or y- direction Λ_{kr} can be approximated as follows (Harris, 2001):

$$\Lambda_{kr} = 0.2453 m_k Q_{kr} \delta_{kr}^{1.11} \cos\gamma_k, \ (k = a,b,c,d; r = x_1, y_1, x_2, y_2). \qquad (4.16)$$

The coefficient Q_{kr} is the reduced non-linear coefficient of the inner and outer raceways contact with the bearing roller, and can be determined as follows (Harris, 2001):

$$Q_{kr} = \frac{7.86\times10^4 l_k^{8/9}}{2^{1.11}}. \qquad (4.17)$$

Combining the equations above yields the following expression for the radial restoring force Λ_{kr}:

$$\Lambda_{kr} = \frac{l_k^{8/9} m_k \cos\gamma_k}{1.12\times10^{-4}} \delta_{kr}^{1.11} = K_k \delta_{kr}^{1.11}. \qquad (4.18)$$

Where, γ_k is the contact angle, l_k is the roller length, and m_k is the number of rollers per row of the k^{th} bearing. The radial deformation (pseudo-penetration) δ_{kr} can be estimated, using a suitably small time step, from the instantaneous displacement d_k of the shaft at the relevant bearing support (figure 4.6):

$$\delta_{kr} = \begin{cases} d_k - \Delta_k, & d_k > \Delta_k \\ 0, & -\Delta_k \le d_k \le \Delta_k \\ d_k + \Delta_k, & d_k < -\Delta_k \end{cases} \tag{4. 19}$$

Where, Δ_k is the radial clearance of bearing k (figure 4.6); and the displacement d_k is equal to $x_{1a}, y_{1a}, x_{1b}, y_{1b}, x_{2c}, y_{2c}, x_{2d}$, or y_{2d}, which correspond to x and y displacements at bearings a, b, c and d, respectively. Since rocking motions of the shafts are not considered, it is assumed that:

$$\left.\begin{aligned} x_{1a} &= x_{1b} = x_1, \\ y_{1a} &= y_{1b} = y_1, \\ x_{2c} &= x_{2d} = x_2, \\ y_{2c} &= y_{2d} = y_2. \end{aligned}\right\} \tag{4. 20}$$

Hence, with the existence of clearance, the radial reaction force is a piece-wise nonlinear function and can be expressed as follows:

$$\Lambda_{kr} = \begin{cases} -sign(d_k) K_k |\delta_{kr}|^{1.11}, & d_k > \Delta_k, d_k < -\Delta_k \\ 0, & |d_k| \le \Delta_k \end{cases}. \tag{4. 21}$$

4.5 The 12-Degree of Freedom Eigen-Value Problem:

In order to determine the natural frequencies and mode shapes of the system, the equivalent linear hydrodynamic contact stiffness is obtained using Fourier expansion, and then the linearised equations of motion, the stiffness and inertia matrices are formed. The natural frequencies and mode shapes are, finally, obtained by solving the eigen-value problem.

By differentiating the hydrodynamic reaction in equation (3.25) with respect to the film thickness, an implicitly time-dependent stiffness expression is obtained:

$$K_i(\varphi_i) = \sum_{j=1}^{N_{total}} \left| \frac{\partial W_{ij}}{\partial h_i} \right| \sim \frac{1}{h_i^2}. \tag{4. 22}$$

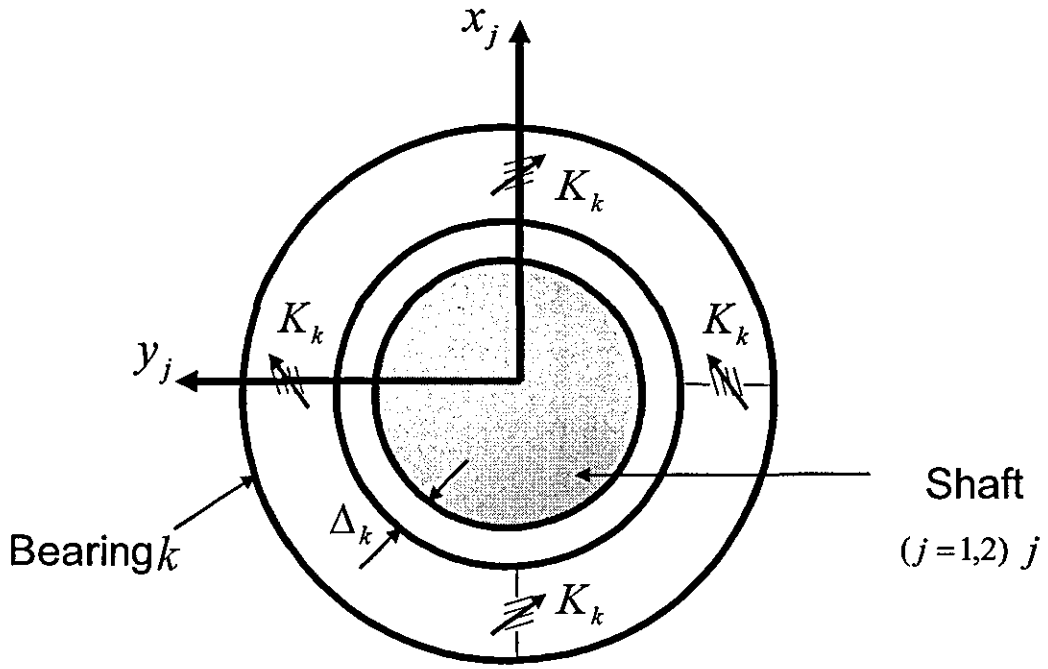

Figure 4.6: Bearing stiffness and clearance

The subscripts ij here denote "of the i^{th} gear pair and j^{th} tooth".

Neglecting the tooth-to-tooth variations and assuming that the oil film stiffness is a periodic function of the displacement, the stiffness can be Fourier-expanded with a fundamental period equal to $2\pi/N_i$ (Theodossiades and Natsiavas, 2001b):

$$K_i(\varphi_i) = K_{0i} + \sum_{\kappa=1}^{\infty}\left(K_{cik}\cos(\kappa N_i\varphi_i) + K_{sik}\sin(\kappa N_i\varphi_i)\right) \qquad (4.23)$$

Where, K_{0i}, K_{cik}, and K_{sik} are the Fourier coefficients of the hydrodynamic stiffness associated with the i^{th} wheel ; N_i is the tooth number of i^{th} wheel; and $\kappa = 1,2,3,\ldots$.

Likewise, the linearised stiffness coefficients of the bearing are obtained by differentiating equations (4.7), (4.9), (4.10), (4.11) and (4.18):

$$\left.\begin{aligned} K_r &= \frac{d\Lambda_{kr}}{d\delta_{kr}} \propto \delta_{kr}^{0.11} \\ K_{ri} &= \frac{\partial F_r}{\partial \varphi_i} \\ K_{rin} &= \frac{\partial F_r}{\partial \varphi_{in}} \end{aligned}\right\} k = a,b,c,d; r = x_1, y_1, x_2, y_2; i = 1,\ldots,7 \ . \qquad (4.24)$$

Obtaining stiffness coefficients from equations (4.7), (4.9), (4.10), and (4.11) is necessary to maintain the coupling between the torsional degrees of freedoms and the translational ones.

The natural frequencies being sought in this chapter are the un-damped natural frequencies. Hence, the terms describing the flank friction and bearing drag (Petrov's tractive force) are dropped since they are essentially damping terms.

Utilising the first term of the stiffness Fourier expansion (e.g. K_{0i} in equation (4.22)), the linearised equations of motion are as follows:

The input shaft:

$$I_{in}\ddot{\varphi}_{in} + \sum_{i=1}^{4} K_{0i} r_{pi}\left(r_{pi}\varphi_{in} - r_i\varphi_i - y_1\right) + \sum_{i=5}^{6} K_{0i} r_{pi}\left(r_{pi}\varphi_{in} - r_i\varphi_i - y_2\right) = 0 \qquad (4.25)$$

1st speed idle gear:

$$\left.\begin{aligned} &I_1\ddot{\varphi}_1 + K_{01} r_1\left(r_1\varphi_1 + y_1 - r_{p1}\varphi_{in}\right) + \\ &K_{07} r_{p7}\left(r_{p7}\varphi_1 + x_1\sin\varepsilon_1 + y_1\cos\varepsilon_1 - r_7\varphi_7 - x_2\sin\varepsilon_2 + y_2\cos\varepsilon_2\right) = 0 \end{aligned}\right\} \qquad (4.26)$$

2nd, 3rd, and 4th speed loose gear wheels which lie on the first output shaft:

$$I_i\ddot{\varphi}_i + K_{0i} r_i\left(r_i\varphi_i + y_1 - r_{pi}\varphi_{in}\right) = 0 \qquad (4.27)$$

Here $i = 2,3,4$.

The 5th and 6th speed loose wheels which lie on the second output shaft:

$$I_i\ddot{\varphi}_i + K_{0i} r_i\left(r_i\varphi_i + y_2 - r_{pi}\varphi_{in}\right) = 0 \qquad (4.28)$$

Here $i = 5,6$.

7^{th} (reverse) speed loose wheel:

$$I_7\ddot{\varphi}_7 + K_{07}r_7\left(r_7\varphi_7 + x_2\sin\varepsilon_2 - y_2\cos\varepsilon_2 - r_{p7}\varphi_1 - x_1\sin\varepsilon_1 - y_1\cos\varepsilon_1\right) = 0 \quad (4.29)$$

The first output shaft in the x-direction:

$$M_1\ddot{x}_1 + \sum_{i=1}^{4} K_{x1i}\varphi_i + K_{x17}\varphi_7 + K_{x1in}\varphi_{in} + K_{x1}x_1 = 0 \quad (4.30)$$

The first output shaft in the y-direction:

$$M_1\ddot{y}_1 + \sum_{i=1}^{4} K_{y1i}\varphi_i + K_{y17}\varphi_7 + K_{y1in}\varphi_{in} + K_{y1}y_1 = 0 \quad (4.31)$$

The second output shaft in the x-direction:

$$M_2\ddot{x}_2 + \sum_{i=5}^{6} K_{x2i}\varphi_i + K_{x27}\varphi_7 + K_{x2in}\varphi_{in} + K_{x2}x_2 = 0 \quad (4.32)$$

The second output shaft in the y-direction:

$$M_2\ddot{y}_2 + \sum_{i=5}^{6} K_{y2i}\varphi_i + K_{y27}\varphi_7 + K_{y2in}\varphi_{in} + K_{y2}y_2 = 0 \quad (4.33)$$

The eigen-value problem is constructed as follows (Rao, 2004):

$$\left[\mathbf{K} - \omega_n^2\mathbf{I}\right]? = \mathbf{0} \quad (4.34)$$

Where, $\mathbf{K}$ is the stiffness matrix driven from equations (4.25) to (4.33) as shown in figure 4.7. The scalar value ω_n^2 is the eigen-value associated with the eigen-vector ? as is explained below. The matrix $\mathbf{I}$ is the inertia diagonal matrix, where its diagonal is expressed as follows:

$$diag(\mathbf{I}) = \left[I_{in} \quad I_1 \quad I_2 \quad I_3 \quad I_4 \quad I_5 \quad I_6 \quad I_7 \quad M_1 \quad M_1 \quad M_2 \quad M_2\right]. \quad (4.35)$$

In order to avoid having a trivial solution for equation (4.34), then

$$\left|\mathbf{K} - \omega_n^2\mathbf{I}\right| = \mathbf{0}. \quad (4.36)$$

When expanding the above equation, a polynomial of order 12 in ω_n^2 is obtained; hence, there are 12 roots for the equation $\left(\omega_n^2 = \omega_n^2\big|_1, \omega_n^2\big|_2, \cdots, \omega_n^2\big|_{12}\right)$, the square roots of which are the natural frequencies. When substituting each of the natural frequencies back into equation (4.34), the corresponding eigen-vector (mode shape) is found; thus, a set of 12 mode shapes are obtained $\left(? = ?\big|_1, ?\big|_2, \cdots, ?\big|_{12}\right)$.

Here, an equation of motion has been formed for the input shaft due to the fact that the film thickness depends on the relative displacement between the pinion and its wheel and if the input shaft equation is ignored the stiffness matrix will be of the size 11×12, the mass matrix's size will be 11×11 and the eigen-vector's size will be 11×1 and matrix addition and multiplication operations are thus impossible.

4.6 Conclusions:

- The single-degree of freedom model presented in chapter 3 was extended to a seven-degree of freedom torsional model.
- An 11-degree of freedom model considering the translational degrees of freedom of the output shafts that carry the idle gears was formed.
- The bearing restoring forces in the radial direction were determined.
- The eigen-value problem of the linearised transmission model was solved in order to find the un-damped natural frequencies of the system and the associated mode shapes.

$$
\mathbf{K}=\begin{bmatrix}
\sum_{i=1}^{6}K_{0i}r_{pi}^2 & -K_{01}r_{p1}r_1 & -K_{02}r_{p2}r_2 & -K_{03}r_{p3}r_3 & -K_{04}r_{p4}r_4 & -K_{05}r_{p5}r_5 & -K_{06}r_{p6}r_6 & 0 & 0 & -\sum_{i=1}^{4}K_{0i}r_{pi} & 0 & -\sum_{i=5}^{6}K_{0i}r_{pi} \\
-K_{01}r_1r_{p1} & \begin{pmatrix}K_{01}r_1^2+\\K_{07}r_{p7}^2\end{pmatrix} & 0 & 0 & 0 & 0 & 0 & -K_{07}r_{p7}r_7 & K_{07}r_{p7}\sin\varepsilon_1 & \begin{pmatrix}K_{01}r_1+\\K_{07}r_{p7}\cos\varepsilon_1\end{pmatrix} & -K_{07}r_{p7}\sin\varepsilon_2 & K_{07}r_{p7}\cos\varepsilon_2 \\
-K_{02}r_2r_{p2} & 0 & K_{02}r_2^2 & 0 & 0 & 0 & 0 & 0 & 0 & K_{02}r_2 & 0 & 0 \\
-K_{03}r_3r_{p3} & 0 & 0 & K_{03}r_3^2 & 0 & 0 & 0 & 0 & 0 & K_{03}r_3 & 0 & 0 \\
-K_{04}r_4r_{p4} & 0 & 0 & 0 & K_{04}r_4^2 & 0 & 0 & 0 & 0 & K_{04}r_4 & 0 & 0 \\
-K_{05}r_5r_{p5} & 0 & 0 & 0 & 0 & K_{05}r_5^2 & 0 & 0 & 0 & 0 & 0 & K_{05}r_5 \\
-K_{06}r_6r_{p6} & 0 & 0 & 0 & 0 & 0 & K_{06}r_6^2 & 0 & 0 & 0 & 0 & K_{06}r_6 \\
0 & -K_{07}r_{p7}r_7 & 0 & 0 & 0 & 0 & 0 & K_{07}r_7^2 & -K_{07}r_7\sin\varepsilon_1 & -K_{07}r_7\cos\varepsilon_1 & K_{07}r_7\sin\varepsilon_2 & -K_{07}r_7\cos\varepsilon_2 \\
K_{x1in} & K_{x11} & K_{x12} & K_{x13} & K_{x14} & 0 & 0 & K_{x17} & K_{x1} & 0 & 0 & 0 \\
K_{y1in} & K_{y11} & K_{y12} & K_{y13} & K_{y14} & 0 & 0 & K_{y17} & 0 & K_{y1} & 0 & 0 \\
K_{x2in} & 0 & 0 & 0 & 0 & K_{x25} & K_{x26} & K_{x27} & 0 & 0 & K_{x2} & 0 \\
K_{y2in} & 0 & 0 & 0 & 0 & K_{y25} & K_{y26} & K_{y27} & 0 & 0 & 0 & K_{y2}
\end{bmatrix}
$$

Figure 4.7: The stiffness matrix of the linear 12-degree of freedom model

Chapter 5: Experimental Methodology

5.1 Introduction

The aims of the experimental studies are to validate and to direct the further developments of the numerical models. The experimental studies comprise two parts: actual vehicle tests on a front-wheel drive passenger car equipped with a turbo-charged four-cylinder in-line Diesel engine, and rig-based investigations with an induction AC electric motor. All the experiments were carried out on a seven-speed (including the reverse) manual transaxle transmission.

The chapter consists of the following sections:

- Description of transducers and data acquisition used in the experiments.
- Description of the experimental rig.
- The experimental procedure.

5.2 Objectives of the Experiments

The objectives of the vehicle and rig experiments are:

- To better understand the structural response of the manual transmission to a fluctuating input rotational velocity under idling conditions.
- To validate the model developed in chapter 4 by correlating its results with the experimental findings.

5.3 Instrumentation and Data Acquisition

In general, a data acquisition system consists of five components:

1. The transducer, which converts the physical phenomenon under investigation into an electrical signal.
2. The signal, which can be analogue or digital.

3. The signal conditioning equipment, which conditions the signals generated by the transducers in order to maximise their amplitude.
4. The DAQ (data acquisition) hardware, which converts the analogue signals into digital form.
5. The signal processing software, which analyses and presents the digital signal received from the DAQ hardware.

The rattle experiments' data acquisition system consists of the following:

1. Transducers: piezoelectric accelerometers, free-field pre-polarized condenser microphones, PT100 resistance temperature transducer, torsional laser vibrometer.
2. Signals in analogue form (voltage).
3. Signal conditioning equipment: preamplifiers for microphones, charge amplifiers for accelerometers, and the connector block.
4. DAQ hardware: data acquisition cards connected to a laptop.
5. Signal generation and processing software packages: PULSE (Brüel & Kjær), LabVIEW (National Instruments), MATLAB® (Pratap, 2002; and The Mathworks online documentation) and AutoSignal (SeaSolve, 2003). The signal processing and analysis will be dealt with in chapter 6.

Signal generators:

For vehicle tests, the input to the transmission was provided by the vehicle engine; a turbo-charged four-cylinder in-line 2.0L Diesel engine.

The input RPM signal for the rig test (.wav file) was created using MATLAB® then imported into a Brüel & Kjær portable data acquisition unit type 3560C (figure 5.1) customised to 4 channels (3 inputs and 1 output). The 3560C, functioning here as a signal generator, transformed the digital signal to an analogue signal with maximum amplitude of 5V, a zero DC offset, and zero phase. The analogue signal was amplified and fed into an inverter with speed control capability before being delivered to the transmission using an AC three-phase motor of maximum power 11 kW.

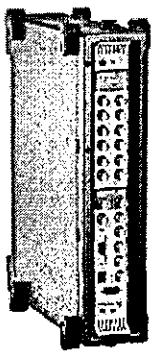

Figure 5. 1: Data acquisition unit type 3560C (courtesy of Brüel & Kjær)

Accelerometers:

Brüel & Kjær high frequency piezoelectric accelerometers: type 4393V, figure 5.2, were used to measure the (output) structural vibration of the transmission housing. This type of accelerometer was chosen due to its high natural frequency (85 kHz), low mass (2.4 grams) and wide temperature range (-74 – 250 C); see Brüel & Kjær (2004).

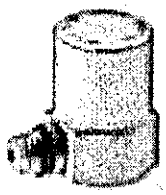

Figure 5. 2: Brüel & Kjær accelerometer type 4393V (courtesy of Brüel & Kjær)

Microphones:

The microphones used to capture radiated noise were Brüel & Kjær's free-field pre-polarized condenser microphones comprised of type 4155 cartridges, each mounted on a pre-amplifier type 2671, (figure 5.3). The rattle frequency range is well below the microphone's resonance frequency of 14 kHz, also no corrections were needed due to the presence of microphone since the wavelength range of rattle is not comparable with the microphone's diameter of approx. 13mm; see Brüel & Kjær (1997). The preamplifier type 2671 has the merit that it can be connected to long BNC cables which are readily available at the university; see Brüel & Kjær (2003).

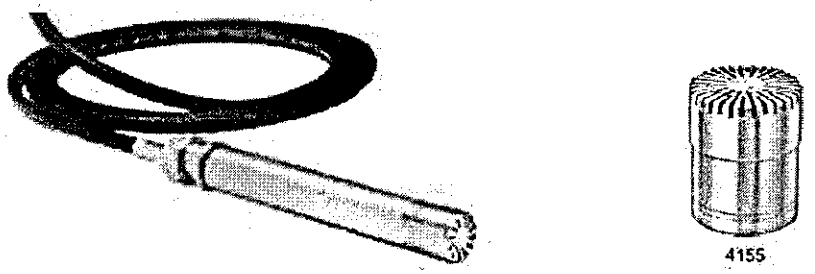

Figure 5. 3: Microphone (right), and microphone attached to a preamplifier type 2671 (left) (courtesy of Brüel & Kjær)

Amplifiers:

Three types of signal conditioning devices were used to amplify the signal from the transducers on its way to the connector block. Figure 5.4 shows the four-channel Nexus conditioning amplifier type 2692 from Brüel & Kjær. It converts the output charge signals of the accelerometers into corresponding amplified voltage signals. Figure 5.5 shows the single-channel charge amplifier type 2635, also from Brüel & Kjær. It also converts the charge output signal from an accelerometer into an amplified voltage signal. Figure 5.6 shows the ISOTRON conditioner ENDEVCO model 4416 B, which functions as a gain amplifier with two gain settings (1 and 10). Three of these conditioners were used with the microphones.

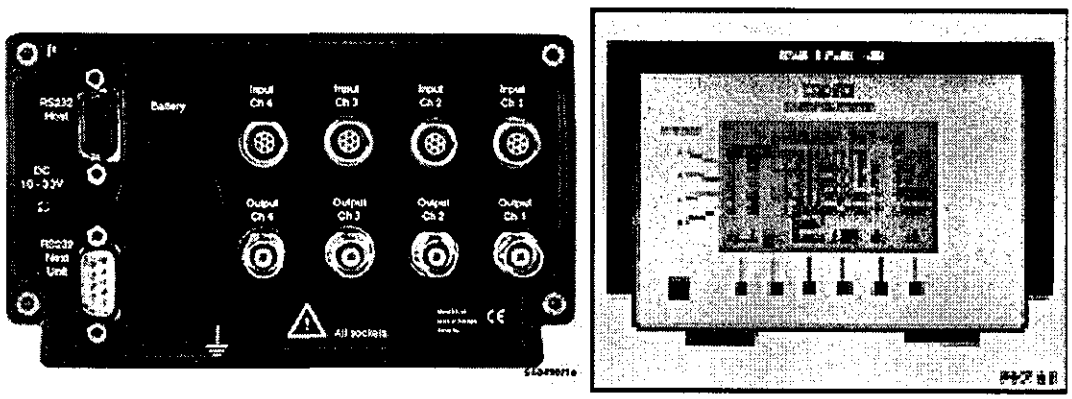

Figure 5.4: Four-channel Nexus conditioning amplifier type 2692 (courtesy of Brüel & Kjær)

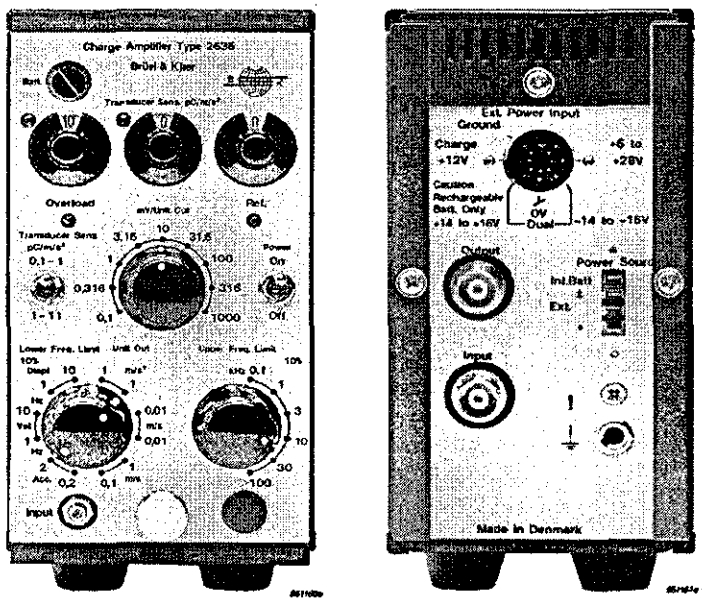

Figure 5. 5: Single-channel charge amplifier type 2635 (courtesy of Brüel & Kjær)

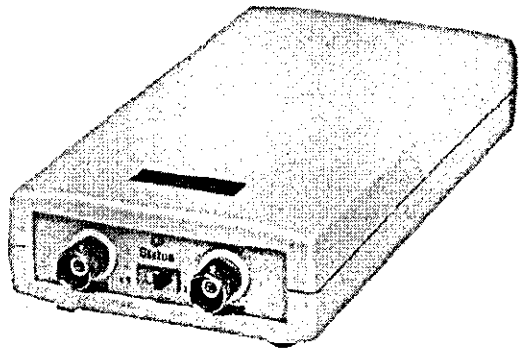

Figure 5. 6: Single-channel Endeveco ISOTRON conditioner model 4416B (picture courtesy of Brüel & Kjær)

Connector block:

A National Instrument connector block type BNC-2110, figure 5.7, was used to provide signal shielding and simultaneous sampling for up to eight channels.

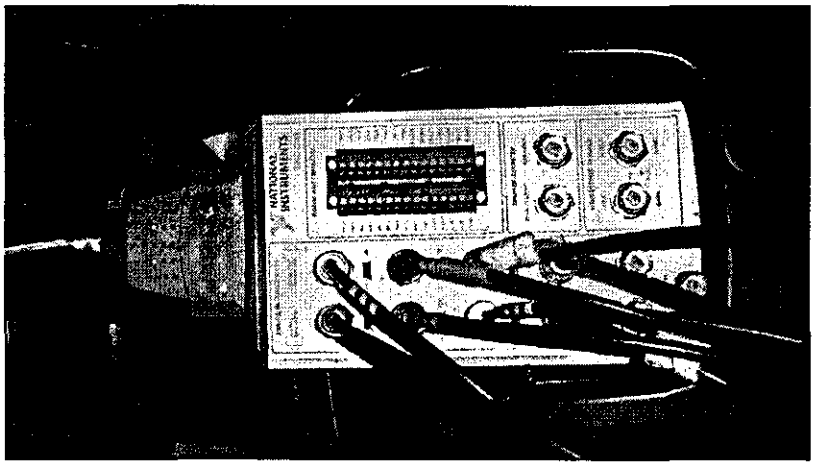

Figure 5. 7: Connector block type BNC-2110

Laser Torsional Vibrometer

The LTV is used to record the input from the AC motor to the transmission input shaft. It is a non-contact transducer and composed of two parts (figure 5.8):

1. Sensor head with dual beam capability: OFV 400.
2. Controller: OFV 4000.

It can perform RPM (revolution per minute) measurement within –7,000 RPM to +11,000 RPM with an accuracy of ±5 RPM.

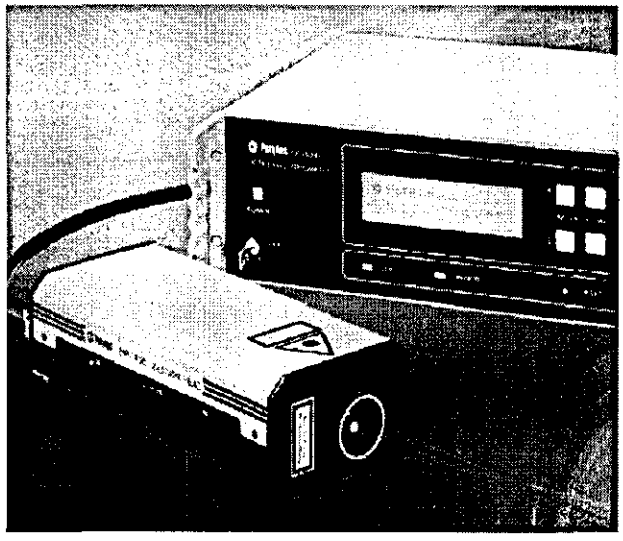

Figure 5. 8: 4000 Series rotational vibrometer (courtesy of Polytec)

National Instruments DAQCard-6036E:

This data acquisition card, figure 5.9, functions as an analogue to digital (A/D) converter; it converts the analogue signals it receives from the connector block into a digital signal accepted by the computer. The NI DAQCard-6036E fits into portable computers (e.g. laptops) with type II PC Card slot. It is a low power card and uses analogue I/O, digital I/O, and timer I/O operations.

The specifications of DAQCard-6036E:

- Number of analogue input (AI) channels: 16.
- Number of differential AI channels: eight.
- Number of digital I/O lines: eight.
- Resolution: 16 bit.

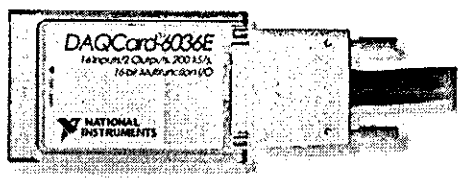

Figure 5.9: DAQCard-6036E (courtesy of National Instrument)

Temperature transducers:

During the vehicle-based experiments, the temperature measurements were undertaken using a hand-held thermocouple type K, screwed into the oil draining hole of the transmission's sump. The thermocouple was utilised independently from the data acquisition system described above.

For the rig test experiments, however, a PT-100 was screwed to the transmission draining plug. The PT-100 is connected to a multi-meter, where the resistance output was read; the temperature was then determined from a standard PT-100 resistance table. Since the suppliers of the actual PT-100 and the multi-meter were different, the

calibration of the PT-100 was tested in a hot water tank and the readings of the multi-meter were compared with the PT-100 resistance-temperature tables, which were found to agree.

National Instruments LabVIEW 6.1:

LabVIEW is visual programming software, which is used for acquiring, processing and saving the data from the DAQ hardware at a user-specified sampling rate.

Brüel & Kjær PULSE 8.0:

Pulse 8.0 is graphical user interface based software used for generating and monitoring the signal to the motor controller during the rig-based experiments.

5.4 Experimental Rig Design

The main specifications taken into account in the design of the rig were:

1. It should closely replicate vehicle conditions.
2. It should ensure the repeatability of the input signal.
3. The internal combustion engine could be very noisy and interfere with the acoustic measurements. Hence, the rig is to be operated by an electric motor, which in addition to being quieter is also easier to install, maintain and operate.
4. The motor controller should be able to accept a fluctuating velocity signal from a signal generator to represent engine input torsional components.
5. The electric motor and the transmission should be mounted separately to minimise the excitation transmitted directly from the motor to the transmission housing and ensure that the fluctuations transmitted via the input shaft are the sole excitation to the transmission gears (and subsequently the housing).
6. The test rig is to be portable such that it can be tested in an anechoic chamber or a suitable test cell.

Transmission test rig characteristics:

The rig accommodates an electric motor, coupling, a shaft, two bearings, and the transmission under investigation. Figure 5.10 represents a CAD drawing (the transmission and motor are only schematic) and a top view photograph of the test rig. By having all the components of the rig built on a single solid base-plate, the issue of alignment has been simplified. Furthermore, this has made the test rig highly portable. The plate and the up-right (for mounting the transmission) are 50 mm thick and made of steel. This dampens the vibrations originating from the motor and other vibrations transmitted through the floor of the laboratory. The whole bed (plate and up-right assembly) was fastened onto two I-section beams representing the laboratory mounting rails.

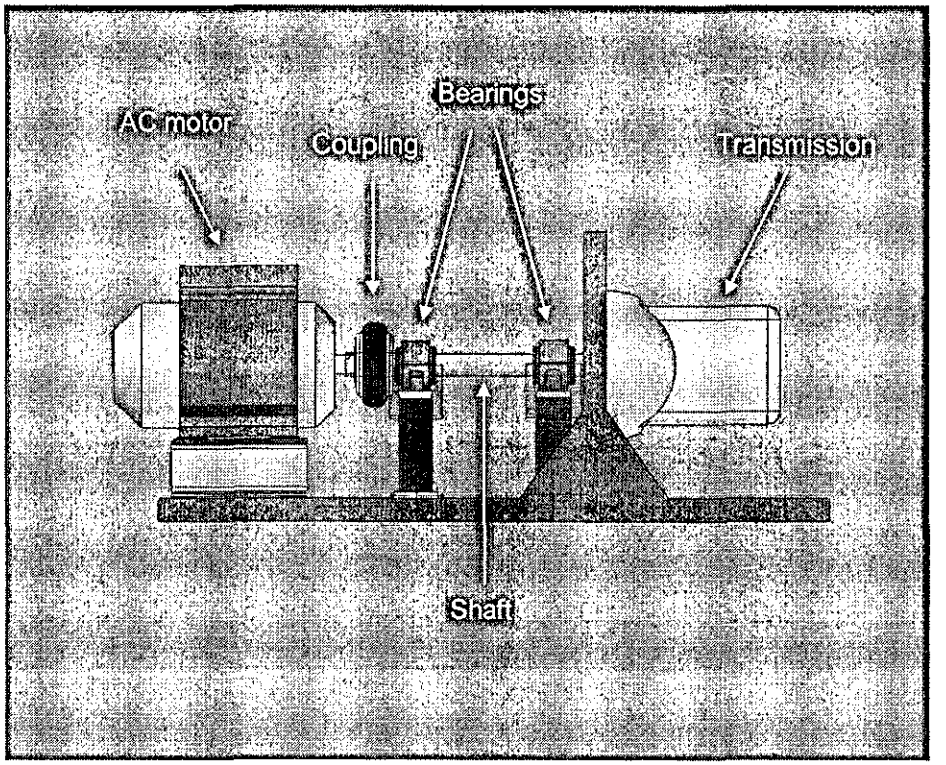

Figure 5.10 (continued)

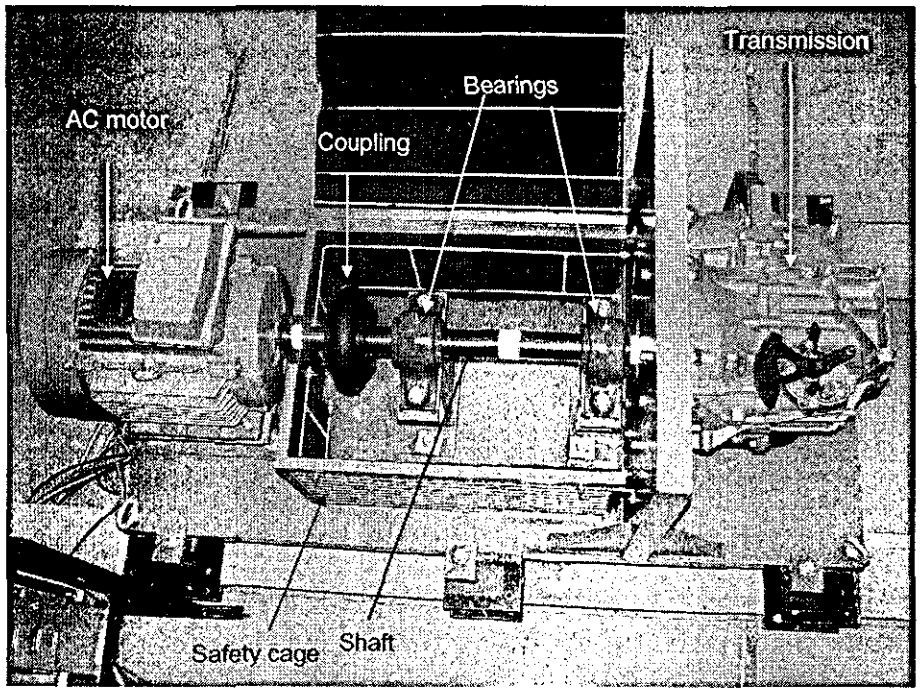

Figure 5.10: Transmission test rig

Motor characteristics:

The main motor characteristics are:

- Maximum power: 11 kW.
- Maximum RPM: 1500.
- Maximum torque: 72 Nm.
- No. of poles: 4.

Coupling characteristics:

A Fenaflex® rubber coupling was used to connect the motor shaft to the rig shaft (figure 5.10); on the shaft side a key locking mechanism is used while on the rig shaft side the coupling is press-fitted. Since in idling conditions the input torque is very low, there are no concerns regarding the rubber twisting under load.

The main characteristics of the coupling:

- Maximum RPM: 3600.
- Nominal torque: 250 Nm.
- Torsional stiffness: 41 Nm/° (2349.3 Nm/rad.).
- Maximum parallel misalignment: 1.9 mm.

- Mass: 0.7 kg.

Bearing characteristics:

Two double row Dodge® type E-XTRA Plummer tapered roller bearings supports the rig shaft (50 mm diameter). The choice of bearing considers possible future tests in loaded conditions.

Main characteristics:

Bore: 50 mm.

Weight: 12 lbs.

5.5 Experimental Procedure

The vehicle experiments were carried out in a semi-anechoic chamber (figure 5.11). The main characteristics of the chamber are:

1. There is an air gap to isolate the chamber from the rest of the building in which it is situated.
2. The chamber is supported on vibration isolation mounts.
3. The walls, ceiling and the floor of the chamber absorb sound frequencies above 100Hz.

The instrumented vehicle is placed as shown in figure 5.11 and the necessary external instruments (i.e. the microphones) were added as explained below.

All the vehicle experiments were performed, while the vehicle was under idling condition, with transmission in neutral position. Various throttle positions were experimented with; they correspond to various engine speeds, ranging from idling speed (810-820 rpm) up to 2000 rpm; those speeds were tested in order to distinguish meshing frequencies from resonances. Also, tests were carried out at various sump temperatures.

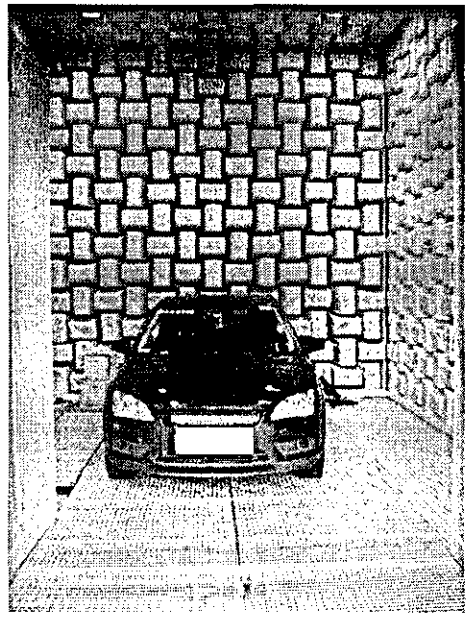

Figure 5.11: The semi-anechoic chamber

The rig-based experiments were carried out in the powertrain labs, where there is a provision for testing both loaded and unloaded (idling) conditions; the scope of the thesis, however, is limited only to unloaded conditions. The rig was run at mean RPM of 600 rpm and sinusoidal frequency of 10 Hz. This was due to noise encountered when trying to impart a real life engine signal from the signal generator. It was concluded that a noise from the motor affects the input signal and that only a sufficiently low frequency sinusoidal signal is suitable for the experiment.

Accelerometers:

The mounting positions for the accelerometers were chosen, so that they follow the path of rattle response: from the bearing housings area to the transmission mountings via the transmission wall.

A total of five accelerometers were used in the vehicle measurements and three during the rig measurements; the extra two, in case of vehicle measurements, were attached to the transmission mountings.

The three common accelerometers are arranged as follows:

- Two accelerometers were mounted on the transmission wall at locations of the bearings of input shaft (indicated by (1) in figure 5.12) and the second output shaft (indicated by (2) in figure 5.12).
- An accelerometer was mounted to the under-side of the transmission housing (indicated by (3) in figure 5.12), where the wall is relatively less rigid (away from the ribs).

The extra two accelerometers used in the vehicle measurements were attached to the mounts of the transmission housing to the vehicle sub-frame and exhaust pipe as shown in figure 5.13. Table 5.1 summarises the sensitivities and locations of the accelerometers in both experiments.

Temperature transducer:

The PT-100 was fitted to the transmission through the lower oil draining plug hole as indicated by arrow (4) in figure 5.12; the measurements show the transmission sump temperature. The thermocouple used in the vehicle measurements was mounted through the upper oil filling hole; as a result only the transmission air or oil spray are obtained.

Microphones:

During the vehicle measurements two microphones (figure 5.14) were located at the left side and under the sub-frame at a distance of 1.5 m; those two locations were useful since they were the nearest locations to the transmission However, during the rig experiments, due to space restrictions, only two microphones were used, they were placed at approximately 1.0 m at the top of the transmission and at the rear (figure 5.15). Table 5.2 summarises the microphones setup for both the vehicle and the rig experiments. The locations of the microphones were selected such that they lie in the free field, where measurements are easier to conduct; measuring too close to the transmission surface implicates complex calculations, while measuring too far from the transmission surface is compromised by reverberation effects (see Hassall and Zaveri, 1979). The distances of the pick-up points from the transmission can then be

used to determine the necessary corrections for reverberation effects, the details of which are reported by Hassall and Zaveri (1979), and Thoden (2006).

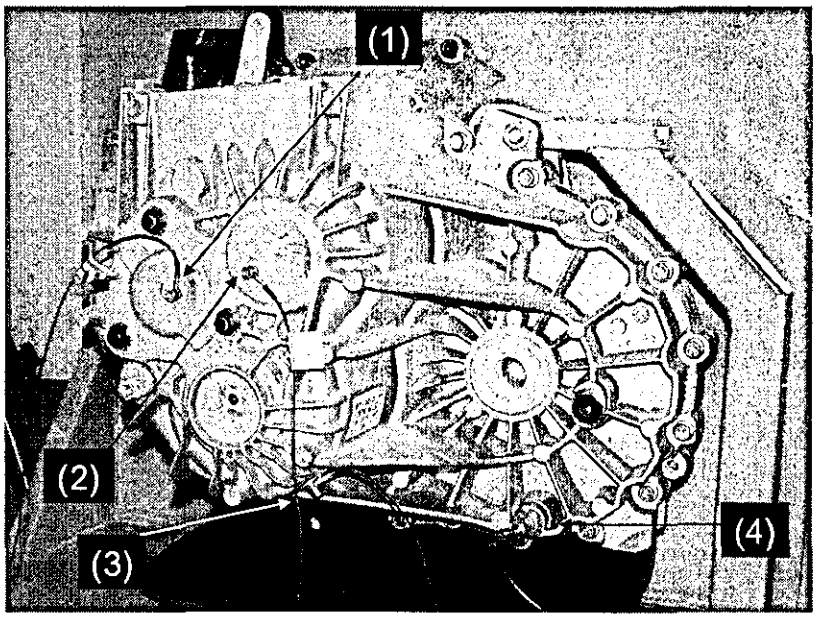

Figure 5. 12: Accelerometers and PT-100 (rig configuration)

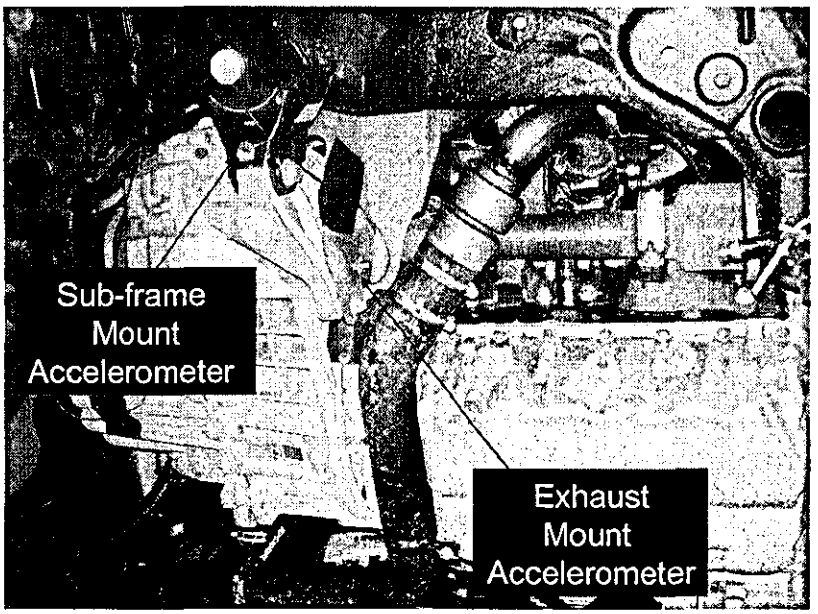

Figure 5. 13: Accelerometers attached to transmission mountings (vehicle configuration)

Experiment	Transducer	Total Sensitivity	Location	Figure
Vehicle only	Accelerometer	100 mV/ms^{-2}	Transmission wall	Figure 5.12
	Accelerometer	100 mV/ms^{-2}	Input shaft bearing	Figure 5.12
	Accelerometer	100 mV/ms^{-2}	Upper output shaft bearing	Figure 5.12
	Accelerometer	100 mV/ms^{-2}	Transmission exhaust bracket	Figure 5.13
	Accelerometer	100 mV/ms^{-2}	Transmission to sub-frame mount	Figure 5.13
Test rig	Accelerometer	10 mV/ms^{-2}	Transmission wall	Figure 5.12
	Accelerometer	10 mV/ms^{-2}	Input shaft bearing	Figure 5.12
	Accelerometer	10 mV/ms^{-2}	Upper output shaft bearing	Figure 5.12

Table 5. 1: Accelerometer pick-up points (rig and vehicle configurations)

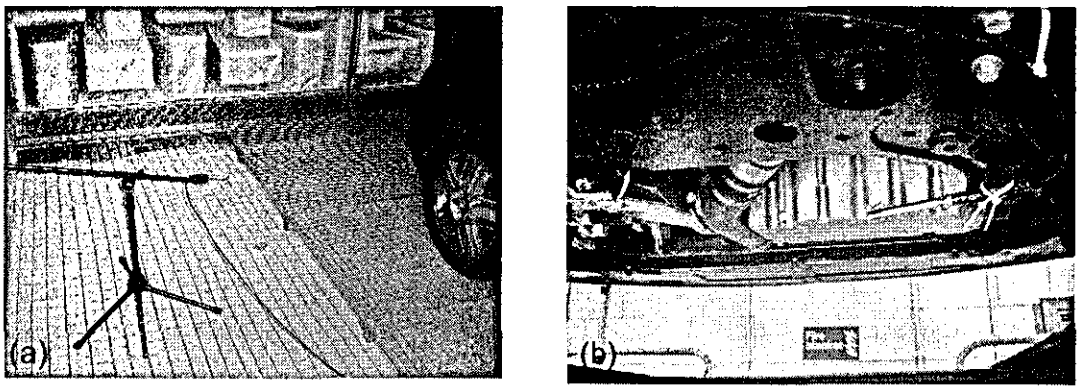

Figure 5.14: Microphone pick-up points (vehicle configurations) (a) Left, (b) under sub-frame

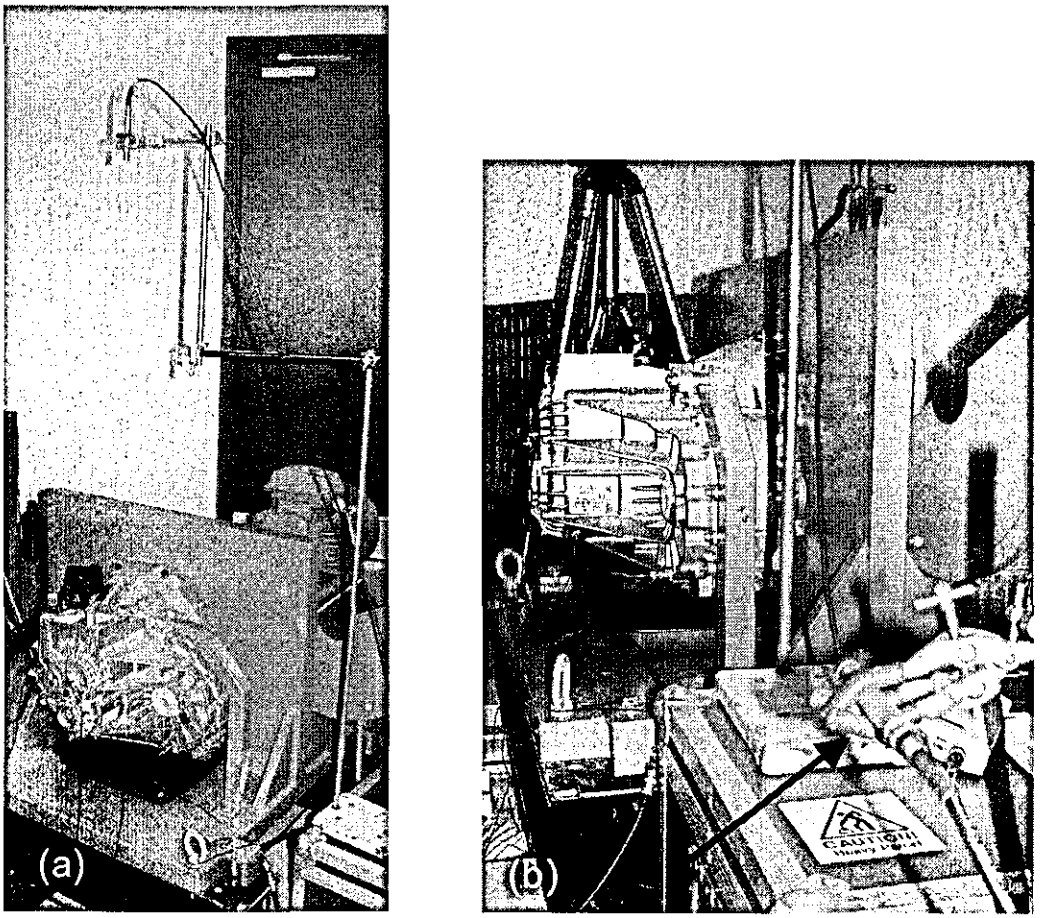

Figure 5.15: Microphone pick-up points (rig configurations) (a) Upper, (b) rear

Experiment	Transducer	Total Sensitivity	Location	Figure
Vehicle	Microphone	500 mV/Pa	Under the engine	Figure 5.14
	Microphone	500 mV/Pa	Outside left (1.5m)	Figure 5.14
Test rig	Microphone	500 mV/Pa	Above the transmission (1.0 m)	Figure 5.15
	Microphone	500 mV/Pa	Behind the transmission (1.0 m)	Figure 5.15

Table 5. 2: Microphones pick-up points (rig and vehicle configurations)

Laser Doppler vibrometer:

A retro-reflective tape was pasted around the transmission input shaft and the dual beam of the laser vibrometer is aimed at it. The aim was to obtain the RPM and acceleration of the input shaft. Figure 5.16 shows the laser Doppler vibrometer. The acceleration of the input shaft was obtained by direct differentiation of the velocity differential output from the laser Doppler vibrometer. The sensitivity of the RPM was 1 mV/rpm, and the sensitivity of the velocity differential was 100°/s/V. It should be noted that due to difficulties in accessing the vehicle input shaft mainly because of the packaging of the drive system, no measurement of the input rotational velocity were possible.

DAQ:

The DAQ sampling rate was set to 12000 Hz; hence giving a Nyquist frequency of 6000 Hz (anti-aliasing filter), which is reasonable for rattle measurements and could capture the structural vibrations of the transmission housing.

It should be noted that the rattle frequencies tend to be in the lower spectral contributions.

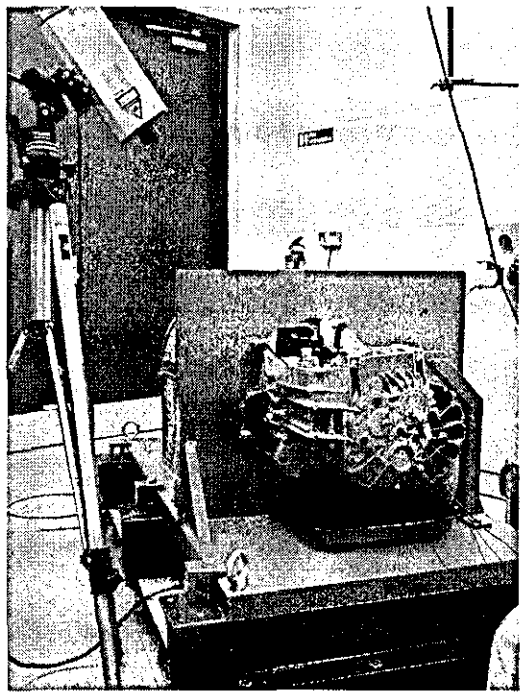

Figure 5.16: Laser Doppler vibrometer

Impact hammer test:

Since the accelerometers measure the structural vibrations of the transmission housing, it is necessary to determine the housing natural frequencies. This will help understanding whether gear rattle actually excites the natural frequencies of the transmission housing. The hammer test is conducted by applying an impact to the transmission structure, the response of which (a wide range of frequencies) contains excitations at each of the transmission housing's natural frequencies (Inman, 2001). The Brüel & Kjær portable data acquisition unit type 3560C (figure 5.1) was used with Brüel & Kjær Pulse 8.0 to analyse the signals coming from the accelerometers, which were mounted as shown in figure 5.12, when they were excited by the hammer impact. The impact excitations were conducted at points (1) and (2) (figure 5.12), where the tooth impact excitations imparted via the bearing housings. The Pulse 8.0 software provides both the frequency response function (FRF) and the coherence of

the output. Thus, it can be determined, which frequencies were excited by the impact and which frequencies were mere noises.

5.6 Summary of Equipment Used

- The main equipment used in the experiments were:
    - Accelerometers for structural vibration measurements.
    - Microphones for acoustic measurements.
    - PT 100 and thermocouple for oil temperature measurements.
    - Laser Doppler vibrometer to measure the rotational velocity of the transmission input shaft.
- Signal conditioning and amplification of transducers' signals was carried out to improve the data acquisition process.
- The main experiments were:
    - Vehicle-based experiments in a semi-anechoic chamber.
    - Rig-based experiments in a powertrain laboratory.
- Chapter 6 details the signal processing and analysis of the data obtained from the experiments described in this chapter.

Chapter 6: Discussion of Results

6.1 Introduction:

The results from chapter 4 on the transmission numerical models and chapter 5 on the experimental data are discussed and compared in this chapter. The analysis is commenced with a seven-degree of freedom torsional model, and then expanded to include the two shafts' lateral degrees of freedom (the 11-degree of freedom model).

6.2 The Seven-Degree of Freedom Model:

Engine order vibrations lead to torsional oscillations of the transmission input shaft, superimposed upon its nominal angular velocity (Rahnejat, 1998). The vibration spectrum of the transmission input shaft acceleration is shown in figure 3.10. The model is run at 39.4 ° C with a 10μm bearing clearance.

Figure 6.1 shows the simulated time histories and FFT spectra of the 2nd and 6th idle gears' angular acceleration. With the vibration severity clearly varying between the two gear pairs, it can be concluded that the overall response of an idle gear consists of two particular motions: the carrier type motions, and the infinitesimal fluctuations, containing different frequency characteristics (the former modulates the latter). The lower frequency engine orders are expected to dominate in the carrier regions, while the higher vibro-impact frequencies are expected to govern the smaller fluctuations. Similar behaviour is also encountered in the time domain graphs of figure 6.2, where the lubricant film thickness time histories of the 2nd and 6th idle gear pairs are presented. Nevertheless, in both cases the size of the lubricant film thickness is within a range compatible with the initially assumed hydrodynamic conditions, varying between 1.5 - 15μm, depending on the gear pair's kinematic conditions and load. Moreover, the 6th gear pair demonstrates higher frequency content in the corresponding vibration spectra (figure 6.2). The way the film thickness changes

reveals the frequencies under which the gear flanks approach and depart. It is noteworthy that in most gear wheels, the highest amplitude contributions coincide with the various engine order harmonics, which are contained in the motion of the transmission input shaft. The 2nd idle gear pair (figure 6.2 (a)), which possesses the higher inertia, generally exhibit higher amplitude of oscillations and lower frequency spectral components compared to the 6th pair (figure 6.2 (b)).

The spectral composition of the loose wheels' acceleration also reveals two types of infinitesimal vibration: those which are due to the separation/squeeze action and those which are due to the rolling action. The spectral components of the squeeze/separation action can be observed more clearly in the FFT spectra of the film thicknesses (figure 6.2). The frequencies associated with rolling are proportional to the meshing frequencies*. They are obtained by dividing the meshing frequency of each gear by its transverse contact ratio (Table 6.1). These frequencies arise due to the change of number of teeth in simultaneous contact. The frequencies 576 and774 Hz, shown in figure 6.1 (a) and (b), are the third harmonics of the rolling frequencies of the 2nd and 6th gears, respectively. They can be calculated from Table 6.1 together with the other harmonics. The frequencies 121 and 418 Hz, on the other hand, are dominant in the film thickness responses (figure 6.2 (a) and (b), respectively) suggesting that they are the main squeeze frequencies. As shown in chapter 3, the squeeze/separation action components appear as bands of frequencies (mainly reflecting modulation at 13 Hz, the input shaft's rotational frequency), while the rolling components tend to show up as mildly modulated single peaks accompanied by some harmonics. From figure 6.2 modulations around 121 Hz (2nd), and around 418 Hz (6th) are observed. In chapter 3, it has been shown that there is a link between such frequency bands and rattling: as the system approaches and crosses the rattle threshold, the band shifts towards the lower end of the frequency spectrum. On the other hand, the frequencies associated with rolling change in terms of their amplitudes only, but their spectral positions remain unchanged as the system approaches rattling condition.

* The meshing frequency is obtained by multiplying the gear rotational speed in cycle per second by its tooth number.

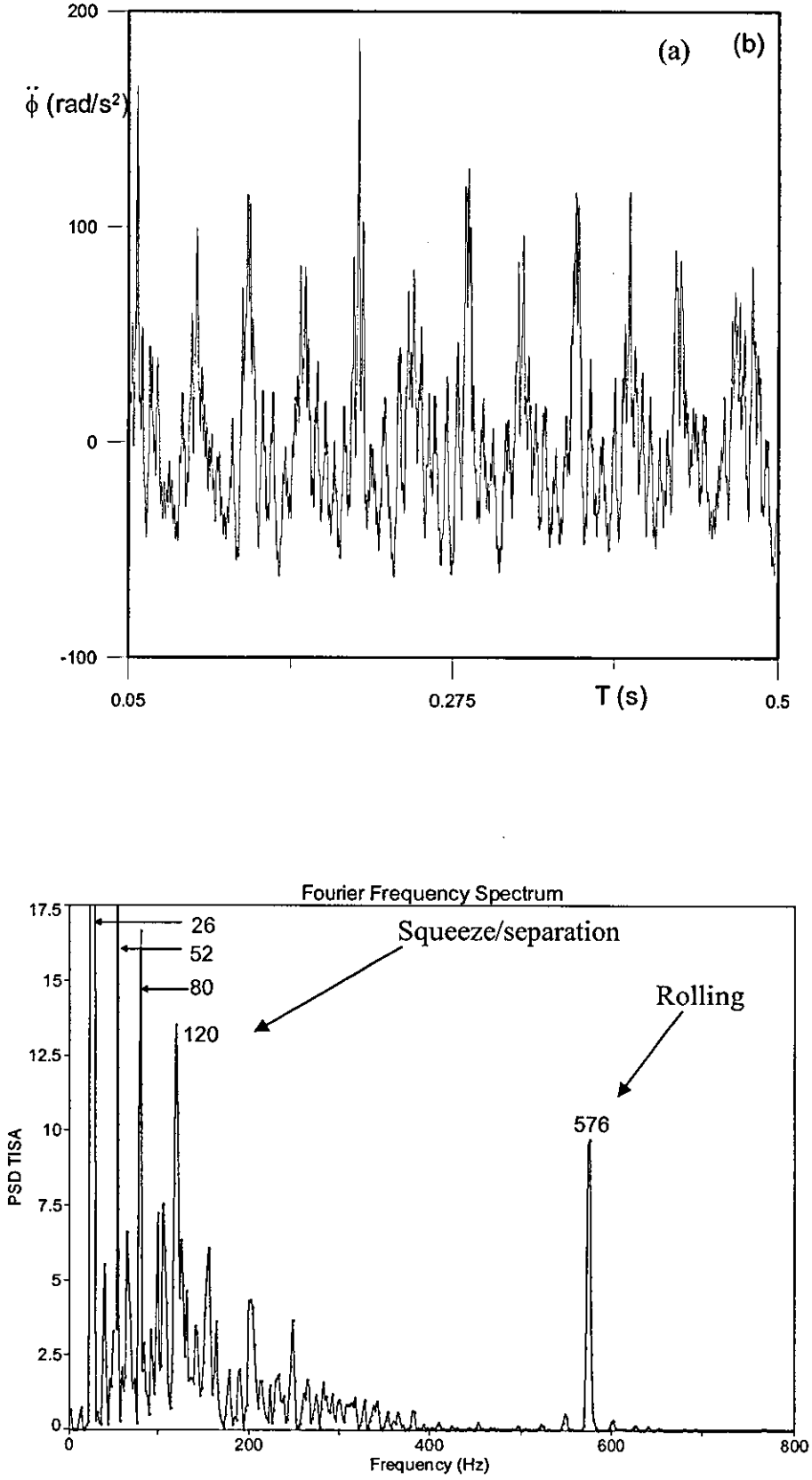

Figure 6.1 (continued over)

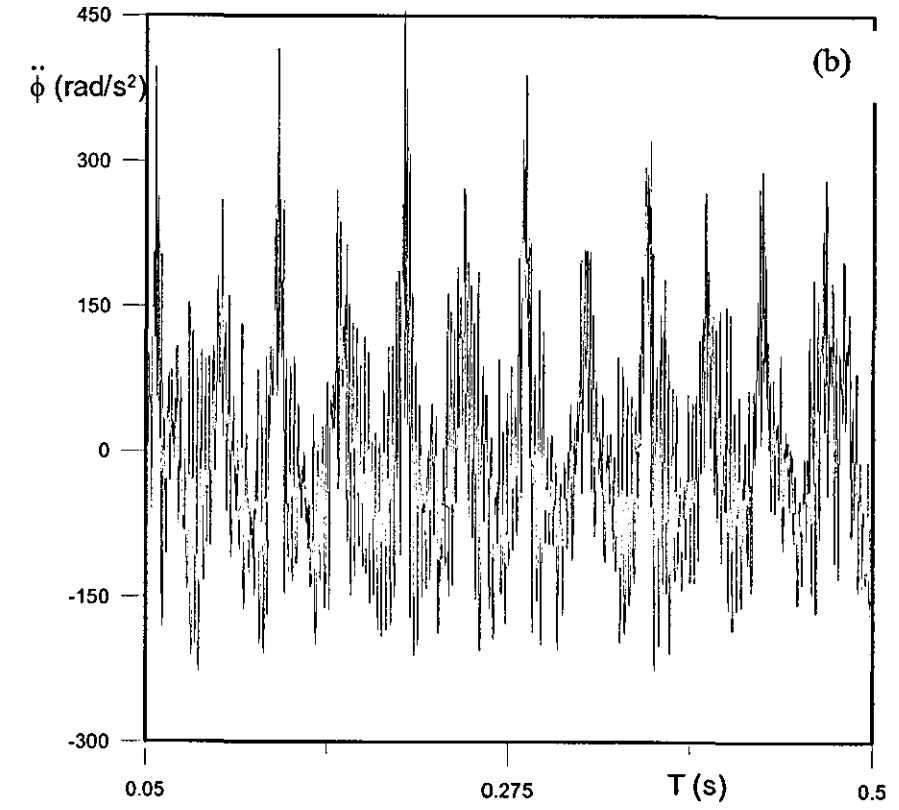

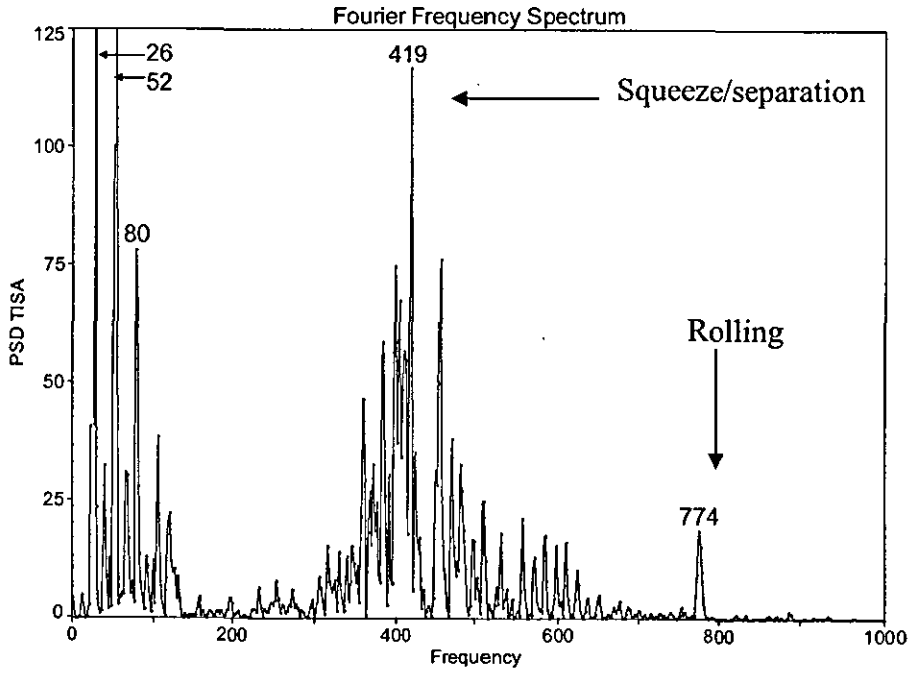

Figure 6.1: Simulated time histories and FFT spectra of $\ddot{\varphi}$ for (a) 2nd Gear and (b) 6th Gear (39.4 ° C and 10μm bearing clearance)

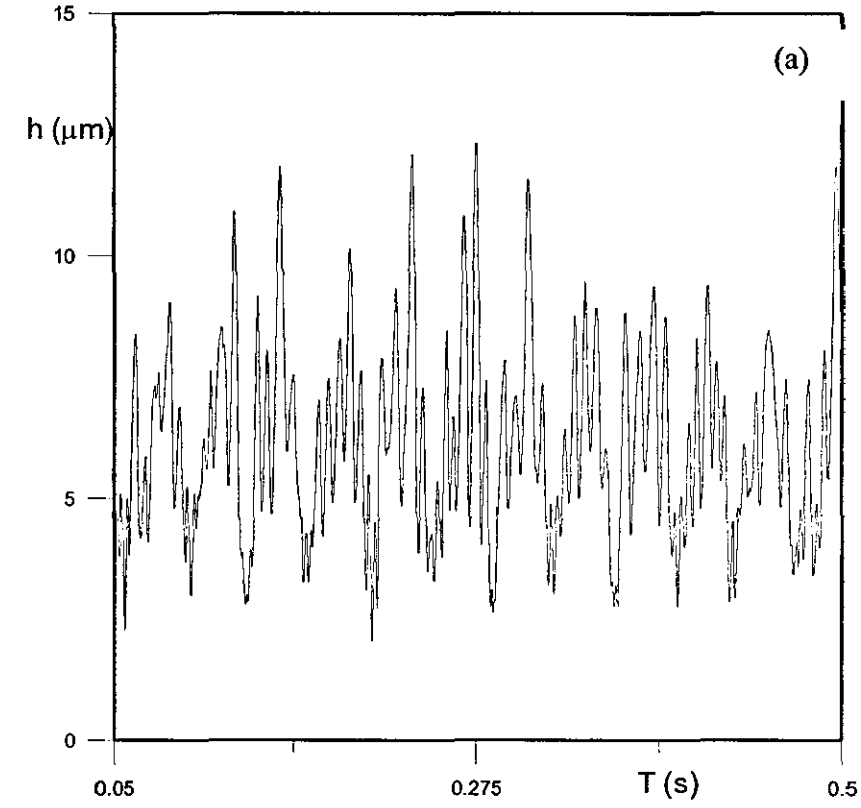

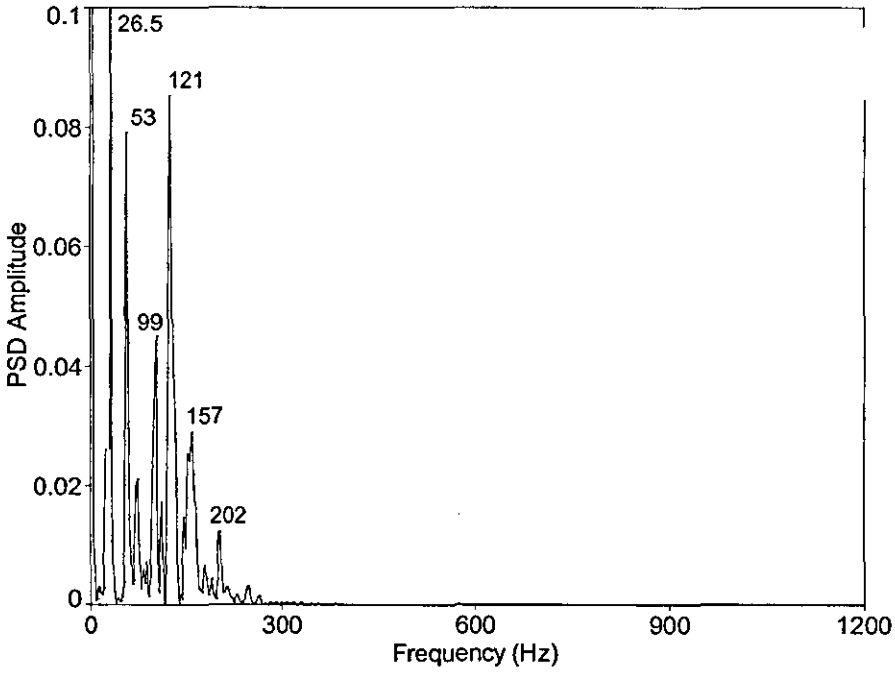

Figure 6.2 (continued over)

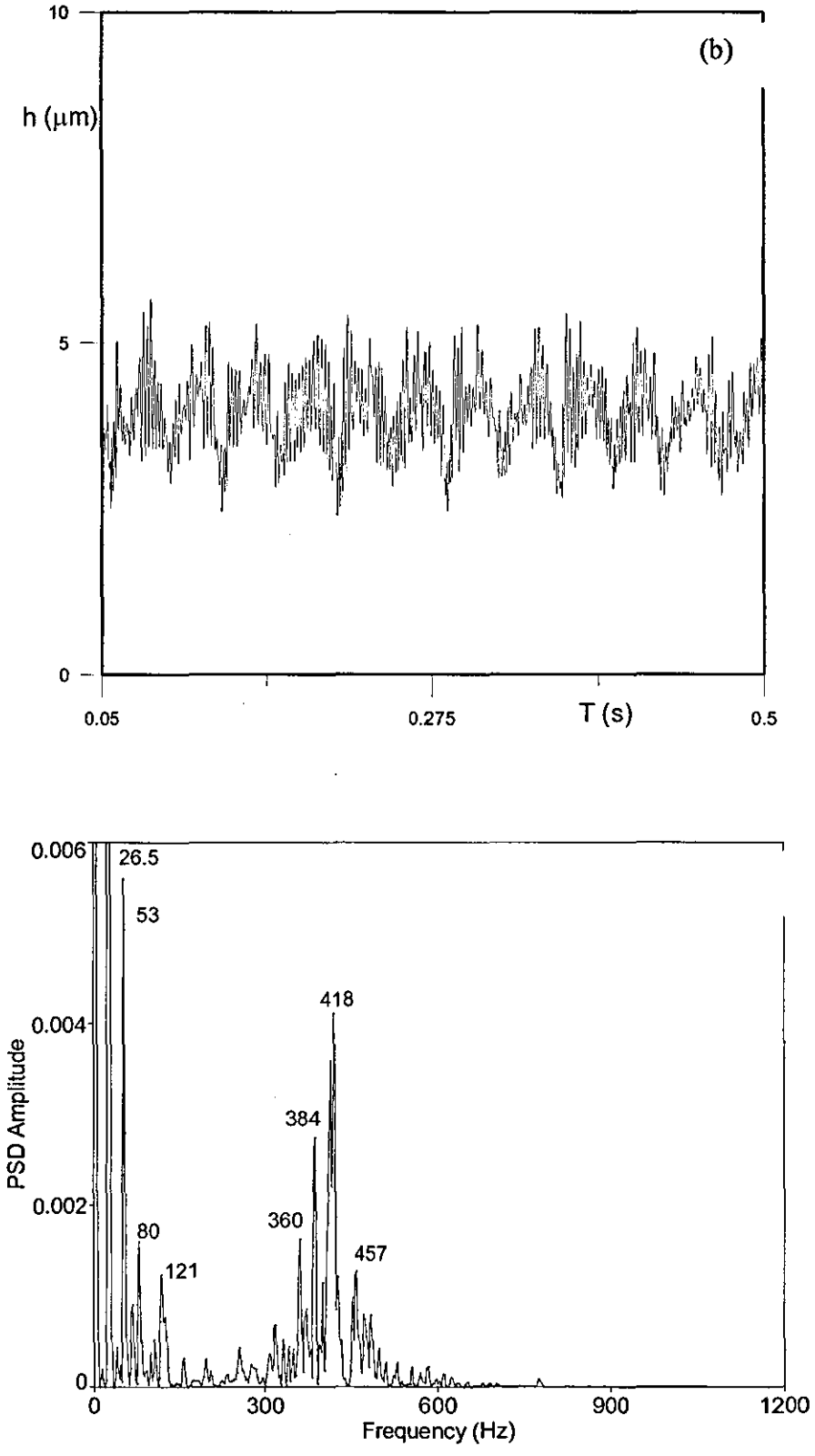

Figure 6.2: Simulated time histories and FFT spectra of h for (a) 2nd Gear and (b) 6th Gear (39.4 ° C and 10μm bearing clearance)

Figure 6.3 and 6.4 show the rattle ratios of both gear pairs. Only the 2nd gear crosses the rattle threshold. From figure 6.2, it can be seen that the rattling pair is exhibiting higher levels of tooth separation (higher film thickness amplitude).

Gear set	1st	2nd	3rd	4th	5th	6th	7th
f_m	173.33	293.33	386.67	506.67	466.67	506.67	108.33
CR_t	1.45	1.52	1.28	2.10	1.82	1.95	1.64
f_{roll}	119.54	192.98	302.09	241.27	256.41	259.83	66.05

Table 6.1: Meshing and rolling frequencies at 800 rpm

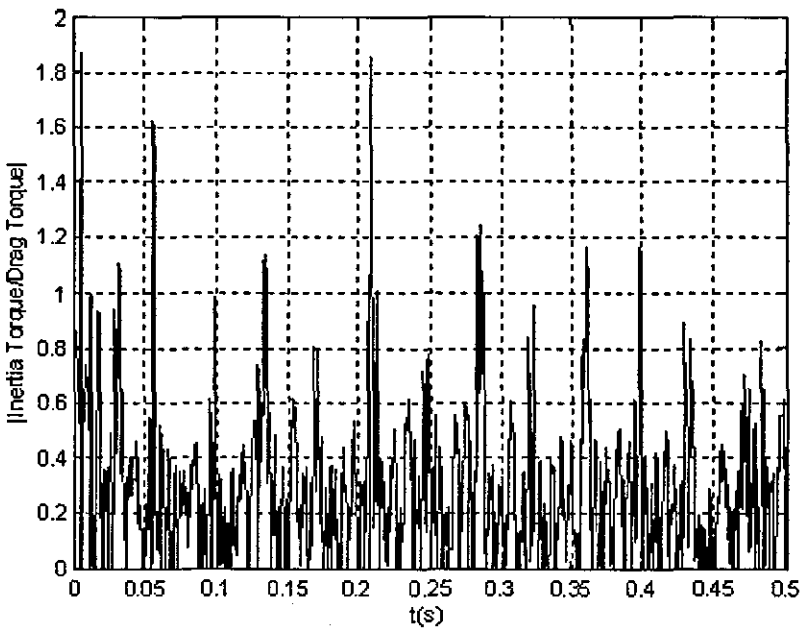

Figure 6.3: The rattle ratio of the 2nd gear

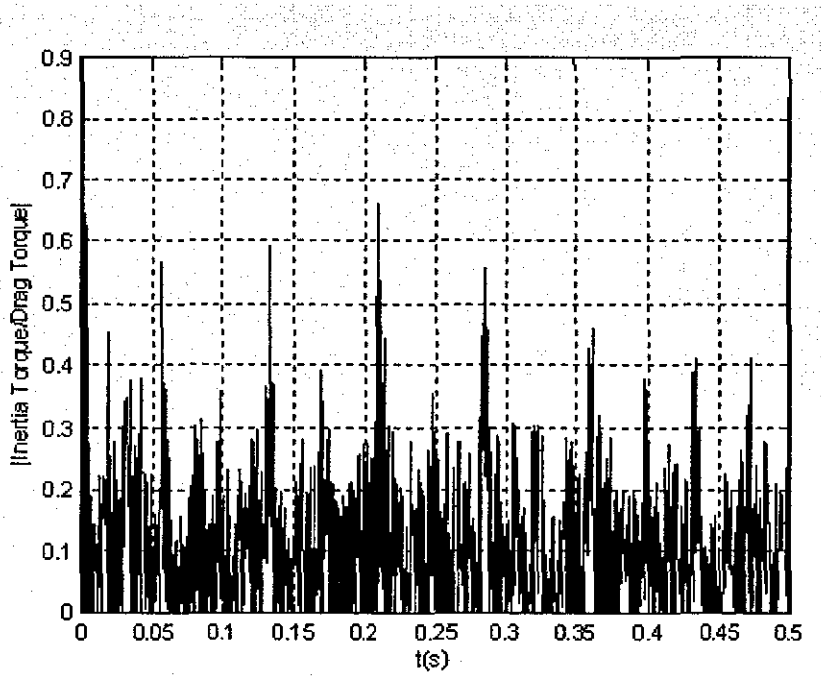

Figure 6.4: The rattle ratio of the 6th gear

Moreover, the parametric study of lubricant viscosity and its effect on the mechanical system response reveals an interesting scenario, which is shown in figure 6.5. The Root Mean Square (RMS) values of the idle gears' rotational acceleration clearly show a downward trend towards a minimum value in a certain temperature range. This phenomenon is in agreement with the findings of Fujimoto and Kizuka (2001), who have shown that rattle noise levels are particularly low within a specific temperature range, which is reached in the gearbox after a given period of engine operation. The downward trend seems to suggest that the reduction of lubricant viscosity, as temperature increases, has a positive effect on the gear rattle noise radiated to the environment. This effect seems to be true for only a small range of temperature. In the aforementioned temperature range, the lubricant stiffness becomes critically small to permit smooth transmission of motion between the gear teeth pairs during the meshing cycle. Considering equation 3.25, this indicates the dominance of the rolling (first) term rather than the squeeze (second) term. The multiple impacts between teeth are significantly reduced by the cushioning effect of the rolling term in equation 3.25 and thus, vibration amplitudes are generally lowered. The graphs in figure 6.5 show that vibration levels are particularly low in the range 40-50°C for the particular examined transmission system.

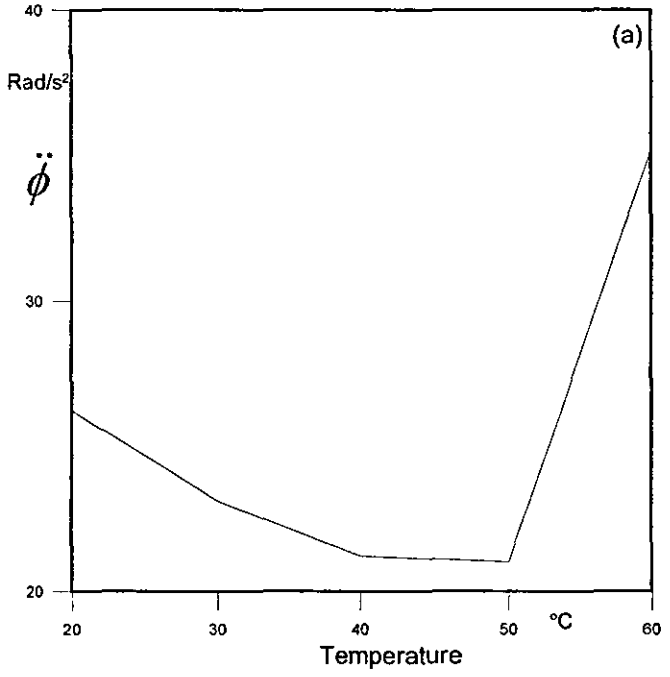

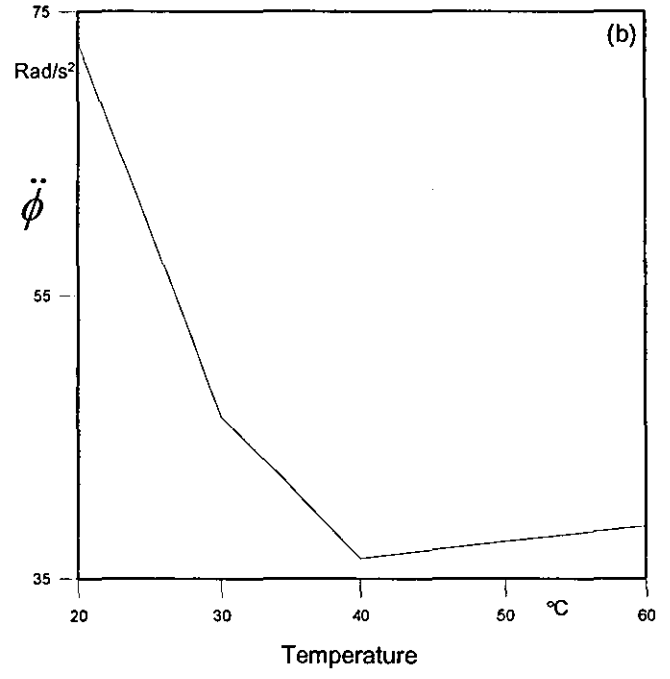

Figure 6.5 (continued over)

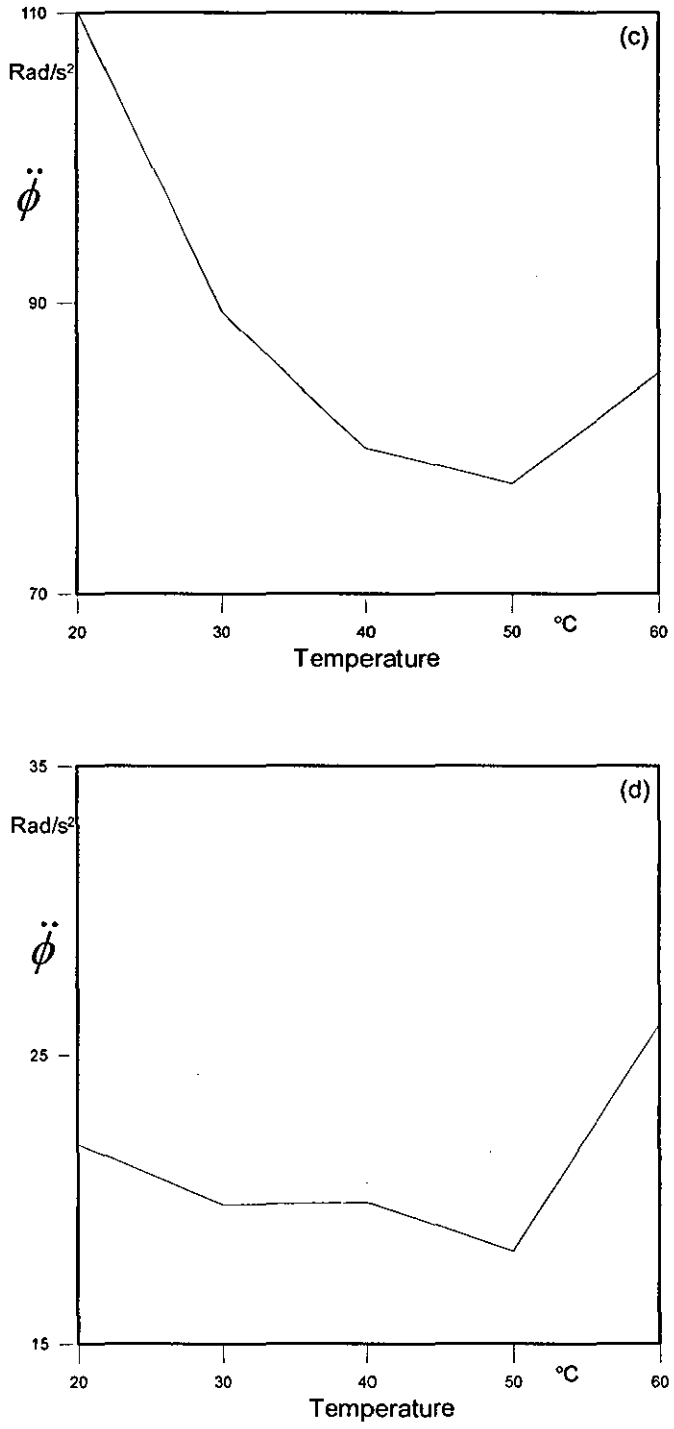

Figure 6.5: RMS Values of $\ddot{\varphi}$ with respect to Temperature for (a) 1st Gear, (b) 2nd Gear, (c) 4th Gear and (d) Reverse Gear.

The investigations here show the existence of an inter-play between the effects of hydrodynamic reaction in meshing pairs and the drag torque between the loose gear

and the supporting output shaft. Since the same lubricant is used in both cases and the geometry of contact differs, changes in lubricant viscosity can make one dominate in certain circumstances and the other in other occasions, depending on contact kinematics and number of meshing pairs. The situation is, therefore, complex, but the significant role of this interaction is clear. Variations between mechanical systems – affecting the overall system behaviour – are generally expected, since the geometric characteristics of the gears change significantly between different types of vehicles.

6.3 The 11-Degree of Freedom Model and the Vehicle Experiments:

The first case examined corresponds to typical values for gear backlash (from 80 to 150 μm, with the larger values corresponding to the higher inertia gear pairs), lubricant dynamic viscosity (0.05122 Pa·s, corresponding to 39.4 °C temperature of the bulk transmission lubricant) and engine speed in idle (810 rpm). The vibration spectrum of the transmission input shaft acceleration is the same as the one shown in figure 3.10. Similar temperature conditions had also been recorded experimentally in the test vehicle, and measurements were captured for comparative purposes.

Figures 6.6 and 6.7 show the FFT spectra of the (modelled) output shafts' rectilinear motions. There are high frequency contributions in both x and y directions, due to the bearing stiffness affecting the motions of the shafts. More specifically, the first output shaft (figure 6.6) exhibits lower frequencies (1775 and 1800 Hz) compared to the second shaft (2016 and 2139 Hz), as shown in figure 6.7. This is because of the larger mass of the first shaft assembly. The characteristics of the shafts' vibration are important, since these components are in the path of vibration transfer from the input shaft to the transmission case (the bell housing). These frequencies are observed in the spectra of the transmission housing accelerometers' responses (figure 6.8 to 6.10) within 3% difference. The natural frequencies and normal modes of the rectilinear motion of the two output shafts (the translational degrees of freedom) are given in figure 6.11. The black spots represent (from left to right) the degrees of freedom of the model corresponding to the generalised coordinates $\varphi_1, \varphi_2, \ldots, \varphi_7, x_1, y_1, x_2, y_2$.

The direction of the dot displacement indicates whether the coupling between the degrees of freedom is in- or out of phase. The figure shows that the shaft response frequencies predicted by the model are identical (within 2%) to the natural frequencies obtained from the linearised model. Figure 6.11 also reveals strong coupling between the fifth wheel and the second output shaft in the y_2 direction). It should be noted that during idling conditions neither shaft is rotating. Hence, apart from their natural frequencies, no other bearing frequencies, such as the ball passing frequency, exist.

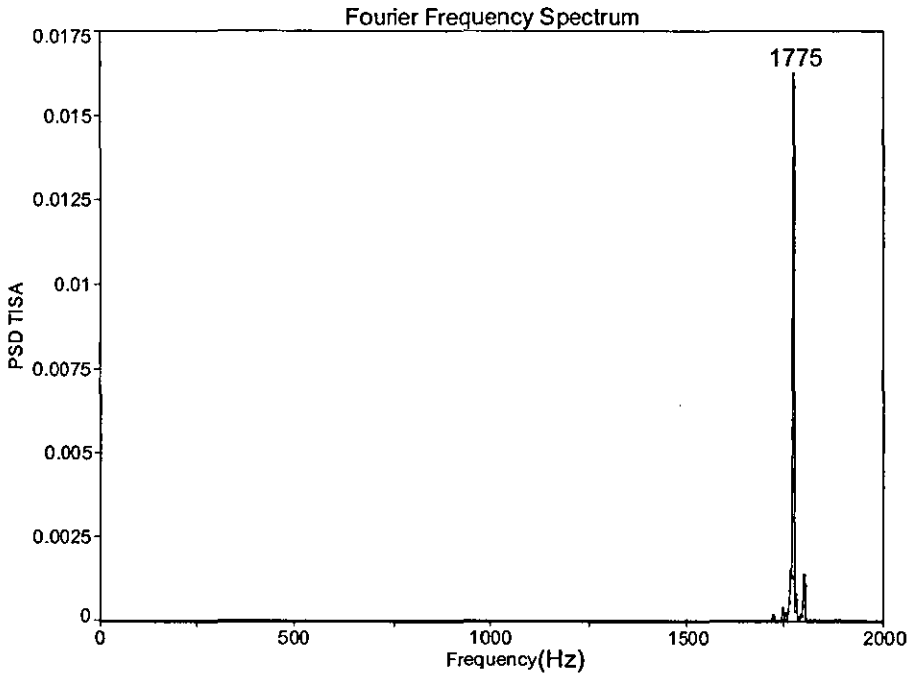

Figure 6.6 (Continued over)

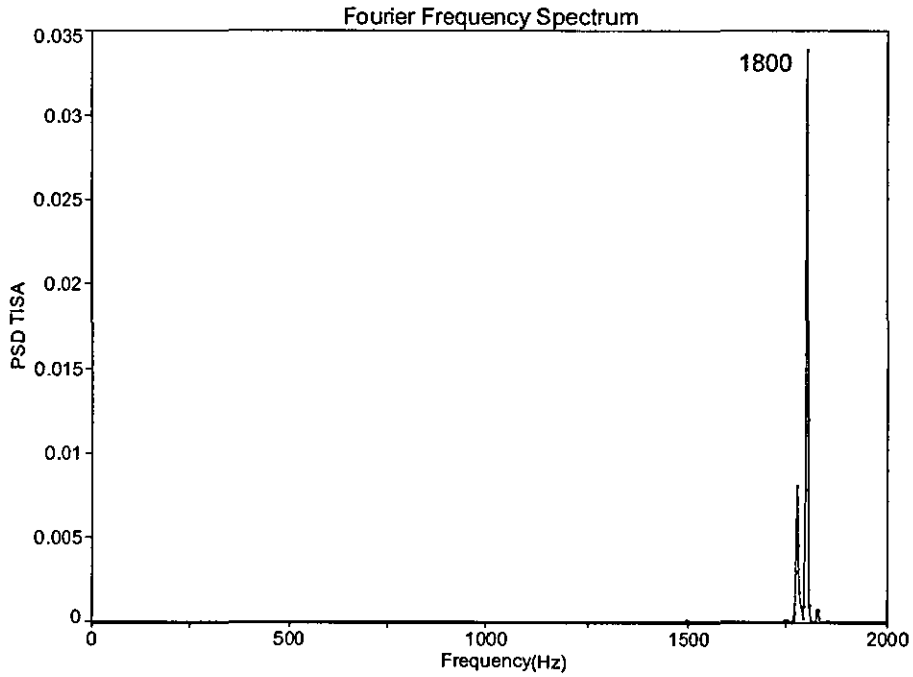

Figure 6.6: The simulated first output shaft spectra in x- (top) and y- (bottom) directions (1st case)

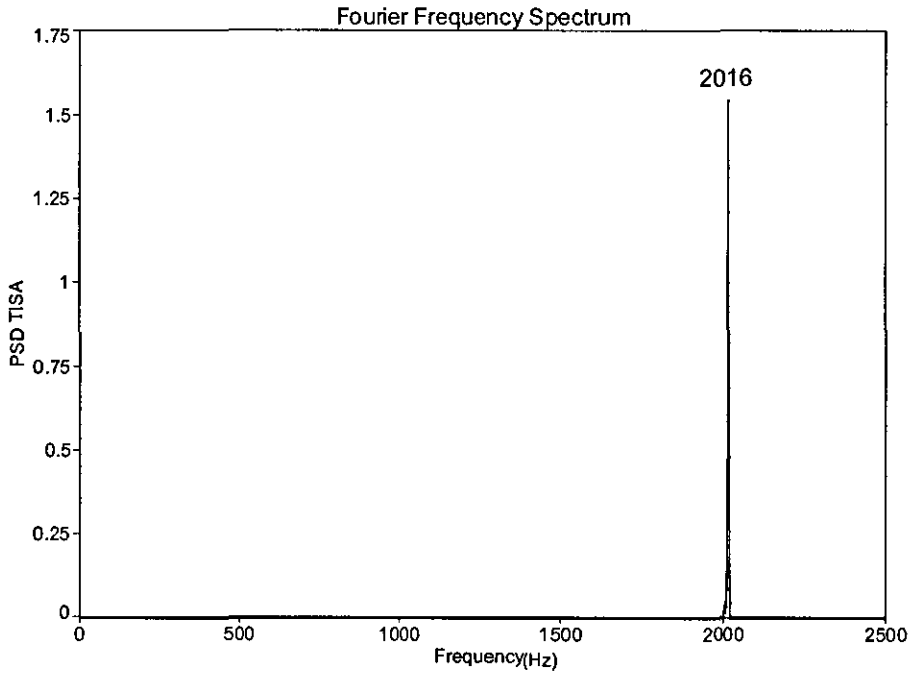

Figure 6.7 (Continued over)

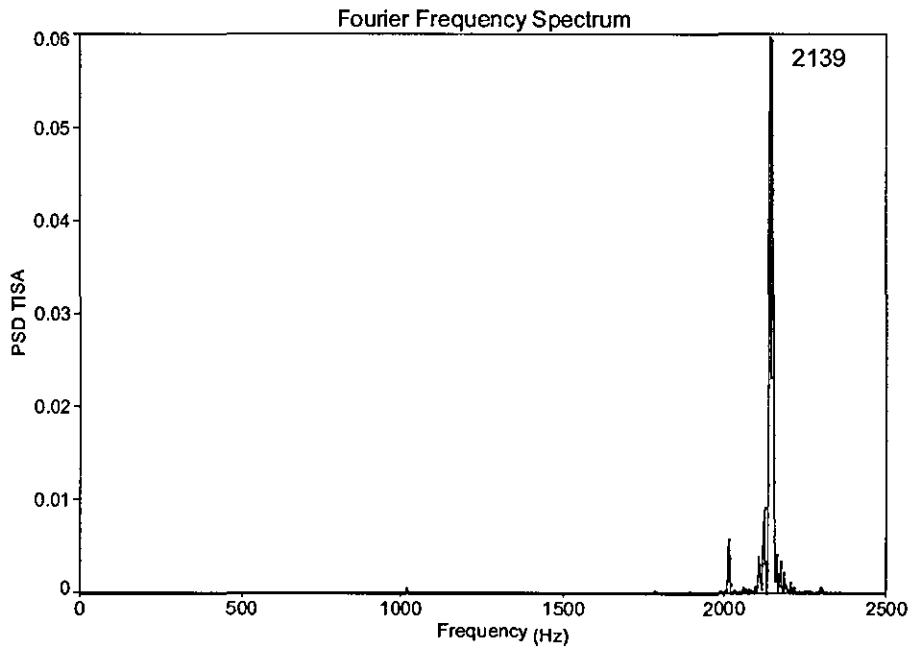

Figure 6.7: The simulated second output shaft spectra in x- (top) and y- (bottom) directions (1st case)

Further inspection of the housing spectra by the transmission wall accelerometer (figure 6.8) shows more engine harmonics (26, 53, 78, and 106 Hz) than the other two accelerometers (figures 6.9 and 6.10), because of its proximity to the engine block (it would capture the engine harmonics directly). There are strong components at 350 and 700 Hz, but when running the engine at various speeds (figure 6.12), these frequencies do not shift, suggesting that they are not associated with the meshing.

The natural frequencies of the housing structure are listed in Table 6.2 (up to 3 kHz). The frequency 1750 Hz lies, within 2% error, near 1781 Hz (figure 6.9), which is associated with the first shaft's response in x-direction (figure 6.6); the response at 2422 Hz (figure 6.9) lies within less than 2% difference from the housing natural frequency 2380 Hz (table 6.2). The housing natural frequency 2070 Hz (table 6.2) is clearly excited as shown in figure 6.10 (appears 2071 Hz).

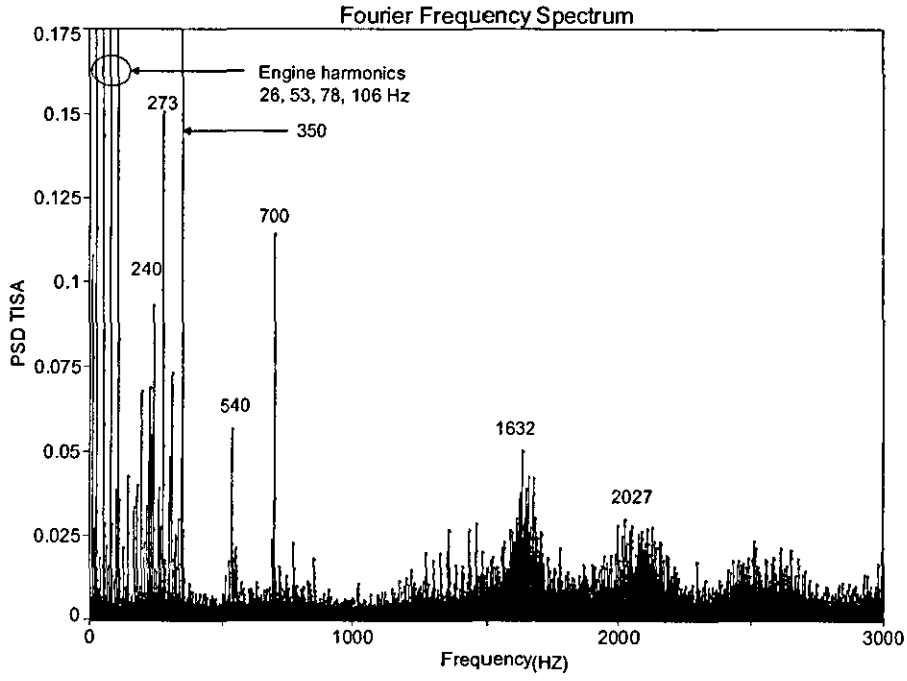

Figure 6.8: FFT Spectrum of the transmission wall accelerometer's response (1st case)

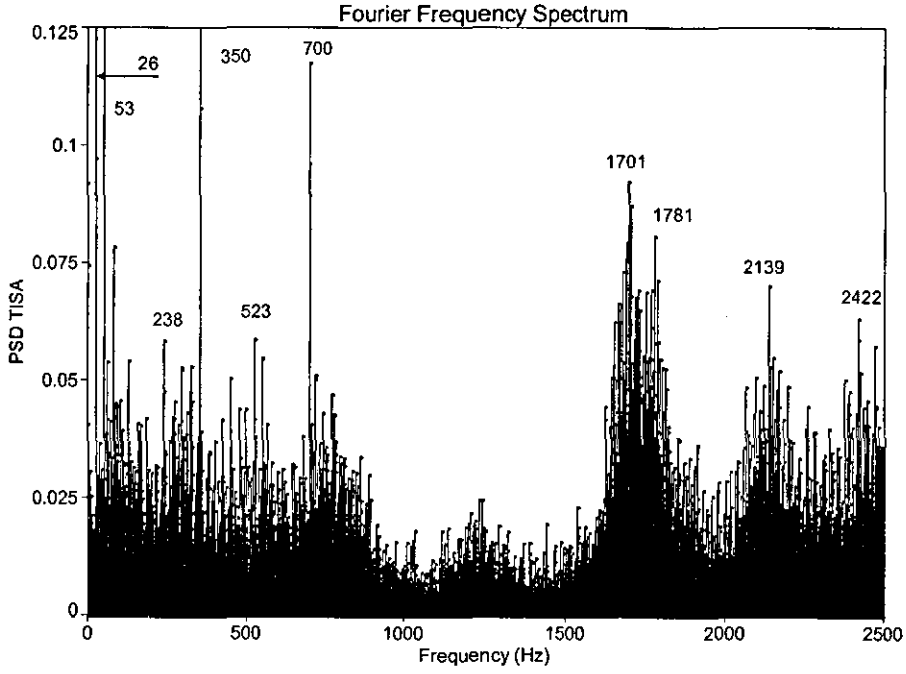

Figure 6.9: FFT spectrum of the transmission input bearing housing accelerometer's response (1st case)

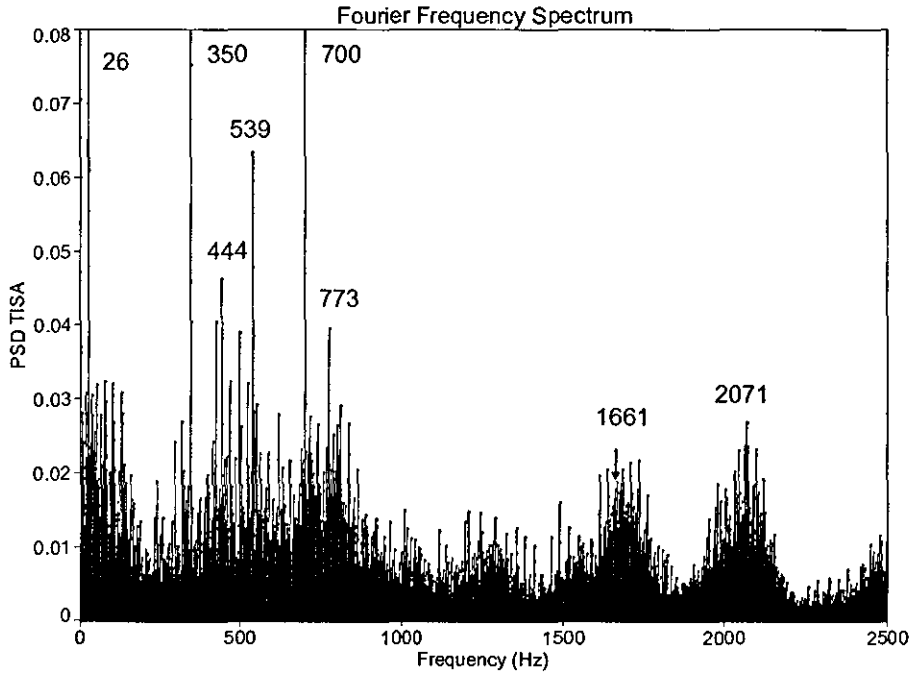

Figure 6.10: FFT spectrum of the transmission upper output bearing housing accelerometer's response (1st case)

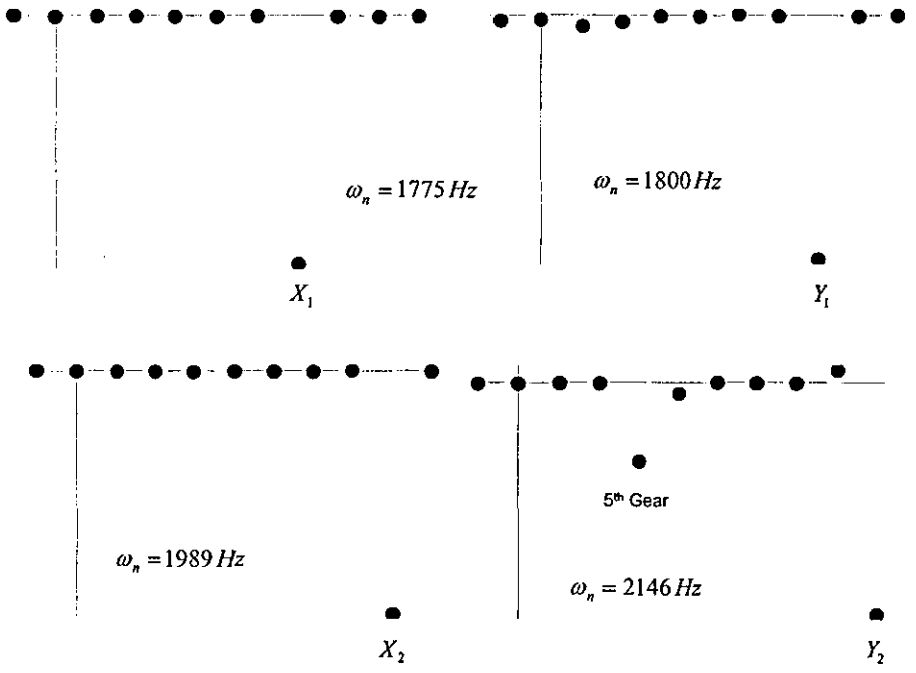

Figure 6.11: Natural frequencies and mode shapes of the output shafts (1st case)

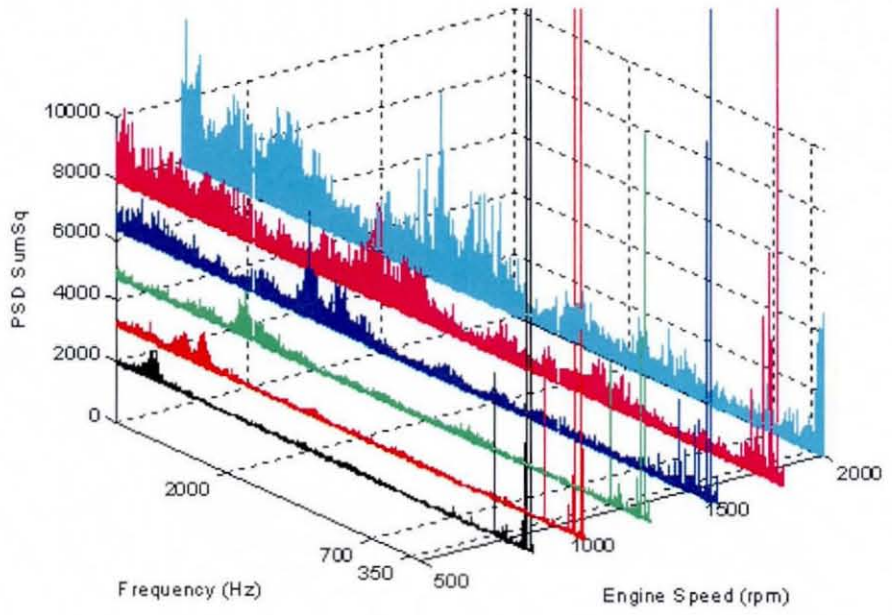

Figure 6.12: Transmission wall spectra at 810, 1000, 1250, 1500, 1750 and 2000 rpm

1020 Hz	1200 Hz	1430 Hz	1750 Hz	1845 Hz
2070 Hz	2380 Hz	2700 Hz	2890 Hz	3065 Hz

Table 6.2: Natural frequencies of the gearbox in the frequency region up to 3 kHz

The responses of the housing captured by the accelerometer mounted at the housing wall (figure 6.8) and at the input bearing (figure 6.9) contain components at 240 and 238 Hz, respectively. These two components can be linked to the 1st or 4th wheel acceleration responses at 238 and 248 Hz (within 4% error), respectively, (figures 6.13 and 6.14). When consulting table 6.1, these two frequencies can be linked to the rolling action of each gear (the second and first harmonic of the 1st and 4th wheel rolling frequency, respectively). In figure 6.13, the 356 Hz component is the third harmonic of the first gear rolling response, and the 132 Hz component could be due to the 7th (reverse) gear rolling response (second harmonic), as could be deduced from table 6.1. The lower contributions (26, 52, 80) in figure 6.13 are the engine orders.

Similarly in figure 6.14 the lower contributions are the engine orders. An activity in the region around the 248 Hz component between 198 Hz and 286 Hz is observed in figure 6.14 suggesting possible modulation at 13 Hz.

Additionally, the 1st gear natural frequency (250 Hz), which was obtained by solving the eigen-value problem (chapter 4), lies within 5% error margin from 238 Hz. Furthermore, when inspecting the normal mode of the 1st gear (figure 6.15), a strong coupling with the 4th gear is observed.

The component at 286 Hz (4th gear response in (figure 6.14) is within a margin of 5% difference from the 273 Hz component captured by the transmission wall accelerometer (figure 6.8). The 540 Hz (figure 6.8) and 539 Hz (figure 6.10) represent approximately the second harmonic of 273 Hz.

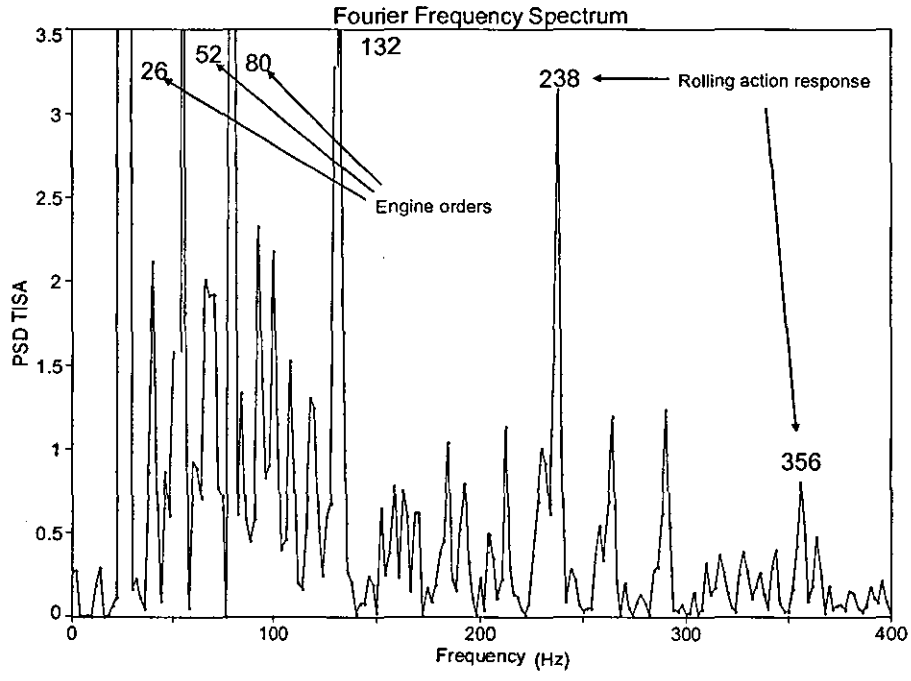

Figure 6.13: FFT spectrum of the simulated 1st wheel acceleration (1st case)

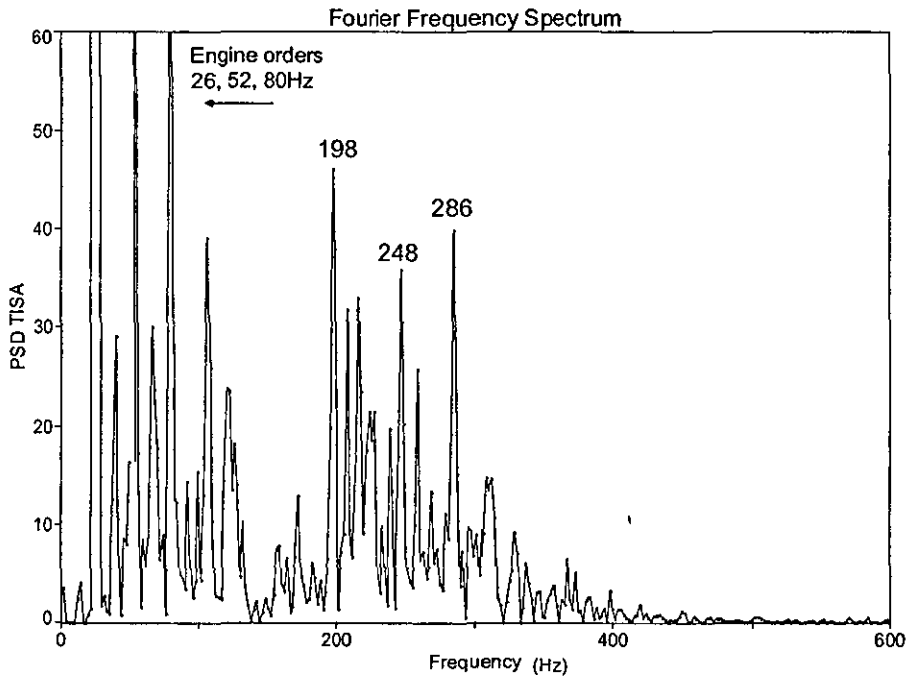

Figure 6.14: FFT spectrum of the simulated 4th wheel acceleration (1st case)

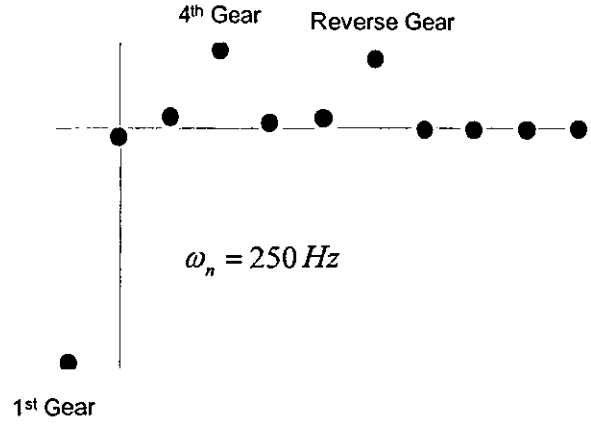

Figure 6.15: Natural frequency and normal mode of the simulated 1st gear contact (1st case)

Figures 6.16 to 6.18 show the rattle and squeeze-to-rolling ratios of the 1st, 4th, and 6th gears, respectively. Only the 1st gear crosses the rattle threshold, mainly due to the higher inertia of its loose wheel. The film reaction due to rolling action is clearly dominant in all the three gears since their corresponding squeeze-to-rolling force ratios are less than unity, suggesting mild rattling. The squeeze-to-rolling ratio assesses the contribution of squeeze action (approach leading to impact) to the system

dynamic and it is obtained by dividing the squeeze term (second term) of equation (3.25) by the rolling term (first term) of equation (3.25):

$$\left.\begin{aligned}\text{Squeeze}-\text{to}-\text{roll force ratio} &= \frac{3\pi}{2\sqrt{2}}\frac{\left|\frac{\partial h}{\partial t}\right|}{u_{ent}\sqrt{\frac{h}{r_{eq}}}}, \quad if \quad \frac{\partial h}{\partial t} < 0 \\ \text{Squeeze}-\text{to}-\text{roll force ratio} &= 0.0, \qquad\qquad if \quad \frac{\partial h}{\partial t} \geq 0\end{aligned}\right\} \tag{6.1}$$

Equation (6.1) indicates that high squeeze rate (film speed) exacerbates rattle as well as high equivalent radius of curvature. On the other hand, high entraining velocity or film thickness attenuates rattle. Thus, for design purposes, by optimising the gear geometry through a parametric study such that reasonably high entraining velocity is achieved and higher film thickness is maintained at the contact, rattling could be attenuated.

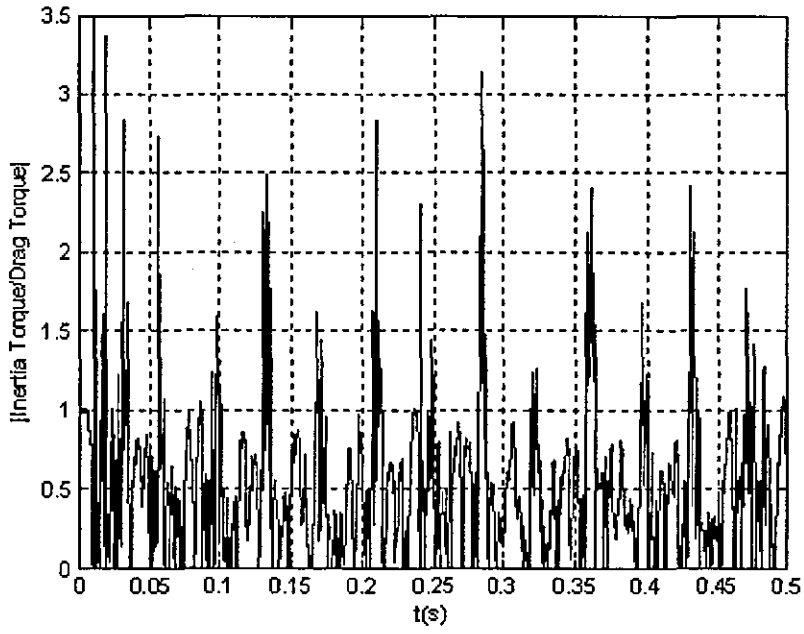

Figure 6.16 (continued over)

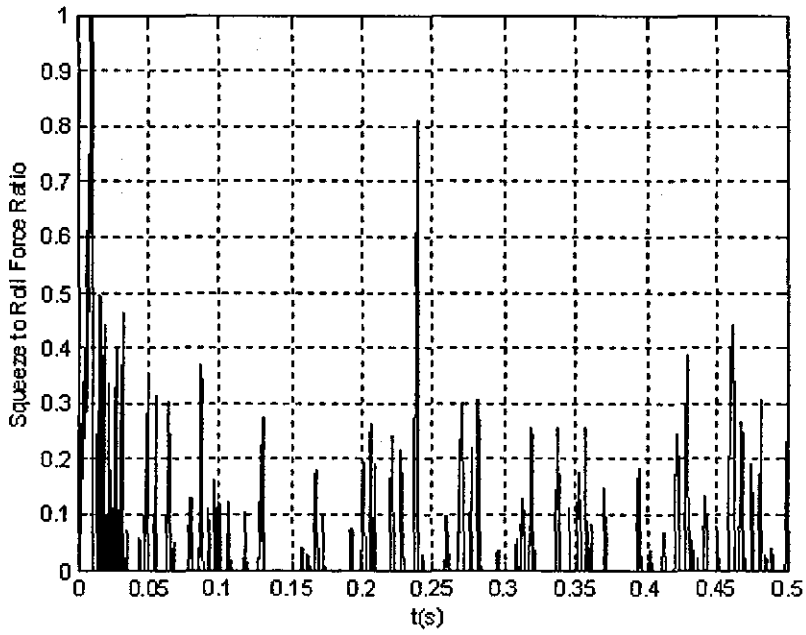

Figure 6.16: Simulated rattle and squeeze to rolling ratios of the 1st gear (1st case)

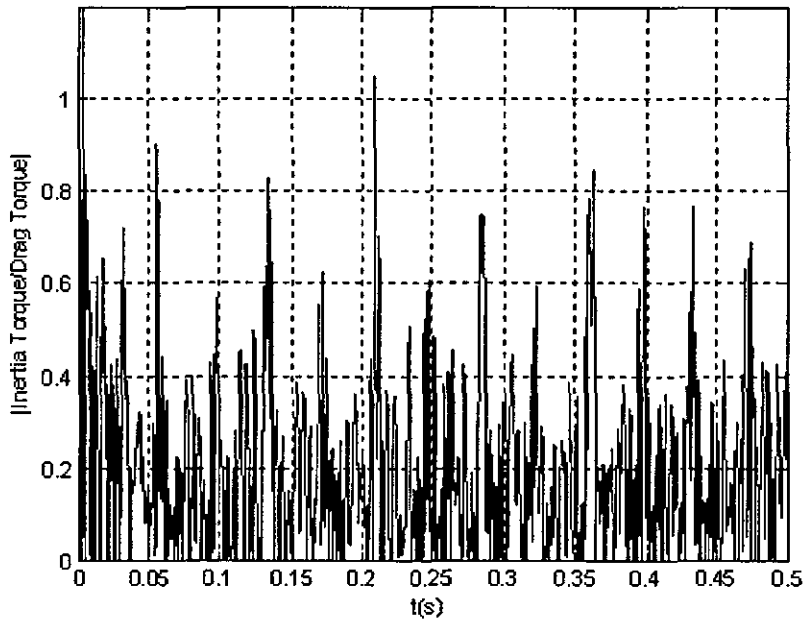

Figure 6.17 (continued over)

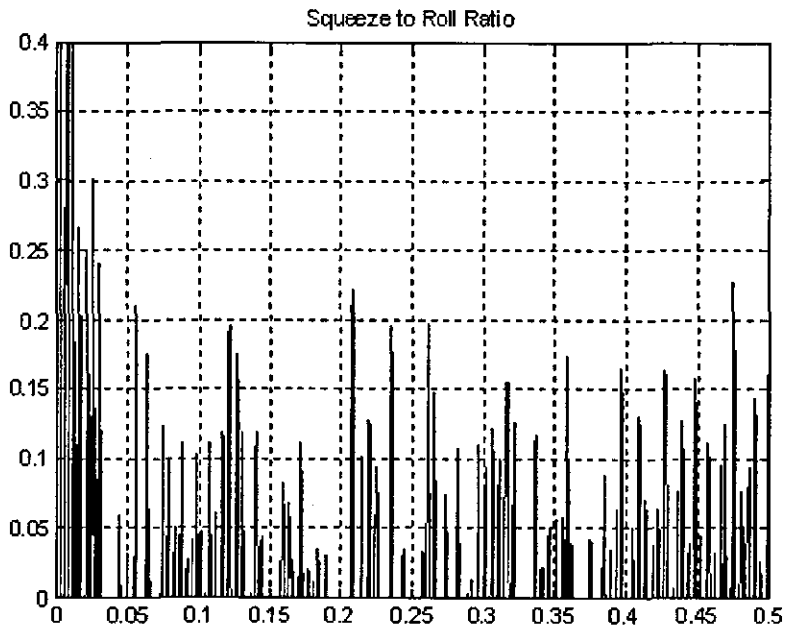

Figure 6.17: Simulated rattle and squeeze to rolling ratios of the 4th gear (1st case)

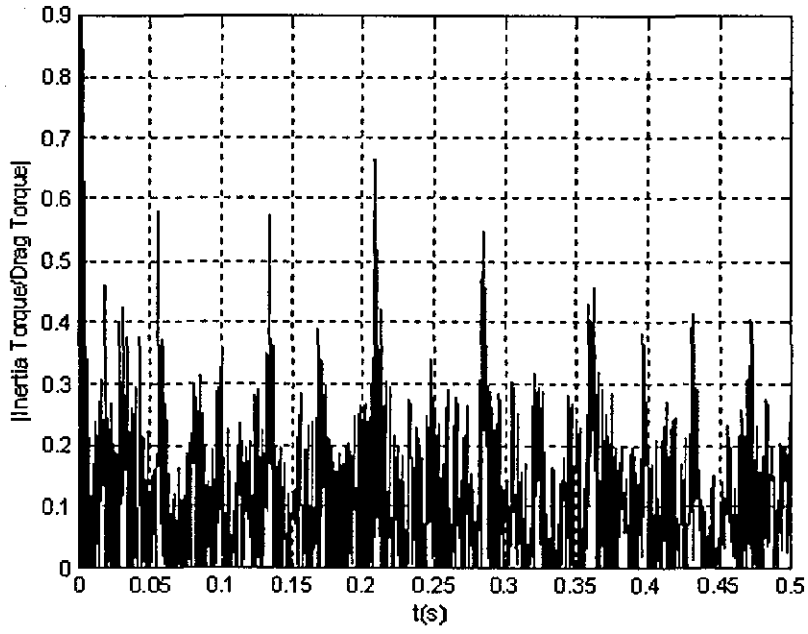

Figure 6.18 (continued over)

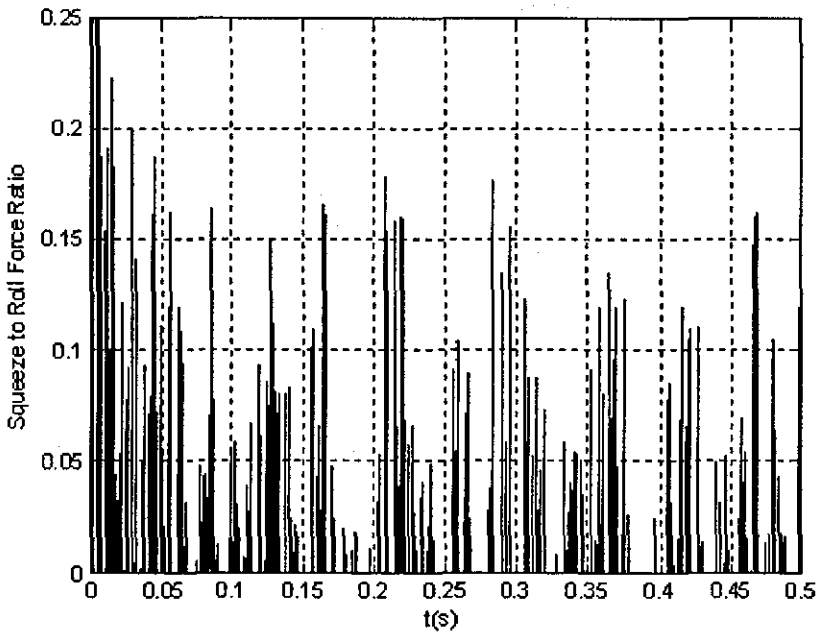

Figure 6.18: Simulated rattle and squeeze to rolling ratios of the 6th gear (1st case)

A second case was examined (using the same vehicle) at a sump temperature of 24.2 °C, thus, viscosity of 0.09512 Pa s. The input to the model is also the same as in first case. Hence, the vibration spectrum of the transmission input shaft acceleration is the same the one shown in figure 3.10. The FFT spectra of the same pick up points (namely the transmission wall, the input bearing housing, and the upper output bearing) are shown in figures 6.19 to 6.21. These figures, when compared to figures 6.8 to 6.10, demonstrate significant responses at higher frequencies due to the lubricant being stiffer at lower temperatures (i.e. higher viscosity).

The shafts' spectral responses, as obtained from the corresponding model, reflect a slight increase in active frequencies (figures 6.22 and 6.23), except in the case of the second shaft's motion in y-direction, where a lower frequency is obtained. The frequencies 1798 and 1816 Hz associated with the first output shaft motion can be found (within 2% error) in the input bearing and the upper (second) output bearing housings spectra (at 1789 Hz and 1784, respectively). The latter finding can be explained by the fact that these housings are parts of the whole (cast) transmission housing and not separate entities. It should be re-iterated that the shafts motion

responses reflect the natural frequencies of the support bearings, which do not rotate in idling condition.

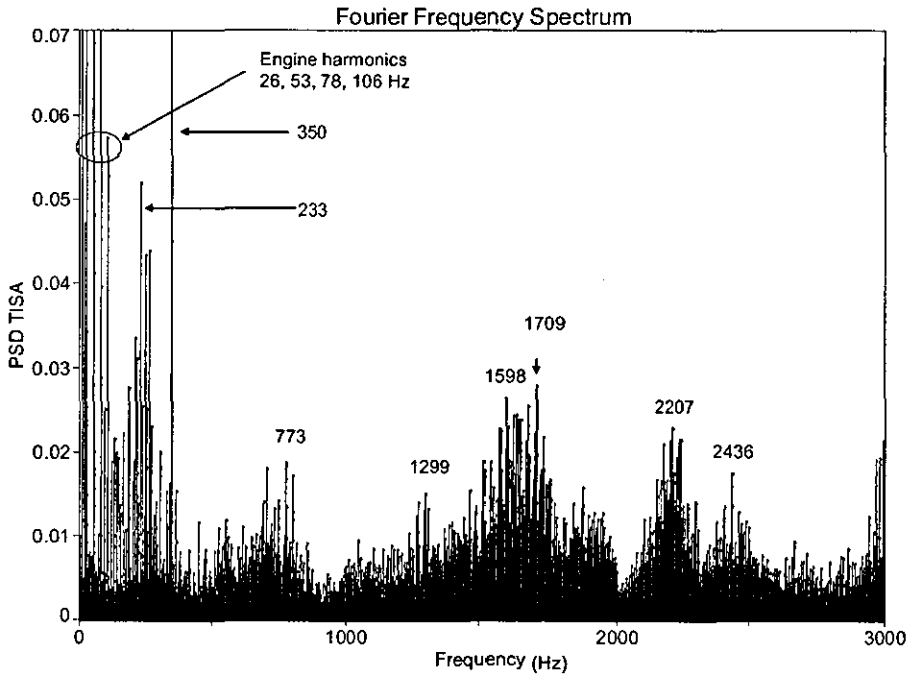

Figure 6.19: FFT spectrum of the transmission wall accelerometer's response (2^{nd} case)

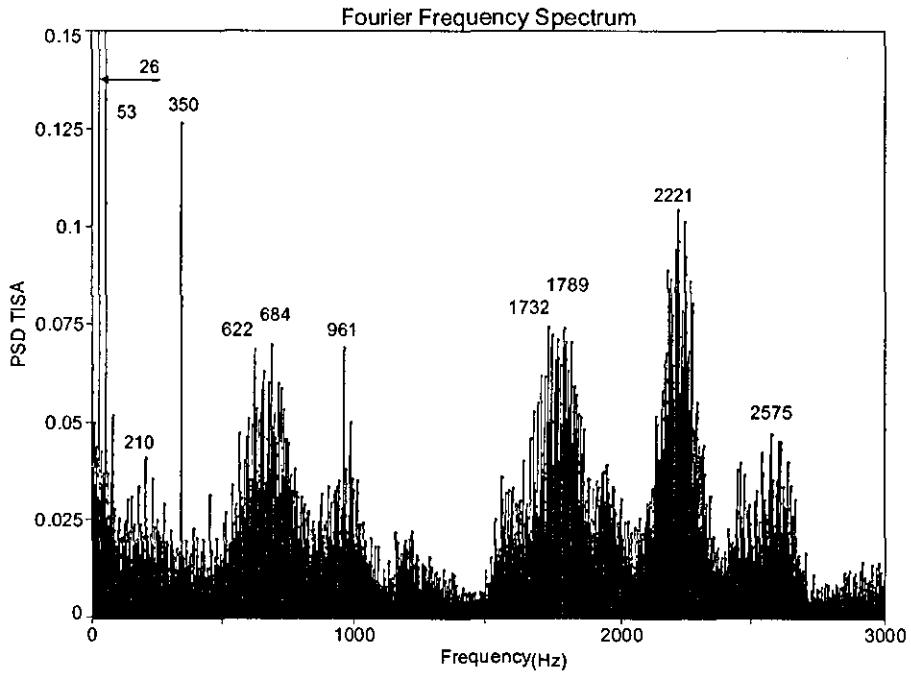

Figure 6.20: FFT spectrum of the transmission input bearing housing accelerometer's response (2^{nd} case)

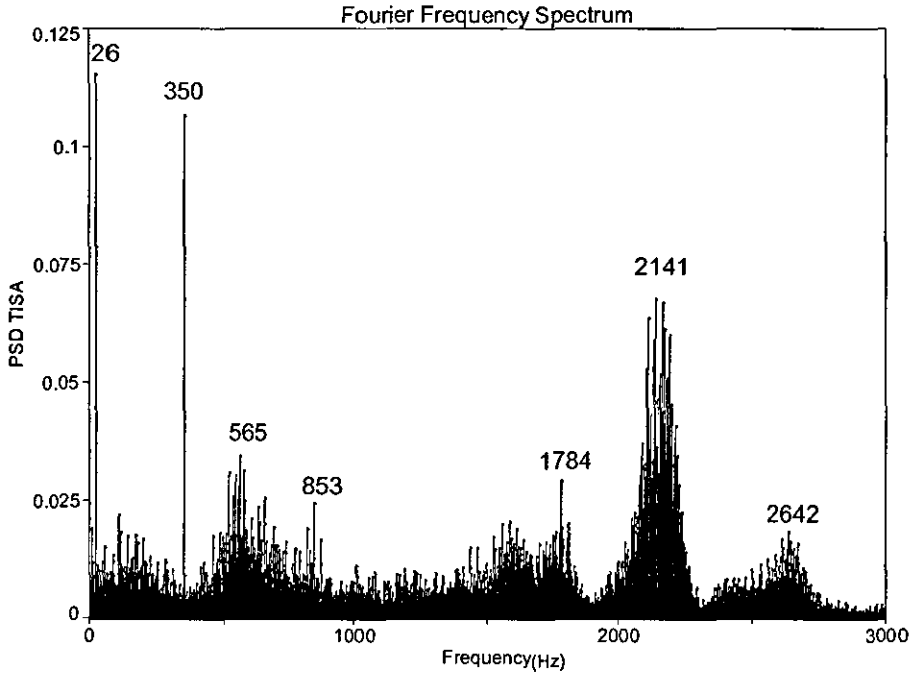

Figure 6.21: FFT spectrum of the transmission upper output bearing housing accelerometer's response (2nd case)

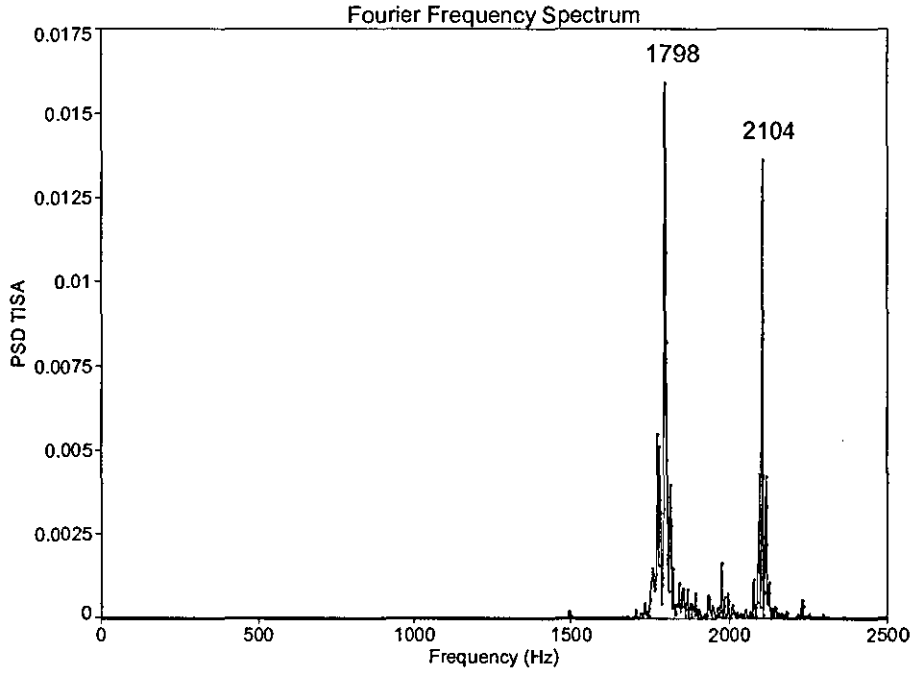

Figure 6.22 (continued over)

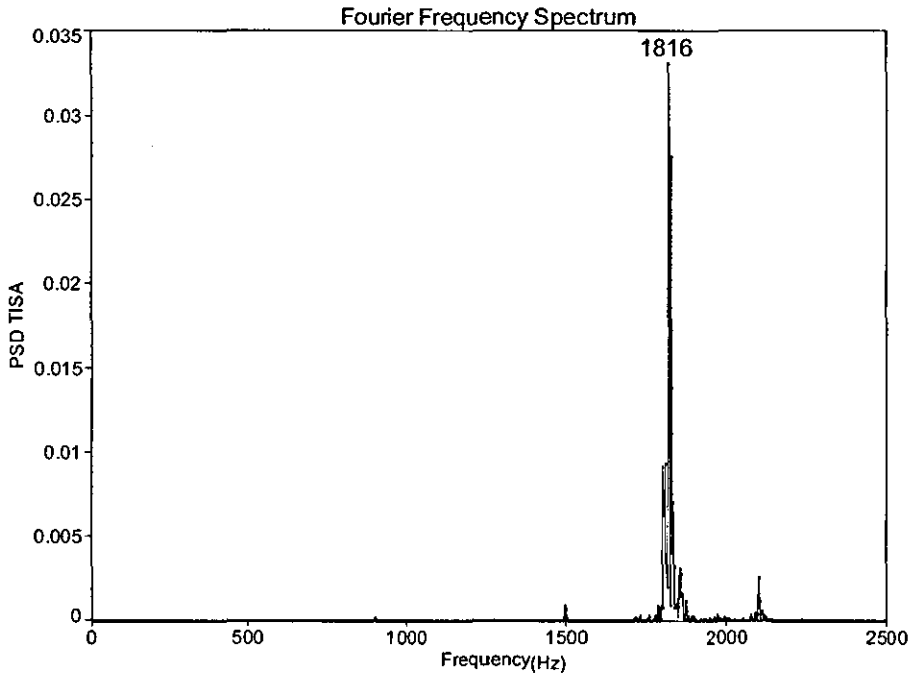

Figure 6.22: The simulated first output shaft spectra in x- (top) and y- (bottom) directions (2nd case)

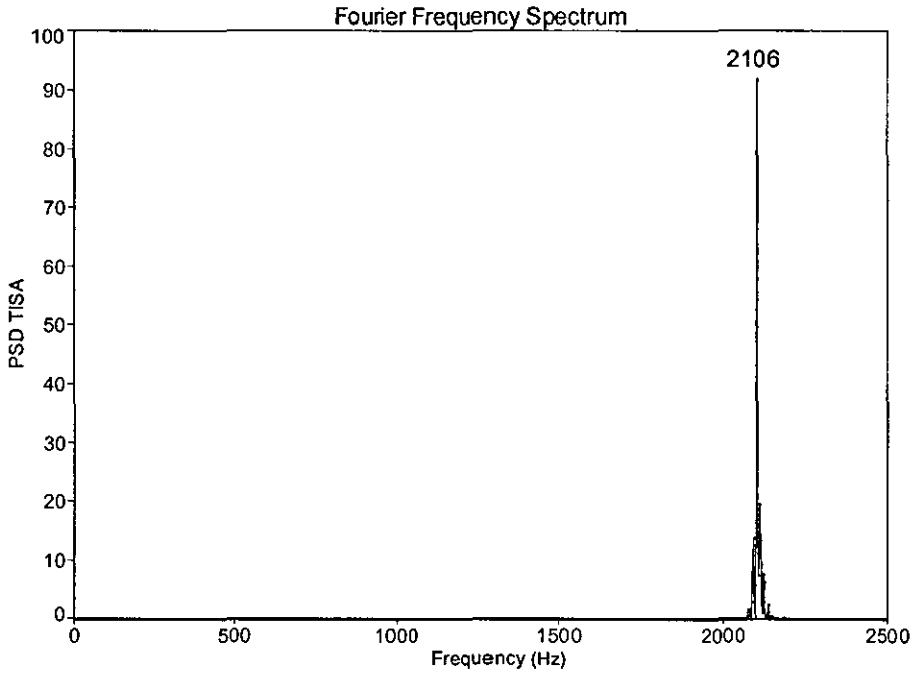

Figure 6.23 (continued over)

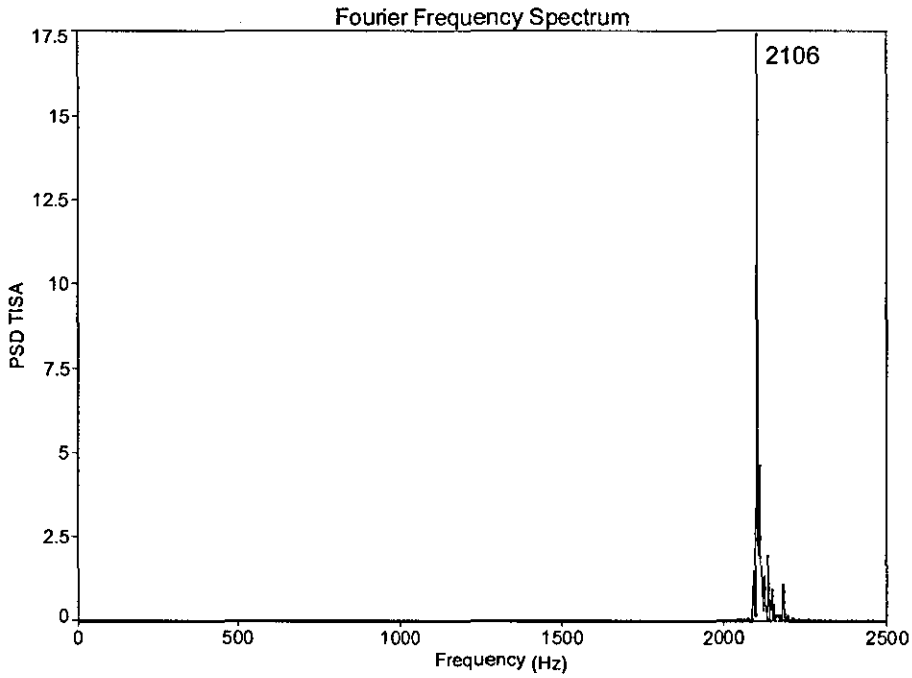

Figure 6.23: The simulated second output shaft spectra in x- (top) and y- (bottom) directions (2nd case)

The predicted responses (natural frequencies of the support bearings) of the second (upper) output shaft, at 2106 Hz (figure 6.23), appear in the upper shaft accelerometer's response at 2141Hz (figure 6.21) within 2% error. Unlike the first case when the temperature was 39.4 °C, it is apparent that the responses of the second shaft in the x- and y- directions are identical. Furthermore, the predicted response of the second output shaft is so dominant that it also appears in the response of the first shaft. In fact, it also appears in the predicted acceleration response of the 1st, 5th, and 6th wheels, as demonstrated in figures 6.24 to 6.26, respectively. While the 5th and 6th gear pairs are directly affected by the motion of the second output shaft, the 1st gear and subsequently the first output shaft are affected indirectly by virtue of the 1st wheel being manufactured with the 7th pinion as one unit.

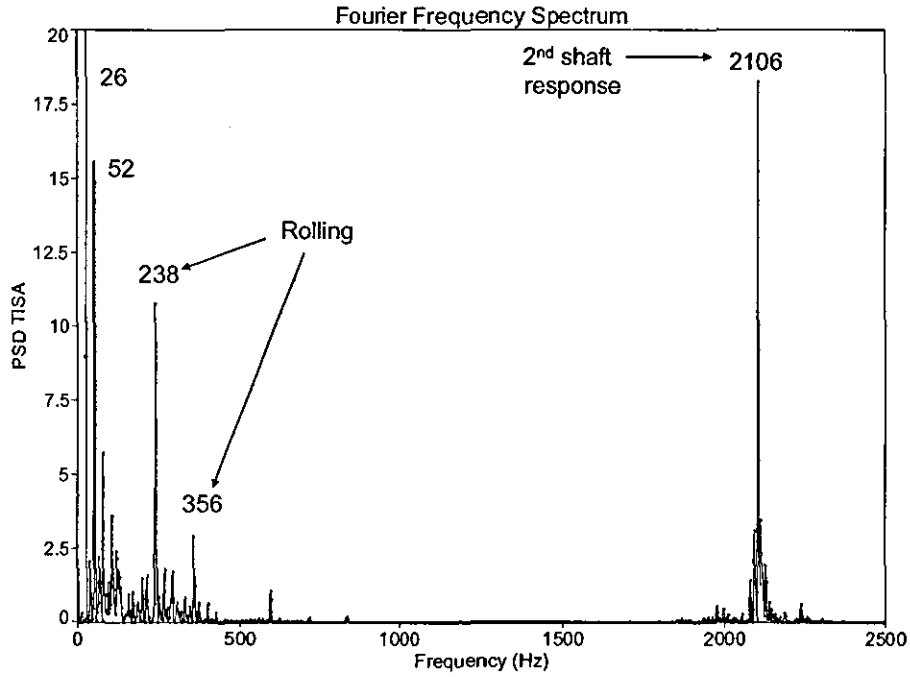

Figure 6.24: FFT spectrum of the simulated 1st gear acceleration (2nd case)

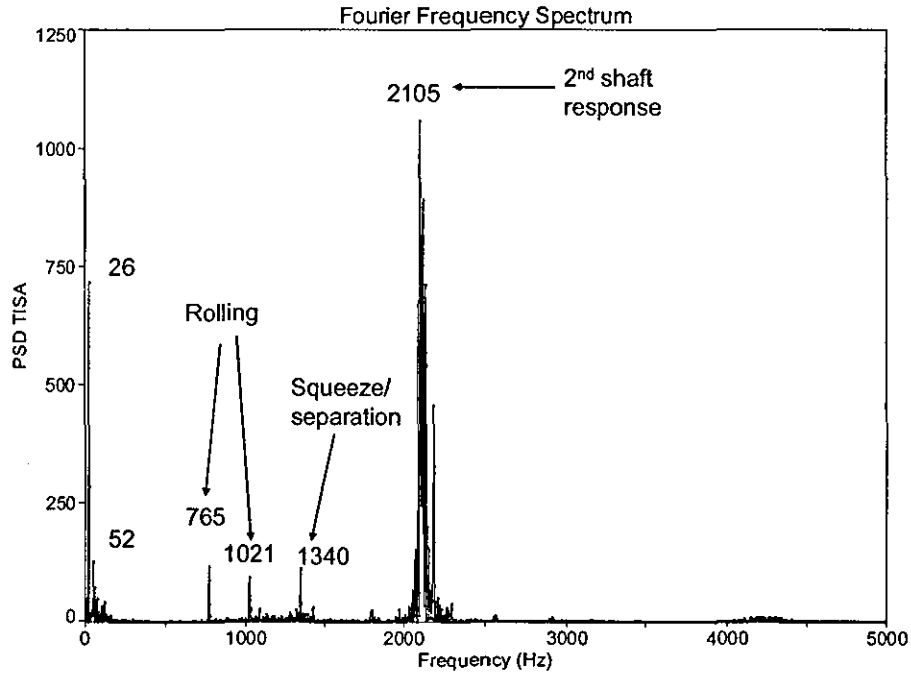

Figure 6.25: FFT spectrum of the simulated 5th gear acceleration (2nd case)

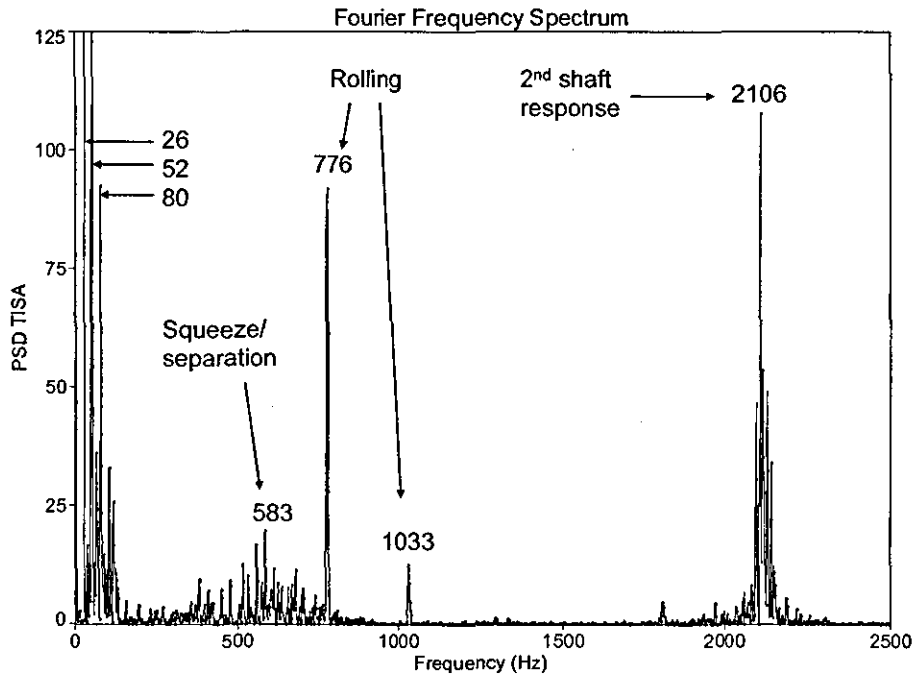

Figure 6.26: FFT spectrum of the simulated 6th gear acceleration (2nd case)

The acceleration response of the first gear is also dominated by the rolling action (figure 6.24), mainly at 238 Hz (second harmonic) and 356 Hz (third harmonics). It should be noted that the fundamental rolling frequency is approx. 118Hz. The 238 Hz is within 3% error from 233 Hz, which appears in transmission wall spectrum (figure 6.19). The 1st gear response and possibly rattling appear to be also influenced by the rolling frequencies (i.e. parametrically excited) and the natural frequency of the second shaft.

Similar strong rolling action response is observed when comparing the corresponding spectra of the 5th and 6th (figures 6.25 and 6.26). The main rolling contributions to the 5th gear's spectrum are the third and fourth harmonics (765 and 1021 Hz, respectively). And the main rolling contributions to the 6th gear's spectrum are the third and fourth harmonics (776 and 1033 Hz, respectively). The remaining frequencies, other than the second shaft's natural frequency, in figures 6.25 and 6.26 (1340 and 583 Hz, respectively) might be associated with the squeeze/separation action, particularly the 583 Hz component, which is clearly modulated. The lower contributions in figure 6.24 (26 and 52 Hz), figure 6.25 (26 Hz), and figure 6.26 (26, 52, and 80 Hz) are the engine harmonics.

The 765Hz component and the sideband 2187Hz of the 5th wheel predicted acceleration response (figure 6.25) can be associated with 773 Hz (approx. 1% error) and the 2207Hz (less than 1% error) components of the transmission wall response (figure 6.19), respectively. The 2187 Hz sideband could also be buried within the side bands of the 2221 Hz component of the input shaft bearing response (figure 6.20) and the 2141Hz component of the upper output shaft bearing response (figure 6.21). The transmission wall's spectral component 773 Hz (figure 6.19) can be more accurately associated with the predicted 6th gear rolling component 776 Hz (figure 6.26). Furthermore, the predicted 6th gear response at 583 Hz is within 4% error margin from the 565 Hz component captured by the upper output shaft accelerometer (figure 6.21).

The predicted responses of the 2nd gear at 200 Hz and 576 Hz (figure 6.27) are observed on the input and upper output shaft accelerometer's FFT spectra at 210 Hz (figure 6.20) and within 2% error at 565 Hz (figure 6.21), respectively. The predicted responses of the 3rd gear at 600 Hz and 900 Hz (figure 6.28) lie within 4% and 7% error margin from the component at 622 Hz and 961 Hz, respectively, which were captured by the input shaft accelerometer (figure 6.20). The dominant 576 Hz in figure 6.27 is the third harmonic of the rolling frequency associated with the 2nd gear. The acceleration response of the 3rd gear is dominated by the second and third harmonics of the rolling frequencies at 600 Hz and 900 Hz, respectively (figure 6.28). The lower contribution in the 2nd and 3rd gear spectra are also dominated by the engine harmonics at 26, 52 and 80 Hz. Both responses of the 2nd and 3rd gears show modulated components at 228 Hz (with strong side bands at 200 Hz and 248 Hz) and 464 Hz, respectively. From the analysis in chapter 3, these two modulated components can be suspected for being squeeze/separation frequencies.

When inspecting the rattle and the squeeze-to-rolling force ratios (figures 6.29 to 6.32), the 1st and 7th gears are observed to be crossing the rattle threshold (figures 6.29 and 6.30). Only the 7th gear has a squeeze-to-rolling force ratio that crosses unity; nonetheless, this occurs at low frequency, thus indicating that there is still a strong rolling influence. This suggests that the severity of rattling is higher at the 7th gear than at the 1st, since rattling is mainly governed by squeeze/separation effects. The

low values of the squeeze-to-rolling ratios indicate dominance of the rolling action. Furthermore, it is clear that the motion of the second shaft plays a significant role in the rattling behaviour of the two gear pairs; such role was not observed at higher temperature.

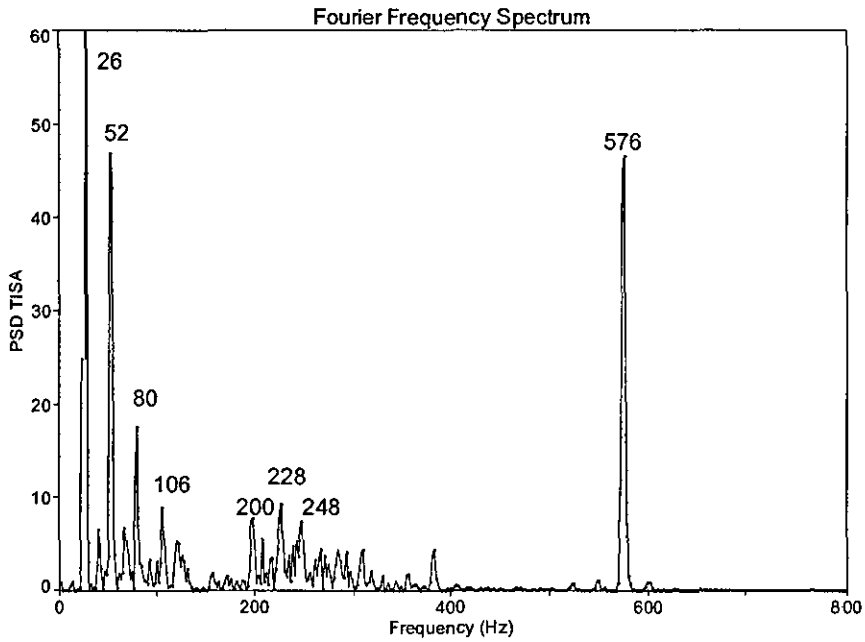

Figure 6.27: FFT spectrum of the simulated 2nd gear acceleration (2nd case)

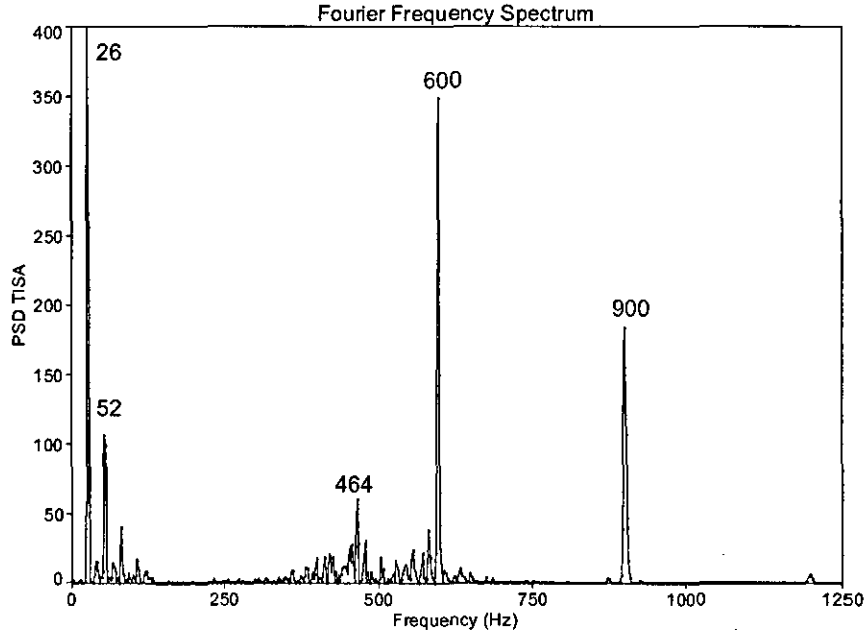

Figure 6.28: FFT spectrum of the simulated 3rd gear acceleration (2nd case)

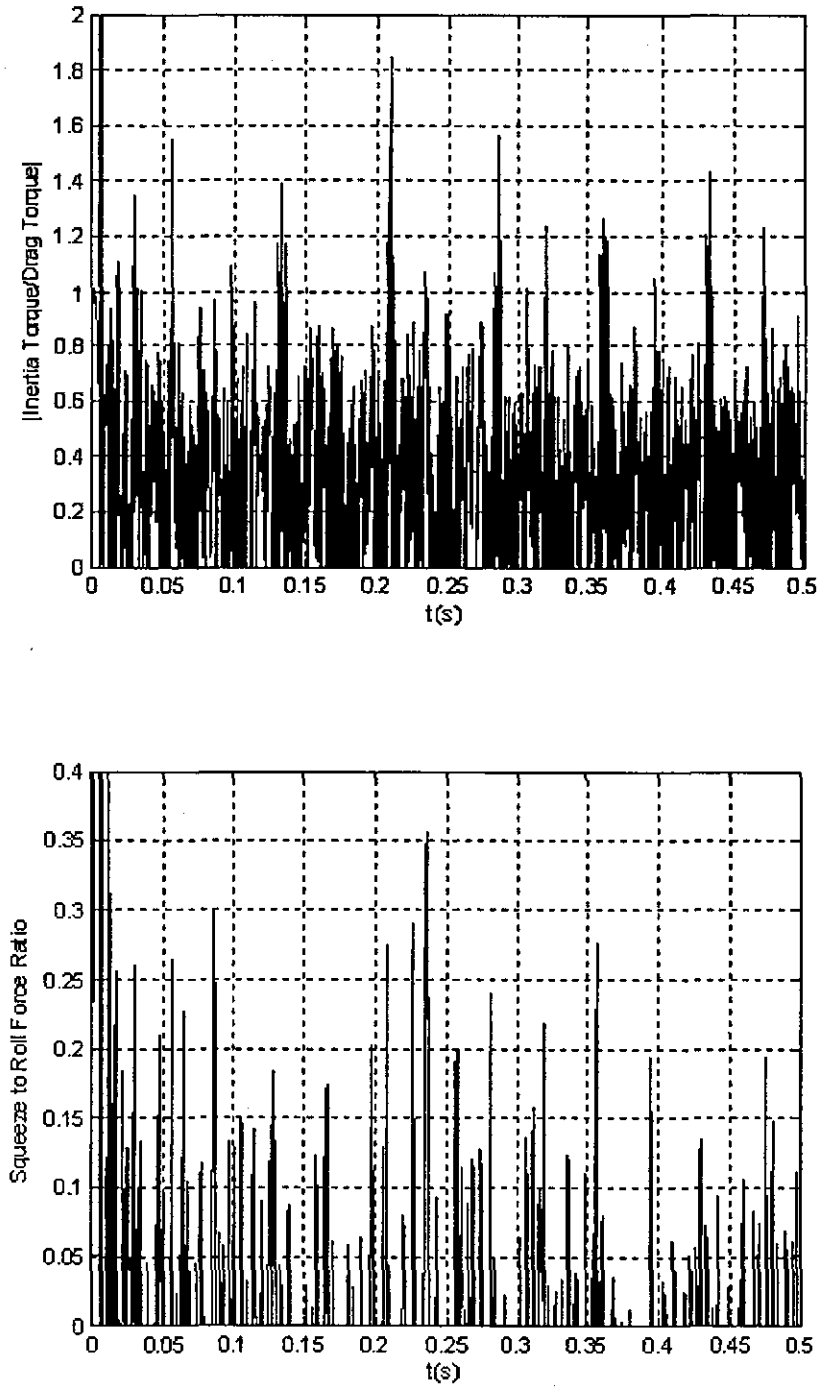

Figure 6.29: The simulated rattle (top) and squeeze to rolling forces (bottom) ratios of the 1st gear (2nd case)

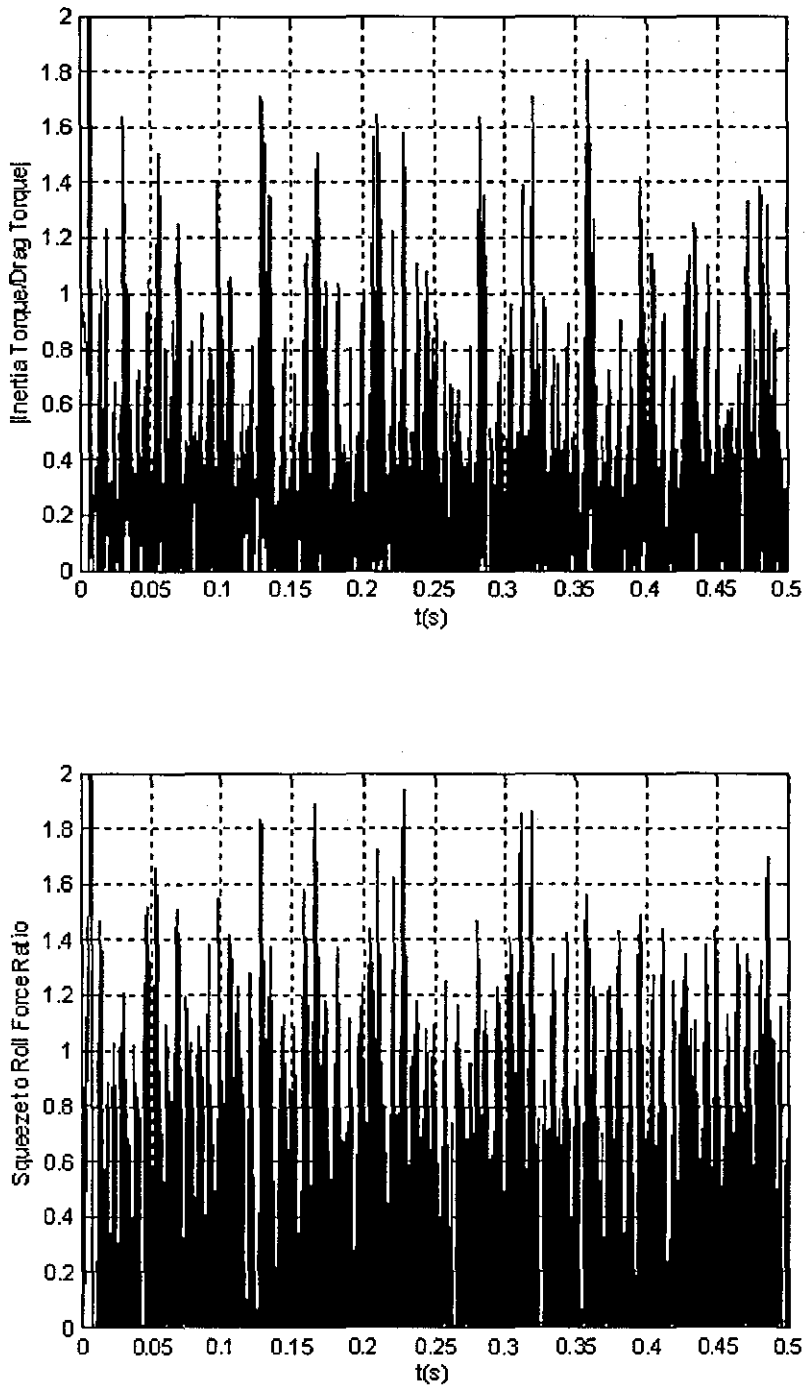

Figure 6.30: The simulated rattle (top) and squeeze to rolling forces (bottom) ratios of the 7th gear (2nd case)

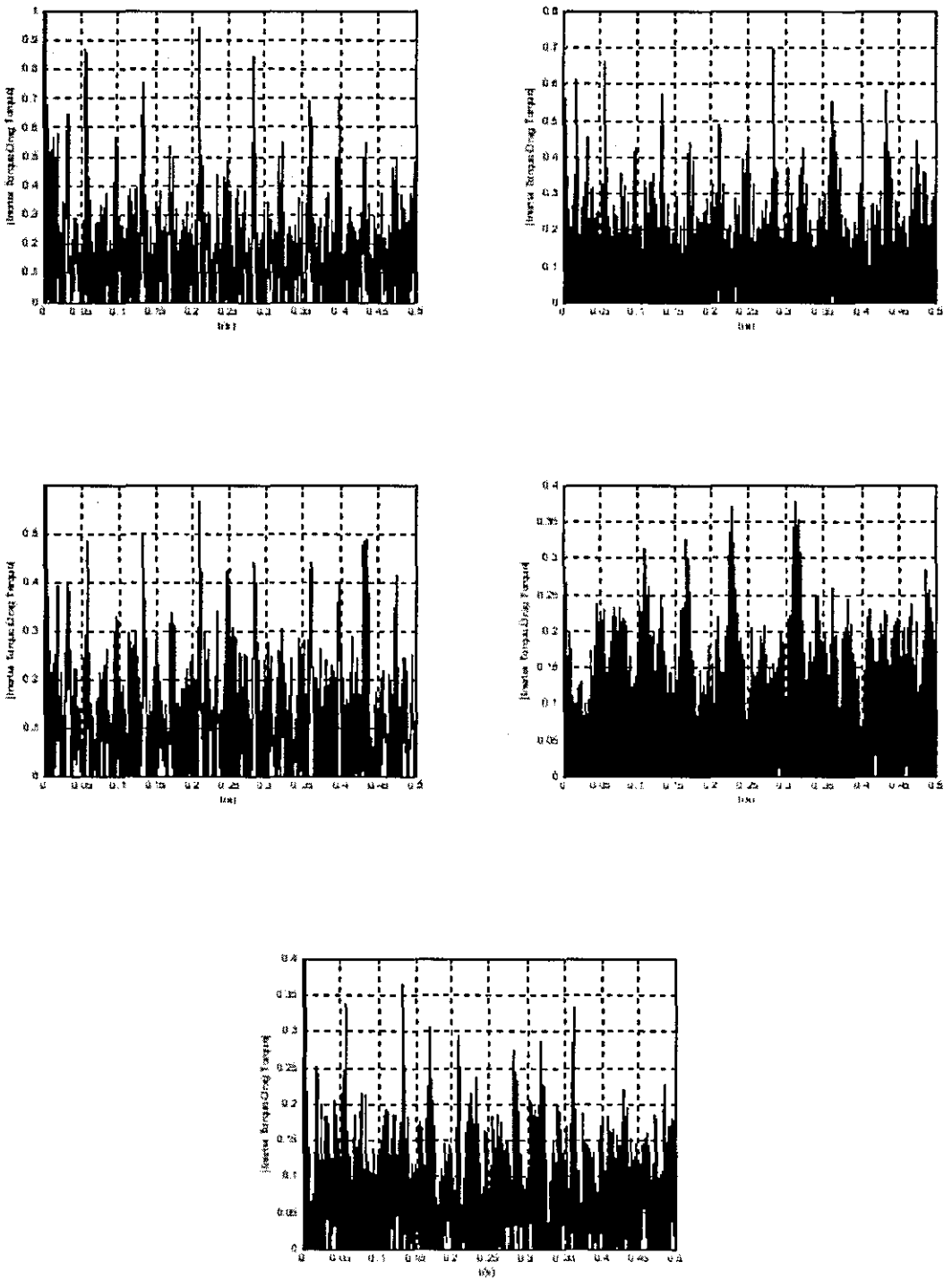

Figure 6.31: The simulated rattle ratios of the 2nd, 3rd, 4th, 5th, and 6th gears (2nd case)

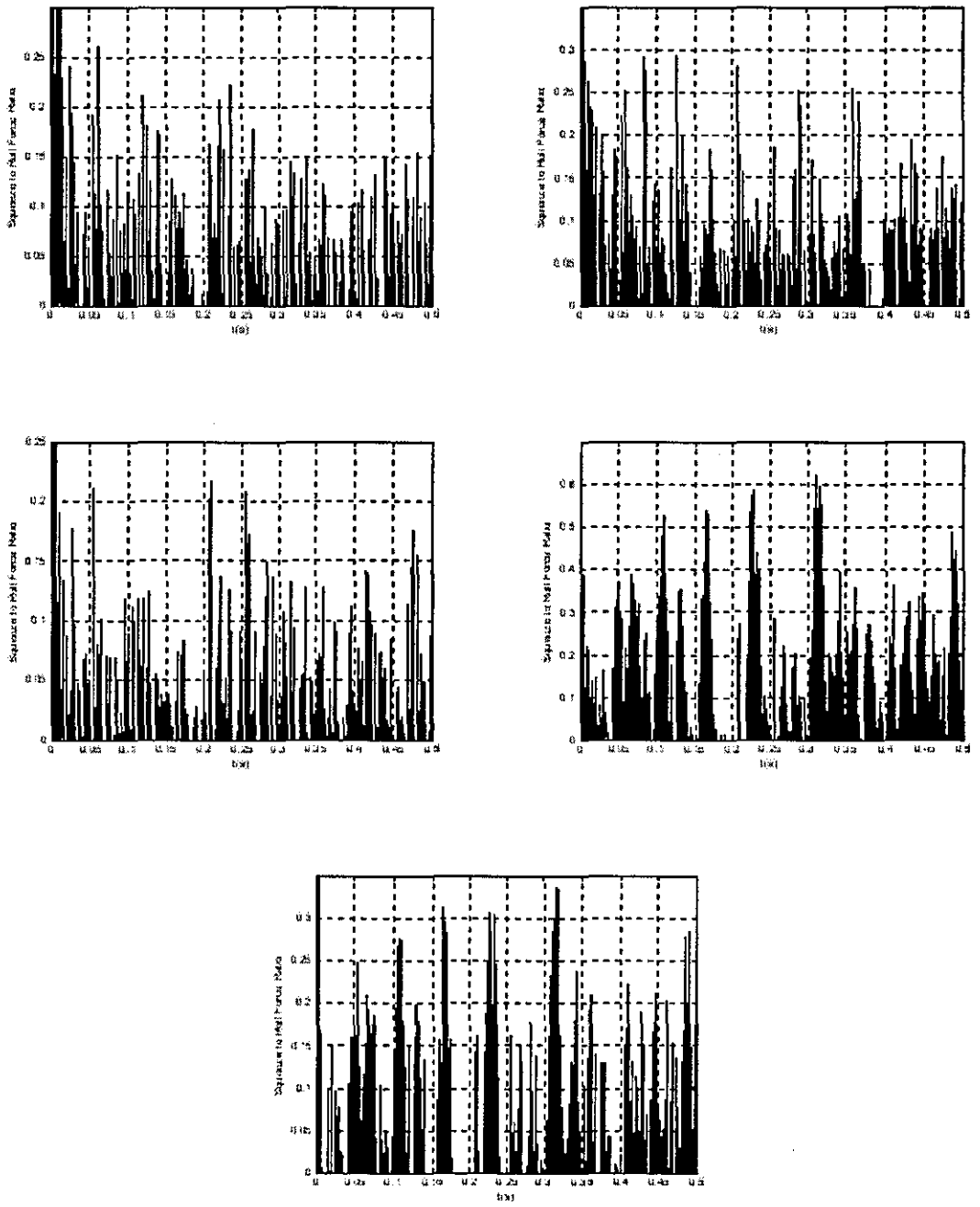

Figure 6.32: The simulated squeeze to rolling force ratios of the 2nd, 3rd, 4th, 5th, and 6th gears (2nd case)

6.4 The 11-Degree of Freedom Model and the Rig Experiments:

The third case is the experiment that was carried out on the test rig with the mean rotational velocity of the input shaft being 616.4 rpm (approx. 10Hz rotational frequency) and the bulk temperature of the transmission oil being 28.51°C. This velocity was chosen because it was the maximum velocity below 800 rpm (vehicle idling speed) that could be achieved by the rig electric motor with minimum noise interference. The same velocity input signal captured from the rig experiment was used in the 11-degree of freedom model to represent the input shaft velocity time history so that similar input conditions are modelled.

Figure 6.33 shows the spectral composition of the test rig transmission input shaft acceleration. The main component is the input 10Hz signal generated by the signal generator. Various harmonics of the fundamental 10Hz signal appear, strong of which are the seventh, eighth and ninth harmonics.

figures 6.34 to 6.36 illustrate the spectral content of the vibration signal captured by the transmission wall accelerometer, the input shaft bearing accelerometer, and the upper output shaft bearing accelerometer, respectively. The spectra show distinctive peaks, particularly strong contributions are observed at 52, 71, 81 and 101Hz.

When comparing this with the FFT spectra of the acceleration responses obtained from the model (figures 6.37 to 6.43), common frequencies are found in the experimental and numerical results as well as some of the meshing frequencies shown in table 6.3.

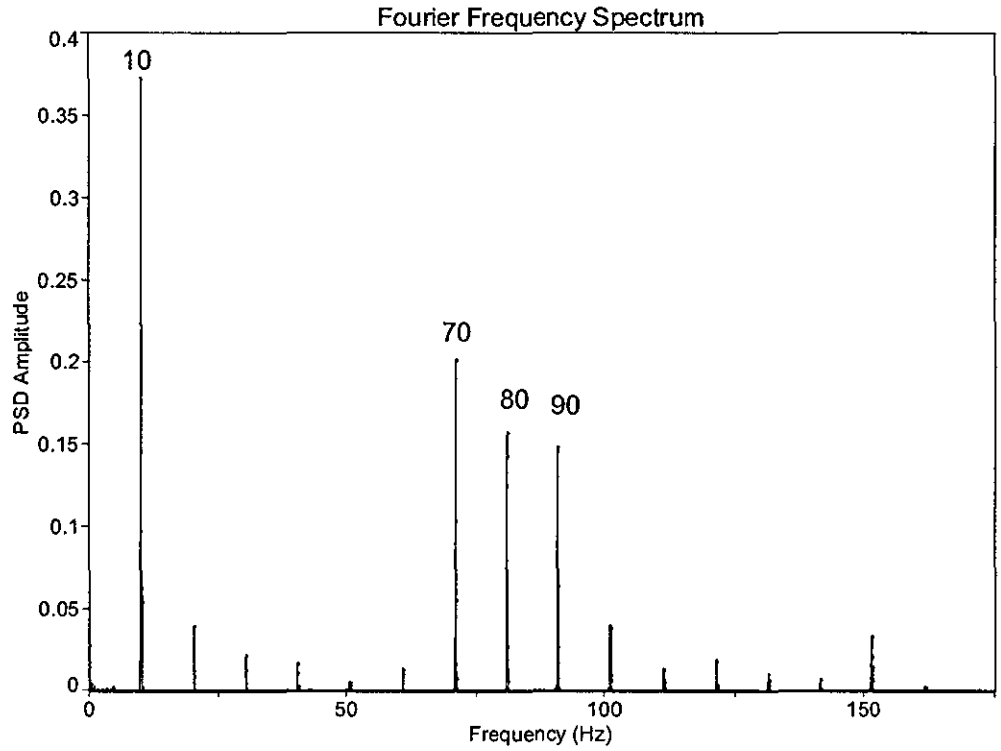

Figure 6.33: FFT spectra of the rig transmission input shaft's acceleration (3rd case)

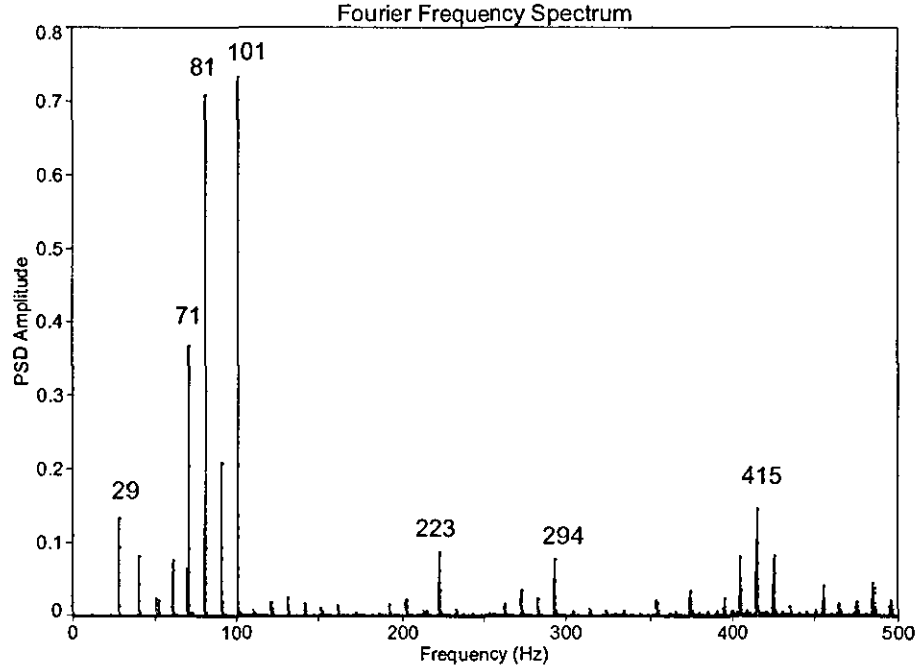

Figure 6.34: Fourier spectrum of the transmission wall accelerometer (3rd case)

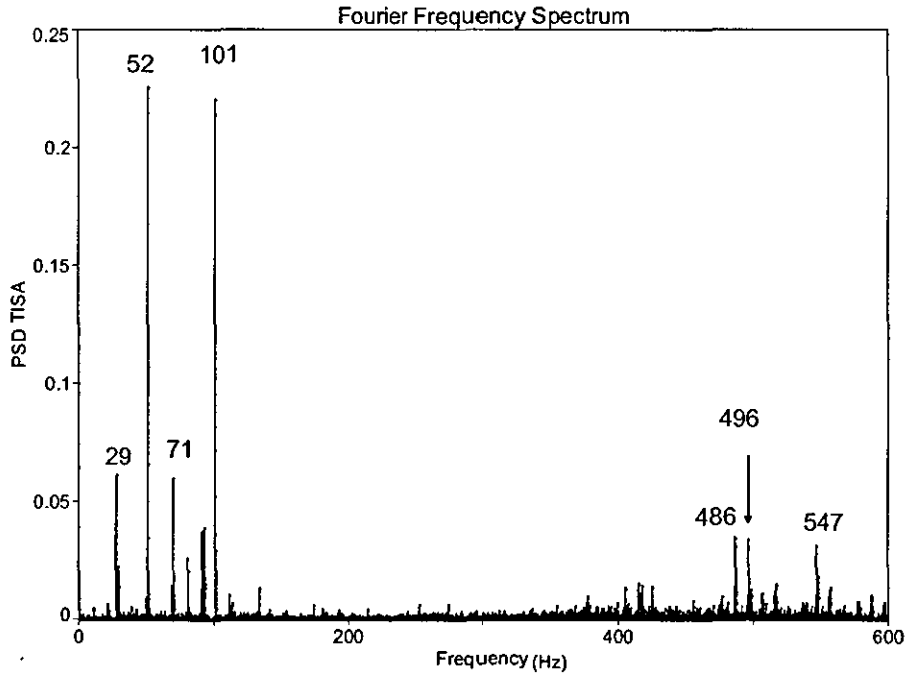

Figure 6.35: Fourier spectrum of the input bearing accelerometer (3rd case)

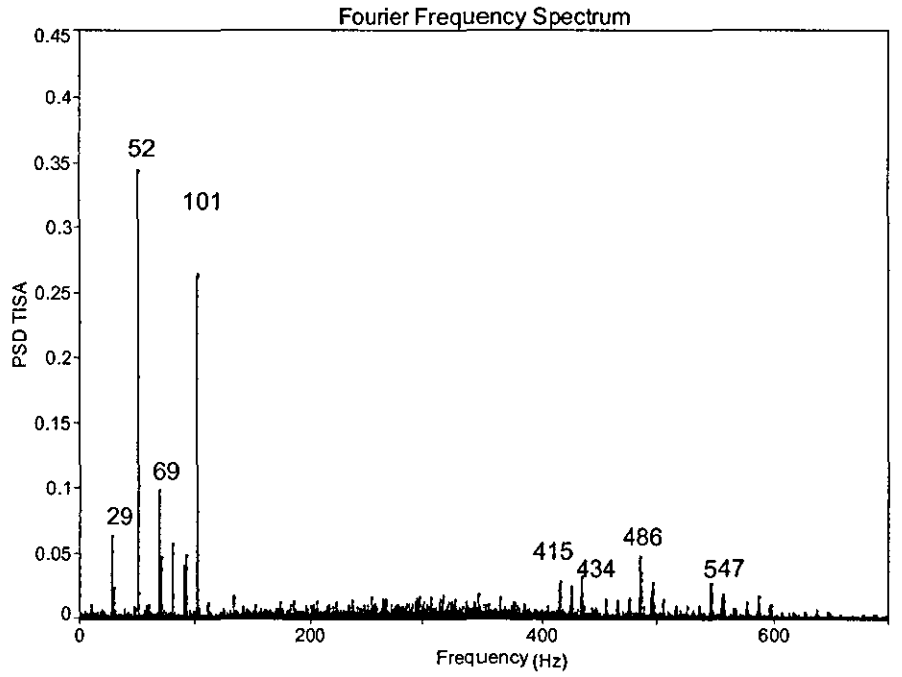

Figure 6.36: Fourier spectrum of the upper output shaft bearing accelerometer (3rd case)

Gear	1st	2nd	3rd	4th	5th	6th	Reverse
f_m (Hz)	133.6	226.0	297.9	390.4	359.6	390.4	83.5

Table 6.3: Meshing frequencies of the gear pairs at 616.4 rpm

The bearings responses obtained by the model show noisy spectrum in the lower contributions. The first shaft bearing response in the x-direction (figure 6.37) reflects the frequency 422 Hz, which was detected by the transmission wall and upper bearing accelerometers (within 2% error). This frequency can also be traced to the first gear modelled response at 432 Hz (figure 6.41) and the modelled second gear response at 436 Hz (figure 6.42). It also reflects the meshing frequency of the first gear (table 6.3), which is also reflected in the 1st gear acceleration response (figure 6.41).

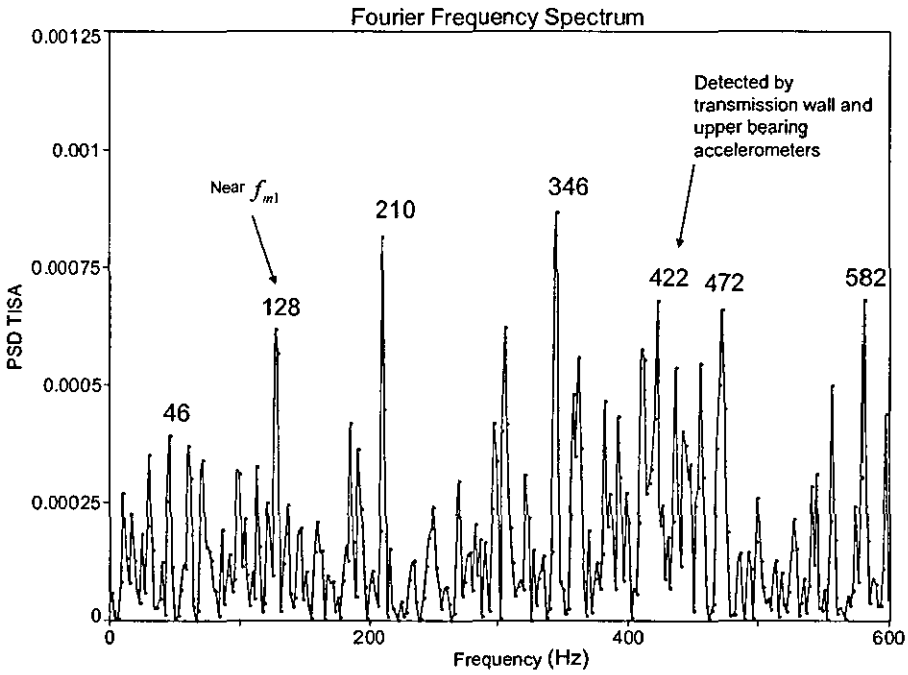

Figure 6.37: The simulated bearing acceleration spectrum in X1 direction (3rd case)

The first shaft bearing response in the y-direction (figure 6.38) reflects the frequencies 30 Hz and 102 Hz, which were detected by all three accelerometers. Furthermore, it

also reflects the frequencies 232 (the meshing frequency of the 2nd gear, table 6.3 and figure 6.42) and 296, which were detected by the transmission wall accelerometer (within 5% error), the 496 Hz, which was detected by the input bearing accelerometer, and the 546 Hz, which was detected by the input and upper output bearings accelerometers. The 102, 296 and 496 Hz can be traced to the first gear acceleration response within 3% error (figure 6.41).

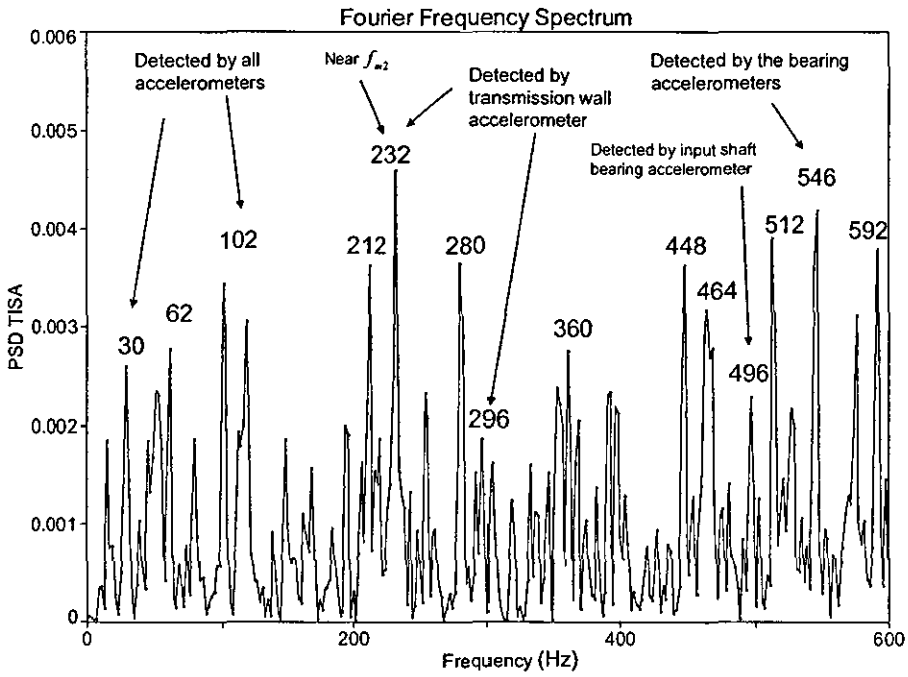

Figure 6.38: The simulated bearing acceleration spectrum in Y1 direction (3rd case)

The second shaft bearing response in x-direction (figure 6.39) reflects the 70 Hz, which was captured by the three accelerometers, the 78 Hz, which was captured by the transmission wall accelerometer and lies within 10 % from the 7th (reverse) gear meshing frequency (table 6.3 and figure 6.43), the 220Hz , which was detected by the transmission wall accelerometer (within 2% error), and the 416, which was also detected by the transmission wall accelerometer and by the upper bearing accelerometer. The frequencies 70 and 416 Hz can be found in the 7th gear's acceleration response with maximum error 2% (figure 6. 43).

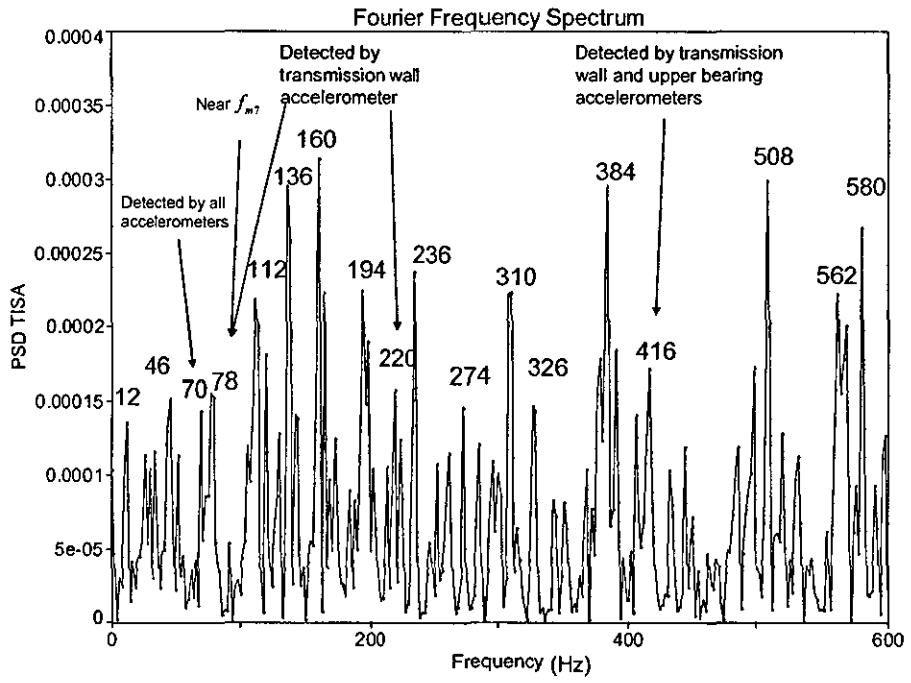

Figure 6.39: The simulated bearing acceleration spectrum in X2 direction (3rd case)

The second shaft bearing response in the y-direction (figure 6.40) reflects the 486, which was detected by the input and upper output bearings accelerometers, and the 498 Hz, which was captured by the input bearing accelerometer.

The acceleration responses of the 1st, 2nd, and 7th gear (figures 6.41 to 6.43, respectively) feature main response components at 150, 142, and 80 Hz, respectively. The latter shows 10 Hz modulation around the peak at 80 Hz.

When inspecting the rattle and squeeze-to-rolling force ratios associated with the 1st, 2nd, and 6th gear (figures 6.44 to 6.46, respectively), the squeeze component of the film reaction appears to dominate. This because the high squeeze to rolling force ratios, together with the high rattle ratios, which indicate significant squeeze forces, indicate that a severe rattling is taking place (compared with the response of the systems in sections 6.2 and 6.3).

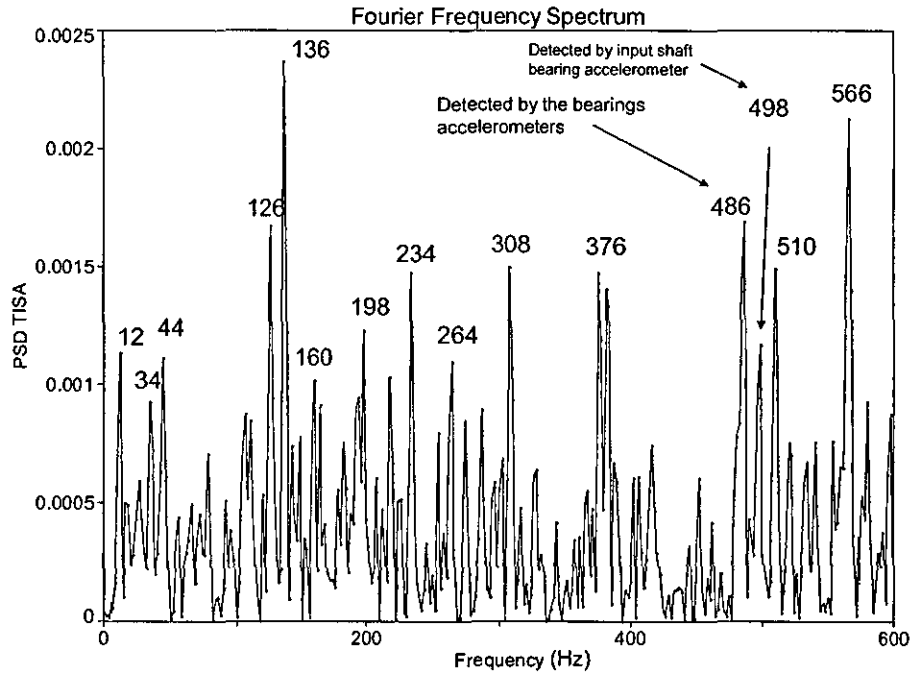

Figure 6.40: The simulated bearing acceleration spectrum in Y2 direction (3rd case)

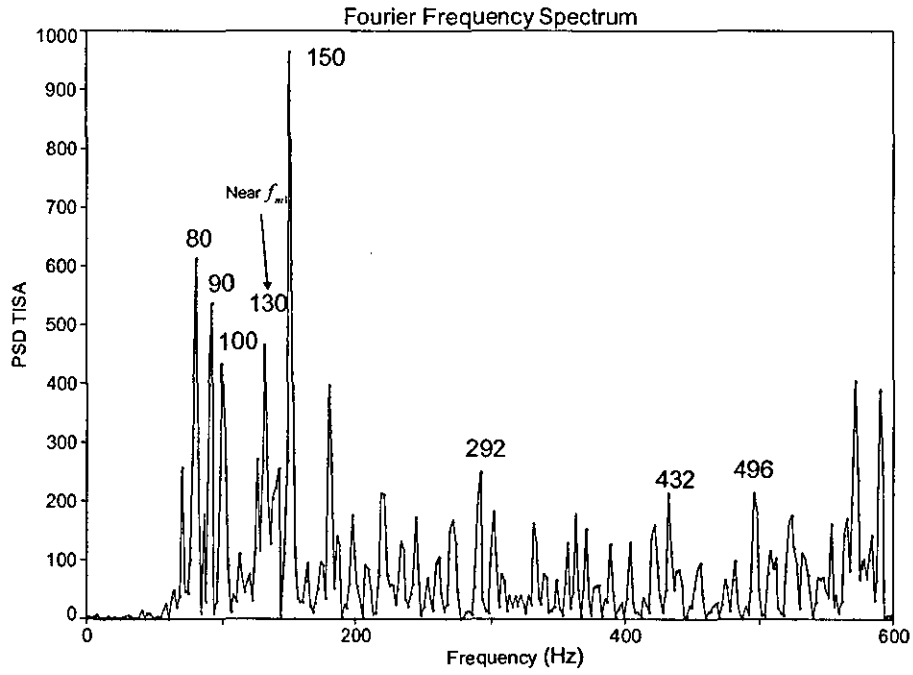

Figure 6.41: FFT spectrum of the simulated 1st gear acceleration (3rd case)

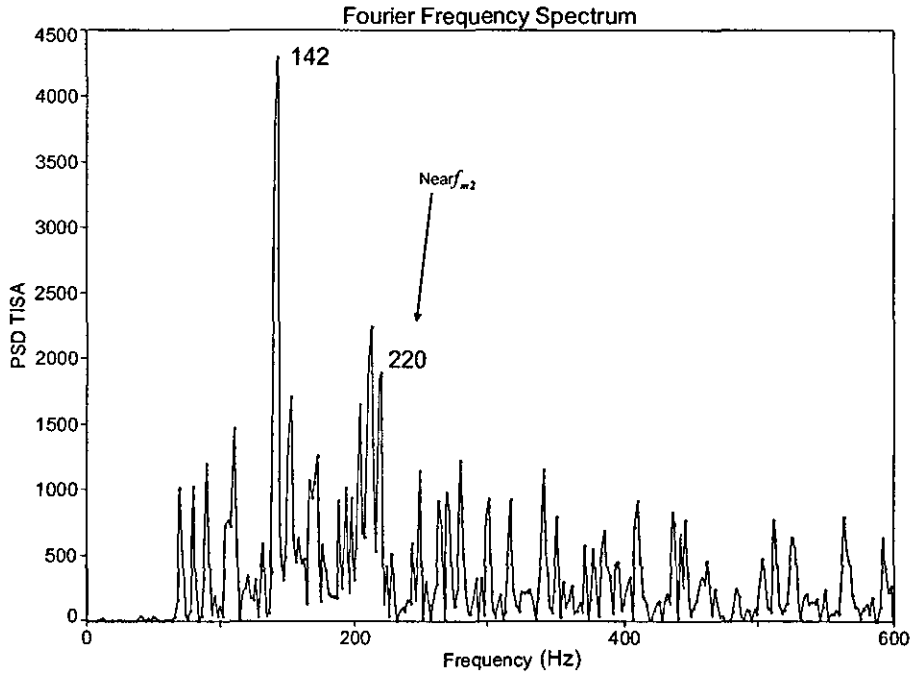

Figure 6.42: FFT spectrum of the simulated 2nd gear acceleration (3rd case)

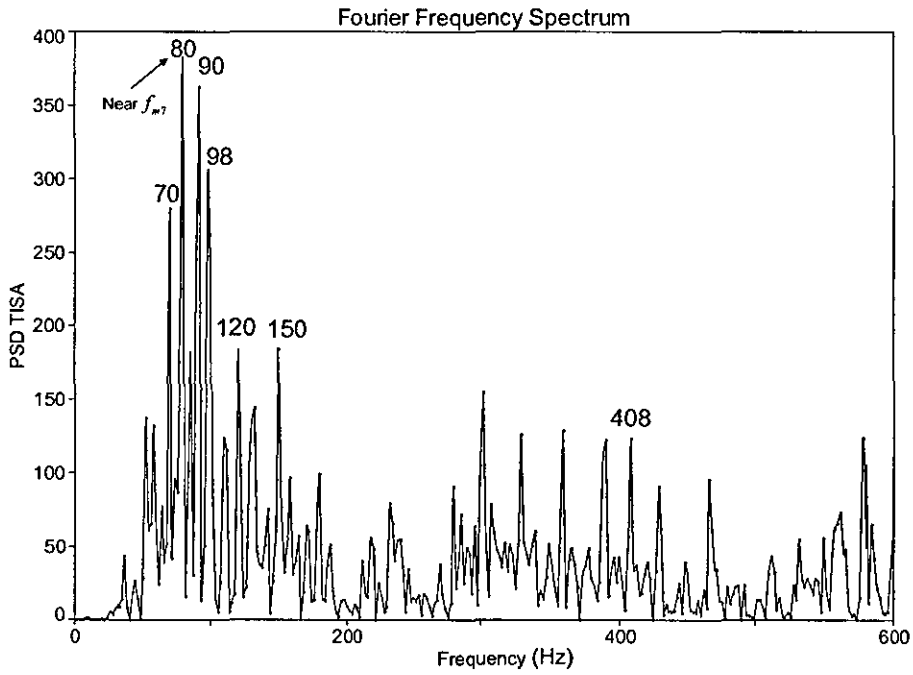

Figure 6.43: FFT spectrum of the simulated 7th gear acceleration (3rd case)

As explained earlier in the text, the rattle response is primarily associated with the squeeze component of the film reaction, since it is the term that explicitly represents the tooth separation and approach (squeeze) that characterises rattling teeth. The 1st and 2nd wheels have high inertias, while the 6th has lower inertia, this indicates that in the third case rattling is not associated with the high-inertia gears, thus, pointing towards an extreme condition of rattling. In fact, when, inspecting the film thicknesses of the 1st and 6th gears (figures 6.47 and 6.48, respectively), the film thicknesses are found to drop below 1μm. When considering that the transmission input shaft is running at lower speed in the third case, there is a possibility that a lubricant regime transition occurs in the contact. Hence, the third case requires further analysis, wherein the instantaneous lubricant regime is determined before calculating the film reaction.

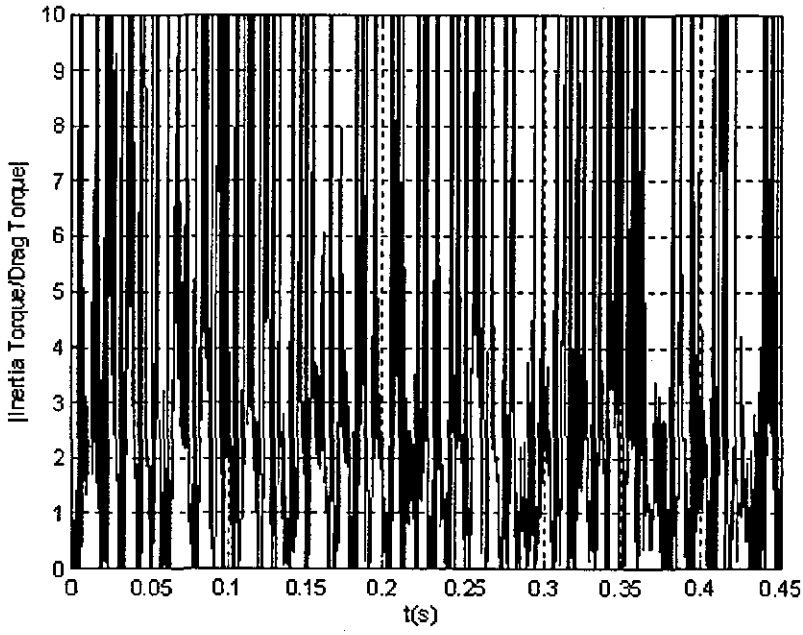

Figure 6.44 (continued)

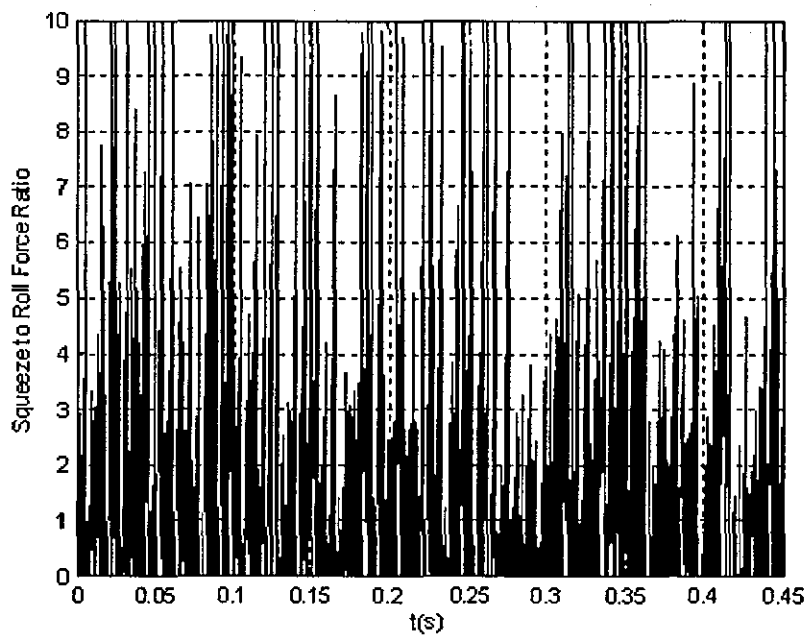

Figure 6.44: The simulated rattle (top) and squeeze to rolling forces (bottom) ratios of the 1st gear (3rd case)

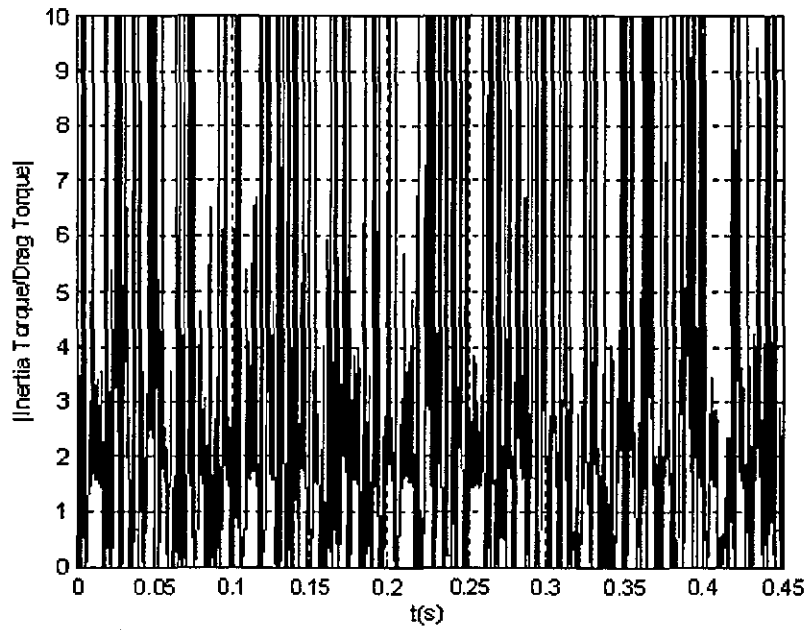

Figure 6.45 (continued)

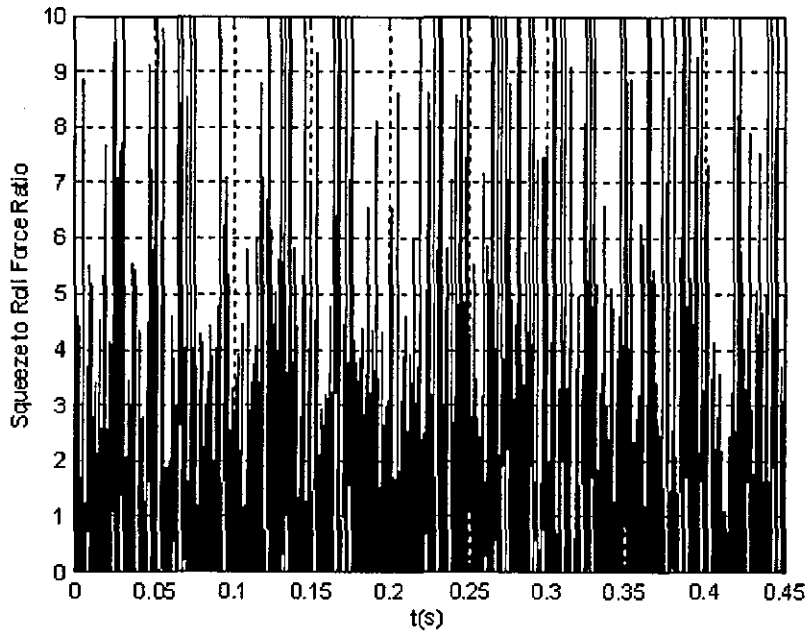

Figure 6.45: The simulated rattle (top) and squeeze to rolling forces (bottom) ratios of the 2nd gear (3rd case)

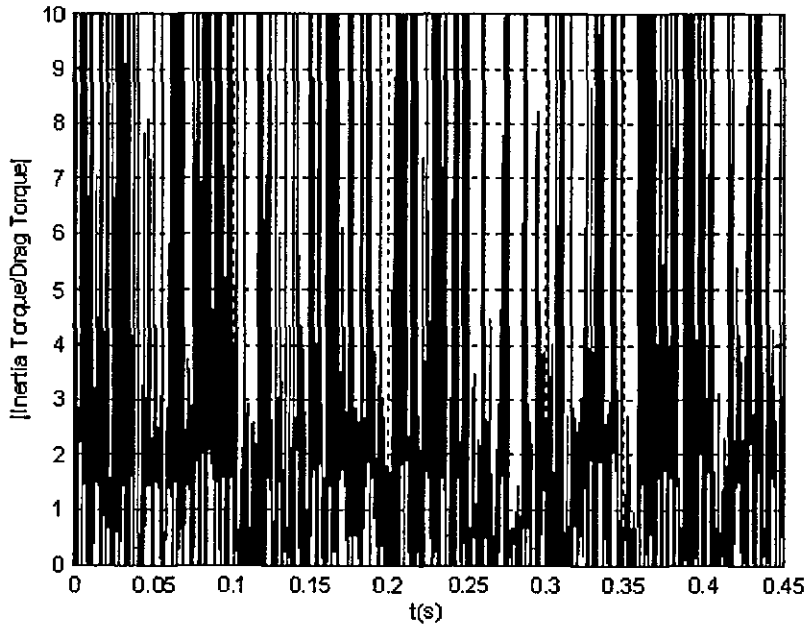

Figure 6.46 (continued)

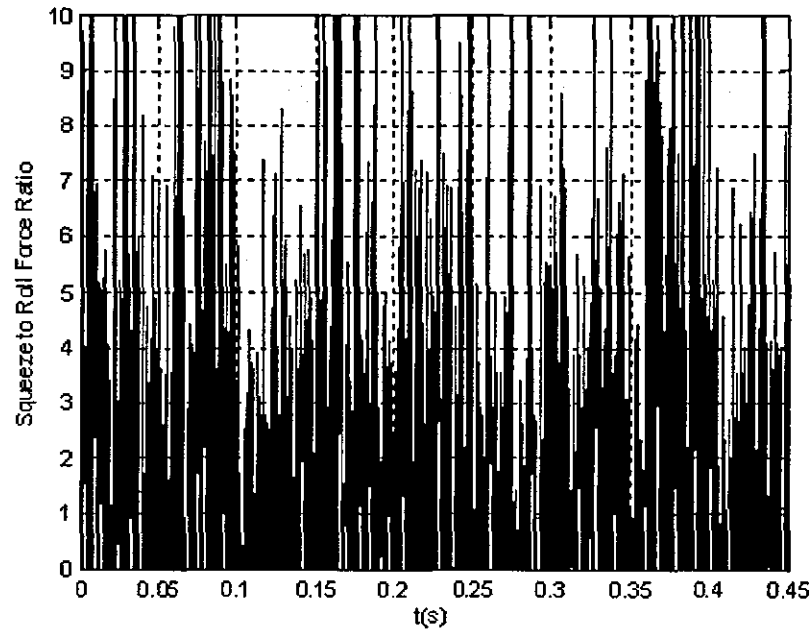

Figure 6.46: The simulated rattle (top) and squeeze to rolling forces (bottom) ratios of the 6th gear (3rd case)

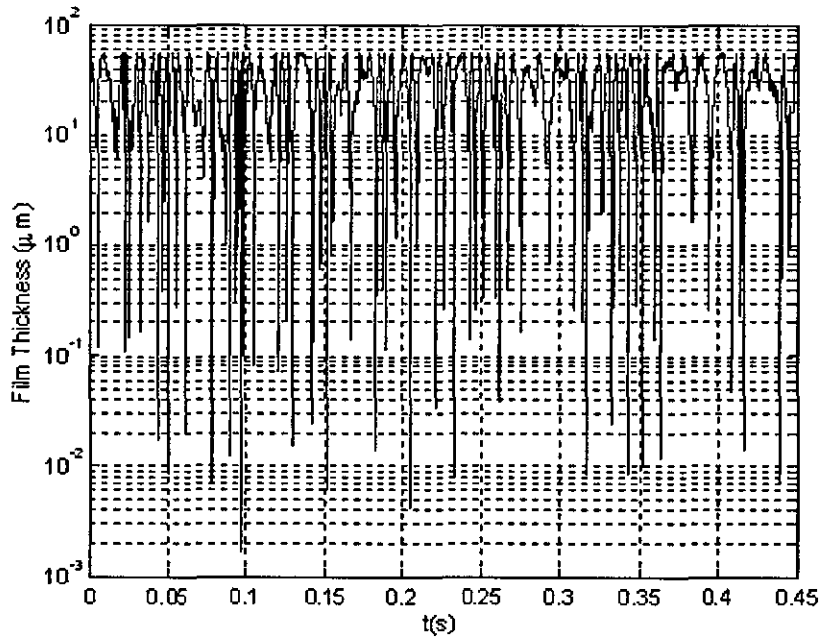

Figure 6.47: The film thickness of the simulated 1st gear (3rd case)

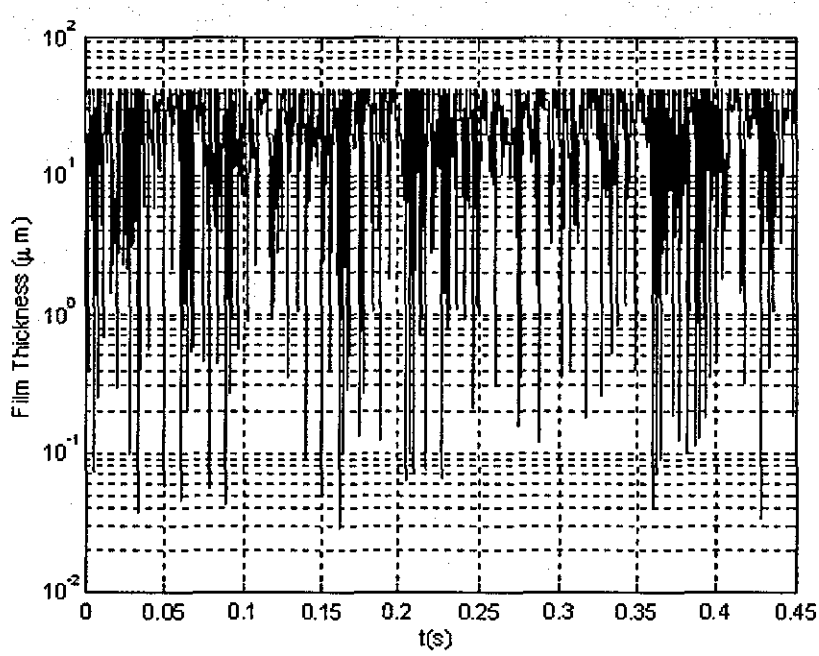

Figure 6.48: The film thickness of the simulated 6th gear (3rd case)

6.5 Conclusions:

The above observations reveal a reasonably good agreement between the numerical analysis and the experimental findings. At this point, it is important to underline the fact that the equation of motion of the input shaft has not been considered in the non-linear analysis (chapter 4), since its rotational kinematics was available from experimental measurements for direct use as input conditions in the numerical model. This has resulted in isolating the input shaft from undergoing backward reactions (i.e. reversals) from the idle gears, which could well be the case in the real system. However, these reaction forces are expected to have little effect on the dynamics of the system, since they are very low compared to the engine excitation. Even though gear rattle is usually associated with rotational input, it should also be mentioned that the translational motion of the input shaft is not included in the input kinematics.

The motion of the shafts could interfere with the gear contact action and play a significant part in determining the rattling behaviour. It is necessary, as a result, to

further investigate the effects of shafts' bearings and their induced vibration on the tooth contact dynamics.

The rattle ratio by itself does not give a comprehensive picture of the behaviour of the system, particularly at low temperatures. By inspecting the ratio of the squeeze component to the rolling component, more information on the severity of rattle could be obtained. The higher the ratio the more severe the rattling, something which highlights the importance of the oil entrainment action in lowering the severity of rattle. Nevertheless, the oil entrainment itself could interfere with the squeeze action and parametrically induce some sort of tooth separation.

Chapter 7: Overall Conclusions, Critical Assessment and Suggestions for Future Work

The thesis proposes a new approach to investigate the problem of idle gear rattle. The approach is based on the assumption that under idling condition the impact loads of the unselected gear teeth pair are sufficiently low to permit the formation of a hydrodynamic lubricant film between the mating gear teeth through combined entraining and squeeze film motions. The following points summarise the findings of the research and provide suggestions for future work:

- A dearth of research into the effect of lubricant on idle gear rattle provided the motivation for the research outlined in this thesis. In fact, most of the literature treats the lubricant as a damping factor only rather than a medium with both spring and damping characteristics. The aim of the current work is to address this shortcoming.
- Due to the high non-linearity of idle gear rattle problem, a numerical solution is sought allowing for more accurate results (because of less simplifying assumptions that usually characterise the existing analytical solutions) to be obtained as well as repeatability and sensitivity studies.
- The work presents a hydrodynamic model that considers the effect of the lubricant film in the gear teeth-pair impact zone under lightly loaded conditions. This film acts as a non-linear spring-damper element that couples the driver and the driven gears. In other words, in the hydrodynamic mode, there is no actual metal-to-metal contact between the mating teeth and the load is transferred via the lubricant film.
- The approach is based on the assumption that during idling conditions the light tooth impact loads are low enough and the gear speeds are sufficiently high to permit the formation of a hydrodynamic lubricant film between the mating gear teeth.
- Further assumptions are:

- The gear tooth profile is perfectly involute.
- No misalignments occur.
- No tooth-to-tooth variations exist.
- The loads on the teeth are too low to cause any tooth local or global deformation (local being due to Hertzian condition and global being due to tooth bending or rocking).
- Changes of viscosity due to generated pressures within the contact zone are negligible due to low hydrodynamic pressures in isothermal analysis.
- No other form of external excitations other than the engine torsional excitations (engine order vibrations) is assumed.

- A single-degree of freedom torsional model is developed in order to establish the low load lubricated impact theory and carry out simple sensitivity study to determine the most influential parameters in the contact conjunction.
- It has been found that oil viscosity and bearing clearance play important roles in determining the dynamics of the system and propensity to rattle mainly due to these bring the dominant factors in determining the ratio of inertia to drag torques, which governs tooth separation (note that a series of iso-viscous conditions have been simulated).
- The model is then expanded into a seven-degree of freedom torsional model and finally into an 11-degree of freedom model, which also includes the lateral motions of the shafts. The 11-degree of freedom model represents a real-life transmission and used for correlation of the hydrodynamic model results with the experimental findings.
- The lateral motions of the shafts carrying the gears have been found to interfere with the gear teeth pair impact action by influencing the relative displacement and velocity between the gear teeth pairs, thus, playing a significant role in determining the rattling behaviour of the gears. It is necessary, as a result, to further investigate the effects of shafts' bearings and their lubrication on the tooth contact dynamics.
- The relationship between the rolling and squeeze film actions determines the severity of rattling condition. When the squeeze action dominates, the system can rattle more severely. By improving the rolling action, the severity of rattle

can be reduced due to an enhanced film thickness. A possible future work can focus on optimising the gear macro- and micro-geometry such that the rolling action is promoted. Nonetheless, improved rolling action (entraining motion) may cause internal excitations and tooth separation.

- Two types of experiments were conducted: Vehicle-based experiments in a semi-anechoic chamber and rig-based experiments in a powertrain laboratory. The experiments were conducted on an actual vehicle transmission, upon which the numerical model is also based. The disadvantage of carrying out experiments on a full transmission is the interference caused by other sources of noise and vibration (such as the synchroniser rings). The transmission acts as a black box, since it is also difficult to reach and directly measure the parameters of the meshing gear pairs.
- By comparing the trend of the frequency response of numerical and experimental output, reasonable correlation between the model predictions and the experimental findings has been found. However, the theory would require further optimisation by removing some of the assumptions that have been made (such as the assumption of perfectly involute teeth).
- In addition to the shortcomings of the approach due to the imposed assumptions, the differences between the model and experiment can also be due to:
    - The effect of interference (from other components of the tested transmission or vehicle parts).
    - The lack of a full model of the transmission housing.
    - Viscosity variation due to temperature effect in a transient manner (not taken into account in the model). Solution of energy equation would be required.
- Also, it is necessary to investigate the structural dynamics of the gear blanks and the shafts, since these transmit structural vibrations due to impacts to the transmission housing (in addition to the rigid body vibrations).
- In general, basic experiments help in building the core science and design guidelines to guard against gear rattle; as a result, in such research, it would be better to optimise the model using a basic gear-pair rig rather than a complete transmission. Such an experiment would minimise interactions with other

sources of noise and vibration and would allow for more direct measurement and control of gear parameters.

- The current approach assumes fully flooded conditions at the inlet of the contact. It does not consider any possible starvation. Since in real transmissions this is unlikely to be exactly the case, it is necessary to extend the work to include this effect, as well as piezo-viscous lubrication and thermal effects.
- The current work concentrates mainly on correlating the vibrations at the surface of the transmission housing with the loose wheel response predicted by the model. It does not consider the acoustic emission due to rattle (even though acoustic measurements were taken during the experiments). Future work can concentrate on relating the hydrodynamic model and the acoustic signature of the transmission housing, for instance, determining whether a relation exists between the squeeze-roll action and rattle noise level. This is best achieved in a basic gear-pair rattle rig.
- It is widely accepted that increasing the drag torque improves the system resistance to rattling, but by increasing the drag in the transmission the efficiency is compromised. Hence, a holistic study of the balance between efficiency and NVH performance (possibly by including other forms of gear rattle) becomes a necessity.

References

Al-Samieh, M.F. and Rahnejat, H. (2002). "Physics of Lubricated Impact of a Sphere on a Plate in a Narrow Continuum to Gaps of Molecular Dimensions", J. Phys., Part D: Appl. Phys., Vol. 35, 2002, pp. 2311-2326.

Bruel & Kjaer UK Ltd., Bedford House Rutherford Close, SG1 2ND, Stevenage, Hertfordshire. Website: http://www.bksv.co.uk/.

Brüel & Kjær, (1997), "Product Data Sheet: Prepolarized Condenser Microphone Cartridges - Type 4129, 4155, 4176".

Brüel & Kjær, (2003), "English Product Data Sheet: Microphone Preamplifier Type 2671: (BP144614)".

Brüel & Kjær, (2004), "English Product Data Sheet: Piezoelectric Accelerometer Charge Accelerometer Type 4393, 4393S, and 4393V. (BP204311)".

Bellomo, P., Cricenti, F., Vito, N. De, Lang, C., and Minervini, D., (2000), "Innovative Vehicle Powertrain Systems Engineering: Beating the Noisy Offenders in Vehicle Transmissions", SAE Technical Paper 2000-01-0033.

Bertin, P., Breton, E., and Mokdad, A., (1995), "Radial Dual Mass Flywheel", SAE Technical Paper 950893.

Biermann, J., Hagerodt, B., (1999), "Investigation of the Clonk Phenomenon in Vehicle Transmissions- Measurement, Modelling and Simulation", Proc. Instn. Mech. Engrs. Vol. 213 Part K, pp. 53-60.

Brancati, R., Rocca, E., and Russo, R., (2005), "A Gear Rattle Model Accounting for Oil Squeeze Between the Meshing Gear Teeth", Proc. IMechE Vol. 219 Part D: J. Automobile Engineering, pp. 1075-1083.

Cai, Y., (1995), "Simulation on the Rotational Vibration of Helical Gears in Consideration of the Tooth Separation Phenomenon (a New Stiffness Function of Helical Involute Tooth Pair)", Transactions of the ASME, Journal of Mechanical Design, Vol. 117, pp. 460-469.

Cavina, N., and Serra, G., (2004), "Analysis of Dual Mass Flywheel System for Engine Control Applications", SAE Technical Paper 2004-01-3016.

Chao, C., (1991), "Special Calculations of Spur and Helical Gears 'In:'", Dennis P. Townsend "Dudley's Gear handbook", McGraw-Hill, Inc., 2nd edition, chapter 5.

Chow, L., and Pinnington, R., (1989), "Practical Industrial Method of Increasing Structural Damping in Machinery, II: Squeeze-Film Damping with Liquids", Journal of Sound and Vibration, 128(2), pp. 333 - 347.

Chu, A., Eller, E., and Whittier, R., (1995), "Vibration Transducers 'In:'", Cyril Harris,"Shock and Vibration Handbook", McGraw-Hill, 4th edition, chapter 12.

Comparin, R., and Singh, R., (1990), "An Analytical Study of Automotive Neutral Gear Rattle", Journal of Mechanical Design , vol. 112, pp. 237-245.

Connor, F., (1982), "Modulation", Edward Arnold, 2nd Edition, London.

Couderc, PH., Callenaere, J., Der Hagopian, J., and Ferraris, G., (1998), "Vehicle Driveline Dynamic Behaviour: Experimentation and Simulation", Journal of Sound and Vibration, 218(1), pp. 133-157.

Croker, M., March, J., Greer, R., (1990), "Transmission Rattle Analysis", IMechE C404/005.

Davis, G., and Brooks, P., (2006), "The Investigation of Automotive Transmission Error Characteristics Subject to Operating Conditions", Proceedings of IPDS 2006 Integrated Powertrain and Driveline Systems 2006, IMechE, Automobile Division.

Dogan, S. N., (1999), "Loose Part Vibration in Vehicle Transmissions – Gear Rattle", Tr. J. Of Engineering and Environmental Science, 23 (1999), 439-454.

Dogan, S. N.,(2001), "Zur Minimierung der Losteilgeräusche von Fahrzeuggetrieben", Berichte Nr. 91, Institut für Maschinenelemente, Universität Stuttgart, PhD Thesis.

Dogan, S. N., and Lechner, G., (1998), "Maßnahmen zur Verringerung von Losteilschwingungen in Fahrzeuggetrieben" , Automobiltechnische Zeitschrift 100 (1998)10, pp. 710-716.

Drago, R., (1988), "Fundamentals of Gear Design", Butterworths.

Driot, N., Rigaud, E., Sabot, J., Perret-Liaudet, J., (2000), "Prediction of Gearbox Noise Variability from Tolerances on Profile and Helix Angle", The 29th International Congress and Exhibition on Noise Control Engineering, 27-30 August, Nice, France.

Driot, N., Perret-Liaudet, J., Rigaud, E., (2001), "Gearbox Critical Speeds Variability Prediction Induced by Manufacturing Dispersion", the 8th International Congress on Sound and Vibration, 2-6 July, Hong Kong, China.

Eren, H, (1999),"Inductive Displacement Sensors 'In:'", John G. Webster, "The Measurement, Instrumentation, and Sensors Handbook", CRC Press LLC, Section 2, Chapter 6, pp. 6-15 to 6-37.

Forcelli, A., Grasso, C., and Pappalardo, T., (2004), "The Transmission Gear Rattle Noise: Parametric Sensitivity Study", SAE Technical Paper 2004-01-1225.

Fudala, G., Engle, T., and Karvelis, A., (1987), "A System Approach to Reducing Gear Rattle", SAE Technical Paper 870396, pp.2.110-2.117.

Fujimoto, T., Chikatani, Y., and Kojima, J., (1987), "Reduction of Idling Rattle in Manual Transmission", SAE Technical Paper 870395, pp. 2.99-2.109.

Fujimoto, T., and Kizuka, T., (2001), "An Improvement of the Prediction Method of the Idling Rattle in Manual Transmission- In the Case of the Manual Transmission with Backlash Eliminator-", SAE Technical Paper 2001-01-1164.

Fujimoto, T., and Kizuka, T., (2003a), "Predictive Calculation of Idling Rattle in Manual Transmissions –Based on Experimental Measurements of Gear Vibration Occurring in Backlashes-", SAE Technical Paper 2003-01-0678.

Fujimoto, T., and Kizuka, T., (2003b), "Audible Noise Simulation –an Attempt to Predict Idling Rattle in Manual Transmissions-", SAE Technical Paper 2003-01-0674.

Gnanakumarr, M, (2001) "Impact Noise and Vibration in Powertrain Systems", First Year Research Report, Loughborough University.

Gnanakumarr, M, (2004) "Integrated Investigation of Impact-Induced Noise and Vibration in Vehicular Drivetrain Systems", PhD Thesis, Loughborough University.

Gnanakumarr, M., Theodossiades, S., and Rahnejat, H., (2002) "The Tribo-Contact Dynamics Phenomenon In Torsional Impact Of Loose Gears Promoting Gear Rattle", SAE 02ATT-138, Society of Automotive Engineers (SAE)-ATT Congress, Paris.

Gnanakumarr, M., Theodossiades, S., and Rahnejat, H., and Menday, M. (2003), "Elasto-Multibody Dynamic Simulation of Impact Induced High Frequency Vehicular Driveline Vibrations", Proceedings of the IMECE 2003: 2003 ASME International Mechanical Engineering Congress and RD&D Expo, November 15-21, Washington, D.C., USA.

Gohar, R., (2001), "Elastohydrodynamics", Imperial College Press, 2nd edition.

Graikousis, R., (1985), "Machine Elements", Vol. 3, 2nd Edition, Greece, (in Greek).

Haberhauer, H., and Bodenstein, F., (2003), "Maschinenelemente: Gestaltung, Berechnung, Anwendung", Springer, 12. Auflage.

Halkon, B., and Rothberg, S., (2006), "Rotor Vibration Measurements Using Laser Doppler Vibrometry: Essential Post-Processing for Resolution of Radial and Pitch/Yaw Vibrations", Transactions of the ASME, Journal of Vibration and Acoustics, Vol. 128, pp. 8-20.

Hall, Brian, (2001),"Noise vibration and harshness 'In:'", Julian Happian-Smith, "An Introduction to Modern Vehicle Design", Butterworth-Heinemann, 1st edition, chapter 8.

Halse, C., Wilson, R., di Bernardo, M., and Homer, M., (2006), "Coexisting Solutions and Bifurcations in Mechanical Oscillators with Backlash" Bristol Centre for Applied Nonlinear Mathematics, University of Bristol, http://hdl.handle.net/1983/374.

Hamrock, B., Schmid, S., and Jacobson, B., (2004), "Fundamentals of Fluid Film Lubrication", Marcel Dekker Inc., 2nd edition.

Harris, T, (2001), "Rolling Bearing Analysis", John Wiley & Sons, Inc., 4th Edition.

Hassal, J., and Zaveri, K., (1979), "Acoustic Noise Measurements", Brüel & Kjær, 4th edition, 1st print.

Heinrichs, R., and Bodden, M., (1999), "Perceptual and Instrumental Description of the Gear Rattle Phenomenon for Diesel Vehicles", Invited Paper, Proceedings of the International Congress on Sound and Vibration, Copenhagen, Denmark, 3103-3112.

Inman, D., (2001), "Engineering Vibration", Prentice-Hall Inc., 2nd Edition.

Johnson, D., (1958), "The Excitation of Resonant Vibration by Gear Tooth Meshing Effects", IMechE Proceedings of the International Conference on Gearing.
Johnson, O., and Hirami, N., (1991), "Diagnosis and Objective Evaluation of Gear Rattle", SAE Technical Paper 911082.
Kahraman, A., and Singh, R., (1991), "Interactions between Time-Varying Mesh Stiffness and Clearance Non-Linearities in a Geared System", Journal of Sound and Vibration, 146(1), pp. 135-156.

Kamo, M.; Yamamoto, H.; Koga, H.; and Umezawa, K.; (1996), "Analysis Method for the Contribution Rate of Each Pair of Gears on the Driveline Gear Rattle", SAE Technical Paper 960726, pp. 221-227.

Karagiannis, K., and Pfeiffer, F., (1991) "Theoretical and Experimental Investigations of Gear-Rattling", Nonlinear Dynamics, 2, pp. 367-387.

Kim, T., Rook, T., and Singh, R., (2005a), "Super- and Sub-Harmonic Response Calculations for a Torsional System with Clearance Nonlinearity using the Harmonic Balance Method", Journal of Sound and Vibration, 281, pp. 965 – 993.

Kim, T., Rook, T., and Singh, R., (2005b), "Effect of Nonlinear Impact Damping on the Frequency Response of a Torsional System with Clearance", Journal of Sound and Vibration, 281, pp. 995 – 1021.

Kim, T., and Singh, R., (2001), "Dynamic Interactions between Loaded and Unloaded Gear Pairs under Rattle Conditions", SAE Technical Paper 2001-01-1553, pp.1934–1943.

Kim, T., and Singh, R., (2002), "Frequency Domain Analysis of Rattle in Gear Pairs and Clutches", the 2002 International Congress and Exposition on Noise Control Engineering, Dearborn, MI, USA, August 19-21.

Laschet, A., (1994), "Computer Simulation of Vibrations in Vehicle Powertrains Considering Nonlinear Effects in Clutches And Manual Transmissions", SAE Technical Paper 941011.

Lechner, G., and Naunheimer, H., (1999), "Automotive Transmissions: Fundamentals, Selection, Design and Application", Springer-Verlag.

Lin, J., (1997), "A New Capacitive Proximity Probe to Overcome Eddy Current Probe Limitations", Uprating and Refurbishing Hydro Powerplants VI, Montreal, Canada.

Lutz, D., (1988), "Kupplungsmanagement – ein Baustein zur Drehschwingungsdämfung" VDI Berichte, Nr. 697, pp. 219-231.

Martin, P., and Rothberg, S., (2006), "Differential Measurements using two Laser Rotational Vibrometers: Dynamic Backlash", 7th International Conference on Vibration Measurements by Laser Techniques: Advances and Applications, Proc. of SPIE Vol. 6345, 63450N.

Mason, J., Homer, M., Wilson, and R., (2006), "Mathematical Models of Gear Rattle in Roots Blower Vacuum Pumps", Bristol Centre for Applied Nonlinear Mathematics, University of Bristol, http://hdl.handle.net/1983/303.

The Mathworks online documentation: http://www.mathworks.com/access/helpdesk/help/helpdesk.html

Mayeux, F., Perret-Liaudet, J., and Rigaud, E., (2002), "Coupled Computation of Meshing and Bearings Stiffnesses: Effect on Radiated Gearbox Noise", the 2002 International Congress and Exposition on Noise Control Engineering, August 19-21, Dearborn, MI, USA.

McFadden, P., (1985), "Low Frequency Vibration Generated by Gear Tooth Impacts", NDT International, Vol. 18, No. 5.

Meisner, S., and Campbell, B., (1995), "Development of Gear Rattle Analytical Simulation Methodology", SAE Technical Paper 951317.

Merritt, H., E., (1971), *Gear Engineering*, Pitman Publishing.

Miura, Y., and Kojima, N., (2003), "Noise Generation Mechanism at Idling for a Four-Cylinder In-line Diesel Engine", SAE Technical Paper 2003-01-1720.

Miura, Y., and Nakamura, S., (1998),"Gear Rattling Noise Analysis for a Diesel Engine", Proceedings of the European Conference of Vehicle Noise and Vibration, 12 – 13 May, London (IMechE Paper C521/001/98).

Naas, J., Stoffels, H., and Troska, A., (2001), "Integrierte Berechnung zur Optimierung des Verzahnungsgeräusches eines Pkw-Handschaltgetriebes", ATZ-Automobiltechnische Zeitschrift 103, 1.

National Instruments Corporation (U.K.) Ltd., Measurement House, Newbury Business Park, London Road, Newbury, Berkshire RG14 2PS. Website: http://www.nationalinstruments.co.uk/

Özgüven, H. N., (1991), "A Non-Linear Mathematical Model for Dynamic Analysis of Spur Gears Including Shaft and Bearing Dynamics", Journal of Sound and Vibration, 145(2), pp. 239-260.

Ohnuma, S., Yahata, S., Inagawa, M., and Fujimoto, T., (1985), "Research on Idling Rattle of Manual Transmission", SAE Technical Paper 850979.

Padmanabhan, C., Rook, T., and Singh, R., (1995a), "Modelling of Automobile Gear Rattle Phenomenon: State of the Art", SAE Technical Paper 951316.

Padmanabhan, C., Barlow, R., Rook, T., and Singh, R., (1995b), "Computational Issues Associated with Gear Rattle Analysis", Transactions of the ASME, Journal of Mechanical Design, Vol. 117, pp. 185-192.

Parker, R., Vijayakar, S., and Imajo, T, (2000), "Non-Linear Dynamic Response of a Spur Gear Pair: Modelling and Experimental Comparisons", Journal of Sound and Vibration, 237(3), pp.435-455.

Pratap, R., (2002), "Getting Started with MATLAB: A Quick Introduction for Scientists and Engineers", Oxford University Press, Inc.

Rahnejat, H., (1984), "The Influence of Vibration on the Oil film in Elasto-hydrodynamic Contacts", PhD Thesis, Imperial College, University of London.

Rahnejat, H., (1985), "Computational Modelling of Problems in Contact Dynamics", Engineering Analysis, Vol.2, No.4, Computational Mechanics, pp.192-197.
Rahnejat, H., (1998), "Multi-body Dynamics: Vehicles, Machines and Mechanisms", Co-publishers: PEP (IMechE) Bury St Edmonds and SAE, Warrendale.

Rao, S. S., (2004),"Mechanical Vibrations", Pearson Prentice Hall, International Edition, 4th Edition.

Reese, S., (2003), "Numerical Methods in Dynamics", Lecture Notes (in English), Numerische Mechanik und Simulationstechnik, Bochum Ruhr-Universität.

Rivin, E., (2000),"Analysis and Reduction of Rattling in Power Transmission Systems", SAE Technical paper 2000-01-0032.

Rook, T. E., and Singh, R., (1995), "Dynamic Analysis of a Reverse-Idler Gear Pair with Concurrent Clearances", Journal of Sound and Vibration, 182(2), pp. 303-322.

Rust, A., Brandl, F. K., and Thien, G. E., (1990), "Investigations into Gear Rattle Phenomena – Key Parameters and their Influence on Gearbox Noise", IMechE, C404/001, pp. 113-120.

Ryborz, J., (2003), "Klapper- und Rasselgeräuschverhalten von Pkw- und Nkw-Getrieben", Berichte Nr. 107, Institut für Maschinenelemente, Universität Stuttgart.

Sakai, T., Doi, Y., Yamamoto, K., Ogasawara, T., Narita, M., (1981), "Theoretical and Experimental Analysis of Rattling Noise of Automotive Gearbox", SAE Technical Paper 810773, pp. 1- 10.

Sasaki, T., Mori H. and Okino, N. (1962)," Fluid Lubrication Theory of Roller Bearings", Trans. ASME, J. Basic Engineering.

Seaman, R., Johnson, C., and Hamilton, R., (1984), "Component Inertial Effects on Transmission Design", SAE 841686, pp. 6.990-6.1008.

SeaSolve (2003), "Auto Signal Version 1.7 User's Manual", SeaSolve Software Inc., Richmond, CA, US.

Sebulke, A., (1987), "The Two-Mass Flywheel – A Torsional Vibration Damper for the Power Train of Passenger Cars – State of the Art and Further Technical Development", SAE Technical Paper 870394.

Shaver, R., (1997), (Editor), "Manual Transmission Clutch Systems", Society of Automotive Engineers, Inc.

Shih, S., Yruma, J., and Kittredge, P., (2001), "Drivetrain Noise and Vibration Troubleshooting", SAE Technical Paper 2001-01-2809.

Singh, R., Xie, H., and Comparin,R., (1989) "Analysis of Automotive Neutral Gear Rattle", Journal of Sound and Vibration , pp. 177-196.

Smith, J. D., (1983), "Gears and Their Vibration: A Basic Approach to Understanding Gear Noise", Marcel Dekker, Inc, New York.

Smith, J. D., (1999), "Gear Noise and Vibration", Marcel Dekker, Inc, New York.

Steinel, K., (2000), "Clutch Tuning to Optimize Noise and Vibration Behaviour in Trucks and Buses", SAE Technical Paper 2000-01-3292.

Theodossiades, S, (2000), "Non Linear Vibrations and Dynamics of Mechanical Systems with Gears", PhD Thesis, Department of Mechanical Engineering, Aristotle University of Thessaloniki.

Theodossiades, S., and Natsiavas, S., (2001a), "On Geared Rotordynamic Systems with Oil Journal Bearings", Journal of Sound and Vibration 243(4), pp. 721-745.

Theodossiades, S., and Natsiavas, S., (2001b), "Periodic and Chaotic Dynamics of Motor-Driven Gear-Pair Systems with Backlash", Chaos, Solitons, and Fractals 12, pp. 2427-2440.

Thoden, D., (2006), " Theoretische Analyse der Schallsituation eines PKW-Schaltgetriebes und Vorschläge zu deren Messung", Studienarbeit, Fritz-Süchting-Institut für Maschinenwesen, Technische Universität Clausthal.

Timoshenko, S., Young, D.H., and Weaver Jr., W. (1974), "Vibration Problems in Engineering", John Wiley & Sons, 4th Edition.

Umezawa, K., Suzuki, T., and Sato, T., (1986), "Vibration of Power Transmission Helical Gears (Approximate Equation of Tooth Stiffness)", Bulletin of JSME, Vol. 29, No. 251, pp. 1605-1611.

Wang, Y., (1998), "Transmission Modelling for Gear Rattle Analysis", European Conference Vehicle Noise and Vibration, 12-13 May, IMechE, London.

Wang, M., Manoj, R., and Zhao, W., (2001), "Gear Rattle Modelling and Analysis for Automotive Manual Transmissions", proc. Instn. Mech. Engrs. Vol. 215 Part D.

Wang, M., Zhao, W., and Manoj, R., (2002), "Numerical Modelling and Analysis of Automotive Transmission Rattle", Journal of Vibration and Control, 8, pp. 921-943.

Wedeven, L., (1975), "What Is EHD?", Journal of the American Society of Lubrication Engineers, Lubrication Engineering, Vol. 31, 6, pp.291-296.

Whiston, G. S., (1979), "Impacting Under Harmonic Excitation", Journal of Sound and Vibration, 67(2), pp. 179-186.

Wilcoxon Research, (undated), "Industrial Vibration Sensor Selection: PiezoVelocity Transducers", online documentation, www.wilcoxon.com.

Wilhelm, M., Laurin, S., Schmillen, K., Spessert, B., (1990), "Structure Vibration Excitation by Timing Gear Impacts", SAE Technical Paper 900011.

Wilson, J., (1999), "A Practical Approach to Vibration Detection and Measurement Part 1: Physical Principles and Detection Techniques", Sensors, http://www.sensorsmag.com/sensors/article/articleDetail.jsp?id=330141.

Yakoub, R., Corrado, M., Forcelli, A., Pappalardo, T., and Dutre, S., (2004), "Prediction of System-Level Gear Rattle Using Multibody and Vibro-Acoustic Techniques", SAE Technical Paper 2004-32-0063/20044350.

Yamamoto, K, Umeyama, M., Ishikawa, H., Otake, T., and Kobayashi, K., (1991), "Consideration of a New Type Two-Mass Flywheel", SAE Technical Paper 911059.

Bibliography

Andersson, A.; and Vedmar, L.; (2003), "A Dynamic Model to Determine Vibrations in Involute Helical Gears", Journal of Sound and Vibration 260, pp. 195-212.

Chang, S-L., Tsay, C-B., Tseng, C-H., (1997), "Kinematic Optimization of a Modified Helical Gear Train", Transactions of ASME, Journal of Mechanical Design, vol. 119, pp 307-314.

Changsen, W., (1991), "Analysis of Rolling Element Bearings", Mechanical Engineering Publications Ltd., London, English Language Edition (translated by W. Changsen and Z. Zhaoying).

Chen, N., (1998), "Curvatures and Sliding Ratios of Conjugate Surfaces", Transactions of the ASME, Journal of Mechanical Design, vol. 120, pp. 126-132.

Chen, Y.-C., and Tsay, C.-B., (2002), "Stress Analysis of a Helical Gear Set with Localized Bearing Contact", Finite Elements in Analysis and Design 38, pp. 707-723.
Donely, M., Lim T., and Steyer G., (1992), "Dynamic Analysis of Automotive Gearing Systems", SAE Technical Paper 920762.

Doughty, S., (1988), "Mechanics of Machines", John Wiley and Sons Inc.

Dyson, A., Evans, H., and Snidle, R., (1992), "A Simple, Accurate Method for Calculation of Stresses and Deformations in Elliptical Hertzian Contacts", Technical Note, Proc. Instn. Mech. Engrs. Vol. 206, Part C: Journal of Mechanical Engineering Science, pp. 139-141.

Feng, P.-H., Litvin, F., Townsend, D., and Handschuh, R., (1999), "Determination of Principal Curvatures and Contact Ellipse for Profile Crowned Helical Gears", Journal of Mechanical Design, vol. 121, pp 107-111.

Hassal, J., and Zaveri, K., (1979), "Acoustic Noise Measurements", Brüel & Kjær, 4th edition, 1st print.

Houser, D., (1991), "Gear Noise 'In:'", Dennis P. Townsend "Dudley's Gear handbook", McGraw-Hill, Inc., 2nd edition, chapter 14.

Inman, D., (2001), "Engineering Vibration", Prentice-Hall Inc., 2nd Edition.

Jackson, A. and Rowe, C. N., (1980), "Application of EHL Theory to Gear Lubrication", SAE Transactions, 800670, pp. 2209-22019.

Karu, Z. Z., (1999), "Signals and Systems Made Ridiculously Simple", ZiZi Press, 3rd Printing.

Kushwaha, M., and Rahnejat, H., (2004), "Transient Concentrated Finite Line Roller-to-Race Contact under Combined Entraining, Tilting and Squeeze Film Motions", J. Phys. D: Appl. Phys. 37, 2018–2034.

Larsson, Roland, (1997), "Transient non-Newtonian Elastohydrodynamic Lubrication Analysis of an Involute Spur Gear", Wear 207, pp. 67-73.

Litvin, F. L., (1989), "Theory of Gearing", NASA Reference Publication 1212, AVSCOM Technical Report 88-C-035.

Litvin, F., (1995), "Applied Theory of Gearing: State of the Art", transactions of the ASME, Special 50th Anniversary Design Issue, Vol. 117, pp. 128-134.

Litvin, F., Chen, N.X., Chen, J.-S., (1995a), "Computerized Determination of Curvature Relations and Contact Ellipse for Conjugate Surfaces", Computer Methods in Applied Mechanics and Engineering 125, pp. 151-170.

Litvin, F., Chen, J., -S., Lu, J., and Handschuh, R., (1996), " Application of Finite Element Analysis for Determination of Load Share, Real Contact Ratio, Precision of

Motion, and Stress analysis", Transactions of the ASME, Journal of Mechanical Design, Vol. 118, pp. 561-567.

Litvin, F., Chen, N. X., Lu, J., and Handschuh, R., (1995b), "Computerized Design and Generation of Low-Noise Helical gears with Modified surface Topology", Transactions of the ASME, Journal of Mechanical Design, Vol. 117, pp. 254-261.

Litvin, F., Fan, Q., Vecchiato, D., Demenego, A., Handschuh, R., Sep, T., (2001), "Computerized Generation and Simulation of Meshing of Modified Spur and Helical Gears Manufactured by Shaving", Comput. Methods Appl. Mech. Engrg. 190, pp. 5037-5055.

Litvin, F., Fuentes, A., (2004), "Gear Geometry and Applied Theory", Cambridge University Press, second edition.

Litvin, F., Fuentes, A., Gonzalez-Perez, I., Carvenali, L., Kawasaki, K., Handschuh, R., (2003), "Modified Involute Helical Gears: Computerized Design, Simulation of Meshing and Stress Analysis", Computer Methods in Applied Mechanics and Engineering, 192, pp. 3619-3655.

Litvin, F., Fuentes, A., Gonzalez-Perez, I., Carnevali, L., Sep, T., (2002), "New Version of Novikov-Wildhaber Helical Gears: Computerized Design, Simulation of Meshing and Stress Analysis", Computer Methods in Applied Mechanics and Engineering, 191, pp. 5707-5740.

Litvin, F., and Gutman, Y., (1981), "A Method of Local Synthesis of Gears Grounded on the Connections Between the Principal and Geodetic Curvatures of Surfaces", Transactions of the ASME, Journal of Mechanical Design, vol.103, pp. 114-125.

Litvin, F., Lu, J., Townsend, D., Howkins, M., (1999), "Computerized Simulation of Meshing of Conventional Helical Involute Gears and Modification of Geometry", Mechanism and Machine Theory, 34, pp. 123-147.

Litvin, F., and Seol, I., (1996), "Computerized Determination of Gear Tooth Surface as Envelope to Two Parameter Family of Surfaces", Computer Methods in Applied Mechanics and Engineering, 138, pp. 213-225.

Lu, J., Litvin, F., and Chen, J. S., (1995), "Load Share and Finite Element Stress Analysis for Double Circular-Arc Helical Gears", Mathl. Comput. Modelling Vol. 21, No. 10, pp. 13-30.

McConnell, K. G., (undated), "Notes on Vibration Frequency Analysis", Spring Annual Meeting of the SESA.

Mostofi, A., (1999), "The Incorporation of Damping in Lumped-Parameter Modelling Techniques", Proceedings of the Institution of Mechanical Engineers, Journal of Multi-body Dynamics, Vol. 213, Part K.

Munro, R. G., (1990), "A Review of the Theory and Measurement of Gear Transmission Error", Proceedings of the Institution of Mechanical Engineers, First International Conference, Gearbox Noise and Vibration, C404/032.

Newland, D E (1989),"Mechanical Vibration Analysis and Computation", Longman Scientific & Technical, 1st Edition.

Rao, S. S., (2004),"Mechanical Vibrations", Pearson Prentice Hall, International Edition, 4th Edition.

Tsay, C-B., (1988), "Helical Gears with Involute Shaped Teeth: Geometry, Computer Simulation, Tooth Contact Analysis, and Stress Analysis", Journal of Mechanisms, Transmissions, and Automation in Design vol. 110, December 1988, pp. 482-491.

Zhang, J. J., Esat, I. I., and Shi, Y. H., (1999), "Load Analysis with Varying Mesh Stiffness", Computers and Structures 70, pp. 273-280.

Appendix A: Publications

Tangasawi, O., Theodossiades, S., Rahnejat, R., and Kelly, P., (2005), "Gear Teeth Impact Dynamics in Manual Transmissions Promoting Idle Rattle", Proceedings of the 5th EUROMECH Nonlinear Dynamics Conference, August 7-12, 2005, Eindhoven University of Technology (Netherlands).

Theodossiades, S., Tangasawi, O., Rahnejat, H., and Kelly, P., (2006), "The Effect of Hydrodynamic Conjunctions on Gear Teeth Oscillations", the 2nd International Conference on Nonlinear Normal Modes and Localization in Vibrating Systems, June 19-23 2006, Samos, Greece.

Tangasawi, O., Theodossiades, S., and Rahnejat, R., (2006) "Lightly Loaded Lubricated Impacts: Idle Gear Rattle" (presentation), the 1st International Conference on Vibro-Impact Systems, July 20-22, 2006, Loughborough, UK.

Theodossiades, S., Tangasawi, O., Rahnejat, H., and Kelly, P., (2006), "Theoretical and Experimental Analysis of Automotive Idle Gears rattle" (presentation), the 6th European Solid Mechanics Conference (ESMC), 28 August – 1 September 2006, Budapest, Hungary.

Tangasawi, O., Theodossiades, S., Rahnejat, R., and Kelly, P., (2006) "Gear Teeth Impacts in Hydrodynamic Conjunctions: Idle Rattle", the Integrated Powertrain & Driveline Systems Conference, October 3 2006, IMechE, London, UK.

Theodossiades, S., Tangasawi, O., and Rahnejat, H., (2006) "Gear Teeth Oscillations in Manual Transmissions Promoting Idle Rattle" (presentation), the BGA Technical Awareness Seminar (Gears 2006), 16 & 17 November 2006, Holiday Inn Manchester Airport.

Theodossiades, S., Tangasawi, O., and Rahnejat, H., (2007) "Gear Teeth Impacts in Hydrodynamic Conjunctions Promoting Idle Gear Rattle", Journal of Sound & Vibration 303, pp. 632-658.

Tangasawi, O., Theodossiades, S., and Rahnejat, H., (2007), "Lightly Loaded Lubricated Impacts: Idle Gear Rattle", Journal of Sound & Vibration, in Press.